SSC-409

GUIDE TO DAMAGE TOLERANCE ANALYSIS OF MARINE STRUCTURES
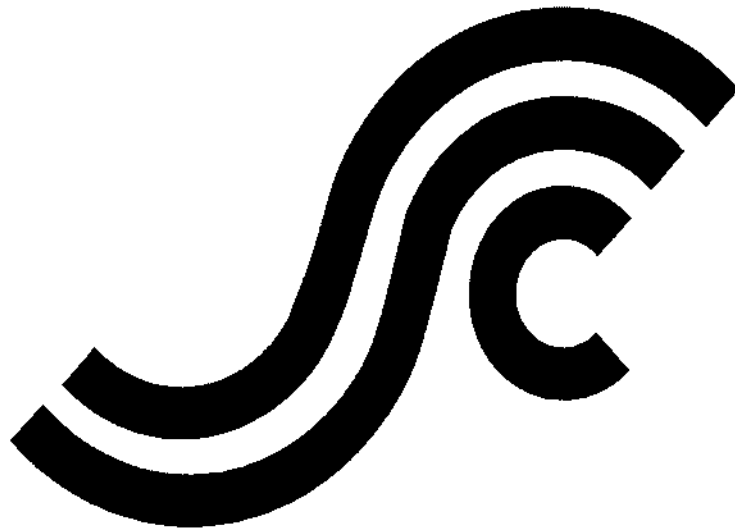
SHIP STRUCTURE COMMITTEE
2000

SHIP STRUCTURE COMMITTEE

RADM Robert C. North
U. S. Coast Guard Assistant Commandant,
Marine Safety and Environmental Protection
Chairman, Ship Structure Committee

Ship
Structure
Committee

An Interagency Advisory Committee

SR-1410
SSC-409

September 2000

GUIDE TO DAMAGE TOLERANCE ANALYSIS OF MARINE STRUCTURES

This report is a revision of SSC 402, "Guide to Damage Tolerance Analysis of Marine Structures". The SSC determined that an update to SSC-402 was necessary to more closely correspond to SSC - 405, "Fatigue Resistant Detail Design Guide for Ship Structures". This report replaces and supercedes SSC - 402.

Ship structures are subjected to various sources of wave-induced loading that may cause fatigue cracks to initiate at welded details during the service life of a ship. The propagation of these cracks may eventually compromise the structural integrity and water-tightness of a ship. The current practice is to repair severe fabrication flaws and any cracks detected in service as soon as possible. However, such a strategy could lead to prohibitive through-life maintenance costs. A useful tool for optimizing the maintenance and inspection of ship structures without compromising the structural integrity and water-tightness of a ship is damage tolerance analysis. This tool makes use of fracture mechanics to quantitatively assess the residual strength and residual life of a cracked structural member.

R. C. NORTH
Rear Admiral, U. S. Coast Guard
Chairman, Ship Structure Committee

TECHNICAL REPORT DOCUMENTATION FORM

1. Report No. SSC-409	2. Government Accession No.	3. Recipient's Catalogue No.	
4. Title and Subtitle Guide to Damage Tolerance Analysis of Marine Structures (Revised December 1999)		5. Report Date September 2000	
		6. Performing Organization Document No. SR-1410	
7. Author(s) I.F. Glen, A. Dinovitzer, L. Malik, R. Basu, R. Yee		8. Performing Organization Report No. 5002C.FR	
9. Performing Agency Name and Address Fleet Technology Limited 311 Legget Drive Kanata, Ontario (CANADA) K2K 1Z8		10. Work Unit No. (TRAIS)	
		11. Contract or Grant No. Req #: 23-99-329E00211	
12. Sponsoring Agency Name and Address Ship Structure Committee CG R&D Center 1082 Shennecossett Road Groton, CT 06340-6096		13. Type of Publication and Period Covered Final Report	
		14. Sponsoring Agency Code G-M	

15. Supplementary Notes
Sponsored by the Ship Structure Committee jointly funded by its member agencies

16. Abstract

In October 1977, Report SSC-402, Guide to Damage Tolerance Analysis of Marine Structures was published. In August 1999, SSC-405, Fatigue Resistant Detail Design Guide for Ship Structures was released. SSC determined that an update to SSC-402 to more closely correspond to SSC-405 was warranted. Therefore, this revised issue of the Guide to Damage Tolerance Analysis of Marine Structures will replace and supercede the previous issue.

Ship structures are subjected to various sources of wave-induced loading that may cause fatigue cracks to initiate at welded details during the service life of a ship. The propagation of these cracks may eventually compromise the structural integrity and water-tightness of a ship. Therefore, the current practice is to repair severe fabrication flaws and any cracks detected in service as soon as possible. However, such a strategy could lead to prohibitive through-life maintenance costs. A useful tool for optimizing the maintenance and inspection of ship structures without compromising the structural integrity and water-tightness of a ship is damage tolerance analysis. The latter makes use of fracture mechanics to quantitatively assess the residual strength and residual life of a cracked structural member. Unfortunately, most naval architects and structural engineers have little or no experience with damage tolerance analysis and fracture mechanics.

This guide is intended to provide naval architects and structural engineers with detailed guidance on the application of damage tolerance analysis to ship structures. The guide begins with a review of the essential elements of damage tolerance assessment. This is followed by guidance on: (i) the use of Failure Assessment Diagrams to assess the local residual strength of a cracked structural detail, (ii) the use of linear elastic fracture mechanics models for fatigue crack growth to predict the residual life of a cracked structural member, (iii) the estimation of peak and cyclic loads over the assessment interval of interest, and (iv) the calculation of stresses and crack driving forces. Towards the end of this Guide, the aforementioned guidance is demonstrated by means of two numerical examples.

17. Key Words Damage tolerance, fatigue, fracture, FAD, ships	18. Distribution Statement Distribution is available to the public through: National Technical Information Services (NTIS) US Department of Commerce Springfield, VA 22151 Phone 703-605-6000		
19. Security Classif. (of this report) Unclassified	20. SECURITY CLASSIF. (of this page) Unclassified	21. No. of Pages	22. Price

Form DOT F 1700.7 (8/72)   Reproduction of form and completed page is authorized

CONVERSION FACTORS

(Approximate conversions to metric measures)

To convert from	To	Function	Value
LENGTH			
inches	Meters	divide	39.3701
inches	Millimeters	multiply by	25.4000
feet	Meters	divide by	3.2808
VOLUME			
cubic feet	cubic meters	divide by	35.3149
cubic inches	cubic meters	divide by	61,024
SECTION MODULUS			
inches^2 feet	centimeters^2 meters	multiply by	1.9665
inches^2 feet	centimeters^3	multiply by	196.6448
inches^3	centimeters^3	multiply by	16.3871
MOMENT OF INERTIA			
inches^2 feet^2	centimeters^2 meters^2	divide by	1.6684
inches^2 feet^2	centimeters^4	multiply by	5993.73
inches^4	centimeters^4	multiply by	41.623
FORCE OR MASS			
long tons	Tonne	multiply by	1.0160
long tons	Kilograms	multiply by	1016.047
pounds	Tonnes	divide by	2204.62
pounds	Kilograms	divide by	2.2046
pounds	Newtons	multiply by	4.4482
PRESSURE OR STRESS			
pounds/inch^2	Newtons/meter^2 (Pascals)	multiply by	6894.757
kilo pounds/inch^2	mega Newtons/meter^2 (mega Pascals)	multiply by	6.8947
BENDING OR TORQUE			
foot tons	meter tons	divide by	3.2291
foot pounds	kilogram meters	divide by	7.23285
foot pounds	Newton meters	multiply by	1.35582
ENERGY			
foot pounds	Joules	multiply by	1.355826
STRESS INTENSITY			
kilo pound/inch^2 inch$^{1/2}$(ksi$\sqrt{}$in)	mega Newton MNm$^{3/2}$	multiply by	1.0998
J-INTEGRAL			
kilo pound/inch	Joules/mm^2	multiply by	0.1753
kilo pound/inch	kilo Joules/m^2	multiply by	175.3
TEMPERATURE			
Degrees Fahrenheit	Degrees Celsius	subtract	32
		& divide by	1.8

CONTENTS

PART A – DAMAGE TOLERANCE ANALYSIS GUIDE OVERVIEW

PART C – DAMAGE TOLERANCE ANALYSIS

PART D – EXAMPLES

APPENDICES
APPENDIX A   NOTCH STRESS CONCENTRATION FACTORS
APPENDIX B   STRESS CONCENTRATION FACTORS FOR SHIP STRUCTURAL
                    DETAILS
APPENDIX C   STRESS INTENSITY FACTORS FOR SHIP STRUCTURAL DETAILS
APPENDIX D   FLAW CHARACTERIZATION CRITERIA
APPENDIX E   PROCEDURE FOR LOAD ANALYSIS BY SPECTRAL APPROACH
APPENDIX F   INPUT DATA FOR WAVE LOAD ESTIMATION METHODOLOGIES

LIST OF FIGURES

LIST OF TABLES

Nomenclature

ABS		American Bureau of Shipping
AP		Aft perpendicular
A_i		Stress coefficient
a		**Half flaw length for through-thickness flaw, or flaw depth for surface flaw**, or
		Half the flaw depth for embedded flaws; or
		Length of double bottom panel; or
		Scale parameter of the basic S-N curve, or
		Acceleration (m/s^2)
	a_l	Combined longitudinal acceleration (m/s^2)
	a_o	Acceleration constant
	a_{px}	Longitudinal component of pitch acceleration (m/s^2)
	a_t	Combined transverse acceleration (m/s^2)
	a_v	Combined vertical acceleration (m/s^2)
	a_x	Surge acceleration (m/s^2)
	a_y	Acceleration due to sway and yaw (m/s^2)
	a_z	Heave acceleration (m/s^2)
$a_1\ a_2$		Fatigue design curve parameters
B		**Moulded breadth of ship (m or ft);** also
		Plate thickness
BSI		British Standards Institute
b		**Transverse width of double bottom panel,** or
		Half plate width
C		Paris constant
C_B		Block coefficient
C_t		Correction function for combined stress
C_w		Wave coefficient
CTOD		Crack Tip Opening Displacement
CVN		Charpy Vee-Notch Test Value
D_m		Moulded Depth of Ship (m)
DNV		Det Norske Veritas
E		Young's Modulus
FAC		Failure Assessment Curve
FAD		Failure Assessment Diagram
FAP		Failure Assessment Point
FEA		Finite Element Analysis

FP	Forward perpendicular
FTL	Fleet Technology Limited
$f(\sigma)$	probability density function for short-term response
$F(\sigma)$	Cumulative distribution function of response
F(Sea State)	Probability of occurrence of a given sea state
$F_{\Delta\sigma i}(\Delta\sigma)$	Rayleigh short-term stress range cumulative distribution function for the ith operational condition
f	Freeboard at the transverse section considered (m or ft.)
f_f	Correction factor to convert from one probability level to another probability level
$f_{mc}(H_s)$	Composite distribution of significant wave heights
$f_{mc}(H_s;T_z)_{composite}$	Composite distribution of wave heights and zero crossing periods (composite scatter diagram)
f_s	joint probability of significant wave height and speed
f_{stotal}	Total probability (three-dimensional probability) or percent of time for each operational condition
$f_V(V\mid H_s)$	Conditional probability of speed, V, given a wave height, H_s (or sea state) – all periods included
f_w	finite width correction factor
$f_\theta(\theta\mid H_s)$	Conditional probability of heading, θ , for given wave height, H_s, - all periods included
g	Gravitational constant
G(x)	General form for the Limit State equation in a First Order reliability analysis
GM	Metacentric height
HAZ	Heat Affected Zone
HSE	UK Health and Safety Executive
H_s	Significant wave height (m or ft.)
h	**Shape parameter for Weibull Distribution (general)**; also Weld height
h_n	Weibull shape factor for n^{th} loading condition
h_o	Basic long-term Weibull shape parameter, modified for location of Point of Interest
h_s	Vertical distance from point considered to surface inside a tank (m)
$H_v(\omega\mid\theta)$	RAO for vertical bending moment
$H_h(\omega\mid\theta)$	RAO for horizontal bending moment
$H_t(\omega\mid\theta)$	RAO for torsional bending moment
$H_p(\omega\mid\theta)$	RAO for external pressure
$H_c(\omega\mid\theta)$	RAO for liquid loads
$H_\sigma(\omega\mid\theta)$	RAO for stress
I	**Moment of Inertia (general)**
I_a, I_b	Moment of inertia about the transverse neutral axis, including the effective width of plating, of long stiffeners
I_h	Hull cross section moment of inertia about the vertical neutral axis

I_v Hull cross section moment of inertia about the transverse neutral axis

IIW   International Institute for Welding

ISSC   International Ship and Offshore Structures Congress

i_a, i_b Blended stiffness per unit (girder and plate) about transverse (longitudinal) neutral axis of double bottom

J		Fracture property derived from tests (ASTM E1737)

K		Stress concentration factor (general)
	K_{app}	Stress intensity factor
	K_b	Stress concentration factor dependent on aspect ratio, ρ, and panel's boundary conditions
	K_G	Global stress concentration factor to account for gross structural geometry (e.g., hatch openings, shear lag) affecting the local nominal stress field
	K_g	Stress concentration factor due to the gross geometry of the detail
	K_I	Mode I (open) Stress Intensity Factor
	K_{II}	Mode II (sliding) Stress Intensity Factor
	K_{III}	Mode III (tears) Stress Intensity Factor
	K_{jc}	Fracture toughness from "j" integral test
	K_{mat}	Fracture toughness
	K_{IC}	Fracture toughness
	K_n	Stress concentration factor due to non-symmetric stiffeners
	K_{te}	Stress concentration factor due to eccentricity
	$K_{t\alpha}$	Stress concentration factor due to angular mismatch
	K_{th}	Threshold range of stress intensity factor range
	K_w	Notch stress concentration; local weld configuration stress concentration
K_0		Stress transfer function relating vessel load response to detail hot spot stress
k		Number of stress blocks or stiffener fixity factor
k_r		Roll radius of gyration (m)
k_{wm}		Moment distribution factor

L		Rule length of ship (m or ft)
LR		Lloyd's Register
ℓ_e		Effective span of stiffener or longitudinal (m or ft.)
l_s		Distance (span) between bulkhead and transverse frame (m or ft.)

M		**Bending moment (MNm or LTft.)**
	M_d	Vertical bending moment range (MNm or LTft.)
	M_{dh}	Design wave-induced hogging moment amplitude (MNm or LTft.) including the effects of whipping
	M_{ds}	Design wave-induced sagging moment amplitude (MNm or LTft.) including the effects of whipping
	M_h	Horizontal bending moment amplitude at the location of interest (MNm or LTft.)
	M_{hog}	Hogging moment (MNm or LTft.)
	M_{sw}	Stillwater bending moment (MNm or LTft.)
	M_{sag}	Sagging Moment (MNm or LTft.)
	M_v	Vertical (sagging or hogging) bending moment amplitude at the location under consideration (MNm or LTft.)

M_k	Stress Intensity Magnification Factor
M_e	Maximum allowable misalingment measured from the centerlines of intersecting plates (mm or in.)
MEDS	Marine Environmental Data Services
m	**Location parameter of the Weibull distribution;** also
	Weight function
m_1, m_2	Fatigue design curve slope parameters
m_0	Spectral zeroth moment employed in spectral analysis
m_k	Spectral kth moment employed in spectral analysis
m_δ	Moment factor due to relative deflection between transverse supports
N	Total number of cycles (wave encounters or stress reversals) experienced by the structure within a time, t; used to express Fatigue Life.
N_i	Average number of loading cycles to failure under constant amplitude loading at the ith stress range
N_t	Total number of loading cycles to failure
N_B	Number of cycles associated with reference stress range $\Delta\sigma_B$
N_o	Number of cycles associated with reference stress range $\Delta\sigma_o$
N'	Total number of Marsden Zones along the route
N_s	Number of cross ties in cargo or ballast tank
NOAA	National Oceanic and Atmospheric Administration
NDT	Non-destructive Testing
NDTT	Nil Ductility Transition Temperature
n_i	Number of stress cycles in stress block "i"
n_o	Number of wave encounters corresponding to the service level of probability for load/stress
P_f	Probability of fatigue-induced failure
POD	Probability of Detection (of a flaw)
POI	Point of Interest
p	Effective lateral pressure
p_d	Dynamic pressure amplitude (kPa)
p_{dp}	Combined pressure dominated by pitch motion in head/quartering seas
p_{dr}	Combined pressure dominated by roll motion in beam/quartering seas
p_e	External pressure amplitude (half pressure range) related to the draft of the load condition considered (kPa)
p_{ext}	External pressure (kPa)
p_i	**Fraction of time at the ith operational condition;** or
	Probability of occurrence of a stationary condition, i
p_{int}	Internal pressure (kPa)
p_1	Pressure due to vertical acceleration
p_2	Pressure due to transverse acceleration
p_3	Pressure due to longitudinal acceleration

p_{ip} Dynamic pressure term (kPa) for pitch-induced pressure

p_{st} Static pressure

p_n Fraction of design life in the nth load condition

prob(H_s)   Marginal probability of wave heights

prob(H_s; T_z)   Marginal probability of the sea state

prob(V and (H_s; T_z))   Joint probability of speed and sea state

prob(θ and (H_s; T_z))   Joint probability of heading and sea state

q   Scale parameter for Weibull distribution

R   Ratio $\sigma_{min}/\sigma_{max}$

RAO   Response amplitude operator

RMS   Root mean square

r_a Distance from point considered to the transverse neutral axis of panel (m or ft.)

r_b Distance from point considered to the longitudinal neutral axis of panel (m or ft.)

r_i Ratio of the ith zero crossing rate, to the average zero crossing rate for all operational conditions

r_{ij} Relative number of stress cycles in short-term condition i, j against the total number of cycles in the vessel life

r_δ, r_π Moment factors for interpolation to crack location along stiffener length

r_p Reduction of pressure amplitude in the wave zone

r_y Radius of plastic zone at crack tip

SCF   Stress Concentration Factor

SIF   Stress Intensity Factor

SSC   Ship Structure Committee

S_r Stress ratio = σ_n/σ_f

$S_\eta(\omega_e)$ Modified wave height spectrum (m^2*s)

$S_\sigma(\omega_e)$ Stress spectrum

s   Stiffener spacing (mm or in.)

s_a Transverse spacing between girders or longitudinals running in the longitudinal direction (m or ft.)

s_b Longitudinal spacing between girders or web frames in the transverse direction (m or ft.)

T   **Draft of ship at load condition (m); also**
Period (s); also
Temperature

T_{act} Stillwater draft at the considered load condition (m)

$\overline{T}$ Long-term average stress period (s)

T_o Reference temperature

T_P Peak wave period (s)

T_R Period of roll (s)

T_S Significant wave period (s)

T_z Zero crossing period (s)

t		**Time(s);** also
		Thickness
	t_b	Bracket thickness (mm or in.)
	t_{corr}	Corrosion thickness allowanced
	t_d	Design life of ship expressed in seconds (s)
	t_f	Stiffener flange thickness (mm or in.)
	t_n	Net plate thickness (mm or in.)
	t_r	Reference thickness (mm or in.)
	t_s	Continuous plate thickness (mm or in.)
	t_w	Web thickness (mm or in.)
TAPS		Trans-Alaska Pipeline Service
u_r		Crack opening displacement
V		Vessel speed (knots)
VLCC		Very Large Crude Carrier
W		Plate width
x		**Length measurement variable (general),** or
		Longitudinal distance from the AP to the section considered (m or ft.)
	x_c	Distance from end of stiffener to crack location (mm or in.)
	x_s	Longitudinal distance from centre of free surface of liquid in tank to pressure point considered (m or ft.)
Y		Stress intensity correction factor
Y′		Modified magnification factor accounting for effective flaw size (including r_y)
	Y_m	Stress intensity or magnification factor accounting for flaw geometry
y		**Length measurement in variable in transverse direction (general),** or
		Transverse distance from the centre line to the point of interest (m or ft.)
	y_{na}	Transverse distance from vertical neutral axis to point of interest
	y_s	Transverse distance from centre of free surface of liquid in tank to point of interest (m or ft.)
Z		Section modulus
	Z_{deck}	of deck
	Z_s, Z_I	of stiffener or longitudinal (mm^3 or in.^{3})
z		Vertical distance on the hull:
	z_{na}	from the neutral axis to the point of interest (m or ft.)
	z_{bl}	from the baseline to the point of interest (m or ft.)
	z_{wl}	from the still waterline (m or ft.) (ship upright)
	z_1, z_2	Instantaneous immersions of POI due to ship motion (m or ft.)

α	**Maximum roll angle, single amplitude (rad)**, or
	Risk parameter
β	Reliability index derived from limit state equation $G(x)$
γ	Empirical correction for local K_g
Δa	Crack growth increment
ΔK	Stress intensity factor range
$\Delta\sigma_{nom}$	Reference nominal stress range (MPa)
$\Delta\sigma_{notch}$	Notch stress range (MPa)
$\Delta\sigma_o$	**Design stress range for the nth loading condition (MPa),** or
	Reference stress range
$\Delta\sigma_{S-N}$	Design stress range allowed by the relevant S-N curve (MPa)
δ	Deformation of nearest frame relative to transverse bulkhead (mm or in.)
$\quad\delta_{mat}$	Critical CTOD value of material
$\quad\delta_c, \delta_u, \delta_m$	Fracture toughness values from CTOD tests
$\quad\delta_r$	Ratio of applied force to fracture toughness expressed in CTOD terms
ϵ	Strain
ϕ	**Pitch angle, single amplitude (rad),** also
	Flaw shape parameter, measured from plate surface
η	**Fatigue usage factor,** or
	Torsion factor in grillage
Θ_k	63rd percentile toughness (value at mean plus 1 standard deviation)
θ	Ship's heading relative to wave direction (degrees, 0° = head seas), also
	Weld toe angle
θ'	spreading angle for wave spectrum (rad)
μ_i	Proportion of time spent in the ith area (Marsden zone)
ν	Poisson ratio
ν_I	Zeroth crossing frequency for ith condition
ν_o	Average crossing rate
ρ	**Panel aspect ratio,** also
	Weld toe radius
ρ_{sw}	Density of seawater (1.025 t/m^3)

σ	**Stress (MPa)**
σ_a	Stress amplitude
σ_{app}	Applied stress
σ_b	Bending stress (MPa)
σ_{eq}	Equivalent stress (MPa)
σ_f	Flaw stress
σ_G	**Standard deviation of limit state equation G(x),** also Global nominal stress
σ_{HS}	Hot spot stress
σ_{lower}	Stress range bin lower value (MPa)
σ_m	Membrane stress
σ_{mid}	Stress range bin mid value (MPa)
σ_n	Net section stress
σ_{nom}	Nominal stress
σ_{notch}	Notch stress
σ_o	Design stress
σ_p	Peak stress (MPa)
σ_r	Residual stress (MPa)
σ_y	Tensile yield strength (MPa)
σ_t	Total stress at crack location (MPa)
σ_{tp}	Peak total stress at crack location (MPa)
σ_{upper}	Stress range bin upper value (MPa)
σ_1	Primary stresses due to bending, shear and torsion in the main hull girder; peak total stress (MPa)
σ_1, v	Primary vertical hull bending stress
σ_2	Secondary stresses due to local stiffener bending (MPa)
σ_{2L}	Plate/panel secondary stresses (MPa)
σ_3	Tertiary plate bending stress (MPa)
σ_δ	Stresses due to relative deflection between web frame and transverse bulkhead (MPa)

ω	Wave frequency (rad/s)
ω_e	Encounter frequency that accounts for the effects of speed and heading

PART A – DAMAGE TOLERANCE ANALYSIS GUIDE OVERVIEW

A.1   INTRODUCTION

Ship structures are subjected to various sources of wave-induced cyclic loading that may cause fatigue cracks to initiate at welded details during the service life of a ship. The propagation of these cracks may eventually compromise the structural integrity and water-tightness of the ship. Current practice is to repair severe fabrication flaws and any cracks detected in service as soon as possible. However, such a strategy can lead to prohibitive maintenance costs. A useful tool for optimizing the maintenance and inspection of ship structures, without compromising the structural integrity and water-tightness of the ship, is damage tolerance analysis. This technique makes use of fracture mechanics methods to quantitatively assess the residual strength and residual life of a cracked structural member.

In principle, existing techniques based on fracture mechanics for assessing the residual strength and residual life of cracked structure in aircraft, pipelines, bridges, and offshore structures can be adapted to ship structures. These practices have been reviewed for their applicability to ship structures in, for example, References A.1 to A.6, and in previous Ship Structures Committee (SSC) projects [Refs. A.7, A.8]. However, many years have been spent in the development of standardized load histories, material databases, failure criteria, and crack growth models to enable damage tolerance assessment of aircraft, bridges, offshore platforms, pressure vessels and pipelines. Even so, the application of these techniques to the design of welded structures has been limited by the complexity of stress fields around welded details, the presence of welding residual stresses, and the complexity of crack growth.

The adaptation of these practices to ship structures is further complicated by the added complexity of ship details, uncertainty of operational loads, uncertainty of welding residual stress assumptions, and the redundancy of ship structures. As a result, this adaptation is still under development. Nevertheless, there is an immediate need for structural engineers and naval architects to have the capability to assess the damage tolerance of ship structures at the design stage, in service, and when extending the service lives of older ships. The SSC recognised this shortfall and contracted Fleet Technology Limited to develop a document that would guide naval architects and ship structures specialists through the process of damage tolerance assessment. This Guide is the result of this work.

A.2   OBJECTIVE

The objective of the present project is to prepare an engineering guide that will:

1.   lead structural engineers and naval architects through the application of damage tolerance analysis to ship structures at the design and fabrication stages, in service, and when extending the service life of older ships;

2.   provide a framework and guidance/commentary for performing detailed calculations of residual strength and residual life; and

3.   present examples that follow the guide in a step by step manner to illustrate the applications of the damage tolerance methodology.

A.3   APPLICATION OF DAMAGE TOLERANCE ANALYSIS IN SHIP STRUCTURES

A.3.1   Metal Fatigue Process in Ship Structures

Metal fatigue is the progressive failure of metal under cyclic loading. This type of failure can be divided into three basic stages:

1.   the initiation of microscopic cracks at microscopic or macroscopic stress concentrations;

2.   the growth of microscopic cracks into macroscopic cracks; and

3.   the growth of macroscopic cracks to a critical size for failure (e.g., plastic collapse, fracture, or oil leakage).

The absolute and relative magnitudes of these stages depend on material, notch severity, structural redundancy, and environment [Ref.A.1].

Fatigue cracks in steel ships generally initiate at welded structural details. The initiation and subsequent propagation of these cracks can be driven by several sources of cyclic loading including:

1.   longitudinal bending, transverse bending, and torsion of the hull girder as a result of wave loading;

2.   fluctuating hydrostatic pressure on side shell plating, cargo hold boundaries and tank walls; and

3.   machinery and hull vibration [Ref. A.9].

Exposure to corrosive media, such as sour crude oil or sea-water, can accelerate the initiation and propagation of fatigue cracks, either directly through corrosion fatigue mechanisms or indirectly through the higher cyclic stresses that result from localized and general corrosion. Fatigue-prone areas in bulk carriers include hatch corners, coamings, bracketed connections between hold frames and wing ballast tanks, the intersections of transverse corrugated bulkheads with top-side structure, and the intersections of inner bottom plating with hopper plating. Fatigue-prone areas in tankers include the intersections of side shell longitudinals and transverse structure and the end connections of deck and bottom longitudinals [Refs. A.10–A.13].

Although most fatigue cracks in steel ships are not detected by conventional inspection techniques until they are at least several inches long and through the thickness of plating, catastrophic brittle fractures rarely initiate from undetected fatigue cracks because of the relatively good fracture toughness of modern ship steels, the inherent redundancy of ship structures, the use of crack arrestors, and the relatively low rate of normal service loads. Nevertheless, any detected cracks are usually repaired at the earliest opportunity to prevent other problems from arising.

Historically, ship structures have been designed to meet minimum scantling requirements that have included allowances for general corrosion and uncertainties in design methods. Until recently, fatigue cracking was not explicitly considered by designers because fatigue cracking was rarely detected in ships less than 10 years old and because the frequency and costs of repairing fatigue cracks in older ships was acceptable to owners. Since the late 1970's, however, fatigue cracking has occurred more frequently in relatively new ships. This change has been attributed to the design and construction of more structurally optimized ships with thinner scantlings. This optimization, that has been motivated by commercial demands to reduce the fabrication costs and weight of hull structures, has been achieved through the greater use of high strength steels, the use of more sophisticated design tools, and the greater exploitation of classification society rules which have permitted design stresses to increase with tensile strength up to a fraction of the tensile strength defined by the so-called material factor. Unfortunately, stress concentrations of structural details have not been adequately reduced to compensate for the higher design stresses and higher local bending stresses associated with thinner scantlings. Furthermore, the fatigue strength of as-welded steel joints is essentially independent of tensile strength. Therefore, local cyclic stresses at structural details have been permitted to increase without a matching increase in fatigue strength of these details. In addition, corrosive environments have exacerbated this mis-match since the flexibility of thin structure promotes the flaking of rust which accelerates the wastage process and further increases the flexibility of thin structure [Refs. A.14-A.16].

In response to safety concerns and escalating maintenance costs for owners, classification society rules have recently introduced explicit fatigue design criteria for welded structural details in steel ships [Refs. A.12, A.17, A.18]. These criteria, which are largely based on well-established fatigue design procedures for welded joints in bridges and offshore structures [Refs.

A.19-A.21], are intended to ensure that there is a low probability of fatigue failures occurring during the design life of a ship, where failure is generally considered to be the initiation of a through-thickness crack several inches long. However, premature fatigue cracking as a result of fabrication or design errors can still occur. Furthermore, some fatigue cracking can still be expected in properly designed ships. Therefore, quantitative techniques for predicting the residual life and residual strength of cracked structural welded details are needed to develop safe but cost-effective inspection schedules at the design stage. These techniques can also be used to optimize the scheduling of repairs for cracks found in service and to assess whether the operation of existing ships can be extended beyond their original design lives.

A.3.2   Application of Damage Tolerance Methods in Design

Damage tolerance is the ability of a damaged structure to withstand anticipated operational loads without failure or loss of functionality. There are three basic ways that damage tolerance can be designed into structures [A.22, A.23]:

1.   **The safe-life approach** designs a structure for a finite life and requires the imposition of large factors of safety on design loads and material properties to ensure that there is a low probability of failure during the design life. Machine components, bridges, offshore platforms, aircraft landing gear, and aircraft engine mounts are typically designed with this approach.

2.   **The fail-safe approach** allows a structural component to be designed with lower factors of safety and, therefore, a higher probability of failure during its service life. However, multiple load paths (i.e., structural redundancy), crack arrestors, and accessibility for inspection must be built into the structure so that damage is detected before the failure of one or more individual components leads to overall failure. This approach was initially developed by the aircraft industry for airframes because the additional weight of a safe-life design was unacceptable.

3.   While both the above methods are designed to produce damage tolerant structures, the so- called **damage tolerant design approach** is a refinement of the fail-safe approach. Damage is assumed to be initially present in critical structural elements, and explicit analyses are conducted to predict the spread of this damage and to assess residual strength. The results of the analyses are used to develop an inspection program for critical structural elements that will ensure that damage will never propagate to failure prior to detection. If necessary, the structure is re-designed to obtain practical inspection intervals and to improve the durability of the structure (i.e., damage over the service life is limited and can be economically repaired). This approach was developed by the aircraft industry in recognition that the spread of initial and subsequent damage can degrade the integrity of redundant members in a fail-safe structure and relies heavily on fracture mechanics to predict the residual life and residual strength of cracked structure. Since the late 1970's, regulations for civil and military aircraft have required

that these damage tolerance assessment techniques be used to design most components and to re-qualify aging aircraft [A.24-A.28].

The **damage tolerant design approach** is shown schematically in **Figure A.3.1**, and the basic steps of this approach are summarized below:

1. Critical structural elements and potential crack initiation sites in these elements are identified.

2. A crack-like flaw is assumed to be initially present at each of the aforementioned sites. The size of these flaws is assumed to be the smallest size that can be reliably detected by conventional non-destructive inspection techniques.

3. The criticality of each initial flaw is evaluated using stress analysis based on maximum expected service loads or design loads, fracture mechanics, and failure criteria for fracture and other possible failure modes.

4. If the **residual strength** of a critical structural element is smaller than the design strength (i.e., initial flaws exceed a critical size), then the structural member is re-designed with lower stresses and/or more damage-resistant materials. Otherwise, the design of the structural element is accepted, and fracture mechanics analysis of fatigue crack propagation is carried out to determine the **residual life** of the structural element (i.e., the time period/voyages after which the initial flaw will grow to a critical size).

5. Each critical structural element is inspected before the end of the calculated residual life. The inspection interval includes an adequate margin of safety, and it is repeated if no flaws are detected. Detected flaws are repaired immediately.

In principle, a damage tolerance design approach would permit designers to exploit the redundancy of ship structures, and some design codes for bridges and offshore structures now permit designers to use damage tolerance assessment techniques in lieu of conventional fatigue design procedures. However, the widespread use of these techniques has been hindered by the difficulty of analyzing stress fields around complex structural details, particularly in redundant structures, and by the complexity of the fatigue cracking process in welded joints. Therefore, the use of damage tolerance assessment techniques in the design of these structures has been restricted to situations where normal fatigue assessment procedures are inappropriate (e.g., the geometry, size, loading, or operational environment of the structural detail under consideration is unusual, and the detail cannot be reliably assessed with available joint classifications, S-N design curves, and stress concentration factors) and to the development of inspection intervals for designs produced by the conventional approach. In both types of applications, it is necessary to assume that there is a pre-existing initial crack, the size and shape of which is determined by the detection capability of conventional non-destructive evaluation techniques. Until designers have greater access to powerful analysis tools and until there is a greater understanding of the fatigue

and fracture process in welded joints, it is expected that ship designers will use fracture mechanics in the same way.
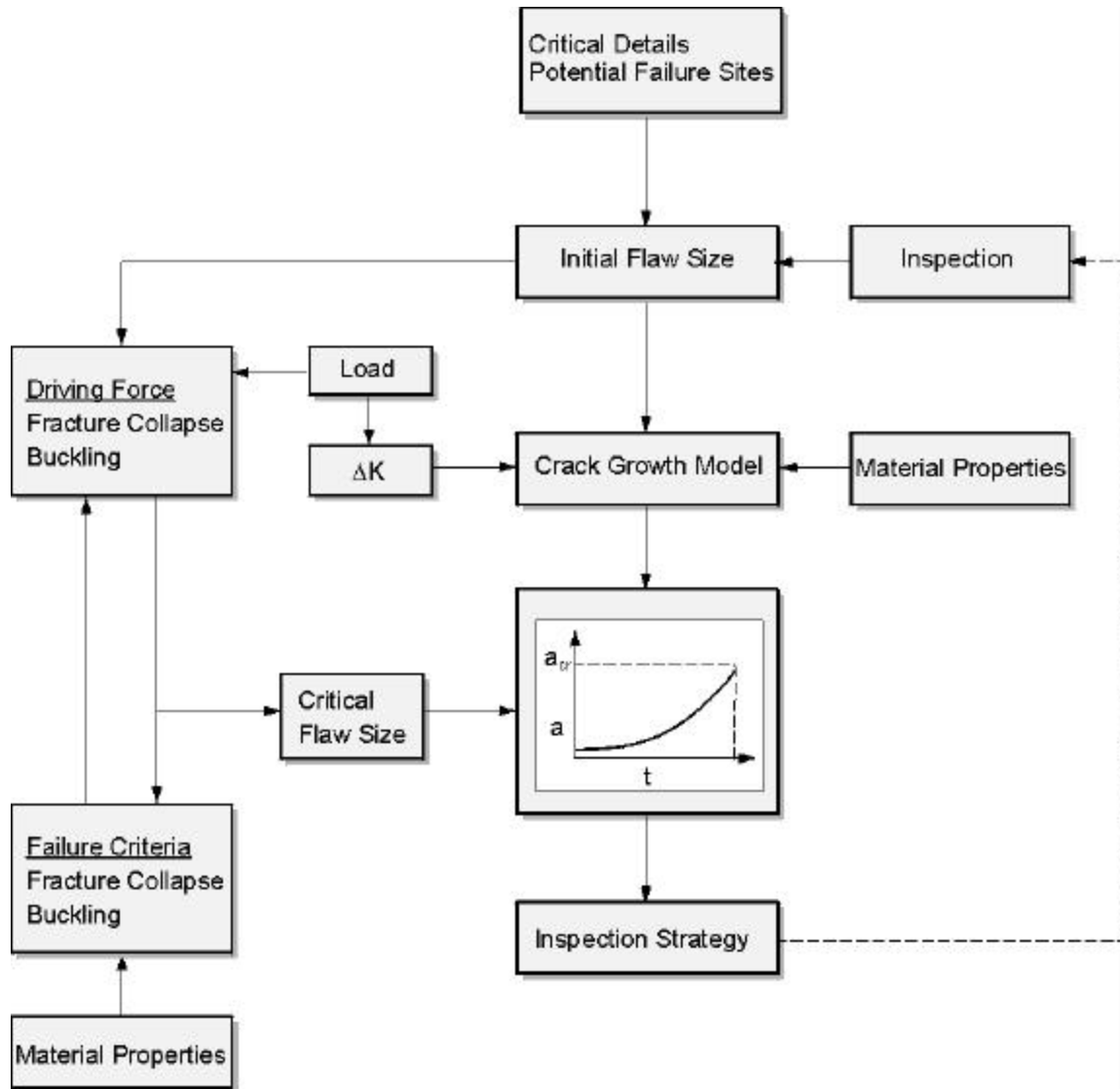
Figure A.3.1: Flow Chart of Procedure for Damage Tolerance Assessment

A.3.3 Fitness-for-Service, Fitness-for-Purpose, or Engineering Critical Assessment

Modern ship structures are mainly fabricated by fusion arc welding processes. These processes enable continuous watertight connections to be produced in an efficient and economical manner. Unfortunately, welding processes can introduce planar and volumetric flaws from which fatigue cracks or brittle fracture could initiate. Such flaws can occur despite careful training of welders and careful design of structures for easy access by welders. Therefore, ship fabricators must rely heavily on inspectors to ensure the quality of fabricated welds. The current practice is to repair defects that do not pass workmanship-based acceptance criteria. These criteria, however, tend to be very conservative, and damage tolerance assessment could be used to screen out unnecessary repairs.

The fatigue design procedures recently introduced by classification societies are consistent with a safe life design philosophy. Such a philosophy will ensure a low probability of fatigue cracking in new ships but it will not completely eliminate it. For example, fatigue cracks could initiate from flaws that have escaped detection during fabrication or from delayed hydrogen-assisted cracking in the heat affected zone of welds. It should also be noted that the majority of existing ships were designed without explicit consideration of fatigue cracking. Fatigue cracking has occurred in these ships, particularly in high strength steel ships, and they will continue to occur as these ships age. As mentioned earlier, the current practice is to repair detected cracks at the earliest opportunity. Damage tolerance assessment could be used to screen out unnecessary repairs, to determine whether needed repairs can be delayed (e.g., to the next scheduled maintenance or port-of-call), to minimize repair costs and down-time, and to establish safe but efficient inspection schedules for unrepaired flaws.

The aforementioned applications of damage tolerance assessment fall within a broader group of applications commonly referred to as **fitness-for-service**, **fitness-for-purpose**, or **engineering critical assessment**. Such assessments have been permitted by design codes for piping and pressure vessels in oil and gas transmission systems, petro-chemical installations, and power generation systems for many years now [A.29,A.30]. The basic procedure is similar to the damage tolerant design procedure shown schematically in Figure A.3.1, and it is summarized below:

1. The criticality of the detected flaw is evaluated using stress analysis based on maximum expected service loads or design loads, fracture mechanics, and failure criteria for fracture and other possible failure modes.

2. If a detected flaw exceeds a critical size (i.e., the **residual strength** of a critical structural element is lower than its design strength), the flaw is repaired before the structure is returned to service. Otherwise, a fracture mechanics analysis of fatigue crack propagation is carried out to determine the **residual life** of the structural element (i.e., the time period/voyages after which the initial flaw will grow to a critical size), and the structure is returned to service.

---

3. Critical structural elements with unrepaired flaws are re-inspected before the end of their calculated residual life. The inspection interval must include a suitable margin of safety, and the criticality of the flaws must be re-evaluated at the end of the interval. The flaw can also be repaired at any convenient time before the end of the inspection interval.

The aforementioned process differs from damage tolerance assessment at the design stage in a few respects. The most obvious difference is that real flaws rather than assumed flaws are considered in a fitness-for-service assessment. In addition, fitness-for-service assessments are usually based on more specific, more up-to-date, and less conservative inputs (e.g., load, material properties, and scantlings) than damage tolerance assessments at the design stage. For example, whenever possible, actual material properties and scantlings rather than design values are used in fitness-for-service assessments to account for any degradation during service.

A.3.4 Life Extension and Changes in Operational Profile

There is a strong economic incentive for ship owners to extend the service lives of existing ships beyond their original design lives and to maximize the utilization of their fleets by using ships in roles for which they were not originally designed. If a hull condition survey is conducted when the original design life of a ship expires, or before the operational profile of a ship is altered, then residual strength assessments could be carried out to determine the criticality of detected flaws and to determine which flaws need to be repaired before the ship is returned to service. Residual life assessments could also be used to assess the residual life of critical structural elements with non-critical flaws and to establish inspection and repair schedules for these flaws. By assuming that initial flaws equal in size to the smallest detectable flaw exist in critical structural members with no detected flaws and by extending the residual strength and residual life assessments to these elements, inspection and repair schedules could be established for the entire ship hull. Therefore, the aforementioned process combines the elements of fitness-for-service assessment with some elements of damage tolerance assessment at the design stage.

A3.5 Fracture Mechanics Basis for Damage Tolerance Assessment

In conventional strength based design, the main objective is to avoid failure by plastic collapse. This goal is achieved by ensuring that the stress that a structural member is subjected to (σ_{app}, the applied stress – the driving force for failure by plastic collapse) due to operational loads does not exceed a certain fraction of the structural material's yield strength (σ_y, the material's resistance to failure). Thus, the limit state equation can be expressed as:

$$\sigma_{app} \leq \beta . \sigma_y \qquad \qquad [A.3.1]$$

where β is a fraction, typically 2/3 to 0.8, that provides a safety margin against the uncertainties in estimates of σ_{app} and σ_y.

The above strength based design approach presumes that the structural member does not contain any crack-like flaws. In reality, this is not the case as crack-like fabrication flaws might be present even in a newly fabricated structure, or fatigue cracks may initiate and grow in welded structures subject to cyclical loads. In the presence of cracks then, it becomes important to determine the rate at which such cracks might grow in response to the operational cyclic loads and the critical crack size that, if reached, might precipitate an unstable catastrophic failure. The discipline of fracture mechanics enables one to determine the driving force and materials resistance relevant to both these situations.

The driving force for crack propagation leading to unstable brittle fracture is expressed in terms of the stress intensity factor (SIF). The stress intensity factor quantifies the severity of the asymptotic stress-strain fields at the crack tip, and is denoted here as K_{app}. For the simple case of a flat plate of width 2b containing a through thickness crack of length 2a perpendicular to an applied stress σ_{app} (see **Figure A.3.2**), the stress intensity factor, K_{app}, is given by the expression

$$K_{app} = Y. \sigma_{app} . \sqrt{(\pi a)} \qquad [A.3.2]$$

where Y is a numeric factor that depends on the geometry of the crack and the structural member, in this case on the ratio a/b. It should be added here that if the crack-like flaw is associated with a weld, then residual stresses of some magnitude, σ_r, are inevitably present in the as-welded (non-stress relieved) structure, and these also contribute to the potential for unstable brittle fracture. The welding residual stresses present in the structural region containing the flaw therefore also need to be estimated and included in calculation of K_{app}.

The material's resistance to unstable fracture in the presence of cracks is called fracture toughness, K_{mat}, and is determined experimentally following one of several standard test procedures developed for this purpose. The limit state equation for prevention of unstable fracture can then be written as

$$K_{app} < K_{mat} \quad \text{or} \quad K_r = (K_{app} / K_{mat}) < 1 \qquad [A.3.3]$$

Thus, in the presence of cracks, K_{app} is analogous to σ_{app}, and K_{mat} is analogous to σ_y.

An evaluation of the residual strength of a structural member containing a crack requires consideration of failure by both plastic collapse and by unstable brittle fracture. A convenient method to do so is by the use of the **Failure Assessment Diagram** (FAD), and one such diagram is shown in **Figure A.3.3**. Here, the ordinate is K_r, a dimensionless ratio of the crack driving force to the material's fracture toughness. Clearly if this ratio is greater than 1, failure by unstable fracture becomes inevitable. Similarly, the abscissa in the figure is S_r, a dimensionless ratio of the net section stress (σ_n) to the material's flow strength (σ_f). The net section stress takes into account the fact that the ligament ahead of a crack tip is subjected to a greater stress

than the calculated stress in the absence of the crack. In the case of the flat plate containing a through thickness crack as shown in Figure A.3.2,

$$\sigma_n = \sigma_{app} / (1-a/b) \qquad\qquad [A.3.4]$$
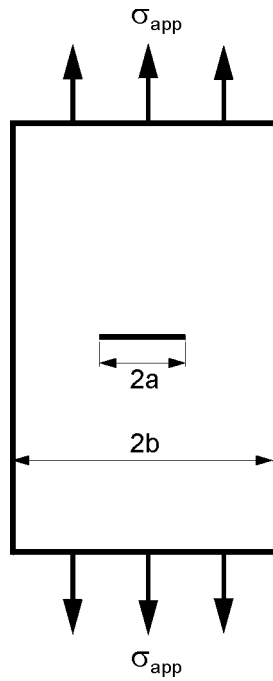
Figure A.3.2: Finite-Width Plate Containing a Through-Thickness Crack
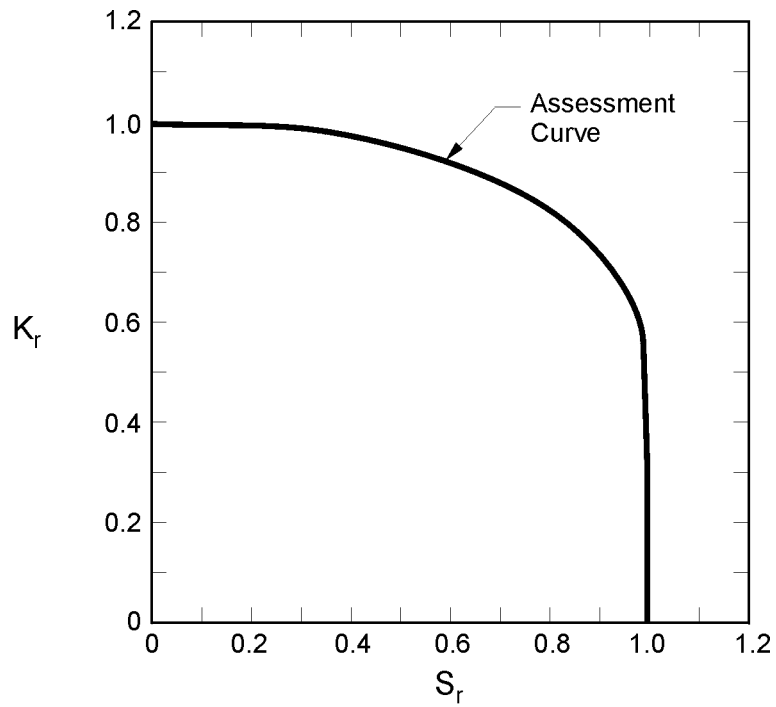
**Figure A.3.3: Failure Assessment Diagram Based on
Strip Yield Model**

The flow strength of the material where the crack tip resides is a function of the material's yield and ultimate tensile strengths, and its calculation is discussed further in Section B.3. (Some FADs use the ratio L_r as the abscissa, where $L_r = \sigma_{app}/\sigma_y$).

As was the case with K_r, when S_r exceeds 1, i.e., σ_n exceeds σ_f, failure is assumed to occur by plastic collapse. Based on the above considerations, the Failure Assessment Diagram would be a square bounded two perpendicular lines at $K_r = S_r = 1$. However, that is true only for materials displaying perfect linear elastic behaviour. Since in most practical cases, there is some plasticity at the crack tip, the locus of the critical conditions deviates from the square and assumes a curve shape.

The concept, selection and use of the Failure Assessment Diagrams are explained further in Part C. Suffice it to add at this point that, if the assessment point for a structural member containing a crack lies within the FAD locus, then the structural member is considered safe; conversely, if the assessment point lies outside the FAD, the structure is unsafe.

Considering next the case of structures subject to cyclic loads, the driving force for failure by fatigue, in the absence of cracks, is the stress *range*. Similarly, in the presence of cracks, the driving force for fatigue crack growth is the stress intensity factor range, ΔK_{app}. Following Equation A.3.2, ΔK can be estimated from Equation [A.3.5]:

$$\Delta K_{app} = Y. \, \Delta\sigma_{app} \, . \, \sqrt{(\pi a)} \qquad\qquad [A.3.5]$$

Once the driving force for fatigue crack growth has been estimated, the actual crack growth rate, da/dN, is estimated from the experimentally established crack growth behaviour of the material of interest. For structural steels and weldments, this behaviour is represented on a log-log plot of crack growth rate (da/dN) versus the stress intensity factor range, ΔK_{app}. As seen in **Figure A.3.4**, this curve has a sigmoidal shape. For most structures, the middle linear region (region II) is of greatest interest. Here, the linear dependence between da/dN and ΔK_{app} can be expressed by the so-called Paris relationship:

$$da/dN = C.(\Delta K_{app})^m \qquad\qquad [A.3.6]$$

where C and m are experimentally determined constants and depend on the test environment. In region I, the fatigue crack growth rate decreases rapidly with stress intensity factor range such that below a threshold value, ΔK_{th}, the cracks can be considered as non-propagating. Conversely, in region III, the crack growth rate is very high and failure becomes imminent

These concepts have been introduced here to allow a better understanding of the whole process. These and other damage tolerance matters will be covered in detail later in this Guide.
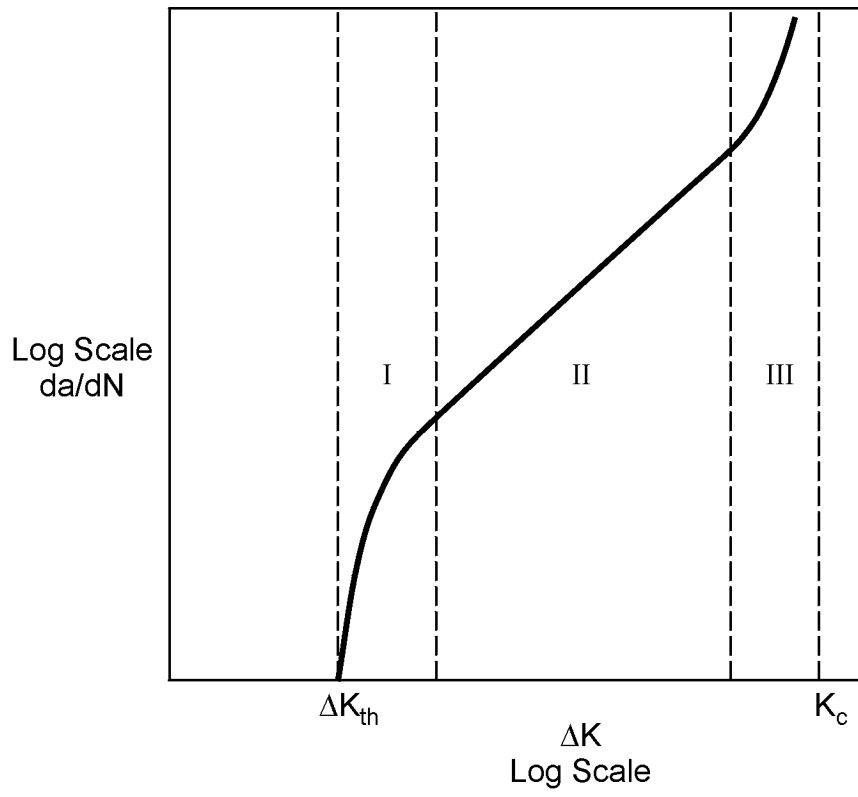
Figure A.3.4: Basic Regions of da/dN vs. ΔK curve

A.4   SCOPE OF THE GUIDE

A.4.1   Layout of the Guide

The guide is organised into four alphabetically identified parts (A, B, C and D) with the first part, Part A, being an introduction reviewing the essential elements of damage tolerance assessment and identifying its potential applications to ship structures. Part B describes the input data and procedures used to develop the fracture mechanics based-damage tolerance assessment. The data development processes include those associated with the applied load statistical distributions, structural stress analysis procedures and material properties. The procedures for developing the damage tolerance analysis input data are described in terms of a level 2 (analytic/empirical equation approach) and a level 3 (first principles/spectral approach) as in the Fatigue Design Guide. The fracture mechanics-based fatigue crack growth and residual strength calculations are described in Section C. The fourth part of this guide, Part D, provides worked examples of damage tolerance analysis applied to ship structural details. References are provided at the end of each section.

In general, a damage tolerance analysis seeks to estimate the safe operational life of a structure containing a flaw. A simplified description of the damage tolerance analysis process is presented in Figure A.4.1b. This process starts with a structure containing a flaw. The loads applied to the structure may be estimated and the response of the structure calculated. This information along with material property data may be used to determine if the residual strength of the structure is sufficient to support the applied loading. If not, the structure fails by fracture or plastic collapse. If the residual strength is sufficient to support the applied load, then the applied load cycle is considered to extend the flaw through a fatigue crack growth mechanism after which the analysis process may be repeated until the residual strength is insufficient to support the applied load and failure occurs.

Figure A.4.1b relates the damage tolerance analysis process to the information presented in this guide by identifying each step in the analysis process to the section in which it is presented by including the section umber in brackets. The figure is subdivided to distinguish input data from the damage tolerance assessment proper.

A.4.2   Relationship to the Fatigue Resistant Detail Design Guide

Since the fatigue design process outlined in the Fatigue Resistant Detail Design Guide for Ship Structures [A.31] provides a structural design process which only considers one limit state, fatigue damage accumulation to initiation, the design process is relatively straight forward. The damage tolerance analysis process, however, considers fatigue crack growth as a mode of degradation leading to two potential limit states (modes of failure), namely fracture or plastic collapse. Therefore, the damage tolerance assessment approach involves both fatigue crack growth due to cyclic load application and limit state evaluations based on a failure assessment diagram (FAD) approach.

a) Fatigue Design Process

Fatigue Design Process

1) Environment and Operational
   Data   [C.3]
2) Statistical Load Analysis   [C.3]

3) Nominal (Global) Stress
   Analysis   [C.4]
4) Local Stress (Stress
   Concentration) Analysis   [C.4]

5) Hot Spot Stresses   [C.5]
6) Short and Long Term Stress
   Range Distributions   [C.5]

7) Fatigue (S-N) Damage
   Summation   [C.6]
8) Reliability / Limit State Analysis[C

b) Damage Tolerance Analysis Process

Damage Tolerance Analysis Data

Flaw Size   [C.2.6]

Applied Loads
(Range and Extreme)   [B.2]

Structural Response
(Stress Analysis)   [B.3]

Env. Data   [B.2]
Vessel Data:
 - Operational   [B.2]
 - Structural   [B.2]
 - Material   [B.2]

Damage Tolerance Assessment

Residual Strength
(Fracture / Plastic
Collapse -FAD)   [C.1]

No Failure   Failure

Fatigue Crack Growth
(Update flaw size)   [C.2]

Service life estimate
based on number of
load cycles

a) Fatigue Design Process

b) Damage Tolerance Analysis Process

Figure A.4.1 presents side-by-side the fatigue design and damage tolerance analysis processes in flow chart form. Each step in each of the analytic processes are referenced back to the sections in each of the guide documents ("Fatigue Resistant Detail Design Guide" and "Damage Tolerance Analysis Guide"). Double-headed arrows are used in the figure to identify the related analytic process steps in the two guides.

In Figure A.4.1a, the appropriate section for the "Fatigue Guide" [A.31] are annotated in parenthesis, as they are in Figure A.4.1b for this Guide.

Topics that are covered by this Guide are the subject of on-going research. Although the procedures presented in this Guide are based on the current state of technology, a number of simplifications have been made to ensure that the guide is practical and accessible to a broad range of users. Where uncertainties exist, conservative assumptions have been made to ensure that a working guide is available now.

It is assumed that users of this Guide will properly document their damage tolerance assessments and provide sufficient analysis or correlation against test data to assure that their assessments are conservative.

This Guide is not intended to replace normal design procedures when such procedures are applicable. For example, it is not intended to circumvent the normal requirements for good workmanship.

A.5 REFERENCES

[A.1] Reemsnyder, H., "Fatigue and Fracture of Ship Structures", Proc. of Symposium and Workshop on the Prevention of Fracture in Ship Structure, March 30-31, 1995, Washington, D.C.

[A.2] Harris, D.O., "Fatigue and Fracture Control in the Aerospace and Power Generation Industries", Proc. of Symposium and Workshop on the Prevention of Fracture in Ship Structure, March 30-31, 1995, Washington, D.C.

[A.3] "The Revisions to the Structural Integrity Assessment Method CEGB/R6", Theme Issue, Vol. 32, Int. Journal of Pressure Vessels and Piping, 1988.

[A.4] Wood, H.A., "Application of Fracture Mechanics to Aircraft Structural Integrity", Journal of Engineering Fracture Mechanics, Vol. 432, 1975.

[A.5] Anderson, T.L., " US Fracture Mechanics Methodologies For Welded Structures", IIW Doc. X-1315-95.

[A.6] Phaal, R., Challenger, N.V., Maddox, S.J., and Garwood, S.J., "Current Status of Revisions to PD6493 - Assessment Procedures For Fusion Welded Structures", IIW Doc. 1314-95.

[A.7] Cramer, E.H., Schulte-Strauthaus, R., and Bea, R.G., "Structural Maintenance Project Volume 1: Fatigue Damage Evaluation", SSC Report 386, Ship Structure Committee, 1995.

[A.8] Ghose, D.J., Nappi, N.S., and Wiernicki, C.J., "Residual Strength of Damaged Marine Structures", SSC Report 381, Ship Structure Committee, 1995.

[A.9] Munse, W.H., Wilbur, T.W., Tellalian, M.L., Nicoll, K., and Wilson, K., "Fatigue Characterization of Fabricated Ship Details for Design", SSC Report 318, Ship Structure Committee, 1982.

[A.10] Bea, R.G., "Marine Structural Integrity Programs", SSC Report 365, Ship Structure Committee, 1991.

[A.11] Lloyd's Register, "Bulk Carriers: Seeking Solutions to the Safety Problem", 100A1, Issue 3, 1991, Lloyd's Register.

[A.12] Cramer, E., Gran, S., Holtsmark, G., Lotsberg, I., Loseth, R., Olaisen, K., and Valsgard, S., "Fatigue Assessment of Ship Structures", DNVC Report No. 93-0432, 1994.

[A.13] Witmer, D.J. and Lewis, J.W., "Operational and Scientific Hull Structure Monitoring on TAPS Trade Tankers"; SNAME Annual meeting Nov. 17-18, 1994, New Orleans.

[A.14] Liu, D. and Thayamballi, A., "Local Cracking in Ships - Causes, Consequences, and Control", Proc. of Symposium on the Prevention of Fracture in Ship Structure, March 30-31, 1995, Washington, D.C.

[A.15] Skaar, K.T., Valsgard, S., Kohler, P.E., and Murer, C, "How Low Can Steel Weight Go With Safety and Economy?", Proc. Third Int. Conf. on "Practical Design of Ships and Mobile Offshore Units", PRADS'87, Trondheim, Norway, June 22-26, 1987.

[A.16] Lloyd's Register, "HTS - Something for Nothing?", 100A1, Issue 3, 1992.

[A.17] Lloyd's Register, "Ship Right - Fatigue Design Assessment Procedure", 1996.

[A.18] American Bureau of Shipping, "Guide for the Fatigue Strength Assessment of Tankers", June 1992.

[A.19] U.K Department of Energy, "Offshore Installations: Guidance on Design and Construction", HMSO, London, April, 1984.

[A.20] British Standards Institution, "Code of Practice for Fatigue", BS 5400: Part 10, 1980.

[A.21] British Standards Institution, "Code of Practice for Fatigue Design and Assessment of Steel Structures", BS 7608, 1993.

[A.22] Swift, T., "Damage Tolerance Assessment of Commercial Airframes", Fracture Problems in Transportation.

[A.23] Goranson, U.G., "Elements of Structural Integrity Assurance", Journal of Fatigue, Vol. 16, No. 1, 1994,

[A.24] Joint Airworthiness Requirements (JAR), " Interpretative Manual on the Substantiation of Fatigue life Behaviour of Aircraft Structures", Issue 2, November, 1976.

[A.25] Airworthiness Notice No. 89, " Continuing Structural Integrity of Transport Aeroplanes", Civil Aviation Authority, United Kingdom, 23 August, 1978.

[A.26] Airworthiness Information Leaflet AD/IL/0067/1-5, " Continuing Structural Integrity of Transport Aeroplanes", Civil Aviation Authority, United Kingdom,   18 August, 1978.

[A.27] Federal Aviation Regulations Part 25, " Airworthiness Standards: Transport Category Airplanes", Para 571, Damage Tolerance and Fatigue Evaluation of Structure.

[A.28] Federal Aviation Administration Advisory Circular 25-571-1, "Damage Tolerance and Fatigue Evaluation of Structure", Sept. 28, 1978.

[A.29] Canadian Standards Association, "Gas Pipeline Systems, Appendix J: Recommended Practice for Determining the Acceptability of Imperfections in Pipelines Using Engineering Critical Assessment", CAN/CSA-Z184-M86, 1986.

[A.30] American Society of Mechanical Engineers, "ASME Boiler and Pressure Vessel Code", Section XI, Rules for In-service Inspection of Nuclear Plant Components, NewYork, 1989.

[A.31] Glen, I.F., Paterson, R.B., Luznik, L., Dinovitzer, A., Bayley, C., "Fatigue–Resistant Detail Design Guide for Ship Structures", SSC Report 405, Ship Structure Report, 1999

[A.32] DesRochers, C., Crocker, J., Kumar, R., Brennan, D., Dick, B., and Lantos, S., "Post-Yield Strength of Icebreaking Ship Structural Members", SSC Report 384, Ship Structure Committee, 1995.

[A.33] St. John, J. and Minnick, P., "Ice Load Impact Study on the NSF R/V Nathanial B. Palmer",SSC Report 376, Ship Structure Committee, 1995.

[A.34] Hughes, O., Nikolaidis, E., Ayyub, B., White, G., and Hess, P., "Uncertainty in Strength Models for Marine Structures", SSC Report 375, Ship Structure Committee, 1994.

[A.35] Jennings, E., Grubbs, K., Zanis, C., and Raymond, L., "Inelastic Deformation of Plate Panels", SSC Report 364, Ship Structure Committee, 1991.

[A.36] Stambaugh, K. and Knecht, J.C., "Corrosion Experience Data Requirements", SSC Report 348, Ship Structure Committee, 1988.

PART B   DETERMINING INPUTS TO DAMAGE TOLERANCE ANALYSIS

B.1   INTRODUCTION

As discussed in Section A.3.2, key elements of damage tolerance assessment are the estimation of fatigue crack growth rate and the residual strength of a damaged structure at a particular point in time - that is the load carrying capacity of the structure in the presence of a crack (or flaw) of known size.

The procedure for performing these calculations are detailed in Part C but may be summarised as a number of steps which have to be performed – not necessarily in sequence, and which, for the design process, are:

1. **Determine the loads acting and the magnitude of applied/service stresses and residual stresses**: These comprise sea loads as well as local loads (e.g., cargo, helicopter landing), as well as stresses built into the structure during fabrication.

2. **Calculate driving force parameters (K_{app}, ΔK_{app} and σ_n)**.

3. **Establish material properties (resistance parameters)**. The material properties of interest are the yield strength, tensile strength, fracture toughness of the material where the flaw resides (K_{mat}), and values for the constants c and m in the Paris relationship.

4. **Determine the flaw size**. This may be already known from inspection reports for evaluating a current flaw. However, if the assessment is for some point in time in the future, then its determination will take into account a flaw's growth under cyclic loading.

5. **Select Failure Assessment Diagram (FAD) for residual strength assessment.**

6. **Perform residual strength assessment**. Calculate K_r and S_r.

7. **Perform crack growth analysis.**

Steps 1 to 4 comprise the *input* to the damage tolerance analysis and are covered in Part B. Steps 5 to 7 comprise the actual damage tolerance analysis and are covered in Part C.

As mentioned earlier, the above steps provide a procedure suitable for "fitness for purpose" analysis, for example at the design stage (all parameters known). If a critical condition corresponding to the failure assessment curve is to be determined, then an iterative procedure will need to be used since one parameter is unknown. This is addressed later.

B.2   LOAD ESTIMATION

B.2.1 Scope of Load Estimation

This section provides guidelines for determining the fatigue loading that a ship structure will experience during a particular period of interest. In the context of a damage tolerance assessment, this period may vary from a few days, up to the life of the ship. Within this period, estimates of the extreme loads as well as the long- term statistical distribution of load ranges are required for an assessment.

It is assumed, as elsewhere herein, that this Guide is being used by a qualified and practicing ship designer or structural engineer, and therefore this Guide does not provide comprehensive direction on how to determine the loads on a ship structure. Rather, it provides guidance on how the loading is estimated for the damage assessment problem.

The ship designer is assumed to be already working with loads to determine the vessel's design strength, and size, the structural elements and scantlings, and with knowledge of the operational area and possibly the operating profile for the vessel. This Guide will show how the information needs to be formulated and used for damage assessment.

The loading imposed on ships depends on several parameters, many of which are highly variable. The dominant load on ships arises from waves, the computation of which is problematic. Apart from the randomness associated with the engineering parameters that determine loading, particularly parameters that derive from climatic phenomena, additional parameters associated with the way operators of ships respond to extreme weather have to be quantified either explicitly or implicitly.

While wave loads are the predominant load effect experienced by ships, any loading that can result in significant stress levels are potentially relevant for damage tolerance assessment. Nevertheless, certain cyclic load types are ignored in this study. Vibration loads are not considered since they tend to be local and generally do not impact the structural integrity of the hull. Also ignored are thermal loads that are difficult to quantify and model. Thermal loads also cycle very slowly and hence their contribution to calculated fatigue damage by linear damage summation is generally small. This observation also applies to the still water bending moment. However, when these loads are superimposed on wave loads, significant interaction effects on crack growth are possible.

Waves may impose loads in several different ways. The primary mechanism is through hull girder bending. The loading is cyclic with periods of the order of several seconds. In severe sea states, phenomena such as slamming may occur which result in transient impact loads; the response to this type of load is characterized by frequencies that are considerably higher than those associated with normal wave loading. Waves may also impose significant loads on a more local scale.

The primary examples include dynamic pressure loads near the waterline, and ship motion, which cause acceleration forces on liquid or solid cargoes and other masses.

The direct calculation of loads on ships requires consideration of a large number of relevant parameters, many of which are highly variable. The primary source of this variability is the environment, and virtually all environmental phenomena are random in character. In addition, the response of ships to waves is a complex fluid-structure interaction problem that is very difficult to model. While methodologies have been developed for this purpose and have met with a measure of success in terms of predicting response with sufficient accuracy for engineering purposes, such methodologies rely on a considerable degree of skill and require sophisticated software tools.

In this context, direct load calculation methods may not always be appropriate. In circumstances where resources are unavailable and/or data is limited, for example, in the early stages of design, simpler, less rigorous, methods are more appropriate.

Guidelines for two methods of load computation with varying degrees of complexity are presented herein. The methods presented are believed to represent the best currently available in terms of accuracy, practicality and cost effectiveness.

These methods are termed Levels 2 and 3 in order of increasing sophistication. Note that the (Load Analysis) "Levels" defined herein correspond to those defined in the companion "Fatigue Design Guide" [Ref. B.1]. Level 1 fatigue design approach was defined therein as applying good design practice against premature fatigue failure by selecting/designing structural details with improved fatigue resistant geometry from a catalogue of details provided in the referenced Fatigue Design Guide. This Load Analysis Level 1 procedure is not included herein. The Level 2 procedure relies heavily on parametric equations, while Level 3 uses the long-term load estimation method. In both the Level 2 and Level 3 approaches described herein, there are alternative methods, depending on the goals, available data, etc.

B.2.2 Definition of Loads

For damage tolerance analysis, loads must be defined in terms that allow derivation of *loads ranges* that will be converted to *stress ranges* based on structural analysis. This may require definition of a load component in hog and sag, or as maximum compressive and tensile load, so that a *range* can be defined. As for overall ship design, loads can be categorized as *global* or *local*. Reviewing these , the important global loads include:

a)   still water loads;
b)   wave loads;
         - low frequency steady-state, response largely rigid-body;
         - high frequency transient (wave impact or slamming), response largely elastic;
         - high frequency steady-state (springing), response largely elastic;

while the main local loads include:

c) hydrostatic pressure loads;
d) pressure loads due to waves, as in b)
e) inertia loads from cargo or fluids (Sloshing) induced by ship motion;
f) functional loads, from machinery and deck equipment;
g) ice loads.

For a further discussion of these load components, see Reference B.1, Section C.

The relative significance of each type of load depends, among other things, upon the ship
type, the payload, structural configuration and location of structure. **Tables B.2.1** to **B.2.5**
[Ref. B.2] provide guidance in identifying the important loads for a selection of ship types.
Additional discussion on the subject is provided in Reference B.3.

B.2.3 Load Estimation Methods

Loads can be determined by calculation, or estimated from full-scale or model-scale tests. In
the context of damage tolerance assessment, the most practicable method is through
calculation. Data gathered in full-scale or model-scale tests are, of course, very useful.
However, in the present context, their value is greatest when used for calibrating and
validating methods for establishing loads based on calculation. Methods for estimating loads
on ships range from simple algebraic expressions to sophisticated analytical approaches that
require computer programs to yield results.

In engineering, it is generally assumed that the accuracy to which a parameter is estimated is
related to the degree of sophistication of the model used to make the prediction. It is
reasonable to suppose that the same applies to ship loading models. In engineering, it is quite
common to select a model, and there may be several potential choices to suit the application.
The engineer implicitly acknowledges that the uncertainty in the result calculated using a
simple rule-of-thumb is probably greater than that computed using a more complex
methodology based on first principles. These approaches are equally valuable depending on
the purpose of the analysis, and depending on the stage of the life cycle of the ship. Early in
design, for example, when the design parameters are not well established, detailed methods
are not justified.

Methods for damage tolerance assessment at different levels of complexity are presented in
this document. It is intended that the appropriate level be selected on the basis of the quality
and detail of the information available, and the accuracy of the assessment required. It is, of
course possible, and perhaps desirable in some circumstances, to use methods of different
levels of complexity at different stages of the analysis. Generally, however, it is most cost-
effective if the levels of accuracy for each stage are broadly consistent throughout the analysis.

Table B.2.1: Highly Loaded Structural Elements - Tankers

STRUCTURE MEMBER	STRUCTURAL DETAIL	LOAD TYPE
Side-, bottom- and deck plating and longitudinals	Butt joints, deck openings and attachment to transverse webs, transverse bulkheads, hooper knuckles and intermediate longitudinal girders	Hull girder bending, stiffener lateral pressure load and support deformation
Transverse girder and stringer structures	Bracket toes, girder flange butt joint, curved girder flanges, knuckle of inner bottom and sloped hooper side and other panel knuckles including intersecting transverse girder webs, etc. Single lug slots for panel stiffeners, access and lightening holes	Sea pressure load combined with cargo or ballast pressure load
Longitudinal girders of deck and bottom structure	Bracket terminations of abutting transverse members (girders, stiffeners)	Hull girder bending, and bending/deformation of longitudinal girder and considered abutting member

Table B.2.2: Highly Loaded Structural Elements - Bulk Carriers

STRUCTURE MEMBER	STRUCTURAL DETAIL	LOAD TYPE
Hatch corners	Hatch corner	Hull girder bending, hull girder torsional deformation
Hatch side coaming	Termination of end bracket	Hull girder bending
Main frames	End bracket terminations, weld main frame web to shell for un-symmetrical main frame profiles	External pressure load, ballast pressure load as applicable
Longitudinals of hopper tank and top wing tank	Connection to transverse webs and bulkheads	Hull girder bending, sea- and ballast pressure load
Double bottom longitudinals [1]	Connection to transverse webs and bulkheads	Hull girder bending stress, double bottom bending stress and sea-, cargo- and ballast pressure load
Transverse webs of double bottom, hopper and top wing tank	Slots for panel stiffener including stiffener connection members, knuckle of inner bottom and sloped hopper side including intersection with girder webs (floors). Single lug slots for panel stiffeners, access and lightening holes	Girder shear force, and bending moment, support force from panel stiffener due to sea-, cargo and ballast pressure load

(1) The fatigue life of bottom and inner bottom longitudinals of bulk carriers is related to the combined effect of axial stress due to hull girder- and double bottom bending, and due to lateral pressure load from sea or cargo.

Table B.2.3: Highly Loaded Structural Elements - Ore Carriers

HULL MEMBER	STRUCTURAL DETAIL	LOAD TYPE
Upper deck plating	Hatch corners and side coaming terminations	Hull girder bending
Side-, bottom- and deck longitudinals	Butt joints and attachment to transverse webs, transverse bulkheads, hatch openings corners and intermediate longitudinal girder	Hull girder being, stiffener lateral pressure load and support deformation
Transverse girder and stringe structures	Bracket toes, girder flange butt join curved girder flanges, panel knuckl at intersection with transverse girde webs, etc. Single lug slots for pane stiffeners, access and lightening hol	Sea pressure load combined with cargo or ballast pressure
Transverse girders of wing tank [1]	Single lug slots for panel stiffeners	Sea pressure load (in particular in ore loading condition)
(1) The transverse deck-, side- and bottom girders of the wing tanks in the ore loading condition a generally subjected to considerable dynamic shear force- and bending moment loads due to large dynamic sea pressure (in rolling) and an increased vertical racking deflection of the transverse bulkheads of the wing tank. The rolling induced sea pressure loads in the ore loadii condition will normally exceed the level in the ballast (and a possible oil cargo) condition due the combined effect of a large GM-value and a small rolling period. The fatigue life evaluatio must be considered with respect to the category of the wing tank considered (cargo oil tank, ballast tank or void). For ore-oil carriers, the cargo oil loading condition should be considered as for tankers.		

Table B.2.4: Highly Loaded Structural Elements - Container Carriers

HULL MEMBER	STRUCTURAL DETAIL	LOAD TYPE
Side- and bottom longitudina	Butt joints and attachment to transverse webs, transverse bulkhea and intermediate longitudinal girder	Hull girder bending, torsion [1], stiffener lateral pressure load and support deformation
Upper deck	Plate and stiffener butt joints, hatch corner curvatures and support detai welding on upper deck for containe pedestals, etc.	Hull girder bending- and torsiona warping stress [2]
(1) Torsion induced warping stresses in the bilge region may be of significance from the forward machinery bulkhead tot he forward quarter length.		
(2) The fatigue assessment of upper deck structures must include the combined effect of vertical and horizontal hull girder bending and the torsional warping response. For hatch covers, additional stresses introduced by the bending of transverse (and longitudinal) deck structures induced by the torsional hull girder deformation must be included in the fatigue assessment.		

Table B.2.5: Highly Loaded Structural Elements - Roll on/Roll off and Car Carriers

HULL MEMBER	STRUCTURAL DETAIL	LOAD TYPE
Side- and bottom longitudinal	Butt joints and attachment to transverse webs, transverse bulkheads and intermediate longitudinal girders	Hull girder bending, stiffener lateral pressure load and support deformation
Racking constraining girders, bulkheads, etc.	Stress concentration points at girder supports and at bulkhead openings	Transverse acceleration load [1]
(1) It should be noted that the racking constraining girders and bulkheads are in many cases largely unstressed when the ship is in the upright condition. Thus the racking induced stresses may be entirely dynamic, which implies that fatigue is likely to be the primary design criterion. For designs which incorporate "racking bulkheads", the racking deformations are normally reduced such that the fatigue assessment may be limited to stress concentration areas at openings of the racking bulkheads only. If sufficient racking bulkheads are not fitted, racking deformations will be greatly increased, and the fatigue assessment of racking induced stresses should be carried out for primary racking constraining members and vertical girder structures over the ship length as applicable.		

Two sets of load data are required for damage tolerance assessment:

- extreme load;
- load (stress) range spectrum.

The importance of assessing both can be illustrated by considering the behaviour of a structure with a crack. The structure starts life with a certain design strength, which degrades with time as the crack grows under the action of cyclic loads; this crack growth can only be estimated with knowledge of the stress range spectrum the structure is subjected to. The structure may degrade to the point where the residual strength is so low that any large (extreme) load will cause the structure to fail; the process is illustrated in **Figure B.2.1**, taken from Reference B.4. In order to be able to assess the risk of the structure failing during a given period of time an estimate of both extreme load and the stress range are required.

Direct methods of wave load estimation are usually categorized as follows:

- short-term estimation;
- long-term estimation.

Both methods, in principle, can yield estimates of extreme load for arbitrary periods of time, a key requirement for damage tolerance assessment. However, of the two, only the long-term method can generate load (stress) range spectra required for crack growth calculation. The short-term method seeks to establish the extreme wave height that will be encountered during the period of interest. This wave height is then used to compute the extreme load. The implicit assumption is that the highest wave height yields the highest load effect. This is not always the case.

A brief description of the long-term methods follows as the methods most suitable for damage tolerance assessment. Level 2 and Level 3 long-term approaches are introduced in Sections B.2.3.1 and B.2.3.2, respectively. This is followed by a more detailed description of each in the subsequent sections.
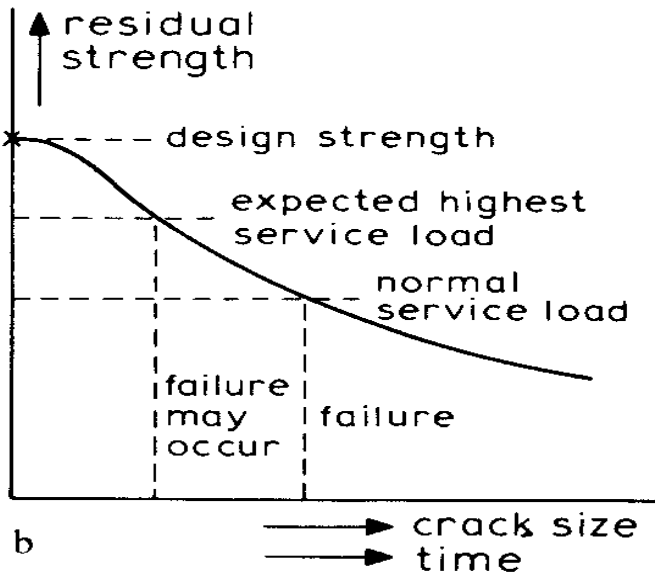
Figure B.2.1: Degradation of Structure with Time

B.2.3.1   Approximate Methods of "long-term" Wave Load Estimation (Level 2 Assessment)

The application of the long-term method requires the gathering of a large amount of input data and the use of advanced software tools. This level of effort may not be possible, or even appropriate. An "engineering" alternative is to use parametric equations that yield the load quantities required for damage tolerance assessment. Parametric equations are often based on the fitting of results from calculations, model tests, and full scale measurements. The results can only be representative of the ship configuration from which the results are obtained and, hence, cannot be generally applicable. It is important to be aware of the limitations; discussion in this regard is contained in Section B.2.6 where three methods based on parametric equations are presented.

B.2.3.2   Direct Methods of "long-term" Wave Load Estimation (Level 3 Assessment)

The long-term method takes advantage of the results of random vibration theory. The main advantage is that the characteristics of the output (response) can be computed very simply when certain requirements in regard to the dynamical system (ship) and the statistical nature of the input (load) are met. The key requirements are that the system is linear and that the input process is statistically ergodic and stationary. Once this assumption is made the responses from different sea conditions, which individually satisfy the requirement of stationarity and ergodicity, can be superimposed to yield an estimate of overall response. Combining this process with certain statistical techniques will yield both an estimate of extreme load and stress range spectrum.

Certain simplifying assumptions are necessary in applying the methodology outlined above. The limitations associated with these assumptions are discussed in Section B.2.7.

B.2.3.3   Probability Level for Extreme Loads

The wave loads ships experiences are highly variable. This is because wave loads result from climatic phenomena that can only be expressed quantitatively in statistical terms. Furthermore, the load levels ships experiences also depend on the behaviour of the operator that is also a variable quantity. Hence, wave loads can only be expressed as probabilistic values. While the damage tolerance assessment approach presented in this document in not formally cast in probabilistic terms, it is necessary to be aware of the probability levels inherent in the guidance.

The statistics of loads from environmental sources are often expressed in terms of the "return period". The return period is the average time between two successive statistically independent events. Hence a particular significant wave height, $\mathbf{H_s}$, with a return period of 50 years means that H_s will be exceeded, on average, once every 50 years. It can be shown that the probability of a particular parameter with a return period of $\mathbf{T}$ years occurring in a period of T years is almost two-thirds. Hence, in the design of structures such as offshore platforms and civil engineering structures, the practice is to design for environmental loads which have a return period considerably in excess of the design life of the structure.

Ochi [Ref. B.5] developed the concept of a "risk parameter" as a means for specifying a lower probability of occurrence of response consistent with design practice. The value of the risk parameter is the probability that a certain extreme load will be exceeded during the period of interest. Reference B.5 recommends a value of 0.01 that is generally consistent with current design practice for marine vehicles. This approximately amounts to increasing the time period to which the structure is exposed, by a factor of 1/0.01, or 100 for design purposes.   This value of 0.01 appears to be broadly consistent with the design of large steel structures in general.

This value is adopted for present purposes. Where possible, a risk parameter of 0.01 is applied in specifying the extreme load. In other words, the extreme load in question has a 0.01 probability of occurring in the duration of assessment. In one case, a Level 2 method, it was not possible to systematically apply this risk level; and this is discussed at the appropriate point.

B.2.4 Load Estimation - Level 3

The overall procedure for Level 3 is illustrated in **Figure B.2.2**. The Level 3 method is a direct calculation method of wave load estimation, sometimes known as the "spectral method". The procedure starts with the definition of the operational profile leading to the encounter conditions between ship and waves.

B.2.4.1   Definition of Operational Profile

In the Level 3 - Direct Calculation method, the loads are determined from a detailed knowledge of the ship's operational profile. In using direct methods for calculating extreme loads, considerable simplifications of the operational profile are usually accepted. For damage assessment calculations, it may be necessary to examine the data in more detail to ensure a reasonably accurate representation of load spectrum shape.

The operational profile information required for a detailed calculation includes:

- The projected route of the vessel described in terms of ocean areas of operation and the % time spent in these areas;

- Vessel loading conditions or missions and relative time spent in each mode; (loading conditions are appropriate for commercial vessels, while the mission may be more appropriate for military or patrol vessels);

- Distribution of time spent at each heading relative to the predominant sea direction;

- Vessel average speed ranges and relative amount of time spent at each speed in a particular sea state or wave height.

In addition, it is necessary to specify the parts of the structure which are to be subjected to the damage tolerance assessment.

In order to make the calculations feasible, each of the parameters is discretized in some manner. For example, the route can be divided into Marsden Zones [Ref. B.6] (or zones of latitude and longitude transited by the vessel) and the time spent in these zones. Loading can be treated in terms of standard conditions. Relative heading can be simplified into head, bow, beam, quartering, and following seas; and speed can be treated as sets of speed ranges.

```
                    ┌─────────────────────┐
                    │   Define Problem    │
                    └─────────────────────┘
                              │
                              ▼
                    ┌─────────────────────┐
                    │ Define Operational Profiles │────────┐
                    │ Based on Mission or │               │
                    │ Loading Conditions  │               │
                    └─────────────────────┘               │
                              │                            │
                              ▼                            │
                    ┌─────────────────────┐               │
                    │ Obtain Wave Climatic Data │          │
                    └─────────────────────┘               │
              ┌───────────────┴───────────────┐           │
              ▼                                ▼           │
    ┌─────────────────────┐         ┌─────────────────────┐│
    │ Calculate Composite │         │ Select Wave Spectra ││
    │ Scatter Diagram     │         └─────────────────────┘│
    └─────────────────────┘                   │            │
              │                                │            │
              ▼                                │            │
    ┌─────────────────────┐                   │            │
    │ Calculate Speed/Heading │◄──────────────┘            │
    │ Probabilities       │                                │
    └─────────────────────┘                                │
              │                                             │
              ▼                                             │
    ┌─────────────────────┐                                │
    │ Calculate Response for │                              │
    │ Each Combination of │                                 │
    │ Speed and Heading   │                                 │
    └─────────────────────┘                                 │
              │                                             │
              ▼                                             │
    ┌─────────────────────┐                                │
    │ Compile Load-Range  │                                 │
    │ Spectrum            │                                 │
    └─────────────────────┘                                 │
              │                                             │
              ▼                                             │
    ┌─────────────────────┐                                │
    │ Obtain Total Load-Range │                            │
    │ Spectrum for Operational │                           │
    │ Profile             │                                 │
    └─────────────────────┘                                 │
              │                                             │
              ▼                                             │
    ┌─────────────────────┐                                │
    │ Compile LIFETIME    │◄───────────────────────────────┘
    │ Load-Range Spectrum │
    └─────────────────────┘
```

Loop over operational profile *Loop over period* *Loop over sea state*

Figure B.2.2: Schematic of Level 3 – Direct Calculation Method

For vessels with significantly varying loading conditions, it is necessary to determine the percentage of time in loaded and ballasted conditions. This applies particularly to tankers, container vessels, and bulk carriers. [If specific data is not available, data presented in Section F.3 of Appendix F can be used.]

When a new design will follow the same operational profile as an existing ship, the existing ship's operations may be studied and characterized from operational logs, [e.g., Ref. B.7]. For new designs, operational profiles can be generated from the operators' plans. The level of discretization of operational and/or environmental data should correspond to the certainty in the operational profile information.

The process of developing a detailed operational profile requires the development of input joint probability tables. These include ship speed versus sea state (or wave height) and then ship relative heading versus sea state (or wave height). These are obtained either from historical data or from operating directions for the vessels (particularly speed in given sea states).

When an operational profile is developed in the absence of historical data, speed, sea state (or wave height) and heading are often assumed to be independent quantities. This may not always be the case, as in severe sea states, the practice is to reduce speed and to orient the ship in preferred directions. However, since the bulk of damage arises from the exposure to moderate conditions, and because the amount of time spent in these severe sea sates is not as significant as that spent in more moderate conditions, the assumption of independence is reasonable, and avoids extremely complex computations that are not justified. When the profile is developed from existing ships logs, it will obviously reflect current practice, which may or may not be modified by other features of the new design.

The next data set required is the distribution of time spent in each geographical area. In order to construct the lifetime operational profile, time spent in port should also be included. A ship that spends 50% of its time alongside will obviously see fewer wave encounters per year than one that is more or less continuously at sea.

These three distributions (speed vs. sea state (or wave height), relative heading vs. sea state (or wave height) and time spent in geographical areas) are combined with the wave data into a probability table of simultaneous occurrence of speed, heading, and sea state for the specific profile. If the operational profile was developed on the basis of wave height (instead of sea state), then, in addition to the speed, relative heading and wave height, wave period represents additional parameter in definition of probability table. The process for producing this final probability table is described in the following sections. Reference B.1 provides a somewhat more comprehensive discussion of this process.

B.2.4.2   Definition of Wave Climate

B.2.4.2.1   Sources of Wave Climate Data

The wave climate experienced by ships varies considerably depending on the area of operation. Wave data is available for most parts of the world including oceans and large bodies of water such as the Great Lakes. Perhaps the most comprehensive compilation of wave data is published by British Maritime Technology [Ref. B.6]. References B.8 and B.9 provide other compilations, and regional wave data is also available, an example being for Canadian Waters - including the Great Lakes [Ref. B.10]. Wave data sites are also available on the Internet for example, at, www.meds.dfo.ca maintained by the Canadian MEDS (Marine Environmental Data Services), and www.nodc.noaa.gov maintained by the U.S. National Oceanic and Atmospheric Administration (NOAA).

Wave climate atlases typically divide the world's oceans into blocks or areas. One such system is that of the "Marsden Zones" used frequently in commercial and offshore applications as presented in Ref. B.6.

Wave climate data is usually expressed in terms of "scatter diagrams" which express the probability of certain combinations of wave height and period occurring.. Typical scatter diagrams are shown in **Tables B.2..8** and **B.2.9**.

B.2.4.2.2   Selection of Wave Spectral Model

In order to use the wave climate data in modelling of response due to wave action , it is generally necessary to select a spectral model for wave height. This is a mathematical representation of the distribution of wave energy as a function of the spectral parameters. (Wave Height, H, and period, T). Several such models have been developed and some are discussed in Appendix F.

B.2.4.2.3   Other Corrections for Wave Encounter

Wave height spectra typically refer to the wave climate at a *stationary* point in the ocean. The frequency of waves that the ship experiences differs from the frequency a stationary observer would experience by virtue of the ships relative speed and heading to the wave train. The former is usually referred to as the "encounter frequency". The spectrum being used in the analysis needs to be modified to account for this fact, and this is usually achieved by modifying the frequency of encounter by:

$$? _e = ? \left(1 - \frac{? \, V}{g} \cos ? \right)$$ (B.2.4.1)

(See Nomenclature for variable definitions).

The wave height spectrum also needs to be modified to account for the transformation of the axes system from a fixed point to one that is translating with the ship, and the modified wave spectrum is given by:

$$S_?(?) = \frac{1}{1 - (2\boldsymbol{w}\ V/g)\cos\ ?} \tag{B.2.4.2}$$

Further, there must be a means of accounting for the variation in wave energy with direction within a single-moded spectrum. As a two-parameter spectrum does not explicitly consider wave direction (only height and frequency), the alternative to assuming uni-directional seas (all wave energy concentrated on one axis) is to apply a cosine-squared spreading function as follows:

$$S_?(?_e, ?') = S_?(?_e) \cdot \frac{2}{p}\cos^2(?') \tag{B.2.4.3}$$

If a software package is used to calculate motions and loads, these corrections will normally be calculated automatically using input from the operator.

B.2.4.2.4   Wave Scatter Diagrams

Wave climate data for both directional and non-directional seas are usually expressed in terms of "wave scatter diagrams" which express the relative frequency of occurrence of certain combinations of wave height and modal period. Hence, using statistical terminology, the diagram represents the joint probability distribution for wave height and period. A typical non-directional wave scatter diagram (in this case for a composite area covering the North Atlantic) is shown in **Table B.2.8**

The direct calculation method is based on the creation of a composite wave scatter diagram derived from the reference wave climate scatter diagrams that comprise the proposed shipping route or operating area. Mathematically, the composite scatter diagram is defined as:

$$(H_s, T_z)_{composite} = \sum_{i=1}^{N'} \mu_i (H_s, T_z)_i \tag{B.2.4.4}$$

where H_s and T_z are the significant wave height and zero crossing period respectively, μ_i is the proportion of time spent in the ith area (Marsden zone), and N' is the total number of areas along the route. In practice, the composite wave scatter diagram is created by:

(1)   multiplying the relative frequency values in wave scatter diagrams for each geographical area by their respective factor μ_i;
(2)   adding all of the modified relative frequency values for common height and period to develop a single weighted scatter diagram.

B.2.4.3   Determination of Wave Load Distribution

Once the ship and wave data required have been developed (sections B.2.4.1, and B.2.4.2 respectively), they are combined into a composite "sea operational profile" containing all the information needed to construct a long-term distribution of loads.

The process is described in detail in Reference B.1 and summarised here. To simplify the presentation, the period data of the used composite scatter diagram has been excluded and only the wave height probabilities are shown (see **Table B.2.6**). In statistical terms, this probability represents the marginal probability of wave heights.

The composite wave height probability distribution (Table B.2.6) for distribution of time in the relevant sea areas is combined with the conditional probability of vessel speed and wave height according to the expression:

$$f_{mc} \cdot f_V (V \mid H_s) = f_s \qquad\qquad (B.2.4.5)$$

where f_s = joint probability of significant wave height and speed.

The term $(f_V (V \mid H_s)$ represents the conditional probability of speed V given wave height H_s, and is calculated from

$$f_V (V \mid H_s) = prob(V \text{ and } H_s) / prob (H_s) \qquad\qquad (B.2.4.6.)$$

where: prob(V and H_s) is the joint probability of speed and wave height, and prob (H_s) is the marginal probability of wave heights. Both terms are obtained from the operational profile joint probability table of speed and wave height. **Table B.2.7** presents the results of the calculation of f_s:

The third parameter, heading, is then incorporated in the analysis. The procedure is similar to that for speed, but is combined directly in the expression to give a total probability (three-dimensional probability), as calculated from the expression:

$$f_{stotal} = f_s \, f_\theta (\theta \mid H_s) \qquad\qquad (B.2.4.7).$$

where

$$f_\theta (\theta \mid H_s) = prob(\theta \text{ and } H_s) / prob (H_s)$$
$$(B.2.4.8)$$

where prob(θ and H_s) is the joint probability of relative heading and wave height, and prob (H_s) is the marginal probability of wave heights. Again, both terms are obtained from an operational profile joint probability table of relative heading and wave height.

Table B.2.6: Composite Distribution of Wave Height Probabilities (f_{mc})

Hs [m]	Marsden Combined
0-1	0.1131
1-2	0.2970
2-3	0.2660
3-4	0.1634
4-5	0.0849
5-6	0.0407
6-7	0.0188
7-8	0.0087
8-9	0.0041
9-10	0.0020
10-11	0.0008
11-12	0.0006

Table B.2.7: Two-Dimensional Joint Probability Distribution (f_s)

SPEED	Significant Wave Height (m)							
(kn.)	**1**	**2**	**3**	**4**	**5**	**6**	**7**	SUM
0-6	0.0014	0.0000	0.0014	0.0000	0.0000	0.0006	0.0062	**0.0096**
6-10	0.0028	0.0012	0.0053	0.0148	0.0075	0.0154	0.0082	**0.0552**
10-14	0.0065	0.0082	0.0800	0.0686	0.0392	0.0527	0.0164	**0.2717**
14-18	0.0457	0.0472	0.2103	0.1826	0.1167	0.0570	0.0041	**0.6636**
SUM	**0.0564**	**0.0566**	**0.2970**	**0.2660**	**0.1634**	**0.1256**	**0.0349**	**1.0000**

The values of f_θ are calculated for every wave height/heading combination and multiplied by each entry in Table B.2.7. For example, if there are four ranges of speeds, five relative headings (head, bow, beam, quartering, and following seas), and seven wave heights, then the matrix of three-dimensional probability of simultaneous occurrence of speed (V), relative heading (θ) for the given wave height (H_s) in the combined operating area has 5 x 4 x 7 = 140 entries. Selective elimination of cells in the matrix by combining their ranges and probabilities can reduce the overall computational effort required considerably. For each cell retained, a set of possible wave periods will also need to be considered. Each speed, heading, wave height, and period combination will generate its own response spectrum.

A full analysis of this matrix could thus require over 1000 separate calculations to be undertaken, and their results combined. Fortunately, a reduced scope will normally be quite sufficient.

For a more detailed description of this process, refer to Reference B.1.

B.2.4.4   Calculation of Response Amplitude Operators and Stress Coefficients

The next stage requires the calculation of the response characteristics in terms of the transfer functions and stress coefficients that together will yield values of field stress, in the vicinity of the details of interest, for unit wave amplitudes for a range of wave periods. These *transfer functions* are generally referred to as Response Amplitude Operators, or RAO's. An RAO represents the response of the ship's structure to excitation by a wave of unit height, and is derived over the full range of (encounter) frequencies that will be experienced. RAO's are complex numbers with real and imaginary components that express the amplitude and phase relationship between the wave load (forcing function) and the response. In general, transfer functions vary with speed and heading. Transfer functions can be determined by model tests, full-scale measurements, or by computer programs.

A number of computer codes for calculating these RAO's are now available. These range from ship motions programs based on the so-called "strip theory" of Salveson, Tuck and Faltinsen [Ref. B.11]– such as ShipmoPC [Ref. B.12] and SMP [Ref. B.13] to programs using "panel methods" [e.g., Ref. B.14] which more accurately represent three dimensional forms, and provide hydrodynamic pressure RAO's over the hull surface, but which require greater computational activity.

This Guide does not develop the mathematical basis for the various ship response RAO's. There are a variety of suitable references [e.g., Ref. 15]. In general, the numerical calculations are computationally demanding and require a computer code. Empirical (model test or parametric) representations have, however, been developed for some specific ship types.

The procedure is to compute RAO's for selected load types. The number of RAO's and stress coefficients that need to be calculated depends on which load types are relevant and which parts of the ship structure are subject to the analysis. In general, the transfer functions for vertical, horizontal and torsional bending moment will be required as well as for external pressure and for liquid loads.

The next stage requires the stress coefficients to be computed. The stress coefficients corresponding to the transfer functions listed above are:

A_v stress per unit vertical bending moment;
A_h stress per unit horizontal bending moment, etc.

Stress coefficients are normally determined from a global finite element model of the ship, or a large part of the ship, for each load case individually (i.e., vertical bending moment, horizontal bending moment, etc.). Each load case is analyzed for a unit value of applied load at the location being considered. The stress coefficient expresses the value of the stress component at the point of interest normalized by the unit load case. (For a more detailed description of using FEA approach in level 3 analysis, refer to Reference B.1.)

The load RAO's and stress coefficients are then combined to yield a stress RAO:

$$H_{\sigma}(w|q) = A_v H_v(w|q) + A_h H_h(w|q) + A_t H_t(w|q) + A_p H_p(w|q) + A_c H_c(w|q) \qquad \text{(B.2.4.9)}$$

where $H_{\sigma}(w|q)$ is the RAO for the part of the structure which is to be subjected to damage tolerance assessment.

In general, a damage tolerance assessment will investigate several parts of the ship. There will be at least one stress RAO for each part. Stress RAO's will be required for each stress component of interest. For example, if axial stress and shear stress are required for a damage tolerance assessment of a detail, then two stress RAO's will be required for each relevant load type.

B.2.4.5   Computation of Response

At this point, all the data required for computing response for a given stationary condition (defined by probability of simultaneous occurrence of speed V, relative heading θ, significant wave height H_s and zero crossing period T_z)are available. The input data comprise:

- Modified wave spectrum, $S_\eta(\omega_e)$ for unidirectional seas (or $S_\eta(\omega_e, \theta')$ for directional seas)
- Ship speed and relative heading (V, θ)
- Wave scatter diagram $(H_s, T_z)_{composite}$
- Stress transfer function(s) or RAO's $(H_\sigma(\omega/\theta)$

The response (stress) spectrum for unidirectional seas is given by:

$$S_s(?_e) = |H_s(?|?)|^2 S_?(?_e) \qquad \text{(B.2.4.10)}$$

where $S_s(?_e)$ is the stress spectrum for a given combination of H_s, T_z and $?$.

Similarly, for directional seas the response spectrum is given by:

$$S_s(?_e,?') = \int_0^{2p} |H_s(?|?')|^2 S_?(?_e,?') \qquad \text{(B.2.4.11)}$$

The spectral moments for the stationary condition in unidirectional seas are given by:

$$m_k = \int_0^\infty ?_e^{\,k} S_s(?_e) d?_e$$
(B.2.4.12)

and in directional seas is given by:

$$m_k = \int_0^{2p} \int_0^{\infty} ?_e^k S_s (?_e, ?') d?_e d?' \tag{B.2.4.13}$$

where m_k is the "k"th moment, and m_0 is the zeroth moment and is equal to the mean square stress response.

More details on numerical calculation of spectral responses and associated spectral moments for unidirectional and directional seas can be found in Reference B.15.

B.2.4.6   Computation of the Spectrum of Stress Ranges

A key assumption of the spectral method is that for each stationary condition the input wave forces are ergodic and statistically stationary. In this circumstance, the response is narrow-banded and is Rayleigh-distributed. Hence, the stress range distribution for a stationary condition is given by:

$$F_{?si} (?s) = 1 - \exp\left[\frac{?s^2}{8m_{0i}}\right] \tag{B.2.4.14)\\}$$

and the response zero crossing frequency for a stationary condition i is given by:

$$\upsilon_i = \frac{1}{2p} \sqrt{\frac{m_{2i}}{m_{0i}}}$$

(B.2.4.15)

B.2.4.7   Compilation of Total Stress Range Spectrum

The purpose of this section is to describe how to compile the total stress range spectrum for the part(s) of the ship structure that are to be subjected to a damage tolerance assessment.

In order to express the total stress range spectrum, the stress range spectra for each stationary condition (characterized by speed, relative heading, wave height and wave period) calculated as described above, are combined as follows:

$$F_{?s} = \sum_{i=1}^{\text{all stationary conditions}} r_i F_{?si}(?s) p_i \tag{B.2.4.16}$$

where

p_i = probability of occurrence of a stationary condition
$r_i = v_i / v_0$ = the ratio between the crossing frequency in a given stationary condition i, and the
average crossing rate

$$v_0 = \sum_{i=1}^{all\,stationary\,conditions} p_i n_i = \text{the average crossing rate}$$

The method as described above does not retain information on sequencing of stress ranges. The sequencing of stress range data is problematic since it is so variable. However, the variations of wave climate from one Marsden zone to another can be captured in an average sense. The stress range data for each combination of H_s, T_z is known and the probability of occurrence of the combination with each Marsden zone is also known. What is still not known is the sequence within each Marsden zone. It may be acceptable to gather the stress range data for each Marsden zone and order the stress range data from high to low. While this is conservative (for certain types of damage assessment) it is not as conservative as sequencing the total stress range data for the duration of the damage tolerance assessment. The degree of conservatism can only be determined by trial and error through simulation exercises.

B.2.4.8   Computation of Extreme Response

The Level 3 method for computing the long-term response presented below was developed by Ochi [Ref. B.5] and is based on combining the "short term responses" that occur during the duration of interest. In the present context, each short-term response has special characteristics. The main assumptions are that the input process (wave loading) is statistically stationary and ergodic, and the system (dynamical model of the ship) is linear. These assumptions are discussed in Section B.2.3.2.

Ochi showed that the probability density function of the long-term response can be expressed as follows:

$$f(s_a) = \frac{\sum_i \sum_j n_* p_i p_j f_*(s_a)}{\sum_i \sum_j n_* p_i p_j} \qquad (B.2.4.17)$$

where

σ_a	=	stress amplitude
$f(\sigma)$	=	probability density function for short-term response
n_*	=	average number of responses per unit time of short-term response
	=	$\dfrac{1}{2p}\sqrt{\dfrac{m_2}{m_0}}$, where m_0 and m_2 are as defined in Section B.2.4.5
p_i	=	weighting factor for ith sea state
p_j	=	weighting factor for jth heading

Implicit in the previous expression is that sea state and heading are the only variable parameters. Other parameters, such as ship speed and wave spectrum could vary significantly over the duration of interest. If this is the case, the expression would have to be modified to include an additional summation for each further variable.

Integration of the probability density function of the long term response yields the cumulative distribution function:

$$F(s) = \int_0^{s_a} f(s)\,ds \qquad\qquad (B.2.4.18)$$

The total number of cycles can be calculated from the following expression:

$$n = \left(\sum_i \sum_j n_* p_i p_j \right) \times T \times (60)^2 \qquad\qquad (B.2.4.19)$$

where T is total exposure time to the sea over the duration of interest.

Applying the asymptotic distribution of extreme values a "design" extreme value can be computed from the following expression:

$$\frac{1}{1 - F\left(\hat{s}\right)} = \frac{n}{a} \qquad\qquad (B.2.4.20)$$

where

$\hat{s}$ = design extreme stress
a = risk parameter discussed in Section B.2.3.3; recommended value 0.01

Caution needs to be applied in calculating an estimate of the extreme response for periods of duration much less than the typical life of a ship. The wave climate model as expressed in terms of scatter diagrams represents an average gathered over many years. Clearly, such a model is not reliable for very short periods, and hence, in these cases, it is incorrect to merely substitute the actual duration for "T" in the expression B.2.4.20.

This is a subject that has not been extensively researched and, therefore, definitive guidance cannot be provided. A limited discussion on one aspect of this subject is presented in Reference B.16.

For very short periods of duration, in the order of days or weeks, a very conservative approach is recommended. In the case of "on-the-spot" analyses, it may be feasible to use weather forecasts upon which to base the wave climate model. Several national and international agencies provide weather forecasts that include forecasts of wave heights over

much of the globe. For the approach to be generally applicable, there is no alternative but to assume an extreme wave climate model.

In the case of intermediate periods of duration there is little alternative but to use the wave scatter diagrams together with conservative assumptions in regard to the duration. Strictly, an analysis should be performed in which the statistical variability of the data upon which the wave scatter diagrams are based is accounted for. As very tentative guidance for periods of less than five years, a period of duration of no less than five years should be used. Where the data allows it, the seasonal variations in wave climate should be included in the analysis.

The treatment of short and intermediate periods of duration outlined above is not based on rigorous analysis, and it is recommended that further analysis be performed before applying any of the above.

B.2.4.9   Slamming Loads

The spectral method, which relies on linearity, is not a convenient framework within which to account for slamming loads. Alternative methods are more conveniently applied. These range from specialist computer programs that compute slamming loads and ship response, to simple empirical rules. As an example of the latter, Mansour et al. [Ref. B.17]suggests that to account for slamming, the wave bending moment for commercial ships should be increased by 20%, and by 30% for warships. When more sophisticated approaches are employed in predicting the response to slamming, it is necessary that a dynamic analysis be performed in which the elasticity of the ship structure is accounted for.

B.2.5 Load Estimation - Level 3b

The Level 3 approach may be modified somewhat when there is insufficient wave data. This method is termed Level 3b as it is identical to the Level 3 approach except for the wave climate model used. While the ideal is to compile a composite wave scatter diagram that reflects the intended route of the ship, this information is not necessarily available. In this situation, it is necessary to use average pre-compiled data. Two such scatter diagrams are presented below, extracted from Reference B.2. **Table B.2.8** is intended for use for routes in the North Atlantic. This is significantly more severe than the "world average" wave climate presented in **Table B.2.9**.

B.2.6 Load Estimation - Level 2

The methodology for determining global stresses described for Level 3 is a first principles approach which requires considerable resources to apply. This applies particularly to the data required and the software tools needed. There are several reasons why such a detailed approach may not be justified. These reasons may include lack of data and lack of appropriate tools. In addition, despite the rigour of the methodology, there are limitations in the method that are not easily overcome.

Several alternative approaches have been developed that are much less demanding in terms of effort required but which are nearly as effective as first principles approaches as long as the limitations are recognized and catered for. These methods are largely empirical in origin and

hence are applicable to the ship types from which the data was derived in the development of the methods. Three methods are presented herein – all as Level 2 analyses.

Short descriptions of each follow:

Method A   A method applicable to a wide range of commercial vessels has been developed by Det Norske Veritas [Ref B.2 or and is adapted here for damage tolerance assessment purposes. The method is based on an estimate of extreme load derived from the DNV Rules, and the stress range spectrum is based on the Weibull model. This is similar in approach to the method devised by the American Bureau of Shipping [Ref. B.18] that forms the basis of the approach used in the ABS SafeHull system [Ref. B.19]. The two approaches are interchangeable in this guide.

Method B   A method based on data gathered on frigate/destroyer size warships was developed by Clarke (Refs. B.20, B.21] and described in Reference B.22.

Method C   A method based on data from both warships and commercial ships was developed by Sikora [Refs. B.23, B.24]

The methods are presented in order of the effort required and comprehensiveness. Method A provides parametric expressions for load calculation for load types considered relevant for several types of ship; these are listed in Section B.2.6.1. Methods B and C are limited to predicting extreme vertical bending moments. Hence these methods cannot predict stresses due to, for example, horizontal or torsional bending. Furthermore, these methods are unable to predict stresses due to local wave action or due to acceleration forces induced by ship motion. These limitations can be a serious drawback in applying the methods unless they are supplemented by other calculation methods where required.

While, in general, wave-induced vertical bending is the major source of high stresses in ship structures, there are potentially other loading modes that may be also be significant sources. For example, torsional moments can cause high stresses at hatch corners in container ships. While this mode can be included in the analysis using the Level 3 method, parametric equations for predicting moments other than those due to vertical bending do not appear to be available except in class society rules. Therefore, in situations where considering vertical bending alone is insufficient, and where Level 3 and 3b methods cannot be applied, it is recommended that Class Society rules be employed. The reference from which Method A is adapted, provides guidance in the use of DNV rules for this purpose [Ref. B.2].

The same observations apply to the calculation of local loads that can be significant for several classes of large commercial vessels that tend to have limited internal structure.

Table B.2.8: Scatter Diagram for North-Atlantic for Use in Fatigue Computations

Tz / Hs(m)	3.5	4.5	5.5	6.5	7.5	8.5	9.5	10.5	11.5	12.5	13.5	14.5	15.5	16.5	17.5	Sum
1	0	72	1416	4594	4937	2590	839	195	36	5	1	0	0	0	0	14685
2	0	5	356	3299	8001	8022	4393	1571	414	87	16	3	0	0	0	26167
3	0	0	62	1084	4428	6920	5567	2791	993	274	63	12	2	0	0	22196
4	0	0	12	318	1898	4126	4440	2889	1301	445	124	30	6	1	0	15590
5	0	0	2	89	721	2039	2772	2225	1212	494	162	45	11	2	1	9775
6	0	0	1	25	254	896	1482	1418	907	428	160	50	14	3	1	5639
7	0	0	0	7	85	363	709	791	580	311	131	46	14	4	1	3042
8	0	0	0	2	27	138	312	398	330	197	92	35	12	3	1	1547
9	0	0	0	1	8	50	128	184	171	113	58	24	9	3	1	750
10	0	0	0	0	3	17	50	80	82	59	33	15	6	2	1	348
11	0	0	0	0	1	6	18	33	37	29	17	8	3	1	0	153
12	0	0	0	0	0	2	7	13	15	13	8	4	2	1	0	65
13	0	0	0	0	0	1	2	5	6	6	4	2	1	0	0	27
14	0	0	0	0	0	0	1	2	2	2	2	1	1	0	0	11
15	0	0	0	0	0	0	0	1	1	1	1	0	0	0	0	4
16	0	0	0	0	0	0	0	0	0	1	0	0	0	0	0	1
Sum	0	77	1849	9419	20363	25170	20720	12596	6087	2465	872	275	81	20	6	100000

Table B.2.9: Scatter Diagram Describing World Wide Trade for Use in Fatigue Computations (Cramer et al., 1995

Tz / Hs(m)	3.5	4.5	5.5	6.5	7.5	8.5	9.5	10.5	11.5	12.5	13.5	14.5	15.5	16.5	17.5	Sum
1	311	2734	6402	7132	5071	2711	1202	470	169	57	19	6	2	1	0	26287
2	20	764	4453	8841	9045	6020	3000	1225	435	140	42	12	3	1	0	34001
3	0	57	902	3474	5549	4973	3004	1377	518	169	50	14	4	1	0	20092
4	0	4	150	1007	2401	2881	2156	1154	485	171	53	15	4	1	0	10482
5	0	0	25	258	859	1338	1230	776	372	146	49	15	4	1	0	5073
6	0	0	4	63	277	540	597	440	240	105	39	13	4	1	0	2323
7	0	0	1	15	84	198	258	219	136	66	27	10	3	1	0	1018
8	0	0	0	4	25	69	103	99	69	37	17	6	2	1	0	432
9	0	0	0	1	7	23	39	42	32	19	9	4	1	1	0	178
10	0	0	0	0	2	7	14	16	14	9	5	2	1	0	0	70
11	0	0	0	0	1	2	5	6	6	4	2	1	1	0	0	28
12	0	0	0	0	0	1	2	2	2	2	1	1	0	0	0	11
13	0	0	0	0	0	0	1	1	1	1	0	0	0	0	0	4
14	0	0	0	0	0	0	0	0	1	0	0	0	0	0	0	1
Sum	331	3559	11937	20795	23321	18763	11611	5827	2480	926	313	99	29	9	0	100000

Methods B and C do not provide explicit models for the stress range spectrum. This is a less serious drawback since the well-established Weibull model can be used. The primary decision to be made in this regard is the choice of a value for the Weibull shape parameter (h). Again the Class societies are a good source of information for commercial ship structure [Refs. B.2, B.18] where values for shape parameter are recommended. In the case of warships, a limited amount of full-scale data for vertical hull girder bending suggests a value of unity [Ref. B.21]. Mansour et al. in Reference B.17, using a computer program based on second-order strip theory, predicted shape parameters somewhat less than unity for two cruisers.

B.2.6.1   Method A

Almost all major classification societies have developed or are in the process of developing structural design methodologies that are a significant departure from past practice. Traditional design methods as expressed in the rules are empirically based and have evolved over many decades of use. While such methods yield adequate designs they suffer from being inflexible and poor at accommodating new materials, innovative structural configurations, and novel hull forms.

In response to this weakness, and for other reasons, the major classification societies have invested considerable resources in developing first-principles methods of analysis and design. These methods have several characteristics in common; principal among them are:

- computer-based systems;
- explicit calculation of loads;
- explicit calculation of structural resistance;
- capability to assess fatigue performance.

While these systems are based on first-principles approaches, they are not generic in terms of the ship types that the approaches can be applied to. The classification societies have developed systems primarily for larger vessels, the main ship types being tankers, bulk carriers, and container ships. Implicit in many of the systems is an assumption of a specific structural configuration.

The degree to which the classification societies have published the background on the methods in the open literature is variable. It would not be appropriate to describe herein all the approaches developed by the classification societies. The method described here is taken from the methodology for fatigue assessment developed by Det Norske Veritas [Ref. B.25,B.2]. While the published approach does not exclude any ship type, it appears by implication to be intended for:

- tankers;
- bulk carriers;
- ore carriers;

- container ships;
- RO/RO and car carriers.

The DNV document presents two methods that are termed "simplified analysis" and "direct analysis". The latter is essentially the long-term method presented earlier. The methodology reproduced below is essentially the simplified analysis presented in the DNV document. It should be noted that in approach the method is similar to that presented by ABS.

The overall approach is to use the DNV Rules to define the following load components based on the Rules [Ref. B.26]:

- vertical bending moment
- horizontal bending moment
- torsional bending moment
- dynamic external pressure loads
- internal pressure loads due to ship motions

The stress range spectrum used for fatigue assessment purposes is modeled using the Weibull distribution. As discussed elsewhere in this document, the Weibull distribution has become the preferred model for representing the stress range spectrum and is illustrated in **Figure B.2.3**
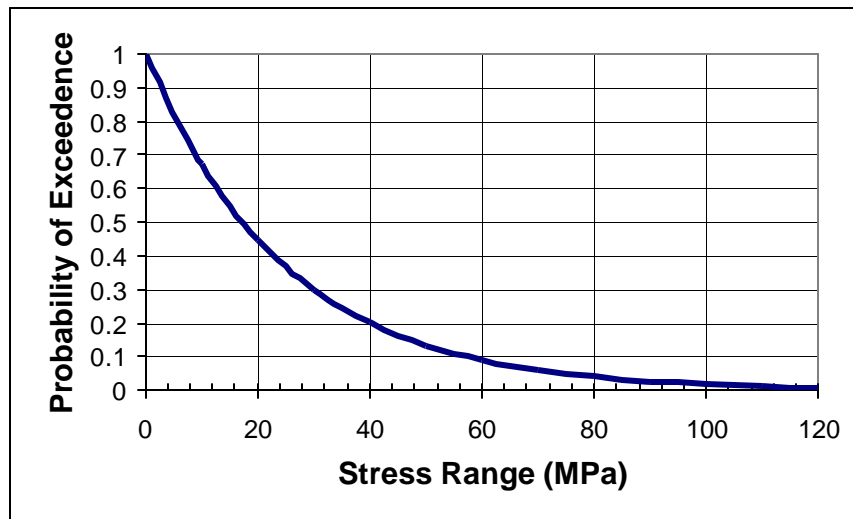

Figure B.2.3: Weibull Distribution (Probability of Exceedance)

The stress range distribution is expressed as follows

$$\Delta s = \Delta s_0 \left[\frac{\log N}{\log N_0} \right]^{1/h}$$

(B.2.6.1)

where

Δs = stress range
Δs_0 = reference stress range
N = number of cycles
N_0 = number of cycles associated with reference stress range

[See also Nomenclature]

h = shape parameter

Reference B.2 provides the following guidance on values for shape parameters (for tankers and bulk carriers). (See Figure B.2.4 also)

h = h_o for deck longitudinals
h = $h_o + h_a (D_m - z_{bl}) / (D_m - T_{act})$ for ship side above the waterline
$T_{act} < z_{bl} < D_m$
h = $h_o + h_a$ for ship side at the waterline $z_{bl} = T_{act}$
h = $h_o + h_a z_{bl} / T_{act} - 0.005 (T_{act} - z_{bl})$ for ship side below the waterline $z_{bl} < T_{act}$
h = $h_o - 0.005 T_{act}$ for bottom longitudinals
h = $h_o + h_a$ for longitudinal and transverse bulkheads

where
h_o = basic shape parameter = $2.21 - 0.54 \log_{10}(L)$

(In the absence of alternatives, h_o can be taken as 1.05 for open type vessels.)

h_a = additional factor depending on motion response period
= 0.05 in general
= 0.00 for plating subjected to forces related to roll motions for vessels with roll period T_R greater than 14 seconds.

In order to avoid sensitivities associated with the Weibull shape parameter, Reference B.2 recommends that the reference number of cycles be taken at 10^4. The methodology described is formulated accordingly.

This section outlines a simplified approach for calculation of dynamic loads. Formulae are given for calculation of global wave bending moments, external sea pressure acting on the hull and internal pressure acting on the tank boundaries.

The simple formula for calculation of loads in this section are based on the linear dynamic part of the loads as defined in the 1993 edition of the DnV Rules [Ref. B.27]. The design loads as defined in the Rules also include non-linear effects such as bow-flare and roll damping and are not necessarily identical with the dynamic loads presented herein.

In general, fatigue damage should be calculated for all representative load conditions accounting for the expected operation time in each of the considered conditions. For tankers, bulk carriers and container vessels, it is normally sufficient to consider only the ballast- and fully loaded conditions. The loads are calculated using actual draughts, T_{act}, metacentric heights GM_{act} and roll radius of gyration, $k_{T,act}$ for each considered loading condition.

B.2.6.1.1 *Wave induced hull girder bending moments*

The vertical wave induced bending moments may be calculated using the bending moment amplitudes specified in the DnV Rules [Ref.B.27]. The moments, at 10^{-4} probability level of exceedance, may be taken as:

$$M_{ds} = -0.11 f_f k_{wm} C_w L^2 B (C_B + 0.7) \quad (kNm) \tag{B.2.6.2}$$
$$M_{dh} = 0.19 f_f k_{wm} C_w L^2 B C_B \quad (kNm) \tag{B.2.6.3}$$

where terms are as defined in the Nomenclature, and

C_w =   wave coefficient
      = $0.0792 L$; $L < 100$ m
      = $10.75 - [(300\text{-}L) / 100]^{3/2}$; 100 m $< L < 300$ m
      = 10.75; 300 m $< L < 350$ m
      = $10.75 - [(L\text{-}350) / 150]^{3/2}$; 350 m $< L$

k_{wm} =   moment distribution factor
      =   1.0 between 0.40L and 0.65L from A.P., for ships with low/moderate speed
      =   0.0 at A.P. and F.P. (linear interpolation between these values.)

f_f =   factor to transform the load from 10^{-8} to 10^{-4} probability level.
      = $0.5^{\frac{1}{h_0}}$

h_o =   long-term Weibull shape parameter
      = $2.21 - 0.54 \log(L)$

For the purpose of calculating vertical hull girder bending moment by direct global finite element analyses, simplified loads may be obtained from Reference B.2

The horizontal wave bending moment amplitude (M_h) at the 10^{-4} probability level may be taken as follows:

$$M_h = 0.22 \ f_f L^{9/4} \ (T_{act} + 0.30 \ B) \ C_B \ (1\text{-}\cos(2p \ x/L)) \quad (kNm) \qquad (B.2.6.4)$$

where x is the distance in metres from the AP to section considered, and L, B, C_B, f_f are as defined in the Nomenclature.

Wave torsional load and moment, which may be required for analyses of open type vessels (e.g., container vessels), are defined in Appendices C and D of Reference B.2.

B.2.6.1.2   Dynamic external pressure loads

Due to intermittent wet and dry surfaces, the range pressure is reduced above a point T_{act}-z_{wl} above the base line, (see **Figure B.2.4**). The dynamic external pressure amplitude (half pressure range), p_e, related to the draught of the load condition considered may be taken as:

$$p_e = r_p p_d \qquad (kN/m^2) \qquad\qquad (B.2.6.5)$$

The dynamic pressure amplitude, p_d, may be taken as the largest of the combined pressure dominated by pitch motion in head/quartering seas, p_{dp}, or the combined pressure dominated by roll motion in beam/quartering seas, p_{dr}, as:

$$p_d = \max \ (p_{dp}, \ p_{dr}) \ (kN/m^2) \qquad\qquad (B.2.6.6)$$

where

$$
\begin{aligned}
p_{dp} \quad &= \quad p_1 + 135 \ \bar{y}/(B + 75) - 1.2(T_{act} - z_{bl}) \\
p_{dr} \quad &= \quad 10[\bar{y}\alpha/2 + C_B((y + k_f)/16)(0.7 + 2z_{bl}/T_{act})] \\
p_1 \quad &= \quad k_s C_w + k_f \\
&= \quad (k_s C_w + k_f) \ (0.8 + 0.15 \ V/\sqrt{L}) \quad \text{if } V/\sqrt{L} > 1.5 \\
k_s \quad &= \quad 3C_B + 2.5/\sqrt{C_B} \qquad \text{at AP and aft} \\
&= \quad 3C_B \qquad\qquad\qquad \text{between 0.2 L and 0.7 L from AP} \\
&= \quad 3C_B + 4.0/C_B \qquad \text{at FP and forward} \\
&\qquad\quad \text{(between specified areas } k_s \text{ is to be varied linearly)} \\
k_f \quad &= \quad \text{the smaller of·}T_{act} \text{ and f (freeboard)} \\
\bar{y} \quad &= \quad \geq B/4 \ (m) \\
f \quad &= \quad \leq 0.8{*}C_w \ (m) \\
r_p \quad &= \quad \text{reduction of pressure amplitude in the surface zone} \\
&= \quad 1.0 \qquad\qquad\qquad\quad \text{for z} < T_{act} \text{ - } z_{wl} \\
&= \quad \frac{T_{act} + z_{wl} - z}{2z_{wl}} \qquad\quad \text{for } T_{act} \text{ - } z_{wl} < z < T_{act} + z_{wl}
\end{aligned}
$$

$$= \quad 0.0 \qquad\qquad \text{for } T_{act} + z_{wl} < z$$

$$z_{wl} \quad = \quad (3/4)^* p_d / \rho_{sw} g)$$

In the area of side shell above $z = T_{act} + z_{wl}$, it is assumed that the external sea pressure will not contribute to fatigue damage.
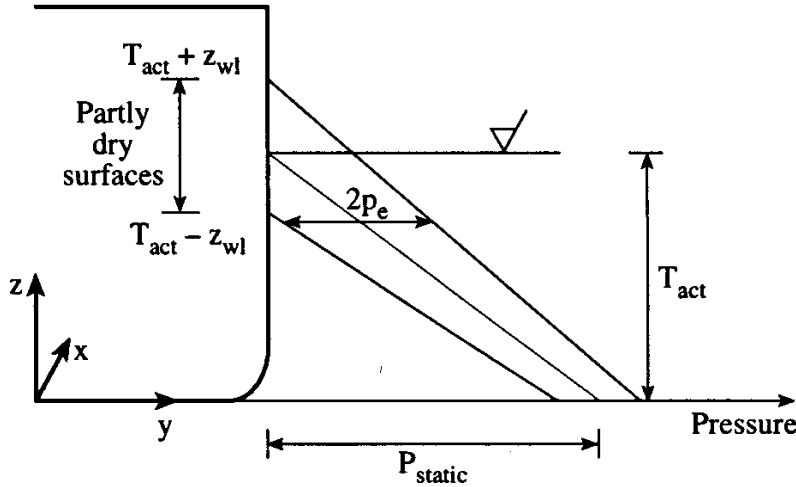
Figure B.2.4: Reduced Pressure Ranges in the Surface Region

B.2.6.1.3   Internal Pressure Loads due to Ship Motion

The dynamic pressure from liquid cargo or ballast water should be calculated based on the combined accelerations related to a fixed co-ordinate system. The gravity components due to the motions of the vessel should be included. The dynamic internal pressure amplitude, p_i in kN/m², may be taken as the maximum pressure due to acceleration of the internal mass:

$$p_i = f_f \max \begin{cases} p_1 = ?_{sw} a_v h_s \\ p_2 = ?_{sw} a_t |y_s| \\ p_3 = ?_{sw} a_l |x_s| \end{cases} \quad (\text{kN/m}^2)$$

(B.2.6.7)

Formulae for the variables in these equations may be found in the Appendix of Reference B.1 and in the original reference [B.27].

However, in general, sloshing pressures may normally be neglected in fatigue computations.

If sloshing is to be considered, the sloshing pressures in partly filled tanks may be taken as given in Section 4 of Reference B.27.

Unless otherwise specified, it may be assumed that tanks (in tankers) are partly filled 10% of the vessels design life. **Figures B.2.5** to **B.2.8** provide a graphical representation of some cargo loading conditions.
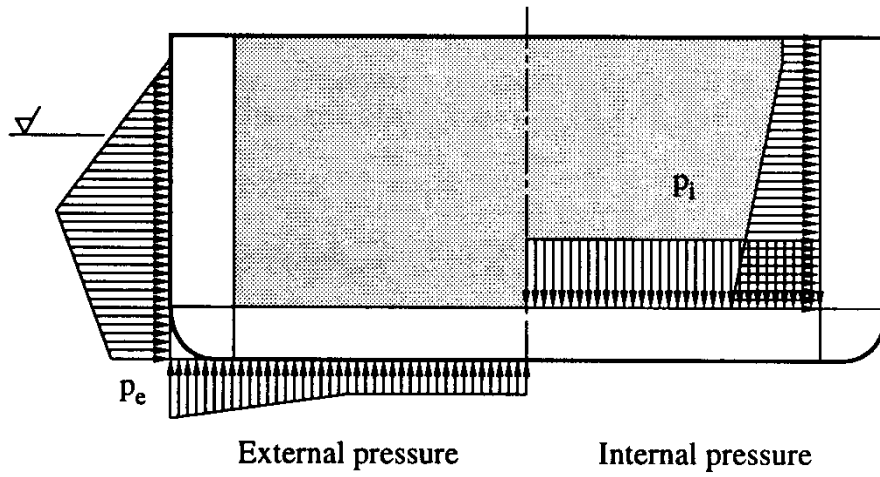
Figure B.2.5: Distribution of Pressure Amplitudes for Tankers in the Fully Loaded Condition
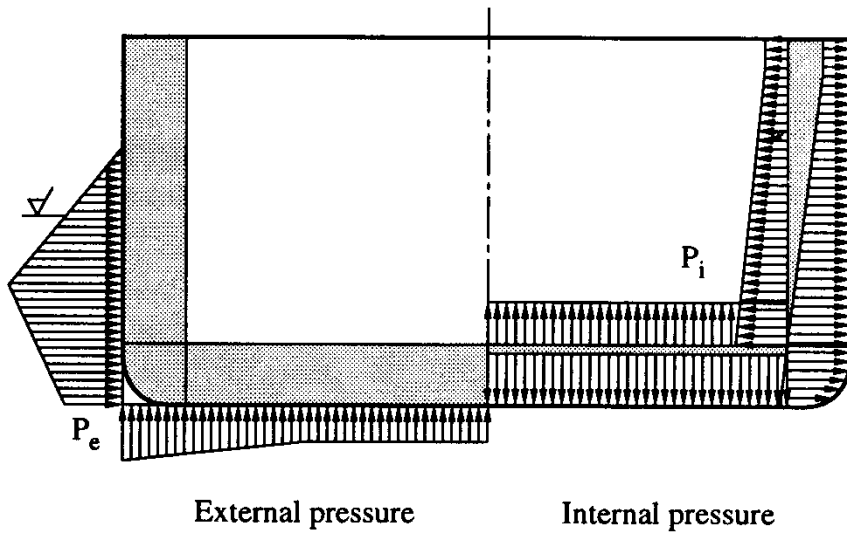
Figure B.2.6: Distribution of Pressure Amplitudes for Tankers in Ballast Condition
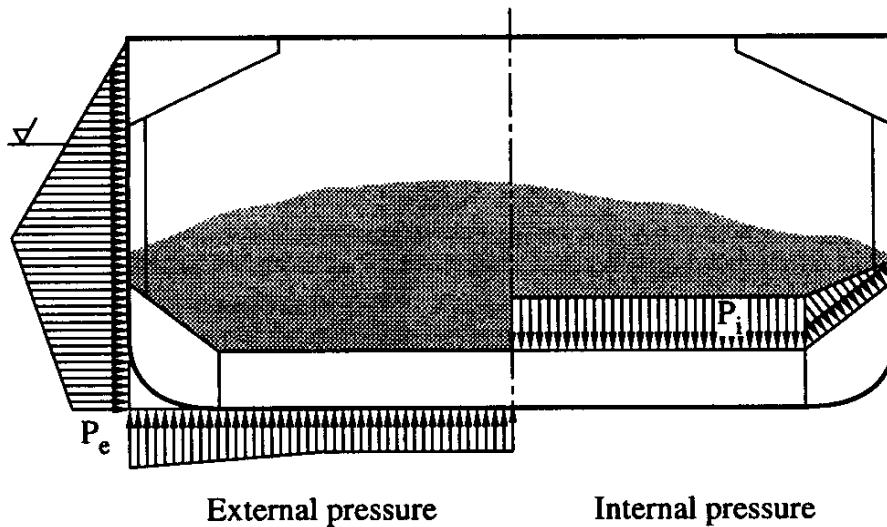
Figure B.2.7: Distribution of Pressure Amplitudes for a Bulk Carrier in the Ore Loading Condition

B.2.6.14   Estimates of extreme load

The methodology summarized above is intended for fatigue analysis and not specifically for estimating extreme loads. However, the fatigue analysis is based on estimates for extreme load for each load component. The DNV methodology uses a reference probability level of 10^{-4} for this purpose and hence a conversion factor is applied to expressions for extreme loads which are generally based on a probability level of 10^{-8} that is representative of the lifetime of the ship. The exception is external pressure loads that are specified directly at probability level of 10^{-4}.

The extreme load levels for a duration other than the lifetime of the ship can be computed by factoring the load as follows:

$$\text{Factor} = \left[\frac{\log \ p_2}{\log \ p_1} \right]^{\frac{1}{h}} \qquad\qquad (B.2.6.8)$$

where:

p_2 = probability level that quantity is to be changed to;
p_1 = probability level that quantity specified at;
h = Weibull parameter.

Caution should be exercised in using the above expression for high probability levels (i.e., periods of short duration). The reasons for this were discussed in Section B.2.4.8.

B.2.6.2   Method B

This method is based on strain measurements made on several warships in the range of 100-200 m length. The method was developed by Clarke [Refs. B.20, B.21] and is described in Reference B.22. The strain data, gathered over a limited time period, was extrapolated to predict a lifetime maximum. Based on a lifetime of 25 years and a 30% exposure, the bending moment expected to be exceeded once in 3×10^7 wave encounters was computed. This was found to have a close correlation with the bending moment calculated by balancing the ship on an 8m wave.

B.2.6.2.1   Lifetime Design Load

On this basis, the following expressions were derived:

$$M_{ds} = M_{sw} + 1.54(M_{sag} - M_{sw})$$
(B.2.6.9)

$$M_{dh} = M_{sw} + 1.54(M_{hog} - M_{sw})$$
(B.2.6.10)

where M_{ds} and M_{dh} are the design sagging and hogging bending moments, M_{sag} and M_{hog} are the sagging and hogging bending moments from static balance on an 8m wave, and M_{sw} is the still water bending moment making proper allowance for its sign.

The multiplier, 1.54, accounts for two effects. The first is a factor of 1.12 which accounts for the systematic biases arising from the mean bias against the 8m wave balance, the underestimate in the measured strain inherent in the type of gauges used, and inaccuracies in the calculation of hull section modulus. The remaining factor is a statistical multiplier that is applied to convert the value of the expected bending moment, which has a probability of being exceeded once in its lifetime, to a probability of exceedance of 1% in its lifetime.

Also inherent in the 1.54 multiplier is 3×10^7 wave encounters. The value of the multiplier for other values of wave encounter is given in **Table B.2.10**.

Table B.2.10: Bending Moment for Various Numbers of Wave Encounters

Number of Wave Encounters	Multiplier
3×10^7	1.54
4×10^7	1.57
5×10^7	1.59
7×10^7	1.63
10×10^7	1.67

B.2.6.2.2   Limited Duration Design Bending Moment

The expressions presented above are intended for design purposes, and hence the numbers of wave encounters are typical of the lifetime of a ship. Damage tolerance assessments may be required for shorter periods. Using an approximation of the methodology upon which the table above is based, multipliers for smaller numbers of wave encounters are derived and presented in **Table B.2.11**. For reasons discussed in Section B.2.4.8, caution must be applied in reducing the multiplier to account for short periods of duration.

Table B.2.11: Bending Moment for Various Numbers of Wave Encounters (adapted from [Ref. B.22])

Number of Wave Encounters	Multiplier
10^6	1.25
3×10^6	1.34
7×10^6	1.41
10×10^6	1.45

The expressions presented above can be used to predict bending moments for any point along the length of the ship. This, however, does not account for slamming effects. To allow for slamming, Reference B.21, recommends extending the length over which the maximum bending moment applies forward by a distance of 15% of ship length and then reducing the bending moment linearly to zero at the forward perpendicular. This is illustrated in **Figure B.2.8** following.

The expressions for the hog and sag bending moment can be added, converted to yield a stress range that has a 1% probability of being exceeded in the duration of interest can be calculated. This, together with the selection of the appropriate Weibull shape parameter, is sufficient to define the stress range spectrum.

The methodology described above is based almost entirely on full-scale data gathered on *warships* ranging in length from about 100m to 200m. Hence the approach should, strictly, not be applied to other types of vessel.

The methodology presented in the next section, Method C, is broadly similar in approach and includes a variety of ship types although the number of ships is small. However, the success of Method C in representing the response of a range of ship types suggests that the present method may be applicable to ship types other than those from which the data was gathered.
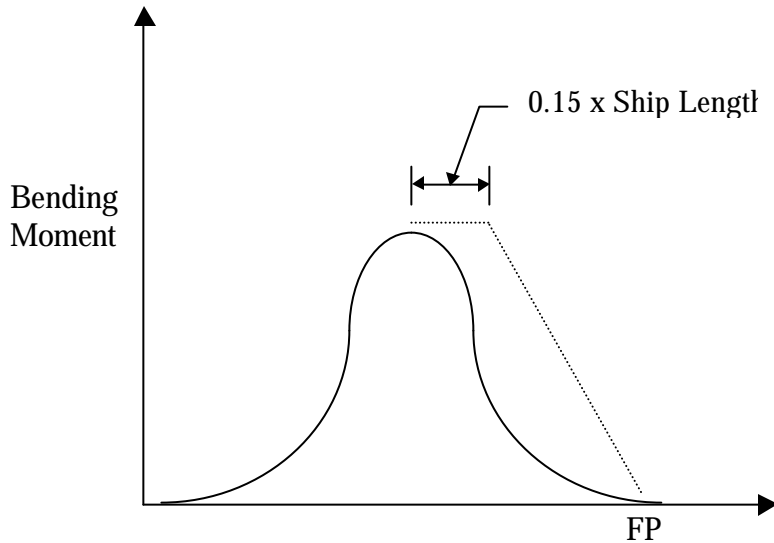
Figure B.2.8: Additional Bending Moment to Account for Whipping

B.2.6.2.3   Stress Range Spectrum

The Weibull distribution, described in Section B.2.6.1, can be used to express the stress range spectrum and guidance on shape parameters can also be found there.

B.2.6.3   Method C

This method is based on work originally reported in Reference B.23 in which a method for predicting lifetime extreme loads and stress range spectra was presented, and further developed in Reference B.24.

The method relies on a generalized response amplitude operator for vertical bending moment at midships. Response data from model-scale results and full-scale trials for a variety of ships was examined and it was found that the RAO for vertical bending at midships could, after appropriate normalization, be represented by a single curve. This generalized RAO is expressed as a function of ship length, breadth, speed and heading

The maximum wave induced bending moment was computed for several ships using the generalized RAO together with assumptions in regard to the wave climate, wave height spectrum, ship speed and direction. The key assumptions are summarized as follows:

B.2.6.3.1   Wave Climate

Wave climates from three areas of the world's oceans were used in the investigation. The frequency of occurrence of sea states for the three areas are presented in **Table B.2.12**. The primary purpose of this part of the work was to establish the sensitivity of structural response, in terms of extreme response and fatigue behaviour, to different wave climates.

B.2.6.3.2   Wave Height Spectrum

The six-parameter wave height spectrum developed by Ochi [Ref. B.5, B.27] was used in the analysis.

B.2.6.3.3   Ship Speed and Heading

The operational profile a ship experiences depends on a number of parameters. A key element is the reduction of speed that usually accompanies high sea states. The degree to which speed is reduced by the captain depends on factors such as slamming, deck wetness, propeller emergence, and accelerations levels experienced by the ship. Depending on the mission, the captain may tolerate some of these phenomena. Similarly, depending on the hull forms, size of ship and mission, the captain may alter heading in high sea states.

For the purposes of developing parametric equations predicting response, it is necessary to make assumptions in regard to the frequency of occurrence of combinations of sea state, ship speed, heading and ship type. References B.23 and B.24 developed estimates of frequency of occurrence for combinations of these parameters. These are presented below in **Table B.2.13**

B.2.6.3.4   Slamming

The role of slamming was also investigated. Using measurements from several ships a simple algorithm was developed for predicting the whipping bending moment. Slamming was assumed to occur on the basis of the criteria presented in **Table B.2.14**.

Table B.2.12: Frequency of Occurrence of Sea States

Significant Wave Height (meter)	Frequency of Occurrence		
	Area A	Area B	Area C
<1	0.0503	0.3692	0.2254
1-2	0.2665	0.3303	0.3849
2-3	0.2603	0.1480	0.2305
3-4	0.1757	0.0723	0.0945
4-5	0.1014	0.0355	0.03033
5-6	0.0589	0.0181	0.01735
6-7	0.0346	0.0110	0.00675
7-8	0.0209	0.0066	0.00390
8-9	0.0120	0.0036	0.00312
9-10	0.0079	0.00247	0.00177
10-11	0.0054	0.00138	0.00058
11-12	0.0029	0.00074	0.00031
12-13	0.0016	0.00040	0.00031
13-14	0.00074	0.00019	0.00010
14-15	0.00045	0.00012	0.00001
>15	0.00041	0.00010	0.0
Area A - North Atlantic			
Area B - Combined Atlantic, Mediterranean and Caribbean			
Area C - Combined Pacific			

Table B.2.13: Frequency of Occurrence of Heading Speed Combinations

Frigates and Small Ships (Displacement <10,000 LT)				
Speed (Kts)	Heading	Significant Wave Height (m)		
		0-5	6-10	>10
5	Head	0.013	0.025	0.0
	Bow	0.025	0.375	0.808
	Quartering	0.025	0.050	0.042
	Following	0.013	0.025	0.0
15	Head	0.088	0.023	0.0
	Bow	0.175	0.338	0.142
	Quartering	0.175	0.045	0.008
	Following	0.088	0.023	0.0
25	Head	0.025	0.0025	0.0
	Bow	0.050	0.038	0.0
	Quartering	0.050	0.005	0.0
	Following	0.025	0.0025	0.0
High Speed Cargo Ships				
5	Head	0.010	0.125	0.175
	Bow	0.020	0.125	0.175
	Quartering	0.020	0.125	0.175
	Following	0.010	0.063	0.088
15	Head	0.096	0.115	0.075
	Bow	0.193	0.115	0.075
	Quartering	0.193	0.115	0.075
	Following	0.096	0.058	0.038
25	Head	0.019	0.010	0.0
	Bow	0.038	0.010	0.0
	Quartering	0.038	0.010	0.0
	Following	0.019	0.005	0.0
Commercial Cargo Ships				
5	Head	0.010	0.125	.175
	Bow	0.020	0.125	.175
	Quartering	0.020	0.125	.175
	Following	0.010	0.063	0.88
15	Head	0.115	0.125	.075
	Bow	0.231	0.125	.075
	Quartering	0.231	0.125	.075
	Following	0.115	0.063	.038

Table B.2.14 Operational Conditions in which Whipping May Occur

Head and Bow Seas		
Displacement (tn)	Speed (Kts)	Significant Wave Height (meter)
<10,000	>10	>5
	> 5	>7
>10,000	>10	>6
	> 5	>9

B.2.6.3.5   Lifetime Design Load

The methodology described above was applied to a range of ships and simple expressions for predicting the extreme lifetime bending moment including the effects of whipping were developed. These expressions are:

$$M_{dh} = M_{sw} + 0.0006L^{2.5}B \qquad\qquad (B.2.6.11)$$

$$M_{ds} = M_{sw} + 0.0009L^{2.5}B \qquad\qquad (B.2.6.12)$$

The equivalent expressions in SI units are as follows:

$$M_{dh} = M_{sw} + 0.000115L^{2.5}B$$
(B.2.6.13)

$$M_{ds} = M_{sw} + 0.000172L^{2.5}B \qquad\qquad (B.2.6.14)$$

where L and B are in metres and the moments are given in MNm units.

Implicit in the expressions presented above is a duration of 3600 days. The risk parameter was found to range from 0.03 to 0.08 for the ships considered. In contrast to the method developed in Reference B.5 where the risk parameter is introduced, the method of Reference B.24 explicitly includes a method for including the loads arising from whipping. The implication is that the actual risk parameter, based on normal wave loads alone, is considerably less.

B.2.6.3.6   Limited Duration Design Bending Moment

The expressions given above are for an operating lifetime of 3600 days. Assuming an average of eight second zero-crossing period, this translates to approximately 3.888×10^{7}

encounters. Assuming an exponential distribution (i.e., Weibull parameter of unity) the limited duration design bending moments can be shown to be:

$$M_{dh} = M_{sw} + 0.000115L^{2.5}B\left[-\frac{\log\frac{1}{n}}{7.59}\right]$$

(B.2.6.15)

$$M_{ds} = M_{sw} + 0.000172L^{2.5}B\left[-\frac{\log\frac{1}{n}}{7.59}\right]$$

(B.2.6.16)

where n is the number of wave encounters.

As stressed before, caution must be applied in reducing the multiplier to account for short periods of duration.

B.2.6.3.7   Stress Range Spectrum

The Weibull distribution, described in Section B.2.6.1, can be used to express the stress range spectrum with guidance for shape parameters also taken from there.

B.2.7 Commentary

Several methods for computing the expected load and stress range spectrum for arbitrary periods of duration have been presented earlier in this section. The methods presented are believed to represent the best currently available in terms of accuracy, practicability and cost effectiveness. However, the subject of wave loading cannot be regarded as entirely mature; it is an area of active research and it is only relatively recently that direct methods of wave load calculation have been applied in the design environment.

Historically, the primary interest was in the development of methods for predicting the extreme loads a ship would likely experience in its lifetime. More recently, interest in estimating the stress range spectrum has also developed. The latter was not a significant issue in the past because fatigue failures were less of a concern. But with the trend towards lighter, optimized structure and the use of high strength steels, the need to explicitly consider fatigue grew.

A parallel development has been the growth in interest in the application of reliability theory principles to the structural design of ships. In concept at least, reliability theory provides an appealing framework within which to develop design methodologies that rely on direct

methods. This is because of the strongly probabilistic nature for the main variables that characterize wave loads on ships. However, the application of these methodologies requires the explicit characterization of all relevant variables. This requires much more data than is typically required using traditional design methods.

The purpose of this commentary is to make the reader aware of the limitations of the methods presented, the implications of the key assumptions and outline some of the progress being made in improving load prediction techniques. The primary interest is in the Level 3 methods that are based on long-term estimation using spectral techniques. The Level 2 methods are semi-empirical in character and their limitations are evident from the limited data sets upon which their load estimation expressions are based.

The key issues in regard to wave loading in the context of damage tolerance assessment can be categorized as follows:

- Arbitrary assessment periods;
- Non-linearities in the wave/load relationship.

Each topic is discussed in turn.

B.2.7.1. Arbitrary Assessment Periods

Virtually all the research in the application of direct methods of wave load calculation has been focused on the lifetime of the ship. In the present context, damage tolerance assessments will be required for shorter periods of duration, perhaps measured in days or weeks. This presents a particular problem because all the methodologies, and the supporting data, have been developed in a framework in which the duration is measured in tens of years.

As discussed by Chen and Shin [Ref B.3] the spectral approach is considered the most appropriate method for fatigue calculations, and, by extension it is reasonable to suggest that is also so for damage tolerance assessment. A key advantage of the spectral approach is its flexibility, in principle, in handling durations of arbitrary length.

Having said that, however, it must be noted that the wave climate data, as exemplified by the typical scatter diagram, is a variable quantity itself. This is much less an issue when 20 or 30 years is the time scale of interest. The problem of using typical wave scatter data for limited duration assessments can only be resolved by further investigation. A related issue in applying the spectral approach is the discretization of wave climate into histograms of wave height and period. Changes between sea states naturally occur gradually. The impact of discretization on the estimate of extreme load does not appear to have been investigated. Time-domain programs could presumably be employed to investigate this aspect.

A recent Ship Structure Committee project [Ref. B.7] has developed sea operational profiles from ship's log data. A major element of the project was the development of operational profiles for arbitrary periods of duration. The statistical variability of the profiles was also established; to provide data for future reliability analyses. While the results of this project, to some extent, were intended to alleviate the current uncertainty in regard to wave load estimates for short- and medium-term time scales, one finding was that observed wave data (from ship's observations at specific times and locations) differ significantly from generalised wave statistics such as those of Reference B.6.

B.2.7.2   Non-linearities in the Wave-Load Relationship

There are other fundamental assumptions made in applying the spectral method. The principle one is linearity in the wave-load relationship as expressed by response amplitude operators (RAO). This may be acceptable for fatigue damage estimation because, generally, moderate seas cause the most fatigue damage. However, the assumption of linearity in computing extreme wave loads is questionable particularly for fast fine-formed ships.

Response amplitude operators (RAO's) are normally developed through model-scale experiments or numerically using computer programs based on strip theory. Several such programs have been developed over the years [e.g., Refs. B.12 and B.13].

The most general of these programs yield RAO's for ship motion parameters and also bending moments and shear forces. A key assumption in virtually all such programs is that of linearity. In particular, the oscillatory motion is assumed to be linear and harmonic. For ships with a vertical plane of symmetry through the ship centreline, the vertical response is assumed to be uncoupled to lateral responses. Despite these severe assumptions, linear strip theory generally yields good agreement between numerical prediction and corresponding full- and model-scale measurement for moderate seas. In severe seas, the wave excitation and the ship response are both non-linear. Because of the wall-sided assumption in linear strip theory the predicted hog and sag bending moments are identical; measurements indicate the sag moments are generally numerically greater than the hog moments. The tendency is for linear strip theory to under-predict the sag moments and over-predict the hog moments.

The prediction of wave loads on ships is an active area of research. As such, providing guidance that is generally applicable is problematic. However, it is reasonable to suggest that for slow full-bodied ships, the predictions of linear strip theory are adequate. Predicting wave loads on faster, finer ships will, in general, require more sophisticated approaches where phenomena such as slamming may need to be accounted for. These observations apply primarily to estimation of the extreme load. In the case of fatigue, the limitations of linear strip theory are much less serious. This topic was investigated by Chen and Shin in Reference B.3 and they conclude that there is a "strong argument" that linearity can be assumed for the purpose of fatigue assessment.

Various corrections have been applied to the linear theory to improve prediction in extreme seas. One of the more successful has been the use of second order strip theory. Second order terms arise from the wave excitation and the angle with the vertical of the side of the ship (zero in linear strip theory). Such a theory was developed by Jensen and Pederson [Ref. B.28]. Mansour developed a simple method for correcting the results of linear strip theory. The method is described in a series of papers and in summary form in a recent SSC report [Ref. B.29]. Three dimensional panel programs [e.g., Ref. B.14] and time domain simulation programs are other approaches into which research is being conducted.

The possibility of slamming exists particularly for faster, finer-formed ships. The Level 2 methods presented account for this phenomenon either explicitly or implicitly. The spectral method is not a convenient framework within which to account for such effects. Specialist programs are available to compute slamming loads. Alternatively, simple multipliers can be applied as described in Reference B.17.

The spectral approach is a demanding methodology in terms of data and tools required. It is not always to appropriate, or possible, to employ an analysis of this detail. Therefore, alternative much simpler methods of lead estimation have been presented. The primary limitation that these methods suffer from is the question of their applicability beyond the ship types upon which their expressions are based. While such methods developed from the Class Societies are quite comprehensive, other methods generally only address vertical hull girder bending.

B.3   STRESS ANALYSIS

B.3.1   Scope of Stress Analysis

Section B.2 outlined several approaches for estimating the statistical distributions, or spectra, of ship loads over a given assessment interval. Section B.2 also outlined how maximum local stresses and the spectrum of the local stress range history may be obtained from the combination of load distributions. This requires the development of local stress coefficients, A_i, which relate the local stresses required for the damage tolerance assessment to the global hull girder bending moments, external sea pressures acting on the hull, and internal pressures acting on the tank boundaries.

The stress coefficients are evaluated by calculating the local field stresses at the point of interest for a unit value of each load component (e.g., vertical, horizontal and torsional bending moment loads, internal and external pressure loads). In general, this will involve conducting stress analyses for unit loads considering each type of loading individually. Strictly, the stress coefficients are a function of wave frequency. However, it appears from Reference B.2, that it is acceptable practice to compute stress coefficients for one particular wave frequency, and/or heading, and apply it to all wave frequencies and/or headings. The total stress spectrum at the location of interest can then be estimated by combining the stress coefficients and load spectra using the methods outlined in Section B.2.

The damage tolerance analysis procedures for residual strength and residual life assessment also require the determination of certain crack driving forces which are used to describe the crack behaviour in fracture and fatigue. Residual strength assessment requires the maximum value of the stress intensity factor (K_I) and the local effective net section stress (σ_n) expected within the assessment interval. For a given crack size, the stress intensity factor is proportional to the local stress state at the crack location (see Section B.3.4). Hence the maximum stress intensity factor can be related to the maximum stress obtained for the extreme loading condition in the assessment interval, bearing in mind that local residual stresses may have to be taken into account. Residual life assessment requires the stress intensity factor range (ΔK) spectrum which is in turn related to the local stress range spectrum ($\Delta \sigma$) for the assessment interval (see Part C).

This section outlines methodologies to determine the local stresses from unit loads (hence determining the stress coefficients), as well as methods of determining the effective net section stresses and stress intensity factors required for damage tolerance assessments.

B.3.2 Definition of Stress Categories

Damage tolerance assessment procedures for fatigue and fracture require knowledge of the stress field local to the crack. The stresses to be considered may be treated directly, or after resolution into four components as shown in **Figure B.3.1** and described below.
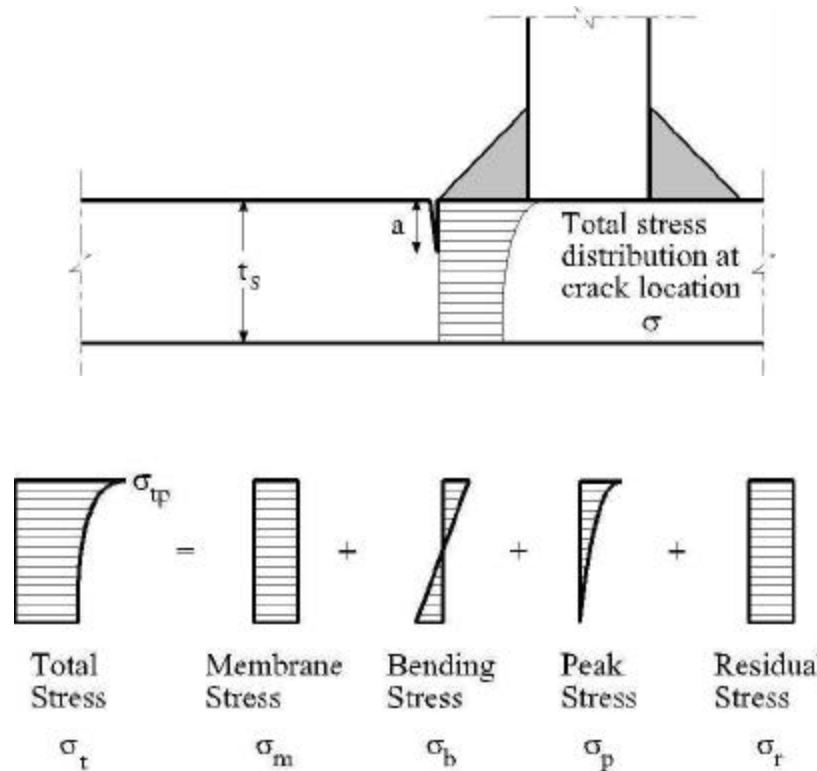

Figure B.3.1: Stress Components in a Welded Joint

(a) Local Nominal Membrane and Bending Stress (σ_m and σ_b): The local nominal membrane stress is the uniformly distributed stress that is equal to the average value of stress across the section thickness. The local bending stress is the component of nominal stress due to applied loading that varies linearly across the section thickness. The nominal stresses satisfy the simple laws of equilibrium of forces and moments from applied loads. They may be derived from simple formulae, beam element models, or coarse mesh finite element analysis (FEA) as described in Section B.3.4. The term local nominal stress is used because stress concentrations resulting from the gross shape of the structure surrounding the local detail under consideration will affect the magnitude of the local field stresses (e.g., shear lag effects) and must be included in the local nominal stresses.

(b) Peak Stress (σ_p): is the component of stress due to applied loads due to stress concentrations at local discontinuities in the vicinity of the crack. The peak stress represents the highest value, usually at the surface at a notch (e.g., weld toe). Peak stresses arise from stress concentrations due to the following effects:

- Geometric Stress Concentrations (K_g): due to the gross geometry of the detail considered. The effect of the geometric stress concentration typically decays over distances of the order of the section thickness.

- Notch Stress Concentrations (K_w): due to the local geometry of the notch (e.g., weld geometry). The effect of the notch stress concentration typically decays over distances of the order 10% to 20% of the section thickness.

- Misalignment Stress Concentrations (K_{te}, $K_{t\alpha}$): Due to bending stresses caused by misalignments including eccentricity tolerance (K_{te}), and angular mismatch ($K_{t\alpha}$). These are normally used for plate connections only. The effect of the misalignment stress concentrations typically decays over distances of the order of the section thickness.

(c) Residual Stresses (σ_r): are local self-equilibrating stresses that arise from fabrication and welding. In general, residual stresses are strain/displacement limited phenomena and, as such, do not contribute to plastic collapse if they relax. However, they do add to the tensile stress field in the vicinity of the crack and have to be included in the calculation of the stress intensity factor for residual strength assessment. Residual stresses may also be resolved into membrane and bending components. However, since there is only limited quantitative data on the distribution of welding residual stresses in ship structural details, it is normal practice to assume a uniform (membrane) residual stress field near tensile yield strength (i.e., $\sigma_r \approx \sigma_y$). This is discussed further in Section B.3.5.3.

(d) Total Stress: is the total sum of the various stress components. The maximum value of total stress at the crack location is referred to as the peak total stress (σ_{tp}). The peak total stress can be evaluated by:

$$\begin{aligned} \sigma_{tp} &= \sigma_m + \sigma_b + \sigma_p + \sigma_r \\ &= K_g \cdot K_w \cdot (K_{te} \cdot K_{t\alpha} \ \sigma_m + \sigma_b) + \sigma_r \end{aligned} \tag{B.3.2.1}$$

In the residual strength assessments the value of total peak stress is conservatively assumed to be uniformly distributed through the plate thickness. Other levels of assessment for fracture and fatigue require taking into account the variation of stress through the load bearing section containing the crack as discussed in Section B.3.4.

The nominal membrane, bending and peak stress components due to applied loadings (excluding residual stresses) may be derived, for a given stress distribution $\sigma(x)$ for $x = 0$ at the surface to $x = t_s$ (through the thickness) by the following analytical expressions [Ref. B.32]:

$$s_m = \frac{1}{t_s} \int_0^{t_s} s(x) \cdot dx \qquad (B.3.2.2)$$

$$s_b = \frac{6}{t_s} \int_0^{t_s} s(x) \cdot \left(\frac{t_s}{2} - x \right) \cdot dx \qquad (B.3.2.3)$$

$$s_p(x) = s(x) - s_m - s_b(x) \qquad (B.3.2.4)$$

B.3.3 Determination of Stresses and Stress Coefficients

B.3.3.1 General

As with other elements of the calculations, there are a number of approaches with varying degrees of complexity and accuracy that can be used to calculate the stresses (or stress coefficients) required for damage tolerance assessments. The approach employed should, in general, be consistent with the complexity and accuracy applied to other elements of the assessment process.

The simplest level of fracture assessment is based on the peak total stress (σ_{tp}) at the crack location as defined in Equation B.3.2.1 and Figure B.3.1. This approach is suitable for a basic screening assessment, and it is preferable that the stress analysis be kept as simple as possible. The simple approach is to calculate nominal global stresses at the stations of interest using the computed hull girder bending moments and shear forces and the relevant sectional properties.

Estimates of stress can be improved somewhat to account for gross effects such as shear lag, openings in decks and the effect of the superstructure using various rules of thumb. Hughes [Ref. B.33] discusses methods of accounting for some of these effects. The total stress at the crack site can then be estimated from available stress concentration factors (i.e., K_w, K_g, K_{te} and $K_{t\alpha}$) for ship details. Alternatively, a combination of coarse mesh finite element methods and available stress concentration factor (SCF) solutions may be used to calculate the peak total stress.

The higher levels of assessments for fatigue and fracture require a more accurate description of the actual stress distribution. When published solutions are used for evaluating stress intensity factors (SIF) (see Section B.3.6.2.2), it is usually sufficient to determine the local nominal

---

membrane and bending stress components (i.e., σ_m and σ_b), and residual stresses (i.e., σ_{rm} and possibly σ_{rb}).

The effects of the local structural geometry (i.e., K_g and K_w, but not stress concentrations due to misalignments) are normally taken into account by the stress intensity magnification factor (M_k) used to determine the SIF. The M_k factor is defined as:

$$M_k = (K \text{ for crack in welded detail}) / (K \text{ for same crack in a flat plate}) \qquad \text{(B.3.3.1)}$$

In the limit, for crack depths approaching zero, it can be shown that the M_k factor is equal to the product of the notch and geometric SCF.

$$M_k = K_w \cdot K_g \qquad \text{as crack depth a} \rightarrow 0 \qquad \text{(B.3.3.2)}$$

The local nominal stresses may be calculated based on global nominal stresses and available factors for global stress concentrations and misalignment effects. Alternatively, coarse mesh FEA that accounts for gross stress concentrations and secondary bending stresses may be used to derive local nominal stresses at the crack location. Where M_k factors are available, it is not necessary to model the local geometry of the detail in the coarse mesh FEA.

Where appropriate SIF and M_k solutions are not available, finite element or weight function methods can be used. When weight function methods are used, the actual stress distribution due to applied loads may be derived from local fine mesh FEA of the uncracked detail, upon which an assumed residual stress distribution can be superimposed to calculate the SIF. When finite element methods are used to compute the SIF, the local detail including the crack is modelled. The actual total stress distribution at the crack location is, therefore, accounted for directly in the calculation of the SIF, although it is usually difficult to include residual stresses in the FEA. The application of weight function and finite element methods for determining stress intensity factors is described in Section B.3.5.2.

B.3.4 Determination of Local Nominal Stresses

As discussed in B.3.2, the local nominal stresses are defined as the stresses that would be calculated in the section containing the crack, in the absence of the crack and the stress concentration due to the local structural detail and weld. This is to say, the local nominal stresses include the stress concentration effects of the overall geometry of the structure surrounding the detail, but not the detail itself.

The local nominal stresses may be calculated, for unit loads, using a combination of parametric formulae for simple structural assemblies and global stress concentration factors to account for the gross geometry of the structure and effects of misalignment. Alternatively, frame models or coarse mesh global FEA may be used to obtain a more precise estimation of the local nominal stresses. The following subsections outline methodologies for evaluating the local nominal stresses using these approaches.

B.3.4.1   Level 2 Approach to Stress Analysis

Calculation of hull girder stresses is the simplest way of getting reasonable approximations to the stress levels in longitudinal hull girder elements and connections and can be used for quick evaluation of stress levels in important details. This approach is most suitable for a Level 2 screening assessment. Global hull girder stresses may be calculated based on gross scantlings. Local stress components should be calculated based on net scantlings, i.e., gross scantlings minus corrosion allowances.

Formulae for calculating hull girder stresses are included in Classification Society Rules. Alternatively, the following formulae derived from those presented in Reference B.26 may be used.

B.3.4.1.1   *Primary Hull Girder Bending*

For Vertical Bending $\sigma_{1,v} = K_G \cdot M_v \cdot Z_{na} / I_v$ (B.3.4.1)

For Horizontal Bending $\sigma_{1,h} = K_G \cdot M_h \cdot y_{na} / I_h$ (B.3.4.2)

B.3.4.1.2   *Stresses due to Internal and External Pressure Loads*

Local secondary bending stresses are the results of bending, due to lateral pressure, of stiffened single skin or double hull cross-stiffened panels between transverse bulkheads (see **Figure B.3.2**). This may be bottom or deck structures, sides or longitudinal bulkheads.

The preferred way of determining secondary stresses is by means of FEA or frame analysis models. Alternatively, secondary bending stresses may be estimated from parametric equations such as the following equations recommended in Reference B.26. Similar equations are given in Reference B.18.

(a)   Longitudinal Secondary Bending Stress in Double Bottom Panels

Longitudinal secondary bending stresses in double bottom panels at the intersection of transverse bulkheads may be estimated by the following formulae**:**

Double Bottom Wider than Long (b > a): Case 1 and 2, **Table 3.1**
          $\sigma_2 = (K_b \cdot p \cdot b^2 \cdot r_a) / \sqrt{(i_a \cdot i_b)}$ $\rho = (a/b) \cdot (i_a / i_b)^{1/4}$ (B.3.4.3)

Double Bottom Longer than Wide (a > b) : Case 3 and 4, Table 3.1

$$\sigma_2 = (K_b \cdot p \cdot a^2 \cdot r_a) / i_a \qquad\qquad \rho = (b/a) \cdot (i_b / i_a)^{1/4}$$

(B.3.4.4)

where :
$$i_a = I_a/s_a \text{ and } i_b = I_b/s_b$$

(b)   Transverse Secondary Bending Stress in Double Bottom Panels

Transverse secondary bending stresses in double bottom panels at the intersection of transverse bulkheads may be estimated by the following formulae.

Double Bottom Longer than Wide (a > b) : Case 3 and 4, Table B.3.1

$$\sigma_2 = (K_b \cdot p \cdot b^2 \cdot r_b) / i_b \qquad\qquad \rho = (a/b) \cdot (i_b / i_a)^{1/4} \qquad\qquad \text{(B.3.4.5)}$$

Double Bottom Wider than Long (b > a) : Case 1 and 2, Table B.3.1

$$\sigma_2 = (K_b \cdot p \cdot b^2 \cdot r_a) / i_a \qquad\qquad \rho = (b/a) \cdot (i_b / i_a)^{1/4} \qquad\qquad \text{(B.3.4.6)}$$

(c)   Secondary Bending Stress in Single Skin Panels

The stresses at transverse and longitudinal bulkheads may be estimated from the same formulae as for double bottom configurations. However, the parameters ρ and torsion coefficient η should be taken as given in **Table 3.2** (also see **Table 3.3**).

(d)   Bending Stress of Stiffeners Between Transverse Supports (e.g., Frames, Bulkheads)

The local bending stress of stiffeners with effective flange between transverse supports may be estimated by:

$$s_b = K \cdot \left(\frac{M}{Z_s} \right) + \left(\frac{m_d EI}{\ell_e^2 Z_s} \right) r_d \cdot d \qquad\qquad \text{(B.3.4.7)}$$

where

M   = moment at stiffener support = $\left(\dfrac{ps\ell_e^2}{12} \right) r_p$

p   = lateral pressure (external or internal pressure load) - taken as unity for evaluation of stress coefficients).

r_δ $= 1 - 2\left(\dfrac{x}{\ell_e} \right)$

r_π $= 6\left(\dfrac{x}{\ell_e} \right)^2 - 6\left(\dfrac{x}{\ell_e} \right) + 1$

K   = stress concentration factor

m_δ = 4.4 at the bulkhead where no stringers or girders support the frames adjacent to the bulkhead; else m_δ must be determined from a beam element analysis.

It is of great importance for reliable assessments that bending stresses in longitudinals caused by relative deformation between supports are not underestimated. The appropriate value of relative deformation, δ, has to be determined for each particular case (Figure **B.3.4**). This usually will require 2-D or 3-D frame analysis or coarse mesh FEA.

(e)   Tertiary Bending Stress of Plates Bounded by Stiffeners

The local longitudinal tertiary plate bending stress in the weld at the plate/transverse frame/bulkhead intersection midway between longitudinals is given by:

$$\sigma_{b,\ell} = 0.343 \cdot p \cdot (s / t_n)^2 \qquad\qquad (B.3.4.8)$$

Similarly the transverse stress at stiffener mid length is:

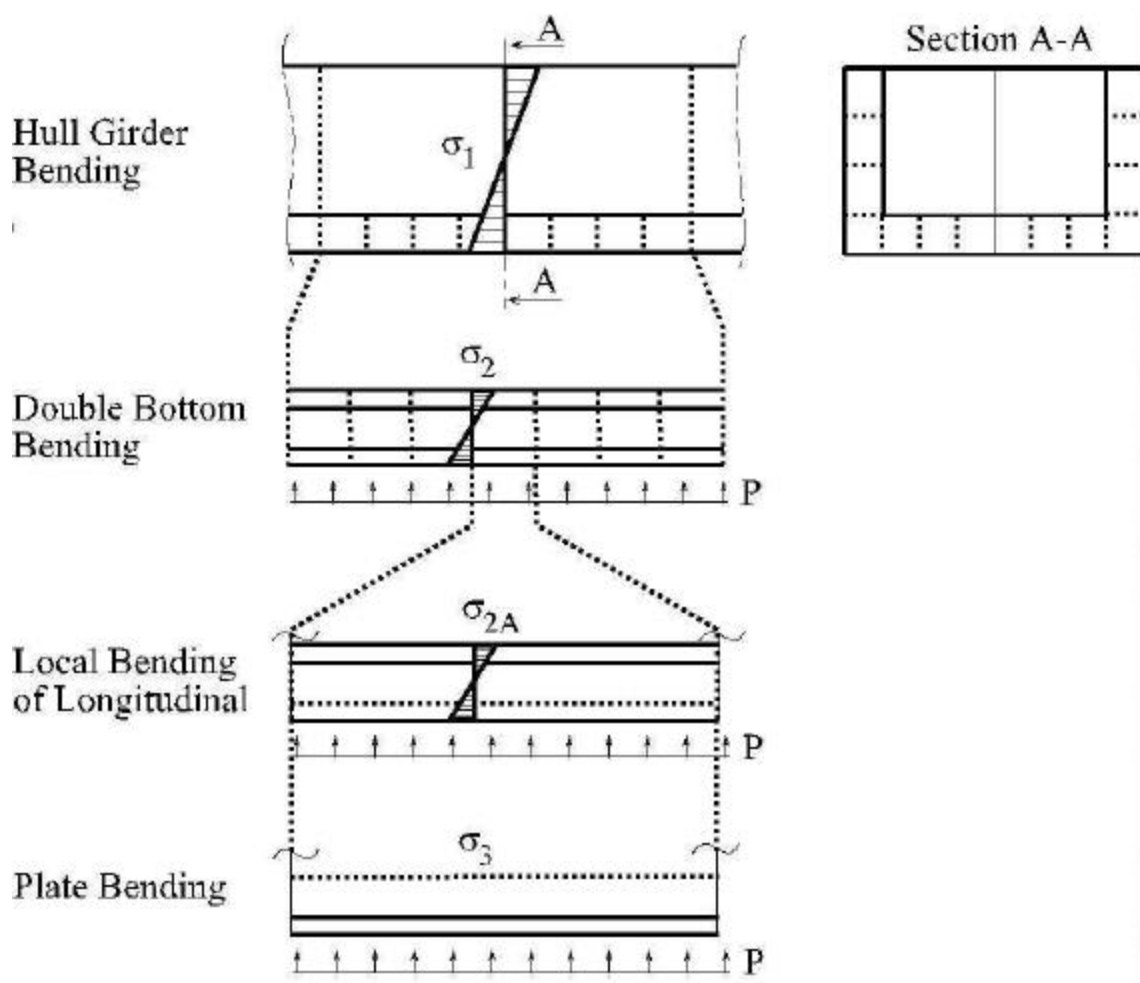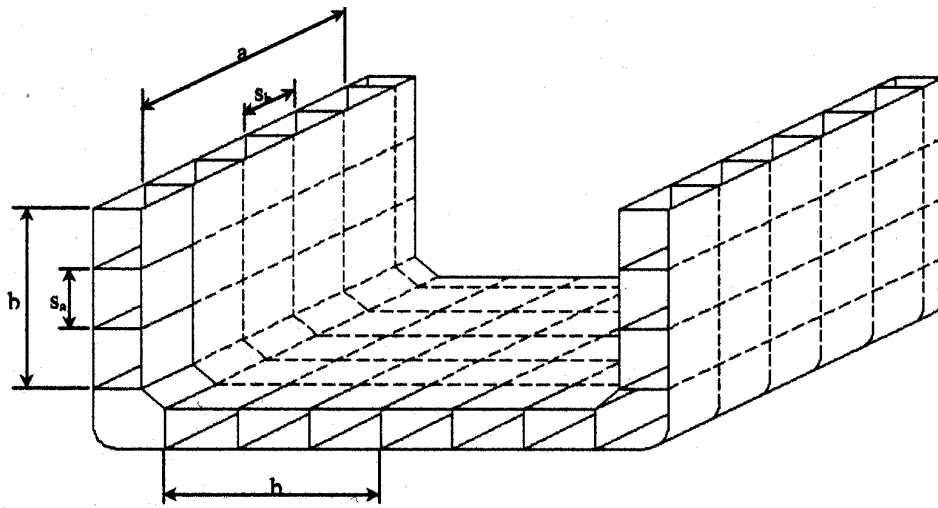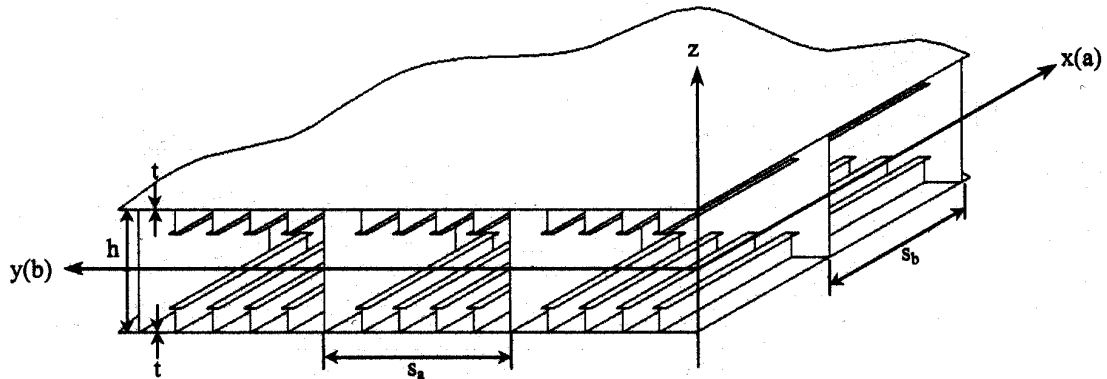$$\sigma_{b,t} = 0.5 \cdot p \cdot (s / t_n)^2 \qquad\qquad (B.3.4.9)$$
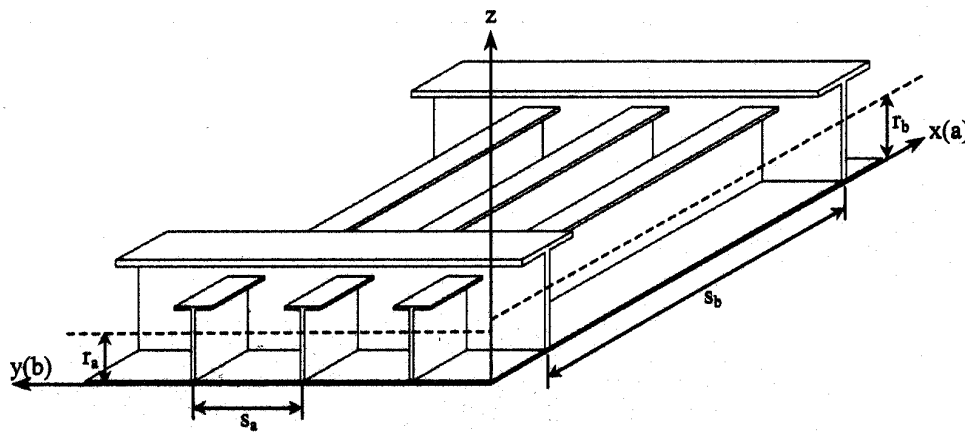
Figure B.3.2: Simplified Stress Analysis of Hull Girder [Ref. B.2]
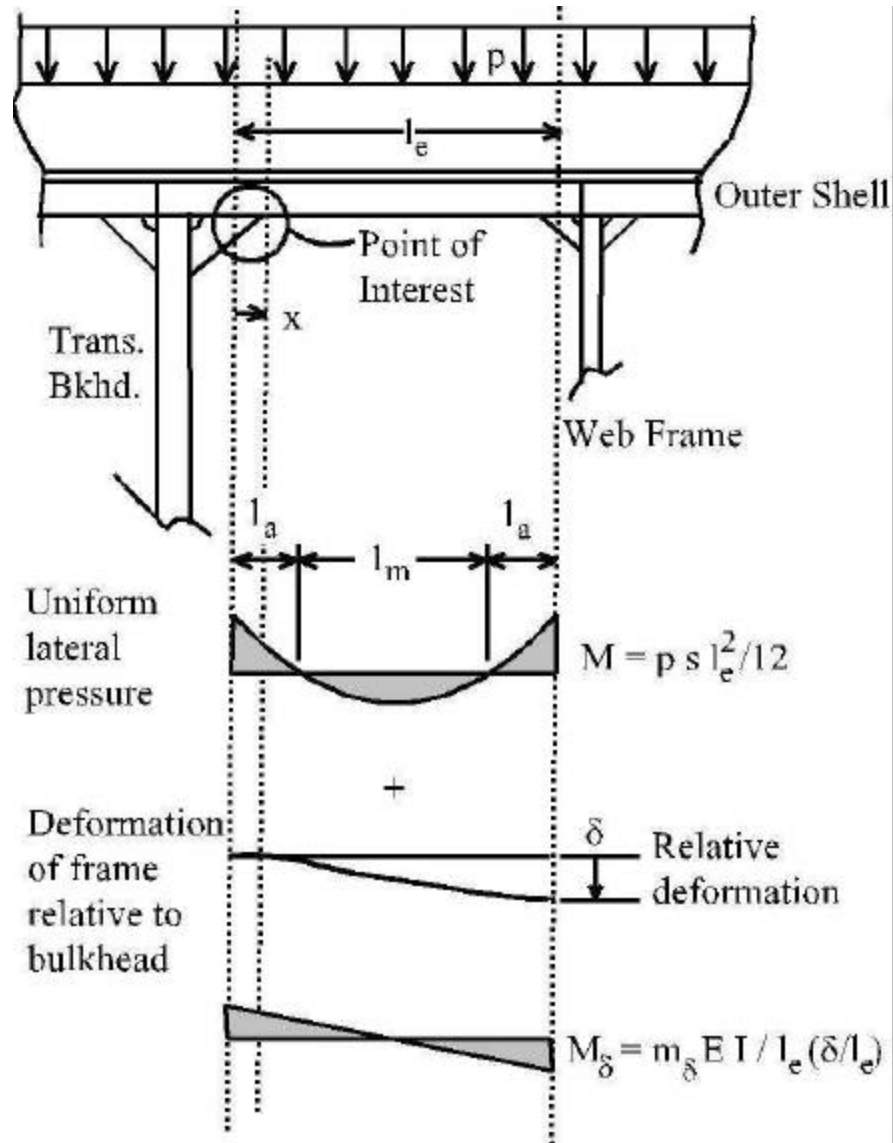
(a) Double Skin Configuration

(b) Double Bottom Configuration

(c) Single Bottom Configuration

Figure B.3.3: Definition of Geometric Parameters for Hull Configurations [Ref. B.2]

Note: l_e is the same as ℓ_e in the previous equations

Figure B.3.4: Stresses in Stiffener [Ref. B.2]

Table B.3.1: Support Bending Stress Coefficients K_b - Double Bottom Panels [Ref. B.2]

(For intermediate values, use linear interpolation)

Case No. & Stress Location	Boundary Conditions	ρ	$\eta = 0.0$	$\eta = 0.5$	$\eta = 1.0$
Case No. 1: Support bending stress in *long* direction at middle of short end	Long edges: Simply supported Short ends: Clamped	1.00	0.0952	0.0845	0.0767
		1.25	0.1243	0.1100	0.0994
		1.50	0.1413	0.1261	0.1152
		1.75	0.1455	0.1342	0.1251
		2.00	0.1439	0.1371	0.1300
		2.50	0.1388	0.1381	0.1356
		3.00	0.1371	0.1376	0.1369
		3.50	0.1371	0.1373	0.1373
		4.00	0.1373	0.1374	0.1373
		& up	0.1374	0.1374	0.1374
Case No. 2: Support bending stress in *long* direction at middle of short end	All edges: Clamped	1.00	-	-	0.0564
		1.10	-	-	0.0591
		1.20	-	-	0.0609
		1.30	-	-	0.0619
		1.40	-	-	0.0624
		1.50	-	-	0.0626
		1.60	-	-	0.0627
		& up	-	-	0.0627
Case No. 3: Support bending stress in *short* direction at middle of long edge	Long edges: Clamped Short edges: Simply supported	1.00	0.0952	0.0845	0.0762
		1.33	0.1026	0.0949	0.0878
		2.00	0.0972	0.0950	0.0926
		2.66	0.0920	0.0925	0.0922
		4.00	0.0912	0.0915	0.0917
		& up	0.0916	0.0916	0.0916
Case No. 4: Support bending stress in *short* direction at middle of long edge	All edges: Clamped	1.00	-	-	0.0564
		1.10	-	-	0.0638
		1.20	-	-	0.0702
		1.30	-	-	0.0755
		1.40	-	-	0.0798
		1.50	-	-	0.0832
		1.60	-	-	0.0857
		1.70	-	-	0.0878
		1.80	-	-	0.0892
		1.90	-	-	0.0903
		2.00	-	-	0.0911
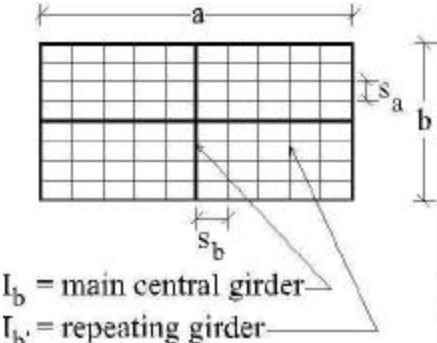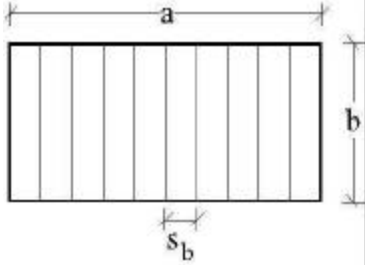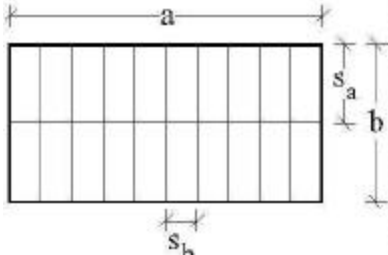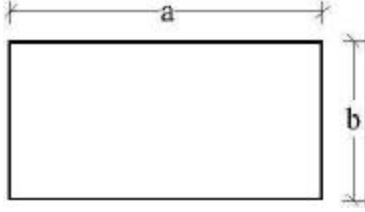
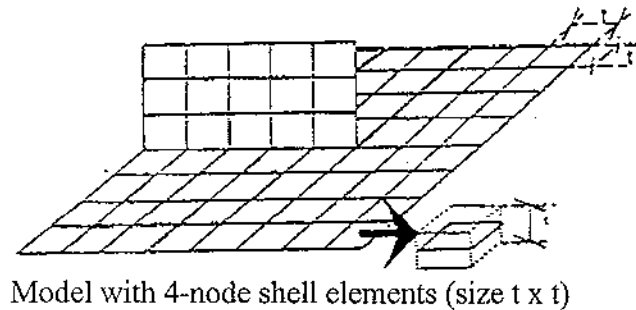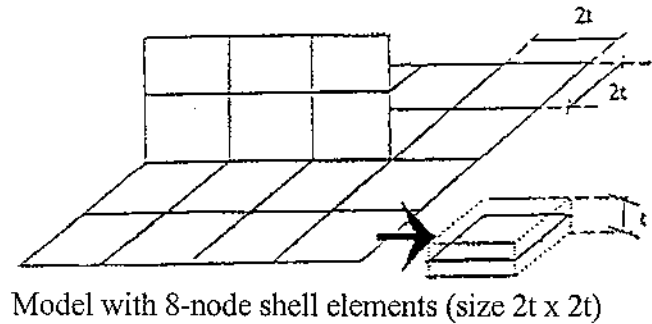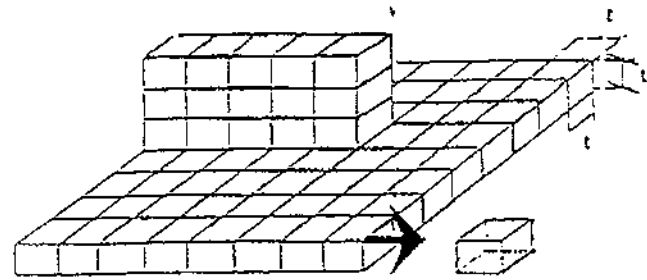|		& up	-	-	0.0911

Table B.3.2: Support Bending Stress Coefficients K_b - Single Skin Panels [Ref. B.2]

(For intermediate values, use linear interpolation)

Case No. & Stress Location	Boundary Conditions	ρ	$\eta = 0.0$	$\eta = 0.5$	$\eta = 1.0$
Case No. 5: Support bending stress in *long* direction at middle of short end	Long edges: Simply supported Short ends: Clamped	1.00 1.25 1.50 1.75 2.00 2.50 3.00 3.50 4.00 & up	0.0866 0.1140 0.1285 0.1324 0.1310 0.1263 0.1248 0.1248 0.1240 0.1250	0.0769 0.1001 0.1285 0.1324 0.1310 0.1263 0.1248 0.1248 0.1240 0.1250	0.0698 0.0904 0.1049 0.1139 0.1191 0.1234 0.1246 0.1246 0.1250 0.1250
Case No. 6: Support bending stress in *short* direction at middle of long end	Long edges: Clamped Short ends: Simply supported	1.00 1.33 2.00 2.66 4.00 & up	0.0866 0.1934 0.0885 0.0837 0.0830 0.0834	0.0769 0.0858 0.0865 0.0842 0.0832 0.0834	0.0698 0.0799 0.0843 0.0839 0.0835 0.0834

Table B.3.3: Definition of Stiffness and Geometry Parameters [Ref. B.2]

Type	Sketch	Formulas for ρ and η
A: Cross stiffening Middle girder/stiffener in both directions are stiffer than the others	 I_b = main central girder $I_{b'}$ = repeating girder	$i_a = \dfrac{I_{na'}}{s_a} + 2\left(\dfrac{I_a - I_{na'}}{b}\right)$ $i_b = \dfrac{I_{nb'}}{s_b} + 2\left(\dfrac{I_b - I_{nb'}}{a}\right)$ $r = \dfrac{a}{b}\sqrt[4]{\dfrac{i_b}{i_a}}$ $h = \sqrt{\dfrac{I_{pa}I_{pb}}{I_{na}I_{nb}}}$
B: Modified cross stiffening One girder/stiffener in a-direction only		$i_a = 2\dfrac{I_a}{b}$ $i_b = \dfrac{I_{nb}}{s_b} + 2\left(\dfrac{I_b - I_{nb}}{a}\right)$ $\rho = \dfrac{a}{b}\sqrt[4]{\dfrac{i_b}{i_a}}$ $\eta = 0.124\sqrt{\dfrac{I_{pb}{}^2 b}{I_a I_{nb} S_b}}$
C: Single stiffening Girders/stiffeners in b-direction only		$i_a = 0$ $i_b = \dfrac{I_{nb}}{s_b}$ $\rho = \inf inite$ $\eta = in\,det\,er\,min\,ate$
D: Unstiffened plate		$i_a = i_b = \dfrac{t^3}{12(1 - \upsilon^2)}$ $\rho = \dfrac{a}{b}$ $\eta = 1.0$

Structural Detail

Model with 20-node solid elements (size t x t x t)

Model with 8-node shell elements (size 2t x 2t)

Model with 4-node shell elements (size t x t)

Element Type	Element Size
20 – node isoparametric solid element	t x t x t
8 – node quadrilateral isotropic shell element	2t x 2t
4 – node quadrilateral isotropic shell element	t x t

**Figure B.3.7: Examples of Local Detail FEA with Recommended Element Sizes
[Ref. B.2]**

Normally, the element stresses are derived at the Gaussian integration points. Depending on the element type, it may be necessary to perform several extrapolations in order to determine the stress at the weld toe. Referring to **Figure B.3.8**, all stress components are used for the extrapolation. The process is as follows:

- Extrapolate the stresses to the surface from the Gauss points based on the assumed distribution function in the element (some FE programs will provide this on request.
- Extrapolate surface stress to a line A-B centred on the hot spot of interest;
- Calculate stress along line A-B at reference points taken at t/2 and 3t.2 from hot spot;
- Linearly extrapolate through reference points t/2 and 3t/2 to determine stress at hot spot;
- Having extrapolated stress components for the hot spot, the principal stresses are calculated at that location for fatigue analysis.

The substructure technique ensures that forces and deformations in the global and local models are compatible and, if the substructure is detailed enough, local stress results may be obtained directly. The substructure technique is very effective where local structural assemblies (i.e., the substructure) are repeated several times in the overall assembly, but it does present added complexity into the analysis.

More commonly, the global and local analyses are conducted separately. Nodal forces and/or displacements obtained from the global model are applied as boundary conditions for the local model. In general the stiffness of the local model should be comparable to that of the global model representation so that forces and displacements between the two models are compatible. However, due to the greater level of geometric detail and mesh refinement of the local model, this is rarely achievable. As such it is preferable that nodal forces be transferred from the coarse model to the local model rather than forced displacements. It is important that the extent of the local model is sufficiently large that boundary effects due to prescribed forces or displacements are away from the areas where accurate stresses need to be determined.

The loads to be applied in the global analysis can be produced using any of the methodologies presented in Section B.2. The global analysis should be conducted for each load case (i.e., vertical bending, horizontal bending, torsional bending, external pressure, internal pressure) individually. Each load case should be analyzed for a unit value of the applied load at the location being considered. In this manner, the stresses derived from subsequent local analysis will correspond to unit loading and therefore be equal to the stress coefficients, A_i , which are required to generate the local stress spectrum from the combined loading spectra.
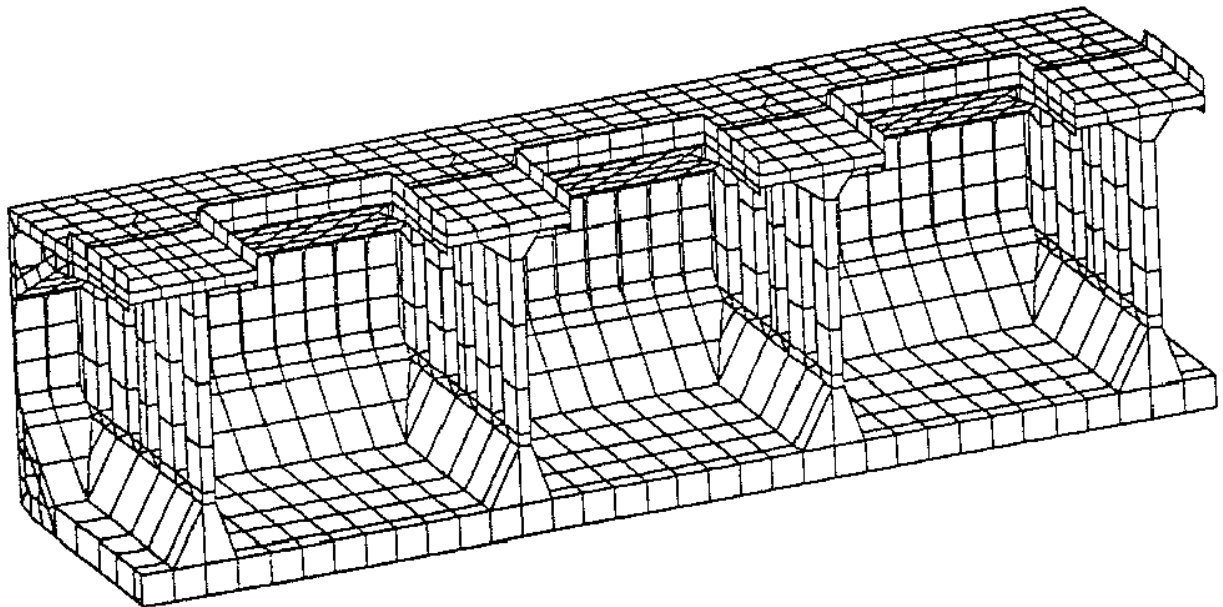

Figure B.3.5: Global Finite Element Model of Bulk Carrier [Ref. B.18]

B.3.5   Determination of Peak Stresses

Peak stresses may be estimated based on parametric approximations of stress concentration factors for ship details, when these are available. Alternatively, they may be determined based on local fine mesh FEA stress analysis of the joint. Peak total stress is determined from Equation B.3.2.1.

B.3.5.1   Stress Concentration Factors for Ship Details

Stress concentration factors (SCF) for a range of details typical of ship structures are given in such references as B.2,,B.18, B.34 and B.35.. Appendix A presents some solutions for notch stress concentrations (K_w). Stress concentration factors for typical ship structural details (K_g) and for misalignment effects (K_{te}, $K_{t\alpha}$) are presented in Appendix B.

The analyst must exercise extreme care when applying stress concentration factors from different sources to ensure that the correct definitions for nominal stress are used. For example, in some cases the nominal stress is defined at the intersection point of a connection, in other cases the global nominal stress may be defined at the weld toe or some distance form the weld toe.

Furthermore, the analyst should be aware that sometimes the published stress concentration factor solutions are designed to calculate the "hot spot" stress or the "notch" stress as opposed to the local nominal stress. The analyst should make certain which form of peak stress will result from the application of the SCF.

B.3.5.2   Local Finite Element Analysis

If appropriate stress concentration factors are not available, the total stress distribution including local peak stresses may be calculated by local FEA. The crack itself is usually not modelled unless the local FEA is going to be used to calculate stress intensity factors directly. As discussed previously in Section B.3.4.2, the extent of the local model should be large enough that the calculated results are not significantly affected by assumptions made for boundary conditions and application of loads.

Figure B.3.6 shows a local finite element model of a ship detail. The local model should have a relatively fine mesh, especially in areas of stress concentration. It is important to have a continuous and not too steep change in the density of the element mesh in the areas where the local stresses are to be analyzed. The geometry of the elements (aspect ratio, corner angles, skewness and warp) at the point of interest should be as near optimal as possible (for example: length/breadth aspect ratio less than 2, corner angles between 60° and 120°, avoid use of triangular elements).
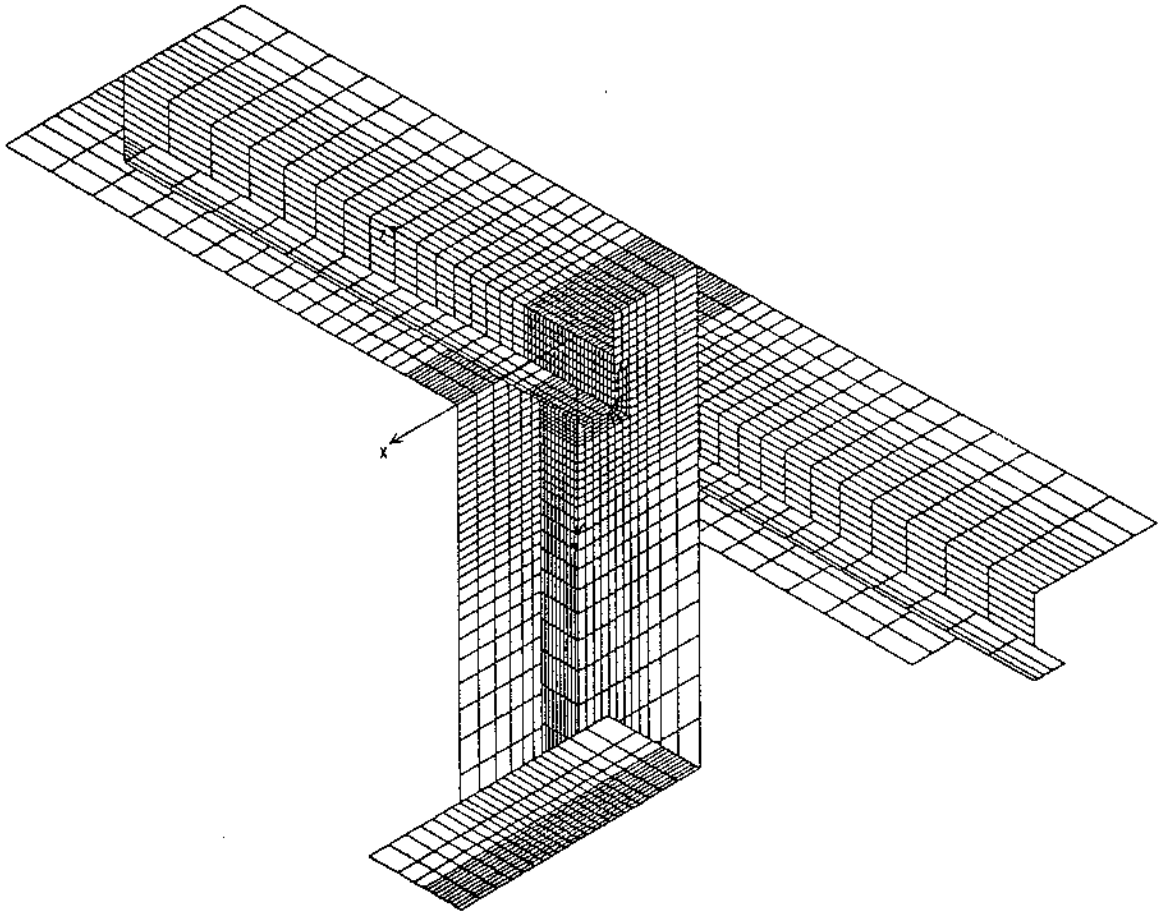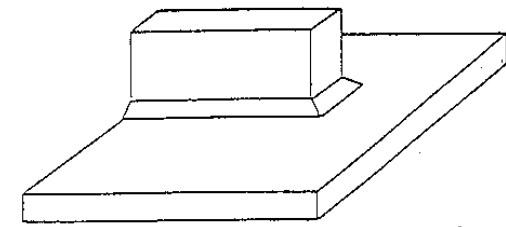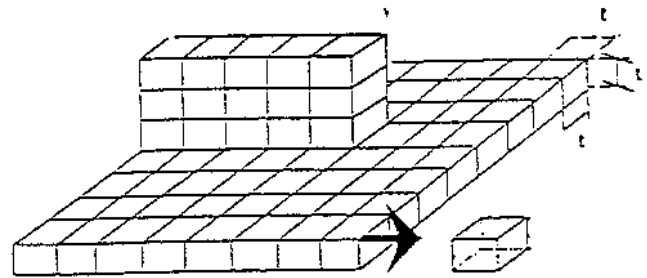
Figure B.3.6: Local Finite Element Model of Ship Detail [Ref. B.36]

Local FEA of a joint is usually conducted to determine the local nominal and hot spot stress at the location of interest, and seldom for direct evaluation of peak notch stress since the weld geometry itself is usually not modelled. If the peak notch stress has to be determined, then the most common approach is to use local FEA to evaluate the hot spot stress. The hot spot stress value is then factored by a weld notch factor, K_w , derived from parametric equations or tables (see Appendix A) to provide an estimate of the peak notch stress in the joint.

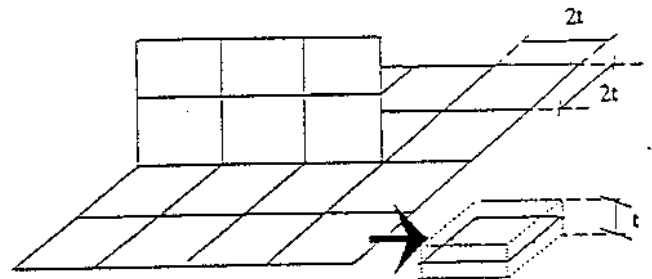Finite element size requirements in the stress concentration region are dependent on the type of element. The mesh size may be determined based on experience or by benchmark testing a similar mesh for a case where results have been presented in the literature. **Figure B.3.7** provides some guidance on element sizes for 20-node solid, 8-node shell and 4-node shell element types suitable for determining the hot spot stress.

Structural Detail

Model with 20-node solid elements (size t x t x t)

Model with 8-node shell elements (size 2t x 2t)

Model with 4-node shell elements (size t x t)

Element Type	Element Size
20 – node isoparametric solid element	t x t x t
8 – node quadrilateral isotropic shell element	2t x 2t
4 – node quadrilateral isotropic shell element	t x t

Figure B.3.7: Examples of Local Detail FEA with Recommended Element Sizes [Ref. B.2]

Normally, the element stresses are derived at the Gaussian integration points. Depending on the element type, it may be necessary to perform several extrapolations in order to determine the stress at the weld toe. Referring to **Figure B.3.8**, all stress components are used for the extrapolation. The process is as follows:

- Extrapolate the stresses to the surface from the Gauss points based on the assumed distribution function in the element (some FE programs will provide this on request.
- Extrapolate surface stress to a line A-B centred on the hot spot of interest;
- Calculate stress along line A-B at reference points taken at $t/2$ and 3t.2 from hot spot;
- Linearly extrapolate through reference points $t/2$ and $3t/2$ to determine stress at hot spot;

- Having extrapolated stress components for the hot spot, the principal stresses are calculated at that location for fatigue analysis.

If FEA is to be used to determine the notch stress, then it should be realised that an extremely fine mesh will be required in order to obtain accurate stresses (much more so than that required for the determination of hot spot stresses). The notch is a relatively severe form of stress concentration and stresses rise very rapidly as the notch root is approached. For example, the calculated stress in a linear elastic analysis of a right angle corner will approach infinity as the element size is decreased to zero. Therefore the local (micro) geometry of the notch (i.e., weld toe radius, angle, etc.) has to be included in the model to obtain reasonable stresses that account for this geometry. Since the notch radius is typically of the order of 1 mm (0.04") and at least one node per 15° of the notch arc radius is required for accurate stresses, a considerable degree of mesh refinement is required which results in a relatively large computer model. Some advantage can be taken by the fact that the effect of the notch on the stresses is very localized, typically only affecting stresses within 10% of the plate thickness (t) at a weld toe. The mesh need not be as refined outside this region, however care must be taken to ensure that the transition from the less refined region to the fine mesh region at the notch is smooth and does not affect the results of interest. Elements within 10% t of the weld toe should be as close to optimal shape as possible.

The stresses obtained from a 2-D or 3-D local FEA of a joint containing a notch are not evenly distributed through the plate thickness direction. The total notch stress can be separated into different components σ_m, σ_b, and σ_p using Equations B.3.2.2 to B.3.2.4.

B.3.5.3   Residual Stresses

Residual stresses caused by welding and fabrication are self-equilibrating stresses necessary to satisfy compatibility in the structure. These stresses in themselves do not contribute to plastic collapse since they arise from strain/displacement limited phenomena, and therefore do not influence the abscissa in the Failure Assessment Diagram (FAD) (S_r or L_r) (See Section A.3.5). However, residual stresses do add to the crack driving force and therefore have to be included in the calculation of K_{app} for residual strength assessments. Residual stresses need not be considered for fatigue since they are accounted for in the constants for the fatigue crack growth law.

Ideally, one would establish the residual stress magnitude based on actual measurements and resolve them into their membrane and bending components (i.e., σ_m and σ_{rb}). However that is impractical and, therefore, conservative estimates of residual stresses based on findings in the technical literature and on the location of the flaw (weld zone or base metal) and orientation with respect to the weld, are incorporated in the analysis.

The following guidelines can be used to estimate the magnitude of residual stresses to be incorporated into the residual strength assessment. As before, the approach depends on the level of fracture assessment being performed. The levels of assessment are referred to as Level 1 FAD, Level 2 FAD, etc., in accordance with the procedure in Reference B.37. Note that these levels of FAD analysis do *not* necessaril*y* correspond to the levels of complexity of

assessment of load, stress, etc., (Levels 2, 3 and 3b) described in the previous section and herein.
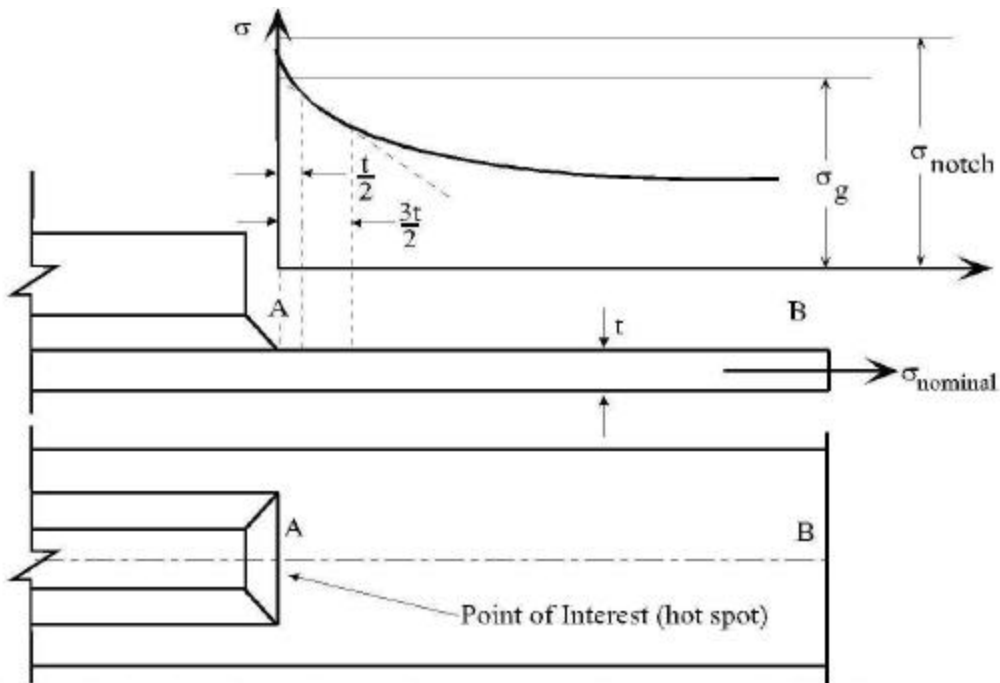
FE Model Hot Spot Stress Extrapolation when weld toe is modeled (i.e. brick elements)
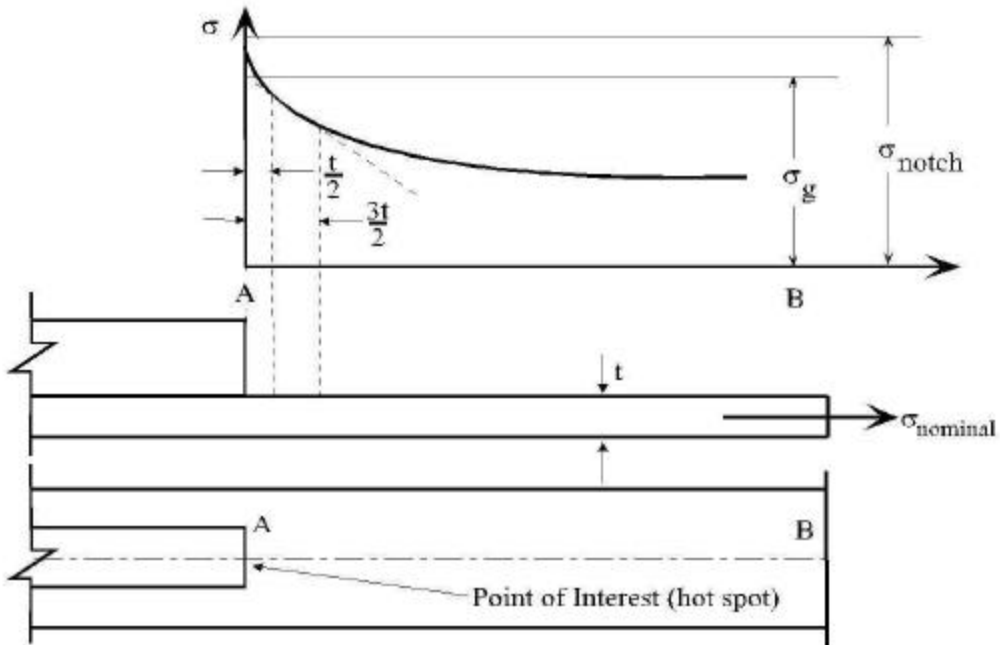
FE Model Hot Spot Stress Extrapolation when weld toe is not modeled (i.e. shell elements)

Figure B.3.8: Stress Distribution at an Attachment and Extrapolation of Stresses at Hot Spot

Level 1 FAD

- In the as-welded condition, and with the flaw plane transverse to the weld axis, tensile (weld longitudinal) residual stress is assumed to be the room temperature yield strength of the material in which the flaw tips are located. However, once the flaw tips grow out of the weld metal and the heat affected zone, and are about one plate thickness from the weld fusion line, the weld longitudinal stresses become compressive and may be neglected. For flaw planes parallel to the welding direction, the tensile (weld transverse) residual stress is assumed the lesser of the yield strengths of the base metal and the weld metal.

- If the welded assembly has been uniformly heated and cooled for a post-weld heat treatment (PWHT) to affect stress relief, then the residual stresses parallel to the weld (for flaws that are transverse to the weld axis) are assumed to be 0.3 times the weld metal yield strength. The residual tensile stresses after PWHT in a direction perpendicular to the weld are suggested to be 0.2 times the weld metal yield strength.

Level 2 FADs

- If the actual distribution of residual stresses is known, then these can be incorporated by linearizing the distribution such that the assumed residual stresses are greater than the actual (measured) stresses over the flaw depth. The linearized residual stress distribution can then be separated into its membrane and bending components.

- A reasonable estimate of residual stresses can be based on some typical residual stress distributions given in Reference. B.37 for butt, fillet and pipe welds (see **Figure B.3.9**). Parametric equations have been developed corresponding to these distributions and their use can reduce the conservatism in the assumption of "yield strength residual stresses in as-welded joints". Still, the use of these parametric equations pre-supposes some knowledge of the weld joint restraint during fabrication.

- The most conservative approach remains the assumption of uniform, yield strength level, residual stresses as in the Level 1 FAD analysis.

If the net section stress is deemed high enough to cause plasticity at the crack tips, a certain amount of residual stress relief occurs and the residual stress can be appropriately reduced to the minimum of:

a) σ_y
b) σ_r based on approximate distributions
c) $(1.4 - \sigma_n / \sigma_f) \sigma_y$ for Level 2 FAD with S_r abscissa
d) $(1.4 - \sigma_n / 1.2\sigma_y) \sigma_y$ for Level 2 FAD's with L_r abscissa

---

The evaluation of net section stress, σ_n, is presented in Section B.3.7. Clearly, the net section stress must be of the order of 50% of the yield strength in order to get any residual stress relief due to plasticity.

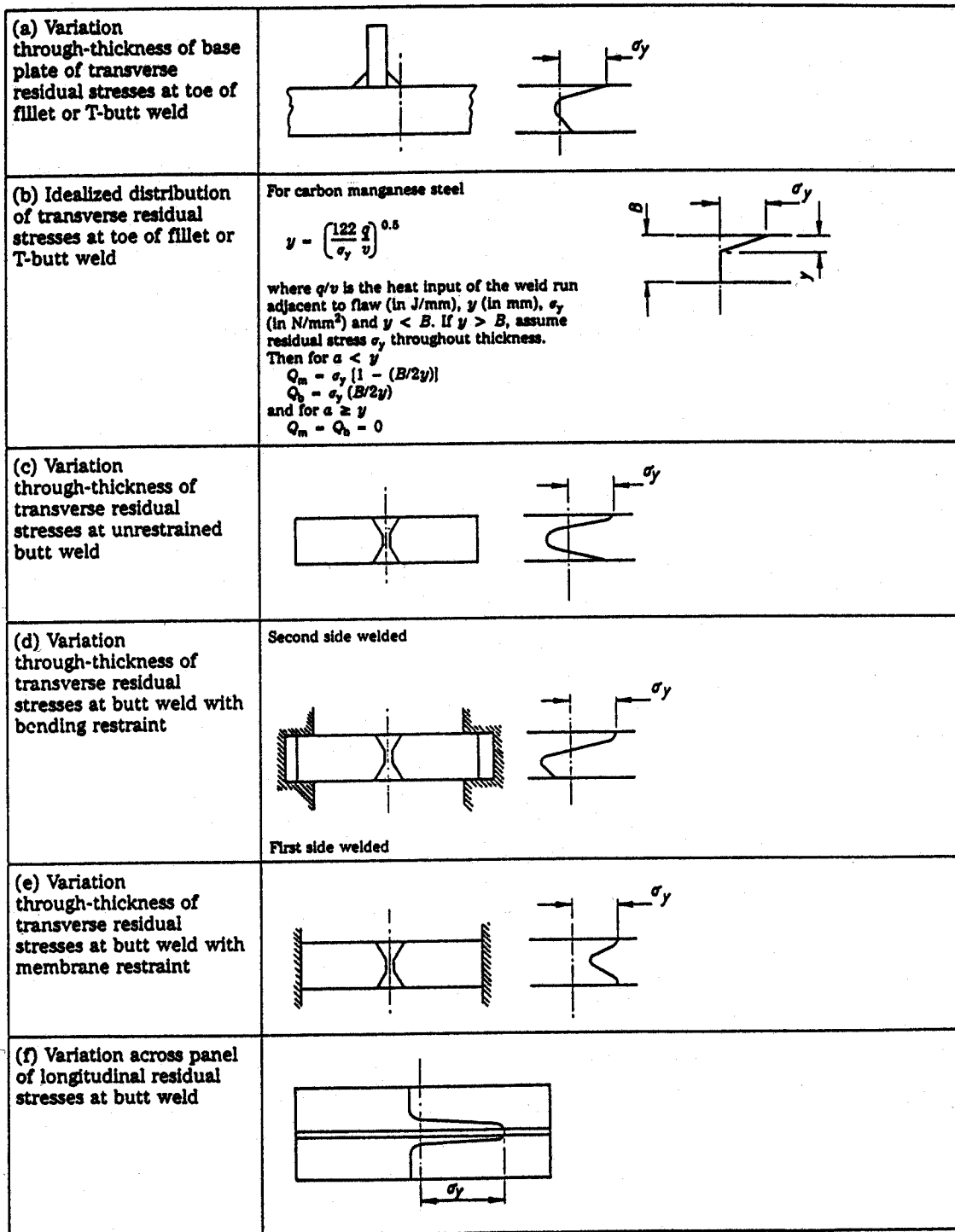|	
(a) Variation through-thickness of base plate of transverse residual stresses at toe of fillet or T-butt weld	
(b) Idealized distribution of transverse residual stresses at toe of fillet or T-butt weld	For carbon manganese steel $$y = \left(\frac{122}{\sigma_y}\frac{q}{v}\right)^{0.5}$$ where q/v is the heat input of the weld run adjacent to flaw (in J/mm), y (in mm), σ_y (in N/mm^2) and $y < B$. If $y > B$, assume residual stress σ_y throughout thickness. Then for $a < y$ $\quad Q_m = \sigma_y [1 - (B/2y)]$ $\quad Q_b = \sigma_y (B/2y)$ and for $a \geq y$ $\quad Q_m = Q_b = 0$
(c) Variation through-thickness of transverse residual stresses at unrestrained butt weld	
(d) Variation through-thickness of transverse residual stresses at butt weld with bending restraint	Second side welded First side welded
(e) Variation through-thickness of transverse residual stresses at butt weld with membrane restraint	
(f) Variation across panel of longitudinal residual stresses at butt weld	

Figure B.3.9: Typical Distributions of Residual Stresses at Welds [Ref. B.37]

When the flaw tips are in the base metal and away from the weld (2 to 3 plate thicknesses), then the weld residual stresses are negligible. However, there are some longer range assembly and construction stresses that still may be present. These may be relieved to some extent with service (shake down effect) or as the crack grows. However, this effect is difficult to predict and therefore, as a conservative measure, longer range residual stresses equal to 20% of the yield strength are recommended to be included in the damage tolerance analysis.

B.3.6   Determination of Stress Intensity Factors

A key requirement of local damage tolerance assessment for fatigue and fracture is the ability to evaluate stress intensity factors (SIF) for ship structural details containing cracks. The following sections review the basic concept of the SIF, and present methods that can be used to calculate SIF's for damage tolerance assessments.

B.3.6.1   General Concepts

The rigorous derivation of the SIF can be found in most advanced texts on fracture mechanics and so only a brief overview will be presented here. A crack represents a very sharp notch (i.e., notch radius $\rightarrow$ 0) and in an ideal elastic body the stresses approach infinity at the crack tip. By studying the conditions near the tip of a crack in an elastic body, it can be shown that the stress and displacement fields can be expressed in terms of three elastic SIF's corresponding to the three modes of fracture (**Figure B.3.10**) : K_I for Mode I (Opening Mode), K_{II} for Mode II (Sliding Mode), and K_{III} for Mode III (Tearing Mode). Any crack problem can be considered to be a combination of these three basic modes of fracture. However, since there is always a tendency for a brittle fracture to propagate in the direction which minimizes the shear loading, the first mode is generally regarded as the most important.
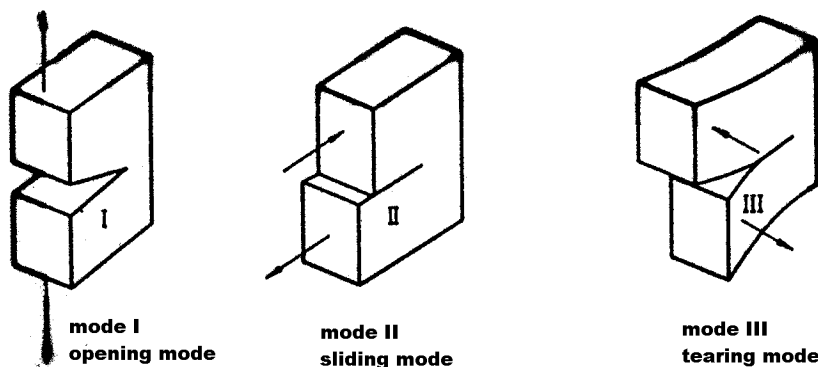

Figure B.3.10: Three Modes of Cracking [Ref. B.38]

The SIF may be described as the amplitude or strength of the stress singularity at the crack tip (**Figure B.3.11**) and includes the influence of loading, crack size, and structural geometry. Since the SIF governs the magnitude of the forces acting in the crack tip region, it plays an essential role in the prediction of brittle strength of bodies containing cracks. The applied Mode I SIF, K_I, (referred to as K_{app} previously) can be correlated to the onset of fracture in brittle materials when it reaches some critical value, denoted K_{Ic}, referred to as the plane strain fracture toughness of the material. This was described earlier and more generically as K_{mat} The cyclic SIF range, ΔK, has also been determined to correlate fatigue crack growth.
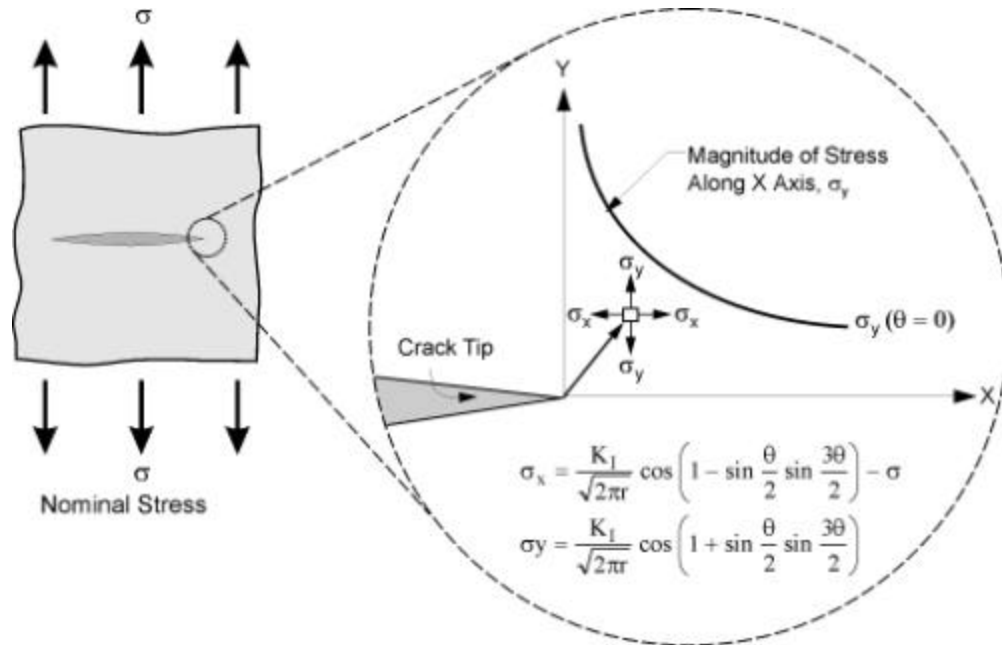

Figure B.3.11: Elastic Stress-Field Distribution Near Crack Tip

The use of the SIF to define the fatigue and fracture behaviour of cracks is the basis of Linear Elastic Fracture Mechanics (LEFM). LEFM follows a similitude approach where identical crack growth and fracture behaviour are assumed to occur for cracks having the same value of SIF. The theoretical basis for LEFM can be justified for brittle materials from thermodynamic arguments. Extension of these arguments to more ductile materials, such as steels used in ship construction, requires simplifying assumptions.

In ductile materials, some non-linear plastic deformation occurs in the highly stressed crack tip region. Provided this plastic zone is "small" in relation to the crack size and well contained within an elastic stress field, the stresses outside this zone will still resemble the K-field stress singularity, and the LEFM approach will suffice to describe the crack behaviour. This condition is generally satisfied in fatigue problems, where cyclic stresses remain well within the elastic range (generally the case for ship structures). In such cases, the LEFM approach based on ΔK can be used for predicting fatigue crack growth behaviour as outlined in Section C.2 for residual life assessment.

However, elasto-plastic conditions usually dominate the fracture behaviour of ship steels at service temperatures, and direct application of LEFM is generally inappropriate. Increasingly attention has focussed on the limitations of LEFM to characterize ductile tearing. Other fracture mechanics theories have also attempted to describe the crack behaviour in terms of a single parameter which accounts for the nonlinear plastic deformation occurring at the crack tip (e.g., J-integral, crack-tip opening displacement, energy release rate). These approaches, generally referred to as Elastic-Plastic Fracture Mechanics (EPFM), continue to be the subject of intense investigations and correlations but, due to added complexity, are not as widely used as in LEFM.

The FAD approach (introduced in Section A.3.5) for residual strength assessment) provides an alternative, and convenient method of assessing fracture behaviour using linear stress and LEFM analysis techniques. The vertical axis of the FAD measures the propensity for brittle fracture using the ratio of the applied crack driving force to material fracture toughness, whereas the horizontal axis of the FAD measures the propensity for stable tearing and plastic collapse using the ratio of the net section stress to the yield strength or flow strength of the material. The failure assessment curve (FAC) represents critical combinations of these ratios.

B.3.6.2 Methods of Calculating Stress Intensity Factors

Various techniques are available to calculate stress intensity factors. However, the method used should be consistent with the level of fracture assessment being applied. The Level 1 FAD approach for calculating SIF, outlined in Section B.3.6.2.1, should be used when applying the Level 1 FAD for residual strength assessment. For other levels of assessment, techniques including numerical methods (e.g., finite element analysis, boundary element analysis) and weight function approaches, can be used to directly calculate K_I at a particular point along a crack front for a given applied stress range, crack size and shape, and structural configuration. When time and resources do not permit the direct calculation of K_I, estimates can be obtained using handbook solutions for simplified geometries and loadings that most closely resemble the actual conditions at the crack location.

A discussion of the various techniques for calculating K_I is presented in the following sections. Key parameters in the following discussion are graphically defined in **Figure B.3.12**. A selection of SIF solutions for basic plate and weld joint configurations is presented in Appendix C.
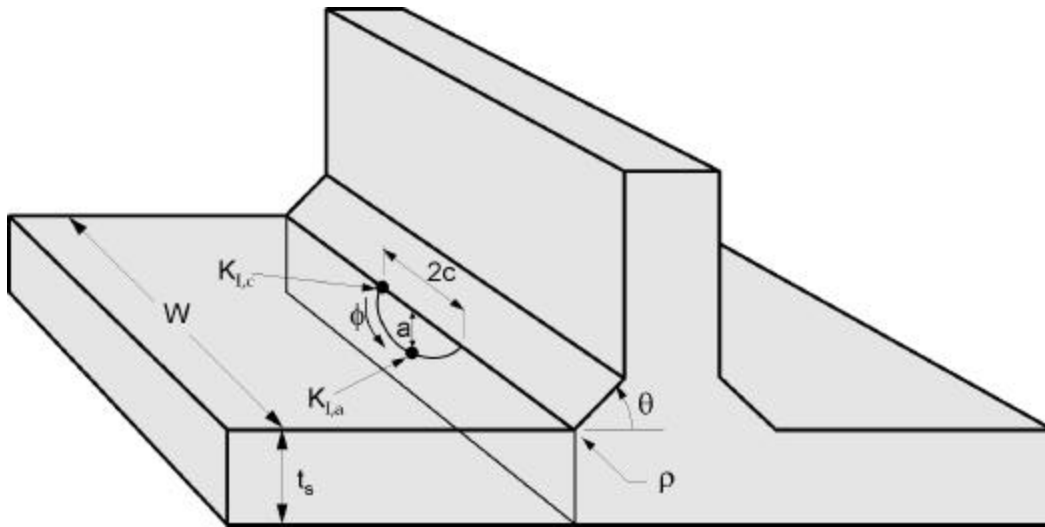
Figure B.3.12: Definition of Parameters for Evaluating Stress Intensity Factors

B.3.6.2.1   Level 1 FAD - Peak Stress Method

The Reference 37 Level 1 FAD for residual strength assessment (see Section C.1) is suitable for a basic screening assessment. It uses an approximate approach for estimating SIF's assuming the maximum total stress is applied as a uniform stress at the crack location and applying the SIF solution for a crack in a finite plate. No account is taken of the local stress profile through the section and, since the maximum or peak value of tensile stress is used, the estimated SIF is generally quite conservative. The basic K_I solutions for through thickness and partial thickness cracks are given as follows.

(a)   Through Thickness Cracks

$$K_I = \sigma_{tp} \sqrt{(\pi a)} \cdot f_w \qquad\qquad (B.3.6.1)$$

$$
\begin{aligned}
\sigma_{tp} \quad &= \quad \sigma_m + \sigma_b + \sigma_r + \sigma_p \\
&= \quad K_w \cdot \sigma_{HS} + \sigma_r && \text{- in terms of hot spot stress} \\
&= \quad K_w \cdot K_g \cdot (K_{te} \cdot K_{t\alpha} \cdot \sigma_m + \sigma_b) + \sigma_r && \text{-in terms of local nominal}
\end{aligned}
$$
stresses
$$
\begin{aligned}
&= \quad K_G \cdot K_w \cdot K_g \cdot (K_{te} \cdot K_{t\alpha} \cdot \sigma_{G,m} + \sigma_{G,b}) + \sigma_r && \text{- in terms of global nominal}
\end{aligned}
$$
stresses

where

2a	=	flaw length.
f_w	=	finite width correction for flaws greater than 10% of the plate width

---

$$= \{\sec(\pi a/W)\}^{0.5}$$

W   =   width of the load bearing section containing the crack.

(b)   <u>Partial Thickness Flaws (Elliptical Embedded or Semi-Elliptical Surface)</u>

$$K_I = Y_m \ \sigma_{tp} \ \sqrt{(\pi a)} \cdot f_w$$

(B.3.6.2)

Where:

Y_m = flaw shape factor given in Appendix C for flaws under membrane loading
f_w = finite width correction when flaw area is greater than 10% of A_l

$$= \{sec(2\pi ac/A_l)\}^{0.5} \quad \text{for embedded flaws}$$
$$= \{sec(\pi ac/A_l)\}^{0.5} \quad \text{for surface flaws}$$

A_l = cross-sectional area of the load bearing section containing the crack.

B.3.6.2.2   *Published Solutions*

Stress intensity factor solutions for general crack geometries and stress fields are included in compendia and handbooks (e.g., Ref. B.37 and Refs. B.39 to B.42). The SIF solutions are obtained either from a simple graphical representation or by evaluating a simple polynomial or analytic expression with given coefficients. The analyst should be careful when using such solutions to ensure that the selected model adequately represents the geometry and boundary conditions of the actual problem.

Stress intensity factor solutions are commonly presented in the following form:

$$K_I = \sigma \cdot Y \cdot \sqrt{(\pi a)} \qquad\qquad (B.3.6.3)$$

where:

σ =   a reference local nominal or "field" stress at the crack location
Y =   stress intensity factor correction
a =   crack size parameter – see Nomenclature.

The stress intensity magnification factor, Y, is a function of crack geometry, structural geometry and mode of loading. The reference nominal stress at the crack location is determined from a local stress analysis of the uncracked body. For residual strength assessments, the reference nominal stress corresponds to the stresses under the extreme load condition (including residual stresses). For residual life assessment, the reference stress range is required to calculate ΔK from:

$$\Delta K = K_{I,max} - K_{I,min} = \Delta\sigma \ \cdot Y \cdot \sqrt{(\pi a)} \qquad\qquad (B.3.6.4)$$

where $\Delta\sigma$ is the reference nominal stress range due to applied cyclic loadings. Welding residual stresses are not included in the calculation of $\Delta\sigma$ since they are usually taken into account in the constants of the crack growth relationship. It should be noted that the reference nominal stress (or stress range), Y factor, and the crack length in Equations B.3.6.3 and B.3.6.4 must be consistently defined for a particular problem.

The membrane and bending components of stress usually require separate correction functions. In addition, self-limiting residual stresses should not be factored by stress concentration factors and therefore need to be separated from the stresses due to applied loading. As a result, Equation B.3.6.3 becomes:

$$K_I = (Y\sigma) \cdot \sqrt{(\pi a)} \tag{B.3.6.5}$$

$$(Y\sigma) = \{Y_m \cdot (M_{km} \cdot \sigma_m + \sigma_{rm}) + Y_b \cdot (M_{kb} \cdot \sigma_b + \sigma_{rb})\} \tag{B.3.6.6}$$

where

Y_m, Y_b	=	magnification factors accounting for the flaw geometry
M_{km}, M_{kb}	=	magnification factors accounting for stress concentrations of the detail
σ_m, σ_b	=	local nominal stresses due to the applied loading
σ_{rm}, σ_{rb}	=	local residual stresses

The subscripts m and b refer to membrane and bending stress components respectively. The stress intensity magnification factors, Y_m and Y_b, account for the crack size and shape and are equivalent to the reference SIF solutions for flaws in a flat plate. M_{km} and M_{kb} are the stress intensity magnification factors due to the stress concentration of the detail, and are functions of the local geometry (i.e., joint configuration, weld toe radius, angle) as well as crack geometry (shape and depth).

Reference solutions for Y_m and Y_b for through-thickness cracks, elliptical embedded, and semi-elliptical surface cracks in membrane and bending loading have been published in Reference B.37 and are included in Appendix C. M_{km} and M_{kb} solutions for several basic weld joint configurations are also presented in Appendix C. In practice, M_{kb} solutions are not available for many configurations. In such cases, it is usually conservative to assume $M_{kb} = M_{km} = M_k$.

Most M_k solutions for cracks at welds have been calculated by 2-D finite element or weight function methods. The 2-D M_k solutions are generally presented as follows:

$$M_k = \alpha(a/t)^\beta \tag{B.3.6.7}$$

Where:

α, β =   functions of crack size and weld geometry.

The 2-D M_k solutions are, strictly speaking, applicable to the case of a straight fronted crack (i.e., $a/2c = 0$). Due to the complexity and costs of the analyses, only a few 3-D solutions exist for semi-elliptical cracks at welds, see for example References B.43 to B.45. However, experience indicates that 2-D solutions can be applied for semi-elliptical cracks (provided $0 \leq a/2c \leq 0.5$) as described below.

For most practical cases, the analysis of semi-elliptical cracks requires only the solutions at the point of deepest penetration (i.e., $K_{I,a}$ at $\phi = \pi/2$) and at the surface (i.e., $K_{I,c}$ at $\phi = 0$):

$$K_{I,a} = \{Y_{m,a} \cdot (M_{km,a} \cdot \sigma_m + \sigma_{rm}) + Y_{b,a} \cdot (M_{kb,a} \cdot \sigma_b + \sigma_{rb})\} \cdot \sqrt{(\pi a)} \qquad (B.3.6.8)$$

$$K_{I,c} = \{Y_{m,c} \cdot (M_{km,c} \cdot \sigma_m + \sigma_{rm}) + Y_{b,c} \cdot (M_{kb,c} \cdot \sigma_b + \sigma_{rb})\} \cdot \sqrt{(\pi a)} \qquad (B.3.6.9)$$

where

$$Y_{m,a} = M_m(\phi = \pi/2) \qquad\qquad Y_{m,c} = M_m(\phi = 0)$$
$$Y_{b,a} = M_b(\phi = \pi/2) \qquad\qquad Y_{b,c} = M_b(\phi = 0)$$
$$M_{k,a} = M_k(\phi = \pi/2) \qquad\qquad M_{k,c} = M_k(\phi = 0)$$

If 3-D solutions are available, the values of $M_{k,a}$ and $M_{k,c}$ can usually be obtained directly. Alternatively, 2-D solutions for M_k may be used to estimate the semi-elliptical crack solutions using the formulae given in Reference B.46.

$$M_{k,a} = M_k \, (2\text{-D}) = \alpha(a/t)^\beta \qquad (B.3.6.10)$$

$$M_{k,c} = M_{k,a} + 1.15 \, \exp^{(-9.74 \, a/t)} \qquad (B.3.6.11)$$

The available SIF solutions for welded joints are generally limited to simple basic weld joint configurations (e.g., butt joint, T-joint, cruciform joint, etc.). Ship details may be considered to be built up of various simple joints, however the stress distributions in actual ship details are somewhat more complicated than that of the simple joints due to the load flow in the structure surrounding the detail as well as the local stress concentration effect of the basic detail. The reference stresses to be used in the SIF solutions should correspond to the local nominal stresses at the crack location. When applying published SIF solutions to actual ship structural details, it is not always clear which stress(es) is (are) to be used as the reference stress.

As noted previously, the SIF solutions for basic welded joints account for the stress concentration for weld (K_w^{basic}) and basic joint configuration (K_g^{basic}) through the M_k factor for the basic joint. In the limit, as the crack depth approaches zero, it can be shown that the M_k factor approaches the value of the stress concentration factor for the basic detail, including the notch effect of the weld toe; that is:

$$M_k = K_w^{basic} \cdot K_g^{basic} \text{ as } a \rightarrow 0 \qquad (B.3.6.12)$$

When stress intensity factor solutions for basic welded joints are applied to complex ship details, then global nominal membrane stresses ($\sigma_{G, m}$) and global nominal bending stresses ($\sigma_{G, b}$) must be corrected with: (i) a stress concentration factor (K_G) that accounts for the gross structural configuration that surrounds the detail, and, (ii) a stress concentration factor (K_g^*) that accounts for the difference between the stress concentration of the detail's configuration (K_g^{detail}) and the contribution to the latter from K_g^{basic}.

$$\sigma_m = K_g^* \cdot K_G \cdot \sigma_{G,m} \qquad (B.3.6.13)$$
$$\sigma_b = K_g^* \cdot K_G \cdot \sigma_{G, b} \qquad (B.3.6.14)$$

As evident in Table B2 of Appendix B, K_g^{basic} is approximately equal to unity for most basic joint configurations, and it is more convenient but not unduly conservative to use K_g^{detail} instead of K_g^* in the above equations.

B.3.6.2.3 *PD6493 Level 2FAD - Linearized Stress Method*

The Level 2 FAD assessment procedure provides an approximate method for evaluating SIF's based on taking the linearized stress distribution across the flaw (as determined from local stress analysis of the uncracked body) and applying the basic SIF solutions for flaws in a plate. In this manner, the stress profile at the crack is more accurately accounted for, resulting in a more accurate evaluation of the SIF than the Level 1 procedure. The equations used to calculate the SIF using this method are as follows:

$$K_I = \{Y_m \cdot (M_{km} \cdot \sigma_m + \sigma_{rm}) + Y_b \cdot (M_{kb} \cdot \sigma_b + \sigma_{rb})\} \cdot \sqrt{(\pi a)} \qquad (B.3.6.15)$$

Parametric formulae for Y_m, Y_b, M_{km}, and M_{kb}, are presented in Appendix C.

The application of this Level 2 FAD approach requires linearization of the stress distribution over the crack length as opposed to linearization of the stresses over the plate thickness or width. The method used for linearization of stresses is different for fracture assessments and fatigue assessments and is summarized in **Figure B.3.13**.

B.3.6.3   Finite Element Methods

In cases where published solutions are not readily available for the detail under consideration, finite element methods may be used to calculate SIF solutions. A number of general reviews of the finite element method relating to fracture mechanics are available of which Reference B.47 is a good example.

The application of FEM to LEFM requires modelling the stress singularity that occurs at the crack tip. The first attempts to model cracks simply involved the use of very large numbers of conventional finite elements. No attempt was made to take into account the stress singularity in

the element formulation. It has been demonstrated [Ref. B.48] that many hundreds of elements are required to achieve perhaps 5% accuracy. As a result, this approach has been abandoned in favour of elements that take explicit account of the crack tip stress singularity.

The most important of these formulations include classical solution based singularity elements, polynomial singularity function elements, and modified isoparametric elements.

Isoparametric elements are, perhaps, the most important of these due to their wide availability in commercial FEM programs. Their application to LEFM is based on the ability to represent the $1/\sqrt{r}$ stress singularity by a very simple modification to the standard isoparametric element. By shifting the "mid-side" nodes to the quarter point in a quadratic isoparametric triangular or quadrilateral element, the required singularity results at the nearest node. Barsoum, in a most important paper [Ref. B.49], investigated two and three-dimensional quadratic isoparametric elements. He introduced the idea of "collapsing" nodes along one edge of the element, and placing the adjacent nodes at the quarter point (**Figure B.3.14**).

These collapsed or degenerate elements were later shown by the same author [Ref. B.50] to contain the required stress singularity along any ray from the crack tip, whereas the simple modified elements exhibit the singularity only along the boundaries of the element. The demonstrated accuracy of the collapsed form of isoparametric element, together with their wide availability and ease of application, makes them the preferred choice for elastic crack analysis.

The application of FEM for determining SIF is similar to that described for local stress analysis in Section B.3.4.2 in terms of extent of model and application of loads and boundary conditions. In general, a local model of the detail containing the crack is required with special crack-tip elements applied at the crack tip. Shell element models may be used to derive SIF for through-thickness and 2-D straight-fronted (i.e., a/2c = 0) cracks. The analysis of partial thickness elliptical cracks is somewhat more complicated and requires the use of 3-D solid elements. **Figures B.3.15** and **B.3.16** show typical FEM meshes for 2-D and 3-D cracks.

The 2-D crack mesh shown in Figure B.3.15 was used to model an edge cracked plate. Four triangular crack tip elements are located at the crack tip in the arrangement shown. The rest of the model uses conventional isoparametric plate or shell elements. In this particular example the crack face lies on a plane of symmetry, therefore only half of the crack is modelled. The nodes between the crack tip and the far edge of the plate are prescribed symmetry displacement conditions, nodes along the crack surface are free to move. Note that the crack tip elements are relatively small (typically about 2% of the crack length) and that elements gradually get larger as the distance from the crack tip increases. This is to ensure that the rapid stress gradient at the crack tip is adequately represented.
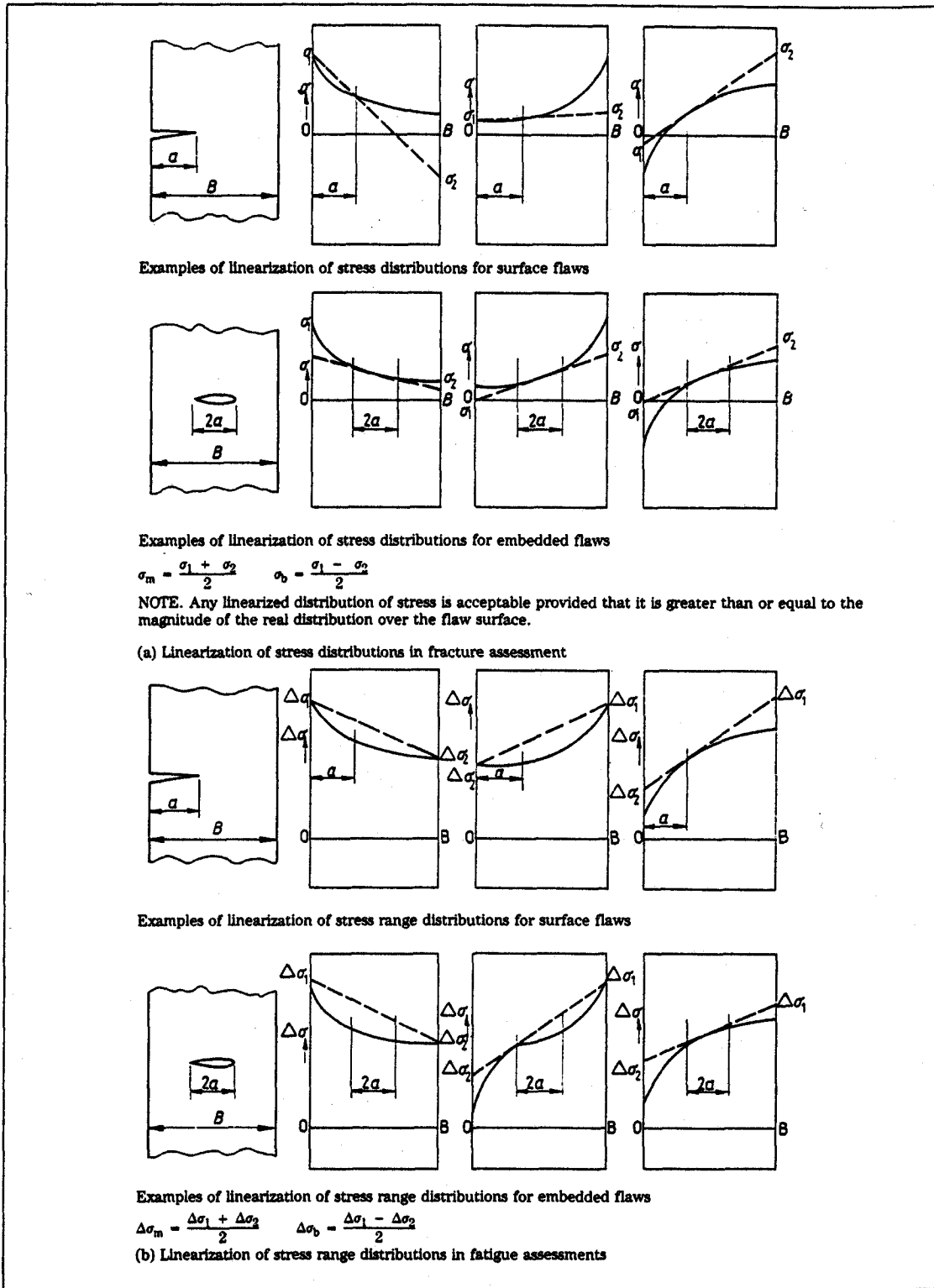
Examples of linearization of stress distributions for surface flaws

Examples of linearization of stress distributions for embedded flaws

$$\sigma_m = \frac{\sigma_1 + \sigma_2}{2} \qquad \sigma_b = \frac{\sigma_1 - \sigma_2}{2}$$

NOTE. Any linearized distribution of stress is acceptable provided that it is greater than or equal to the magnitude of the real distribution over the flaw surface.

(a) Linearization of stress distributions in fracture assessment

Examples of linearization of stress range distributions for surface flaws

Examples of linearization of stress range distributions for embedded flaws

$$\Delta\sigma_m = \frac{\Delta\sigma_1 + \Delta\sigma_2}{2} \qquad \Delta\sigma_b = \frac{\Delta\sigma_1 - \Delta\sigma_2}{2}$$

(b) Linearization of stress range distributions in fatigue assessments

Figure B.3.13: Linearization of Stress Distributions (Ref. B.37)
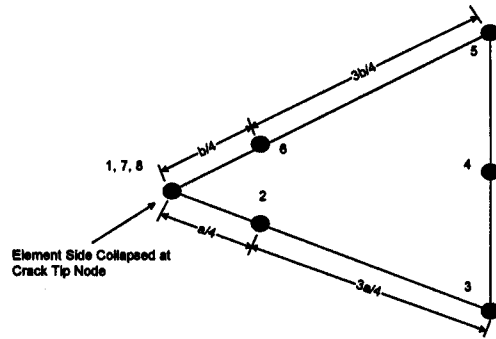
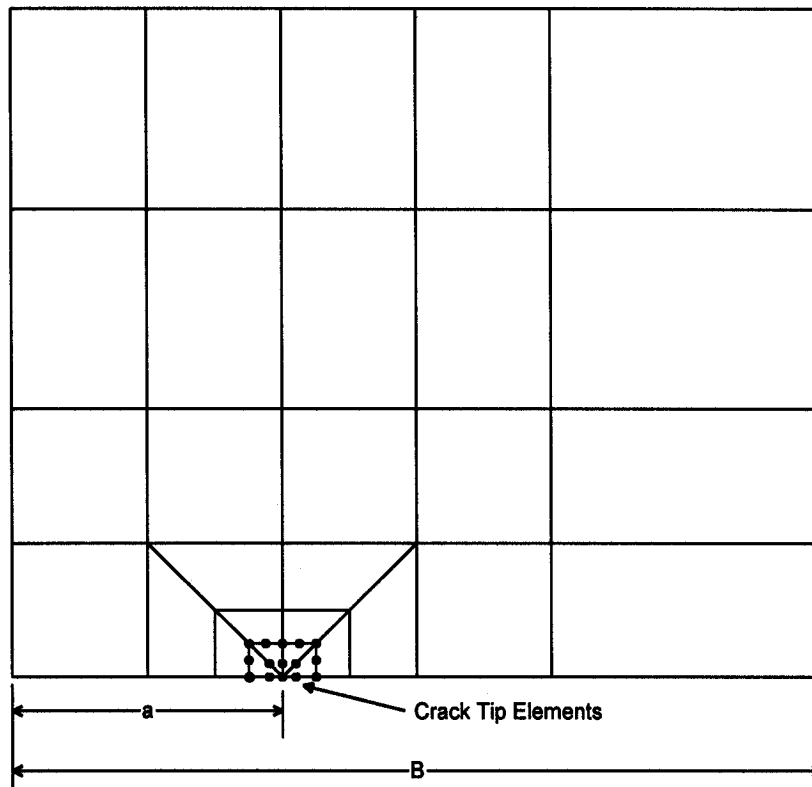**Figure B.3.14: Collapsed Node Isoparametric Crack Tip Element**

Figure B.3.15: Example of 2-D Crack Model of an Edge Cracked Plate

Figure B.3.16 shows a 3-D FEM model of a semi-elliptical surface crack in a plate. The design of the 3-D crack mesh requires analogous considerations for element placing and sizing to those discussed for the 2-D crack mesh. As a guide, the size of the crack tip elements normal to the crack front should be less than 5% of the crack length, a, for acceptable accuracy (2-5%). The length to width aspect ratio of solid crack-tip elements should not exceed 4, where the length dimension of the element is measured along the crack front. The 3-D crack model is considerably more complex than the 2-D problem. In general modelling of 3-D semi-elliptical cracks requires the use of computerized "mesh generation" programs or FEM preprocessors with advanced solids modelling features to facilitate their preparation.
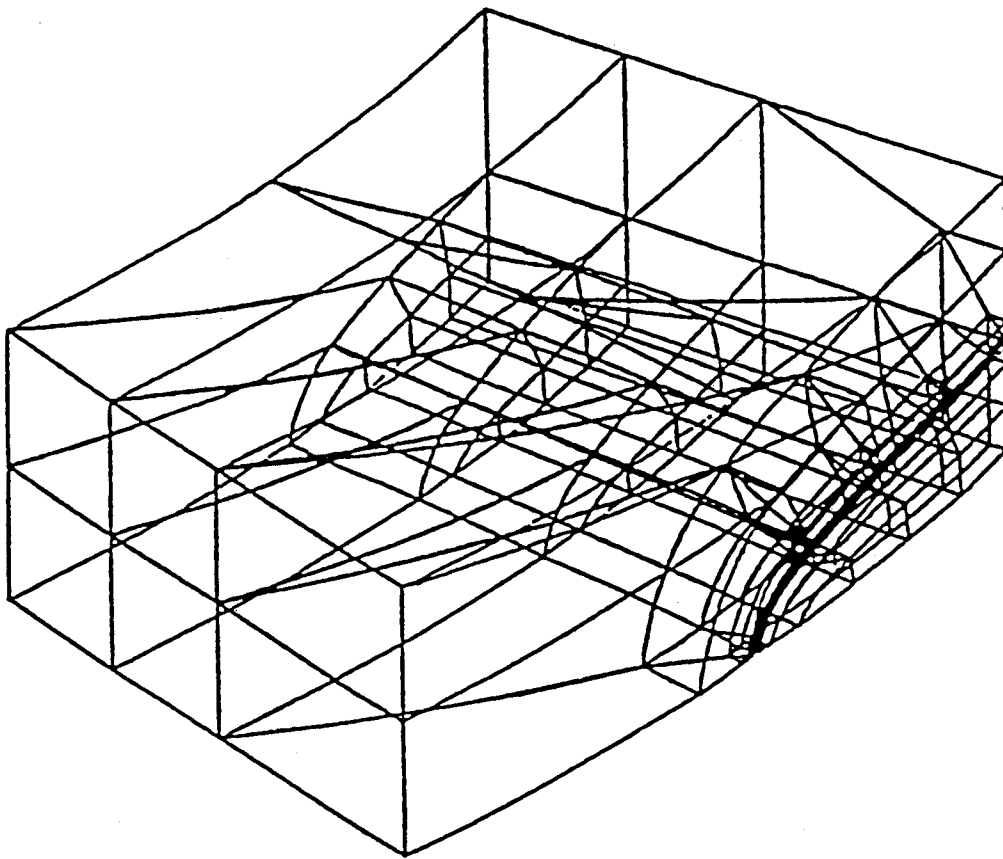

Figure B.3.16: Example of 3-D Crack Mesh for Semi-Elliptical Surface Crack

<u>B.3.6.4 Weight Function Methods</u>

The weight function m(x,a) for a crack in (opening) mode I (Figure B.3.10) is a unique property of geometry and it enables an alternative economical method of calculating SIF solutions for complex geometries and stress profiles. It is particularly well suited for allowing the effects of residual stresses to be incorporated into the SIF solution. The weight function for a 2-D cracked body can be written in the form:

$$K_I = \int_0^a s(x) \cdot m(x) \cdot dx \tag{B.3.6.16}$$

$$m(x, a) = \frac{H}{K_r} \cdot \frac{du_r}{da} \tag{B.3.6.17}$$

$$H = E \quad \text{for plane stress;} \quad H = \frac{E}{(1 - v^2)} \quad \text{for plane strain.} \tag{B.3.6.18}$$

In order to derive the weight function, a reference stress intensity factor K_r for a given geometry and stress system needs to be known together with the corresponding crack opening displacement field $u_r(x,a)$. An appropriate solution for K_r can usually be found from the literature (e.g., K_r solution for a partial thickness crack in a flat plate). However, reference solutions for $u_r(x,a)$ are usually more difficult to find. An approximation for the crack opening displacement function follows:

$$u_r(x, a) = \frac{s_0}{H\sqrt{2}} \left[4Y(a/t) \sqrt{a(a - t)} + \frac{G(a/t)(a - x)^{2/3}}{\sqrt{a}} \right] \tag{B.3.6.19}$$

Generalized weight function expressions were derived assuming this displacement function and are summarized on the following page. Knowing the weight function m(x,a), a stress intensity factor K_{new} can be calculated for any new local stress system $\sigma_{new}(x)$. The local stress distribution $\sigma_{new}(x)$ has to be obtained for the prospective crack plane in the actual structural configuration for which K_{new} is to be derived. This may be achieved by conventional local detail FEA of the uncracked geometry to derive the local stress field, upon which the residual stress field may be superimposed, to achieve the total stress field at the crack location.

Further details of this approach are provided in References B.51 and B.52. Reference B.32 illustrates the use of the weight function technique to calculate SIF solutions for weld details as presented in Appendix C.

$$m(x, a) = \frac{2}{\sqrt{2p(a - x)}} \left[1 + m_1 \frac{a - x}{a} + m_2 \left(\frac{a - x}{a} \right)^2 \right] \tag{B.3.6.20}$$

$$m_1 = \frac{4Y'(a/t) \cdot a + 2Y(a/t) + 3/2G(a/t)}{2Y(a/t)}$$

(B.3.6.21)

$$m_2 = \frac{G'(a/t) \cdot a + 1/2G(a/t)}{2Y(a/t)}$$

(B.3.6.22)

$$Y(a/t) = \frac{K_r}{s_0}\sqrt{pa}$$

(B.3.6.23)

$$Y'(a/t) = \frac{d}{d(a/t)}[Y(a/t)]$$

(B.3.6.24)

$$G(a/t) = \frac{[I_1(a) - 4Y(a/t)\sqrt{a} \cdot I_2(a)]\sqrt{a}}{I_3(a)}$$

(B.3.6.25)

$$I_1(a) = s_0 p\sqrt{2} \int_0^a [Y(a/t)]^2 \cdot a \cdot da$$

(B.3.6.26)

$$I_2(a) = \int_0^a s_r(x) \cdot (a - x)^{1/2} dx$$

(B.3.6.27)

$$I_3(a) = \int_0^a s_r(x) \cdot (a - x)^{3/2} dx$$

(B.3.6.28)

$$G'(a/t) = \frac{d}{d(a/t)}[G(a/t)]$$

(B.3.6.29)

B.3.7 Net Section Stresses

The horizontal co-ordinate of a failure assessment diagram (FAD), the ratio of the net section stress (σ_n) to the material yield strength or flow strength (see Section A.3.5), measures the plastic collapse strength of the cracked section or structure. The net section stress for a uniform applied tensile load and symmetric crack configuration is simply the applied load divided by the net cross-sectional area. In contrast, the net section stress for unsymmetric crack configurations and/or applied bending loads is not obvious and usually defined by an imaginary stress that is obtained in the following manner. The distribution of net section stresses prior to plastic collapse is assumed to be identical in form to the distribution of net section stresses at plastic collapse according to limit load analysis with an elastic perfectly plastic material model.

The net section stress prior to plastic collapse is then obtained by simultaneously solving the equilibrium equations for moment and forces across the remaining uncracked ligament. Closed form solutions for simple cases are given in Ref B.37 and repeated below. Additional guidance and formulae for other geometries are given in References B.53. and B.54, and calculations for a side shell longitudinal are presented in Part D of this guide.

(a) Through Thickness Flaw

$$\sigma_n = \{\sigma_b + (\sigma_b^2 + 9\sigma_m^2)^{0.5}\} / \{3[1 - (2a/W)]\} \tag{B.3.7.1}$$

where: $2a$ = the crack length

(b) Surface Flaw – Normal Bending Restraint

$$\sigma_n = \{\sigma_b + [\sigma_b^2 + 9\sigma_m^2(1 - \alpha)^2]^{0.5}\} / \{3(1 - \alpha)^2\} \tag{B.3.7.2}$$

where $\alpha = (a/t_p) / \{1 + (t_p/c)\}$ for $W \geq 2(c+t_p)$
         $\alpha = (2a/t_p)(c/t_p)$ for $W < 2(c+t_p)$
         a = the crack depth in the plate thickness direction
         $2c$ = the crack length at the surface

(c) Surface Flaw – Negligible Bending Restraint (e.g., pin-jointed)

$$\sigma_n = [\sigma_b + 3\sigma_m\alpha + \{(\sigma_b + 3\sigma_m\alpha)^2 + 9\sigma_m^2(1 - \alpha)^2\}^{0.5}] / \{3(1 - \alpha)^2\} \tag{B.3.7.3}$$

(d) Embedded Flaw

$$\sigma_n = [\sigma_b + 3\sigma_m\alpha + \{(\sigma_b + 3\sigma_m\alpha)^2 + 9\sigma_m^2\{(1-\alpha)^2 + 4p\alpha/t_p\}\}^{0.5}]/\{3(1 - \alpha)^2 + 4p\alpha/t_p\} \tag{B.3.7.4}$$

where: $\alpha = (2a/t_p) / \{1 + (t_p/c)\}$ for $W \geq 2(c+t_p)$
         $\alpha = (4a/t_p)(c/W)$ for $W < 2(c+t_p)$
         d = dimension of the nearest distance of the flaw to the plate surface.

B.4   MATERIAL PROPERTY INPUTS

The material property data required for residual strength analysis are the yield strength (lower yield or 0.2% offset), ultimate strength and fracture toughness of the material (weld metal, heat affected zone or base metal) where the flaw tips reside. For fatigue crack growth analysis, the material data required also include the Paris Law crack growth parameters (C, M, K_{th}). Guidance for obtaining appropriate values for these inputs is as follows:

B.4.1   Tensile Properties

The yield strength and ultimate strength of weld metal and base metal are easily determined following standard test procedures. (When multiple tensile tests are conducted, the scatter in results is usually minimal so that damage tolerance assessment results are not significantly affected when the tensile properties used are obtained from a single specimen or as a lower bound from multiple specimens.) Once the yield and ultimate strength values are established, the flow stress (σ_f) can be computed.

For heat affected zones, tensile properties are not easily determined. To obtain conservative assessments, it is recommended that the HAZ tensile properties be assumed to be the lower of adjacent base metal or weld metal in calculating S_r or L_r values, and higher of adjacent base and weld metals when required for calculating HAZ fracture toughness in experimental procedures (CTOD, K or J tests).

B.4.2   Fracture Toughness

B.4.2.1 General Approach

Since the damage tolerance assessment results are sensitive to the input material toughness and since there usually is a significant scatter in the fracture toughness measurements of a given material (especially weld metal and HAZ), selection of fracture toughness input value has warranted considerable thought. In selecting the input material fracture toughness value for deterministic analysis, the following guidelines are provided:

- For most marine structural steels and weldments, the fracture toughness is most commonly measured as a critical CTOD value (δ_{mat}) that corresponds to either unstable fracture initiation in the specimen without any crack extension (δ_c), unstable fracture after some ductile crack extension (δ_u), or maximum load behaviour in a test (δ_m) [Ref. B.55]. For an analysis based on the Level 1 FAD, this is an ideal choice since the experimentally established CTOD design curve, the basis of the Level 1 FAD, also uses such values.

- The fracture toughness value , K_{mat} , should be computed from critical values of CTOD (δ_{mat}) using Equation B.4.2.1 that is less conservative than the equation implicit in Reference B.37 (see Section 3.6):

$$K_{mat} = \sqrt{\frac{1.6s_f d_{mat} E}{\left(1-?^2\right)}} \qquad\qquad (B.4.2.1)$$

Occasionally, the fracture toughness may be available as J_{mat}, a critical value of J determined in accordance with standards like ASTM E 1737 [Ref. B.56]. In such cases, K_{mat} can be inferred from Equation B.4.2.2:

$$K_{mat} = \sqrt{\frac{J_{mat} E}{\left(1-?^2\right)}} \qquad\qquad (B.4.2.2)$$

- The CTOD tests can be conducted according to ASTM Standard E 1290 [Ref. B.55] and J tests according to ASTM Standard E 1737 [Ref. B.56]. In a new standard [Ref. B.57], both fracture parameters will be calculable from the same test procedure. The tests for determining the fracture toughness must be conducted at the design temperature on full thickness specimens machined from the same material as the welded structure and at the same stress intensity factor rate as that anticipated in service. For welds and the heat affected zone, it means that the welding procedure (welding consumables, heat input, restraint during welding, post-weld heat treatment, etc.) for the test weld for preparing the specimens should be the same as for the production welds. The crack plane and location in the specimen should be the same as that anticipated for the flaw in service. For HAZ specimens, post-test metallography ought to be performed to ensure that the crack tip indeed resided in the microstructural region of interest.

It is a common practice to determine fracture toughness using rectangular $t \times 2t$ (preferred geometry), three point loaded, single edge notched beam specimens where t is, once again, the specimen and plate thickness.

The fracture toughness is most frequently measured at a quasi-static loading rate whereas the loading rates that ship structural members are subjected to are in the intermediate loading rate (strain rate of about 5×10^{-3})[Ref. B.58]. In the absence of such data, it is common practice to input fracture toughness values based on quasi-static loading rate tests though it does introduce a degree of non-conservatism in the assessment.

- An important issue is the number of fracture toughness tests that ought to be done and then which value should be used as a representative fracture toughness. For Level 1 FAD assessment, Reference B.37 recommends conducting at least three tests and then using the lowest one in analysis. The minimum value from a set of three corresponds to a 33rd percentile value (mean minus one standard deviation) with 70% confidence. Further tests are recommended if there is too much scatter within the three results. Excessive scatter is indicated when the minimum CTOD value is less than half the average of three values or if the maximum value is more than twice the average of the three values.

- Further testing would normally comprise an additional set of three specimens and then selecting the second lowest value for material fracture toughness from six values available from the two sets of tests.

- For the remaining FADs described earlier, there are no safety factors built into them, and once again the lowest fracture toughness value obtained from a set of three is normally used subject to the qualifications stated above and provided worst case estimates for stress and flaw size are used. However, it is generally desired that greater volume of fracture toughness data be available. When more than three test results are available, then the statistically equivalent value to the minimum of three that should be used in the damage tolerance assessment is given in **Table B.4.1**.

Table B.4.1: Equivalent Fracture Toughness Values to the Minimum of Three Results

Number of Fracture Toughness Tests	Equivalent Value
3 to 5	Lowest
6 to 10	Second Lowest
11 to 15	Third Lowest
16 to 20	Fourth Lowest

(In reliability based analyses, log normal or Weibull distribution could be fitted to the available data, assuming that all data points represent the same failure mode $(\delta_c, \delta_u,$ or $\delta_m)$ and then a characteristic value equal to mean minus one standard deviation established. Further, it is recommended that a partial safety factor be applied to this value depending on the consequences of the member's failure. Thus, for moderate consequences of failure, the partial safety factor suggested is 1 and it is 1.4 when the fracture toughness is expressed as CTOD (1.2 for K_{mat}) and the failure consequences are severe.)

- An alternate approach to handle the scatter in the fracture toughness value is considered in Reference B.57. The basis of this approach lies in two observations. First, it has been shown that at any test temperature, the cleavage fracture toughness distribution can be described by a three parameter Weibull distribution of slope 4 so that:

$$F = 1 - \exp\left[-\left(\frac{K_{Jc} - 20}{T_k - 20}\right)^4\right] \tag{B.4.2.3}$$

where, F is the cumulative probability, K_{Jc} is the fracture toughness obtained from J integral and Θ_K is the 63rd percentile toughness. Generally, six tests at any one test temperature are expected to be sufficient to establish the Θ_K value first, and then the median (or any other percentile) K_{Jc} value by setting F equal to 0.5 (or appropriate fraction).

Secondly, according to Reference B.59, the temperature dependence of fracture toughness can be expressed by the equation:

$$K_{Jc(median)} = 30 + 70\exp\left[0.019\left(T - T_0\right)\right]$$ (B.4.2.4)

According to this equation, when $T = T_0$, $K_{Jc} = 100$ MPa$\sqrt{m}$. Once this is established, then the K_{Jc} value (any percentile) can be plotted as a function of temperature. This approach should be used only for the ductile-brittle transition region as it is not suitable for the upper shelf region and it may not fit the data well in the lower shelf region.

- Frequently, it is the case that no fracture toughness data is available at all and none can be generated due to material unavailability. On the other hand, CVN toughness for the desired region may be available or could be generated with the limited material available. In such cases, lower bound CVN-K_{mat} correlation may be used but at the risk of obtaining very conservative assessments (small critical flaw size or low residual strength).

Reference B.37 provides two graphs to estimate K_{mat} from the CVN test results. When the CVN absorbed energy (20, 27 or 40 J) transition temperature of the region of interest is known and it is different from the service or design temperature, then **Figure B.4.1(a)** enables one to estimate K_{mat} as a function of (design temperature - transition temperature).

The curve in Figure B.4.1(a) is based on a lower bound to the data generated for ASTM A533 grade B, nuclear pressure vessel steel and includes data from crack arrest and dynamic fracture toughness tests, and is, therefore, quite conservative for relatively thinner ship steels subject to intermediate loading rates rather than dynamic. The transition temperature used in the ASME lower bound curve is the drop weight nil ductility transition temperature (NDTT) as determined by the ASTM E208 procedure. However, for ship and structural steels in general, CVN data is more frequently available than the NDTT and therefore Reference B.37 recommends the use of CVN transition temperature though some recent work suggests that for modern, clean, low carbon steels, the NDTT can be higher than the CVN transition temperature. (Anderson in Reference B.60 uses a similar lower bound curve for pressure vessel steels but based on quasi-static fracture toughness data only. Obviously, this approach gives higher K_{mat} value for the same CVN toughness, however, since the applicable loading rates for ships are in the intermediate range, it is prudent to use the lower bound curve in Reference B.37 rather than the one used in Ref. B.60).

If the CVN absorbed energy at the design or operating temperature is known, then **Figure B.4.1(b)** can be used directly to estimate K_{mat}. If both these pieces of information are available, then use of the lower of the two resulting K_{mat} values is recommended. Secondly, these correlations should be used only for steels with less than 480 MPa yield strength.

Care should be taken to ensure that the CVN data is from specimens that represent the same fracture path and microstructural region as the region of the structure containing the flaw.
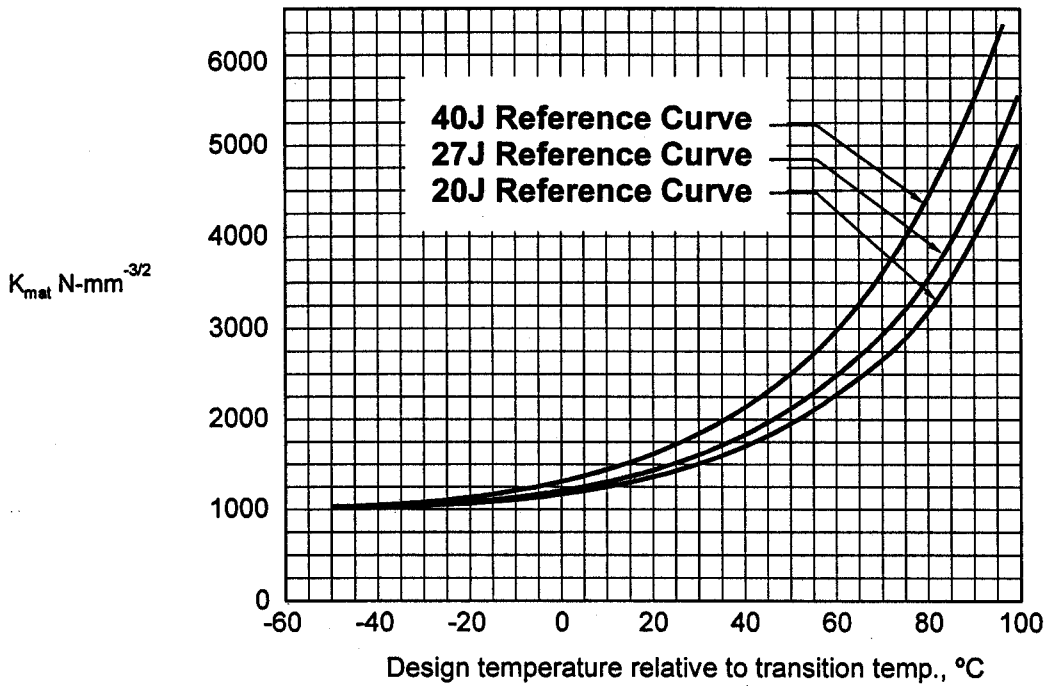
Figure B.4.1(a): K_{mat} Estimate at Design Temperature Based on Design Temperature Difference with Respect to the CVN Transition Temperature [Ref. B.61]
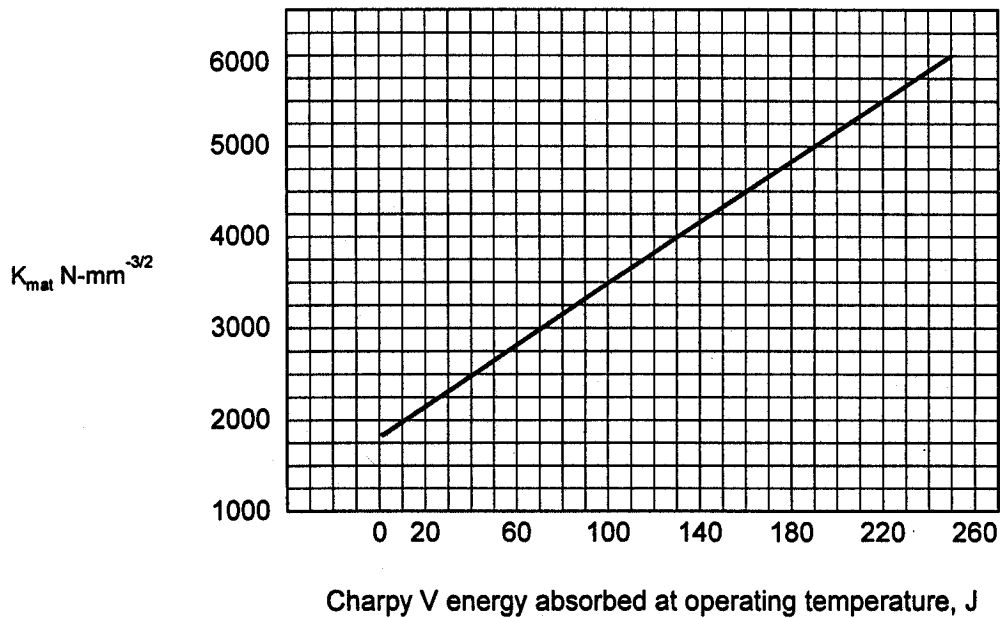

Figure B.4.1(b): Lower Bound K_{mat} Estimate from Energy Absorbed in Charpy Vee-Notch Test at the Operating Temperature [Ref. B.62]

B.4.2.2   Practical Examples of Estimating K_{mat} Values in Various Scenarios

(a)   **Steel of Unknown Specification, and Not Available for Any Toughness Tests**

In such a situation, ideally no damage tolerance analysis will be performed. If one must be performed for whatever reason, then there is no choice but to estimate a lower bound material toughness value. Reference B.60 recommends that for steel of unknown origin, one should presuppose a hot rolled steel and assume the 20 J transition temperature to be $38^{o}C$. For a design temperature of $0^{o}C$, the K_{mat} value using the correlation provided in Ref. B.37 (Figure B.4.1(a)) would be about 1025 Nmm$^{-1.5}$ (32.5 MPa$\sqrt{m}$).

In practice, a similar situation can arise when it is known that the steel used conforms to Grade A that does not have any CVN toughness requirements at all. In developing the guidelines for steel grade application to different regions of the ships, Reference B.63 assumed that Grade A steels would meet a transition temperature of $10^{o}C$. Once again, Figure B.4.1(a) would suggest that the K_{mat} value for a design temperature of $0^{o}C$ for such a steel would be about 1250 Nmm$^{-1.5}$ (39.5 Mpa$\sqrt{m}$).

K_{mat} values of 32 to 40 MPa$\sqrt{m}$ are quite small and are likely to indicate unsafe conditions except in most benign conditions (very low stresses or very small flaws).

(b)   **Steel or Weld Metal of Known CVN Toughness or Specification**

Two cases can be envisaged in this scenario. The steel grade or fabrication specification detailing the minimum requirements is known but the actual values from the mill test report or procedure qualification record may or may not be known. Or, the actual CVN toughness values at a particular test temperature might be available or be determinable, with or without the knowledge of the governing material specifications. Again it is assumed that material is not available for testing and generating the fracture toughness data.

For example, it may be known only that the steel used in fabrication was specified to be EH 36 which is required to meet a requirement of 34 J at $-40^{o}C$ (i.e., the design temperature of $0^{o}C$ is $40^{o}C$ above the CVN test temperature) in the longitudinal direction. Then, assuming the flaw orientation to be consistent with flaw propagation in a direction perpendicular to the rolling direction, Figure B.4.1(a) indicates that lower bound K_{mat} for such a steel is about 2000 Nmm$^{-1.5}$ (63 MPa$\sqrt{m}$) at $0^{o}C$.

 The actual data may indicate that the steel in fact had a CVN toughness range of say, 100 to 110 J at $-40^{o}C$. Clearly, the CVN toughness would be higher at the design temperature of $0^{o}C$. Still, using the 100 J number (lowest value) and Figure B.4.1(b), one would estimate the K_{mat} value to be 3500 Nmm$^{-1.5}$ (110 MPa$\sqrt{m}$). Unfortunately, Reference B.37 implies that one is limited to using the lower of the two K_{mat} values obtained from Figures B.4.1(a) and (b), respectively.

B.4.2.3   Commentary on Fracture Toughness Input

Traditionally, the notch toughness of steels and weldments has been assessed on the basis of absorbed energy in the blunt notched Charpy Vee-Notch specimen, and the minimum requirements for material specification are based primarily on experience. Unfortunately, the CVN notch toughness values cannot be used directly in fracture mechanics analysis described in the previous section. The required input has to be in terms of fracture toughness that is a measure of the material's resistance to fracture initiation from sharp flaws under specific loading conditions. It is conveniently measured by subjecting a single edge (fatigue sharpened) notched specimen to a three point bending load at the test temperature of interest and monitoring load and crack (notch) mouth opening displacement and/or the load line displacement until a fracture occurs in the test or a maximum load condition is reached.

The fracture toughness of a material can be presented in the form of one of three parameters, viz., critical stress intensity factor (K_{Ic}), crack tip opening displacement (CTOD), or the J integral. These parameters, and detailed test procedures to determine them, were initially developed to measure fracture toughness in the three different regimes of fracture toughness-temperature transition curve (**Figure B.4.2**). At low temperatures, the material behaves in a brittle, linear elastic fashion and the extent of plasticity at the crack tip is small compared to specimen thickness. Fracture toughness under these conditions can be expressed in terms of K_{Ic} and measured as per ASTM Standard E399. However, one generally endeavours to avoid using steels that satisfy the requirements of ASTM E399 for valid K_{Ic} values at the design temperature since it would otherwise imply the use of a relatively brittle steel for the intended application.

The CTOD procedure was developed to measure fracture toughness in the ductile-brittle transition region where there is plasticity and stable ductile tearing at the crack tip before the initiation of the brittle cleavage factor. The CTOD toughness can be measured using ASTM Standard E1290 [Ref. B.55] and BSI Standard 7448. Since the extent of plasticity at the crack tip and therefore, the measured CTOD fracture toughness, can depend on the specimen thickness (crack tip constraint), it is recommended that CTOD fracture toughness should be determined using full thickness specimens.

The J integral, on the other hand, was devised for materials that display fully ductile behaviour at the design temperature such as the nuclear pressure vessel steels. The J values are also material thickness dependent and therefore, full thickness specimens should be employed for assessing J value. The ASTM Standards covering measurement of J values are E813, E1152 and E 1737, and recently ASTM E 1820 [Ref. B.57] was introduced that allows CTOD and J to be obtained from the same test.
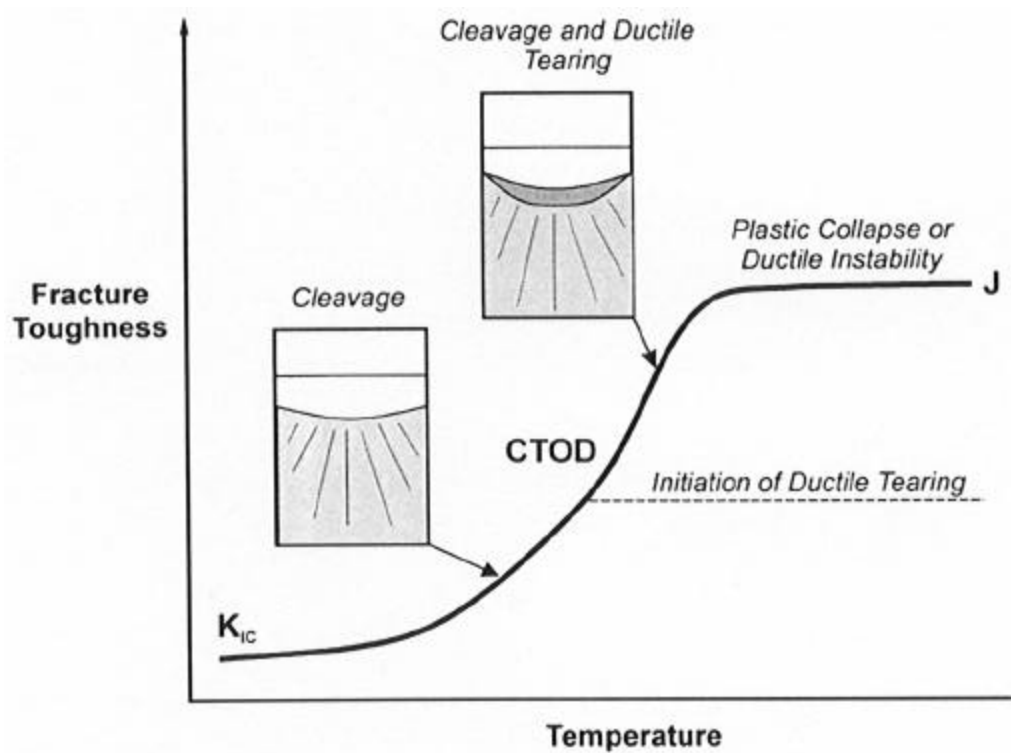
Figure B.4.2: Usually Applicable Measures of Fracture Toughness in the Different Regimes of the Fracture Toughness versus Temperature Curve [Ref. B.60]

In calculating J or CTOD toughness for elastic-plastic materials, another consideration is the stage of the load versus crack mouth opening displacement at which the fracture toughness value should be computed. Referring to the CTOD test load vs CMOD trace shown in **Figure B.4.3**, four CTOD values can be defined. For brittle materials, cleavage fracture is initiated in the elastic load range and an unambiguous CTOD toughness, δ_c, can be calculated. However, in the presence of extensive crack tip plasticity, there are three potential values of CTOD toughness that can be defined. Thus, δ_u denotes CTOD toughness corresponding to the peak load at fracture in specimens that display some ductile tearing at the crack tip before the fracture. Similarly, δ_m refers to the CTOD value corresponding to the maximum load reached in the test for specimens that display ductile tearing only and wherein no cleavage fracture intervenes. In between δ_c and δ_u, there is a potential CTOD value, δ_i, that just corresponds to onset of ductile tearing. Its determination requires a different test procedure so that a CTOD (or J) vs crack growth (Δa) curve (also called the CTOD-R or J-R curve) is generated and then CTOD or J value determined for $\Delta a = 0.2$ mm.
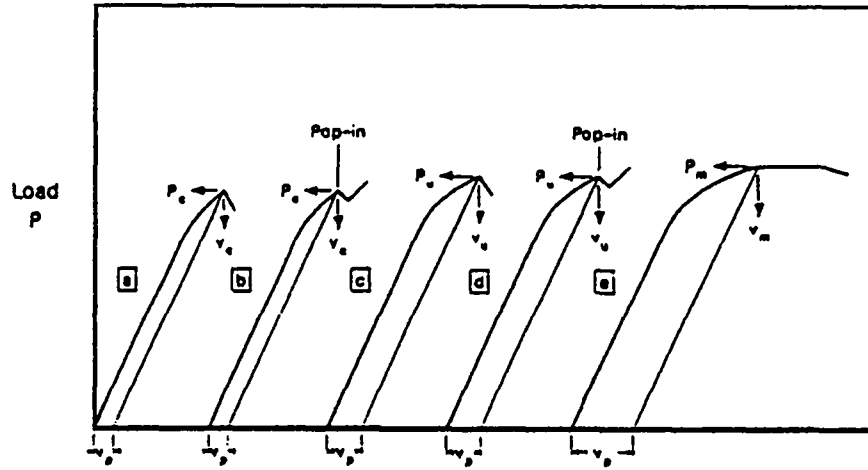
Figure B.4.3: Types of Load versus Crack Mouth Opening Displacement Records [Ref. B.55]

In the linear elastic (plane strain) regime, one can obtain a theoretical relationship between the three measures of fracture toughness:

$$K_{Ic} = \sqrt{\frac{J_{Ic}E}{(1-?^2)}} = \sqrt{\frac{2s_y d_c E}{(1-?^2)}}$$

(B.4.2.5)

where; K_{Ic}, J_{Ic} and δ_c are critical values for fracture toughness expressed in terms of stress intensity factor, J integral and CTOD.

In the presence of crack tip plasticity, however, the relationship between K, J and CTOD breaks down and then one can use the following:

$$K_{mat} = \sqrt{\frac{J_{mat}E}{(1-?^2)}}$$

(B.4.2.6)

where J_{mat} is the J toughness corresponding to 0.2 mm crack extension, i.e., J_{Ic}, though arguments are being developed [Ref. B.60] to accept the use of critical J_u value corresponding to the load at brittle fracture initiation after some stable crack extension.

Based on tests wherein both CTOD and J were measured, Reference B.60 proposes the following for K_{mat} - critical CTOD relationship:

$$K_{mat} = \sqrt{\frac{1.6\sigma_f \delta_{mat} E}{\left(1 - v^2\right)}}$$

(B.4.2.7)

where; σ_f is the flow stress, and δ_{mat} is the critical CTOD for c, u, or m type fracture behaviour. It is presumed that any error caused by the use of these critical values instead of δ_i is small and acceptable.

In the present Guide, following Reference B.60, it is recommended that K_{mat} be estimated from critical CTOD value using Equation B.4.2.7. In comparison, Reference B.37 recommends that if the fracture toughness is available as critical CTOD, it should not be converted to K_{mat}. Instead, the driving force is to be computed in CTOD terms (δ_{app}) using the equation:

$$d_{app} = \frac{K_{app}^2}{s_y E}$$

(B.4.2.8)

Implicit in the above expression is the following relationship between K_{mat} and δ_{mat} :

$$K_{mat} = \sqrt{1.0\, \sigma_y \delta_{mat}\, E}$$

(B.4.2.9)

Equation B.4.2.9 provides a more conservative estimate of the fracture toughness to be used in the analysis. Anderson [Ref. B.60], however, takes issue with this approach because when material toughness data is available both as CTOD and J, their respective use will lead to different answers. The Anderson approach (Equation B.4.2.7) recommended in this Guide provides similar answers when the fracture toughness data used is as CTOD or J from the same test. While this approach is less conservative than the Ref. B.37 approach., the validation studies based on analysis of numerous wide plate tests has indicated that when a lower bound toughness is used (based on a relationship similar to that in Figure B.4.1(a) but a quasi-static loading rate), the predictions with respect to the non-specific material FAD are still safe.

Finally, as mentioned earlier, the use of fracture toughness value, K_{mat}, derived from CVN toughness leads to overly conservative assessment because the K_{mat} - CVN toughness correlation is based on data from thick steels representing plane strain conditions and includes fracture toughness data at dynamic loading rates as well as from crack arrest toughness tests. Therefore, while this method of estimating the K_{mat} value may be fast and convenient, it is the least preferred as well.

B.4.3   Material Data for Fatigue Crack Growth Analysis

B.4.3.1   Crack Growth Characteristics

The fracture mechanics procedure for assessing fatigue crack growth assumes that the Paris equation uniquely characterizes the relationship between da/dN and ΔK for all values of ΔK above a threshold value ΔK_{th}, and that fatigue cracks do not propagate at ΔK values less than ΔK_{th}: (see Section A.3.5)

$$\frac{da}{dN} = C(\Delta K)^m \qquad \text{for } \Delta K > \Delta K_{th}$$

(B.4.3.1)

$$\frac{da}{dN} = 0 \qquad \text{for } \Delta K \leq \Delta K_{th}$$

Whenever possible, specific values of C, m, and ΔK_{th} for the relevant combination of material, direction of crack growth, environment, R-ratio ($\sigma_{min}/\sigma_{max}$), and frequency of cyclic loading should be used in fatigue crack growth predictions, and the chosen values should include a sufficient factor of safety to account for the variability of fatigue crack growth data. If there is any doubt about the applicability of available values in the open literature, then specific da/dN versus ΔK data should be produced in accordance with a relevant test standard such as ASTM E647 [Ref. B.64] or BS 6835 [Ref. B.65].

As discussed later in detail, da/dN versus ΔK data is generated from discrete measurements of crack length during fatigue tests of standard specimens with through-thickness edge cracks or center cracks subjected to Mode I constant amplitude loading. Moving average techniques are used to extract crack growth rates from these measurements, and the corresponding ΔK values are calculated by linear elastic fracture mechanics. It is customary to fit a least squares regression line through log da/dN versus log ΔK data for Region II crack growth (Figure A.3.4) and to report the corresponding C and m values. It is also customary to define an operational value of ΔK_{th} by fitting a least squares regression line through log da/dN versus log ΔK data for Region I crack and by extrapolating the fitted line to the smallest detectable crack growth rate (typically 10^{-10} m/cycle). These values characterize the mean fatigue crack growth behaviour of a test sample, and are usually the values reported in the open literature. Although they can be used as inputs for relative fatigue crack growth assessment, more conservative values are generally required for absolute fatigue crack growth assessments to account for measurement errors, local variations of material properties within a batch of material, and general variations of material properties between different batches of material. If the test specimens and structure being analyzed are fabricated from the same batch of material, then absolute fatigue crack growth assessments should be based on C and ΔK_{th} values that correspond to the mean values of log da/dN in the test sample plus two standard deviations. If it is not possible to fabricate the test specimens from the same batch of material as the structure being analysed, then the test specimens should be fabricated from several other batches of

material to account for the variability of material properties between different batches of material.

B.4.3.2   C and m Values for Region II Crack Growth in Steels in Air

Although Region II crack growth rates for steels in air tend to increase with increasing R-ratio, this dependency is small compared to the dependency of Region I crack growth on R-ratio and it is usually ignored in comparisons of Region II crack growth rates for different steels. For example, Barsom and Rolfe [Ref. B.66] compiled da/dN versus ΔK data for Region II crack growth in a wide range of steels tested at various R-ratios, and divided this data into three groups according to microstructural differences (viz., martensitic, ferritic-pearlitic, or austenitic). They found that most of the measured crack growth rates within each group varied by less than a factor of two at any given ΔK value. Considering the wide range of mechanical properties and chemical compositions represented within each group, Reference B.66 suggested that engineering estimates of crack growth rates in martensitic, austenitic, and ferritic-pearlitic steels could be obtained from the following upper bound relationships[1]:

martensitic steels

$$\frac{da}{dN} \;=\; 1.2 \,\times\, 10^{-10} \Delta K^{2.25} \qquad\qquad\qquad (B.4.3.2)$$

ferritic-pearlitic steels

$$\frac{da}{dN} \;=\; 4.92 \,\times\, 10^{-13} \Delta K^{3} \qquad\qquad\qquad (B.4.3.3)$$

austenitic steels

$$\frac{da}{dN} \;=\; 1.73 \,\times\, 10^{-13} \Delta K^{3.25} \qquad\qquad\qquad (B.4.3.4)$$

Most investigations of fatigue crack growth in steels have not been accompanied by fractographic examinations of fatigue crack growth mechanisms. The few studies that have involved such examinations have shown that Region II fatigue crack growth in a wide range of microstructures occurs by a transgranular striation mechanism, and that crack growth rates associated with this mechanism fall within a common scatter band regardless of R-ratio and tensile strength. Departures from the striation mechanism (e.g., microcleavage in coarse pearlitic steels and steels with brittle second phase particles such as spheroidized carbides, intergranular cracking in tempered martensite tested at low ΔK, void coalescence in tempered martensitic steels tested at high ΔK) are invariably associated with higher crack growth rates that tend to increase with increasing tensile strength and R-ratio.

---

[1] Units for da/dN and ΔK are mm/cycle and MPa√mm respectively.

References B.67 and B.37 recommend, in the absence of specific data, the following relationship for engineering assessments of fatigue crack growth in ferritic structural steels (including plain plate, weld metal, and heat affected zone metal with yield strengths below 600 MPa) operating in air at temperatures up to 100°C:

$$\frac{da}{dN} = .3.0 \times 10^{-13} \left(? \ K^3\right) \quad (striation)$$

(B.4.3.5)

This relationship represents an upper bound on published da/dN versus ΔK data for crack growth by a striation mechanism. If there is a potential for crack growth by non-striation mechanisms (e.g., certain weld metals and heat affected zones as K_{max} approaches its critical value), then both references recommend the following equation:

$$\frac{da}{dN} = 6.0 \times 10^{-13} \left(? \ K^3\right) \quad (non\text{-}striation) \qquad (B.4.3.6)$$

The former equation may be overly conservative for certain steels since the crack growth rate determined by a striation mechanism in different steels can vary by as much as a factor of five for a given ΔK value while the latter equation should be used with caution since it is less conservative than Reference B.66's upper bound relationship for martensitic steels.

Note: Equations B.4.3.6 and B.4.15 correspond to the mean of log da/dN plus two standard deviations for pooled data.

As this Guide is being produced, a new standard has been drafted and circulated for comment by the British Standards Institute, which will eventually replace Reference B.37 [Ref. B.68]. It advocates a two-stage linear relationship, but recommends that for a simplified analysis a one-stage law can be assumed, with no distinction between striation and non- striation mechanisms. It mentions one value of C of 5.21 x 10⁻¹³ as in Equation B.4.3.1.

B.4.3.3 ΔK_{th} Values for Steels in Air

ΔK_{th} values for steels are essentially independent of R-ratio for R-ratios less than 0.1, but tend to decrease with increasing R-ratio for R-ratios above 0.1. Several investigators [Ref. B.69, B.70] have compiled ΔK_{th} values for a wide range of steels in air, and in Reference B.66 can be found the following equations which define a reasonable lower bound on this data:

$$\Delta K_{th} = 190 \ MPa\sqrt{mm} \qquad\qquad for \ R < 0.1 \qquad\qquad (B.4.3.7)$$
$$\Delta K_{th} = 221(1 - .85R) \ MPa\sqrt{mm} \qquad for \ R \geq 0.1 \qquad\qquad (B.4.3.8)$$

The range of compiled ΔK_{th} values for a given R-ratio is nearly 300 MPa√mm at R-ratios less than 0.1, but narrows with increasing R-ratio to about 60 MPa√mm at an R-ratio of 0.9. The greater range of ΔK_{th} values at low R-ratios appears to be related to the strong influence of microstructure on ΔK_{th} for some steels loaded at low R-ratios. In particular, Taylor [Ref. B.71] and Ritchie [Ref. B.72] have noted that ΔK_{th} values for martensitic steels, bainitic steels, and ferritic-pearlitic steels with high ferrite content decrease significantly with increasing yield strength at low R-ratios whereas ΔK_{th} values for ferritic-pearlitic steels with high pearlite content are relatively insensitive to yield strength.

In addition, several investigators [Ref. B.72] reported a marked increase in ΔK_{th} for various low strength ferritic-pearlitic steels loaded at low R-ratios when ferrite grain size was increased, while other investigators [Ref. B.71] found little effect of prior austenite grain size on ΔK_{th} values for martensitic and bainitic high strength steels loaded at low R-ratios.

Finally, it is noted that References B.37 and the new Reference B.68 advocate that ΔK_{th} should not exceed 65 MPa√mm

B.4.3.4   C, m, and ΔK_{th} Values for Fatigue Crack Growth in a Marine Environment

Unprotected areas of steel marine structures are prone to general corrosion as a result of exposure to sea water. Wastage can lead to higher stresses as a result of reductions in net section and load re-distribution away from severely corroded structure, and gross corrosion pitting can introduce significant stress concentrations in plating. In addition to these factors, which effectively increase the driving force for fatigue crack propagation, the resistance of steels to fatigue crack propagation can be reduced by various corrosion fatigue mechanisms.

Various experimental studies have shown that the fatigue crack growth resistance of freely corroding steels in sea water differs from that in air [Ref. B.73, Ref. B.74]. Fatigue crack growth rates under free corrosion conditions approach those in air at high ΔK values (> 1500 MPa√mm) and as ΔK approaches ΔK_{th} (< 300 MPa√mm). At intermediate ΔK values, however, crack growth rates under free corrosion conditions are higher than those in air and can be characterized by a bi-linear relationship between log da/dN and log ΔK. The difference between crack growth rates in air and under free conditions is highest at the knee of the bi-linear relationship and increases with decreasing loading frequency, increasing temperature, and increasing oxygen content. For example, it has been observed that growth rates under free corrosion conditions in $0^{o}C$ sea water are only marginally higher than crack growth rates in air at room temperature, whereas crack growth rates under free corrosion conditions in sea water at room temperature are 3 to 4 times faster than those in air at room temperature. This acceleration of crack growth has been attributed to anodic dissolution at the crack tip that is enhanced by higher temperatures, lower loading frequency, and higher oxygen content. It is also believed that the diffusion of hydrogen to the crack tip contributes to the acceleration of crack growth, but it is not clear whether this is through an embrittlement mechanism or through some other form of hydrogen-assisted cracking.

It is also worth noting that the knee of the bi-linear relationship occurs at a higher ΔK value with decreasing frequency. Furthermore, crack growth rates above this knee increase with decreasing frequency. In contrast, crack growth rates seem to be independent of frequency although there is relatively little data on frequency effects in this regime (Region I).

Cathodic protection is used to control the general corrosion process in steel marine structures. Although it is believed that cathodic protection helps to nullify the anodic dissolution process at a crack tip as well, experimental studies indicate that cathodic protection does not completely restore fatigue crack growth rates in steels to their in-air values [Ref. B.74 to Ref. B.76]. In Region I, cathodic protection reduces crack growth rates in sea water below crack growth rates in air and increases ΔK_{th} values in sea water above ΔK_{th} values in air. Increasing the negativity of impressed potentials increases ΔK_{th} and decreases crack growth rates.

These beneficial effects of cathodic protection have been attributed to the precipitation of calcareous deposits which wedge the crack closed at ΔK values near ΔK_{th}. In Region II, crack growth approaches a plateau of constant rate. Above this plateau, growth rates approach in-air values. Crack growth rates along this plateau increase with increasing impressed potential, decreasing loading frequency, and increasing R-ratio. Impressed potentials of -0.7V to -0.8V (Ag/AgCl) have been found to reduce fatigue crack growth rates in sea water close to air values, whereas highly negative impressed potentials (-1.1 V) have been found to elevate crack growth rates in sea water above growth rates under free corrosion conditions. It is believed that the more negative potentials increase the amount of hydrogen available for adsorption and diffusion to the crack tip and, therefore, promotes hydrogen-assisted cracking.

Recommendations of da/dN versus ΔK relationships for engineering predictions of fatigue crack propagation in steels in a marine environment have been complicated by the sensitivity of crack growth rates to impressed potential, loading frequency, R-ratio, and the complex relationship between da/dN versus ΔK. In the absence of specific corrosion fatigue data, Reference B.37 recommends the following relationships[2] for engineering assessments of fatigue crack growth in ferritic structural steels in a marine environment:

$$\frac{da}{dN} = 2.3 \times 10^{-12} \Delta K^3 \qquad \text{for } \Delta K > \Delta K_{th} \qquad\qquad \text{(B.4.3.9)}$$

$$\frac{da}{dN} = 0 \qquad\qquad\qquad\quad \text{for } \Delta K \leq \Delta K_{th} \qquad\qquad \text{(B.4.3.10)}$$

$$\Delta K_{th} = 63 \qquad\qquad\qquad\quad \text{for } R > 0.5 \qquad\qquad\qquad \text{(B.4..3.11)}$$

$$\Delta K_{th} = 170 - 214R \qquad\qquad \text{for } 0 < R < 0.5 \qquad\qquad \text{(B.4.3.12)}$$

---

[2] Units for da/dN and ΔK are mm/cycle and MPa$\sqrt{}$mm respectively.

$$\Delta K_{th} = 170 \qquad \text{for } R < 0 \qquad (B.4.3.13)$$

These equations, which are similar to relationships recommended by Reference B.77, define an upper bound on crack growth rates over a wide range of ΔK values in structural ferritic steels that are loaded at high R-ratios and cathodically protected at highly negative impressed potentials. Although Equation B.4.3.9 does not clear all of the experimental data for cathodically protected steels in the plateau region, the value of C in this equation has been chosen to ensure conservative fatigue life predictions for steels loaded at high R-ratios and cathodically protected at highly negative impressed potentials.

B.5   REFERENCES

[B.1]   Glen, I.F., Dinovitzer, A., Paterson, R.B., Luznik, L., and Bayley, C.,"Fatigue-Resistant Detail Design Guide for Ship Structures", Ship Structure Committee Report SSC 405, Project No. SR-1386, 1999.

[B.2]   Cramer, E.H., Schulte-Strauthaus, R., and Bea, R.G., "Structural Maintenance Project Volume 1: Fatigue Damage Evaluation", SSC Report 386, Ship Structure Committee, 1995.

[B.3]   Chen, Y. N., and Shin, Y. S., "Consideration of Loads for Fatigue Assessment of Ship Structure", National Research Council Symposium and Workshop on The Prevention of Fracture in Ship Structure, Washington, DC, March 1995.

[B.4]   Broek, D., Elementary Engineering Fracture Mechanics: 4th Edition, Kluwer Academic Publishers, 1986.

[B.5]   Ochi, M. K., "Wave Statistics for the Design of Ships and Ocean Structures", Presentation at the Annual Meeting of the Society of Naval Architects and Marine Engineers, New York, NY, November 1978.

[B.6]   Hogben, N., Dacunha, N.M.C., and Oliver, G.F., Global Wave Statistics, BMT, 1986.

[B.7]   Glen, I., Paterson, R.B., Luznik, L., "Sea Operational Profiles for Structural Reliability Assessments", Ship Structure Committee Report SSC 406, 1999.

[B.8]   Bales, S.L., Lee, W.T., and Voelker, J.M., "Standardized Wind and Wave Environments for NATO Operational Areas", DTNSRDC Report SPD-0919-01, 1981.

[B.9]   Gilhousen, D.B., Quayle, R.G., Baldwin, R.G., Karl, T.R., and Brines, R.O., "Climatic Summaries for NOAA Data Buoys", USDC, 1983.

[B.10] "Wind and Wave Climate Atlas" – 4 Volumes TP10820 Transport Canada 1981

[B.11] Salveson, N., Tuck,E.O. and Faltinsen, O.M., "Ship Motions and Sea Loads" Trans. SNAME 1970.

[B.12] McTaggart, K., "SHIPMO7 – An Updated Strip Theory Program for Predicting Ship Motions and Sea Loads in Waves" Defence Research Establishment Atlantic Tech Memo 96/243, 1997.

B.13] Meyers, W.G., Applebee, T.R., Baitis, A.E., "User's Manual for the Standard Ship Motion Program SMP", DTNSRDC/SPD-0936-01, September, 1981.

[B.14] Huijsmans, R.H.M., and Willemstein, A.P., "PRECAL V 3.0" Marin Report, Dec 1998.

[B.15] "Principles of Naval Architecture – Volume III", Edited by Edward V. Lewis, SNAME 1988.

[B.16] Det Norske Veritas, Structural Reliability Analysis of Marine Structures, Classification Notes No. 30.6, DNV, July, 1992.

[B.17] Mansour, A.E., Wirsching, P., White, G., and Ayyub, B., "Probability-Based Ship Design Implementation of Design Guidelines for Ships: A Demonstration", Report SSC 392, Ship Structure Committee, Washington, D.C., March 1996

[B.18] American Bureau of Ships, "Guide for Fatigue Strength Assessment of Tankers", June 1992.

[B.19] American Bureau of Shipping, *"The ABS SAFEHULL System"*, 1996.

[B.20] Clarke, J.D., "Derivation of Static Balance Wave Height for Estimating Maximum Midships Vertical Bending Moment", Report TM 85118, Admiralty Research Establishment, Dunfermline, 1985.

[B.21] Clarke, J.D., "Wave Loading in Warships", Advances In Marine Structures, Elsevier Applied Science Publishers, London, 1986.

[B.22] Chalmers, D.W., Design of Ships' Structures, HMSO, London, UK, 1993.

[B.23] Sikora, J.P., Dinsenbacher, A., and Beach, J.E., "A Method for Estimating Lifetime Loads and Fatigue Lives for SWATH and Conventional Monohull Ships", Naval Engineers Journal, May 1983.

[B.24] Sikora, J.P. and Beach, J.E., "Automated Method for Predicting Maximum Lifetime Loads and Fatigue Lives of Ships", Current Practices and New Technology in Ocean Engineering , edited by T. McGuiness, presented at the 9th Annual Energy Sources Technology Conference and Exhibition, New Orleans, LA, American Society of Mechanical Engineers, New York, NY, 1986.

[B.25] Cramer, E., Gran, S., Holtsmark, G., Lotsberg, I., Løseth, R., Olaisen, K., and Valsgård, S, "Fatigue Assessment of Ship Structures", DNVC Report No. 93-0432, Rev. 5, Det Norske Veritas Classification AS, February 1993.

[B.26] Det Norske Veritas,"Fatigue Assessment of Ship Structures", Classification Notes No. 30.7, September 1998.

[B.27] Det Norske Veritas, Rules for Classification of Ships, Newbuildings, Hull and Equipment Main Class, Part 3, Chapter 1, Hull Structural Design Ships with Length 100 metres and above, 1993.

[B.28] Ochi, M. and Bales, S., "Effect of Various Spectral Formulations in Predicting Responses of Marine Vehicles and Ocean Structures", presented at the 9th Annual OTC, Houston, TX, 1977.

[B.29] Glen, I., Paterson, R.B., and Luznik, L., "Sea Operational Profiles for Structural Reliability Assessments" SSC Report 406 Project SR1388, 1999.

[B.30] Jensen, J.J., and Pederson, P.T., "Wave-induced Bending Moments in Ships - A Quadratic Theory", Transactions RINA, Supplementary Papers, Vol. 121, 1979.

[B.31] Mansour, A.E., Wirsching, P., et al. "Assessment of Reliability of Ship Structures", Phase 2, Ship Structure Committee Report SSC 398, Project SR 1344, 1997.

[B.32] Hobbacher, A., "Stress Intensity Factors of Welded Joints", Engng. Fracture Mechanics, Vol. 46, No. 2, pp173-182, 1993.

[B.33} Hughes, O., "Ship Structural Design: A Rationally-Based, Computer-Aided, Optimization Approach", Wiley-Interscience, New York, 1983.

[B.34] Stambaugh, K., Lawrence, F., and Dimitriakis, S., "Improved Ship Hull Structural Details Relative to Fatigue", SSC-379, 1994.

[B.35] Yoneya, T., Kumano, A., Yamamoto, N., and Shigemi, T., "Hull Cracking of Very Large Ships", Integrity of Offshore Structures-5, Paper 15, University of Glasgow, Scotland, 1992.

[B.36] Ma, K.T., Bea,R., "Repair Management System for Fatigue Cracks in Ship Critical Structural Details, Report SMP III-1-1, Dept of Naval Architecture and Offshore Engineering, University of Berkeley, CA Dec. 1994

[B.37] PD6493: 1991, "Guidance on Methods for Assessing the Acceptability of Flaws in Fusion Welded Structure", BSI, 1991.

[B.38] Almer-Naess, A., Ed., "Fatigue Handbook – Offshore Steel Structures", Tapir Publishers, Trondheim, Norway, 1985.

[B.39] Murakami, Y., (editor), "Stress Intensity Factor Handbook", Comm. on Fracture Mechanics, Japan, Vol. 2, Pergammon Press, 1987.

[B.40] Tada, H., Paris, P.C., and Irwin, G., "The Stress Analysis of Cracks Handbook", Del Res. Corp., Hellertown, Pa., 1984.

[B.41] Rooke D.P., and Cartwright, "Compendium of Stress Intensity Factors", The Hillington Press, 1976.

[B.42] Sih, G., "Handbook of Stress Intensity Factors, Leheigh University, Bethlehem, Pa., 1973.

[B.43] Bell, R., "Stress Intensity Factors for Weld Toe Cracks in T-Plate Joints", DSS Contract Serial No. OST84-00125, Faculty of Engineering, Carleton University, Canada, May 1987.

[B.44] Nykanen, T., "On the Effect of Weld Shape on the Crack Shape Development at the Toe of a Fillet Weld", Lappenranta University of Finland, Dept. Mechanical Engineering, 1987.

[B.45] Straalen, I., Dijkstra, O., and Snijder, H., "Stress Intensity Factors and Fatigue Crack Growth of Semi-Elliptical Surface Cracks at Weld Toes", Prc. Int. Conf. Weld Failures, Paper 15, pp. 367-376, TWI, 1988.

[B.46] Pang, H., "A Review of Stress Intensity Factors for a Semi-Elliptical Surface Crack in a Plate and Fillet Welded Joint", TWI, 426, November 1990.

[B.47] Bell, R., and Kirkhope, J., "The Evaluation of 3-Dimensional Stress Intensity Factors Using Finite Elemental Methods", Phase 1 Report, DSS Contract 8SV80-00010, Faculty of Engineering, Carleton University, Canada, August 1981.

[B.48] Chan, S.K., Tuba, I.S., and Wilson, W.K., "On the Finite Element Method in Linear Elastic Fracture Mechanics", Engng. Fracture Mechanics, Vol. 2, No. 1, 1970.

[B.49] Barsoum, R.S. "On the Use of Isoparametric Elements in Linear Fracture Mechanics" Int. J. for Num. Methods in Engrg. Vol 10 (1976)

[B.50] Barsoum, R.S., "Triangular Quarter Point Elements as Elastic and Perfectly Plastic Crack Tip Elements", Int. J. for Num. Meth. In Engng., Vol 11, 1977.

[B.51] Niu,X.,Glinka,G.,"The Weld Profile Effect on Stress Intensity Factors in Weldments" Int. J. Fracture, 35,1987

[B.52] Albrecht, P., and Yamada, K., "Rapid Calculation of Stress Intensity Factors", J. Struct. Div., ASCE, 103(ST2), pp. 377-389, 1977.

[B.53] Willoughby, A., and Davey, T., "Plastic Collapse at Part Wall Flaws in Plates", ASTM STP 1020, pp 390-409, 1989.

[B.54] Miller, A., "Review of Limit Loads of Structures Containing Defects", Central Electricity Generating Board Report TPRD/B/0093/N82, Rev 1., December 1984.

[B.55] ASTM Standard E 1290 "Standard Test Method for Crack-Tip Opening Displacement (CTOD) Fracture Toughness   Measurement", American Society of Testing and Materials, Philadelphia.

[B.56] ASTM Standard E 1737 "Standard Test Method for J-Integral Characterization of Fracture Toughness", American Society of Testing and Materials, Philadelphia.

[B.57] ASTM Standard E 1820 "Test Practice (Method) for Fracture Toughness in the Transition Range", (Draft) American Society of Testing and Materials, Philadelphia, 1995.

[B.58] Sumpter, J. D. G. et al., "Fracture Toughness of Ship Steels", The Royal Institute of Naval Architects, "The Naval Architect", July-August 1989, pp 169-186.

[B.59] Wallin, K., "Fracture Toughness Transition Curve for Ferritic Structural steels", Proc. of the Joint FEFG/ICF Intl. Conf. On Fracture of engineering materials, Singapore, 1991, pp. 83-88.

[B.60] Anderson, T.L.: "US Fracture Mechanics Methodologies for Welded Structures", IIW Doc. X-1315-95.

[B.61] Phaal R., et al, "Current Status of Revisions to PD 6493 Assessment Procedures for Fusion Welded Structures", IIW Doc. X-1314-95.

[B.62] "Guidance on the Methods for Assessing the Acceptability of Flaws in Fusion Welded Structures, PD 6493-1991", published by the British Standards Institution.

[B.63] Yajima, H, and Tada, M., "Material Selection of Hull Plates Based on Fracture Toughness", Technical Review (published by Mitsubishi Heavy Industries Limited), February 1981, p 52.

[B.64] ASTM E647, "Standard Test Method for Measurement of Fatigue Crack Growth Rates".

[B.65] BS6835, "Method for Determination of the Rate of Fatigue Crack Growth in Metallic Materials".
.

[B.66] Barsom, J.M. and Rolfe, S.T., <u>Fracture and Fatigue Control in Structures</u>, Prentice-Hall, Englewood Cliffs, New Jersey, 1987.

[B.67] BS7608, "Code of Practice for Fatigue Design and Assessment of Steel Structures", 1993.

[B.68] BSI Document 97/714934 DC, "BS 7910 Guide on Methods for Assessing the Acceptability of Flaws in Structures" Draft for Public comment dated 17th Sep. 1999.

[B.69] Lindley, T.C. and Richards, C.E., "Near-Threshold Fatigue Crack Growth in Materials Used in the Electricity Supply Industry", Fatigue Thresholds - Fundamentals and Engineering Applications, EMAS, U.K., 1982.

[B.70] Priddle, E.K., "The Threshold Stress Intensity Factor for Fatigue Crack Growth in Mild Steel Plate and Weld Metal: Some Effects of Temperature and Environment", Fatigue Thresholds - Fundamentals and Engineering Applications, EMAS, U.K., 1982.

[B.71] Taylor, D., <u>Fatigue Thresholds</u>, Buterworth, London, 1989.

[B.72] Ritchie, R.O., "Near-threshold Fatigue-Crack Propagation in Steels", International Metals Reviews, Review 245, No. 5 and 6, 1979.

[B.73] Jaske, C.E., Broek, D., Slater, J.E., and Anderson, W.E., "Corrosion Fatigue of Structural Steels in Seawater and for Offshore Applications", <u>Corrosion Fatigue Technology</u>, ASTM STP 642, 1978.

[B.74] Bignonnet, A., "Corrosion Fatigue of Steel in Marine Structures - A Decade of Progress", Proc. of 3rd Int. Conf. on Steel in Marine Structures (SIMS'87), Delft, Netherlands, June 15-18, 1987, Paper PS5, pp 119-135.

[B.75] Burnside, O.H., Jr. Hudak, S.J., Oelkers, E., Chan, K., and Dexter, R.J., "Long-Term Corrosion Fatigue of Welded Marine Steels", Ship Structure Committee Report SSC-326, 1984.

[B.76] Vosikovsky, O., "Frequency, Stress Ratio, and Potential Effects on Fatigue Crack Growth of HY130 Steel in Salt Water", J. Testing and Evaluation, 6(3) 1978.

[B.77] "Fatigue Background Guidance Document", Health and Safety Executive, OTH Report 92 390, 1995.

PART C   DAMAGE TOLERANCE ANALYSIS

C.1   ASSESSMENT OF RESIDUAL STRENGTH

C.1.1   Introduction

As discussed in Part A, a key element of damage tolerance assessment is the estimation of the **residual strength** of a damaged structure at a particular point in time (i.e., the load-bearing capacity of the structure in the presence of a crack of known size).

The main purpose of residual strength assessment of a structural member containing a crack is to ensure that it does not lead to unstable brittle fracture or local plastic collapse. The importance of such an assessment is obvious for flaws in primary structure. Residual strength assessment of flaws in secondary structural members may not seem as important since there is a greater possibility of stress redistribution in secondary structural members. However, a brittle fracture that initiates in secondary structure may run into adjoining primary structure before being arrested by stress relaxation or tougher material. For example, brittle fracture of a poorly fabricated splice weld in a longitudinal [Ref. C.1] or brittle fracture initiation from a fatigue crack at the toe of a bracket welded to a longitudinal frame [Ref. C.2] can penetrate the shell and affect the overall structural integrity and water-tightness of a ship.

The residual strength of a structural member containing a crack depends on the potential failure mode (e.g., brittle cleavage fracture, cleavage fracture preceded by ductile tearing, and plastic collapse). Brittle fractures are of greatest concern since low material toughness and/or local stress concentrations can precipitate the initiation of fast catastrophic fracture at nominal stresses that are far below the uni-axial yield strength of the material. Local plastic collapse, on the other hand, occurs when the stresses in the remaining ligament adjacent to the crack exceeds the flow stress of the material. Local collapse should be differentiated from global structural collapse because local collapse may be preceded by structural collapse at some other smaller flaw located in a region of higher stresses (e.g., smaller flaw subject to hoop stress in a pressure vessel compared to another flaw subject to longitudinal stresses). Local collapse may indeed lead to structural collapse if the affected member is a non-redundant one. In between the possibilities of brittle fracture and local plastic collapse, there can be situations where some ductile tearing at crack tips may precede unstable fracture.

C.1.2 Residual Strength Assessment using the FAD Concept

The Failure Assessment Diagram (FAD) was introduced in Part A section A.3.5. The FAD is a graphical model of the potential for failure by brittle fracture or local plastic collapse for different combinations of crack driving force and net-section stress (i.e., stress across remaining uncracked ligament). This diagram consists of two elements (Figure C.1.1), the Failure Assessment Point (FAP) and the Failure Assessment Curve (FAC).

The FAP defines the state of a member containing a flaw under specific service conditions. The vertical co-ordinate of this point (ordinate) is defined by the ratio of the applied crack driving force to the fracture toughness of the material (K_r), while the horizontal co-ordinate (abscissa) of the point is defined by the ratio of the applied net section stress to the yield strength or flow strength of the material. These abscissa ratios are referred to as L_r and S_r respectively.

The FAC, on the other hand, represents critical combinations of the non-dimensionalised crack driving force and non-dimensionalised net section stress.

The structure being analysed is deemed to be safe if the FAP lies within the region bounded by the FAC and axes of the FAD. Failure is predicted if the FAP lies outside of the region bounded by the FAC and axes of the FAD. The failure mode is expected to be brittle fracture initiation in the upper left corner of the FAD, by plastic collapse in the lower right corner of the FAD, and by a mixed mode in between.

The FAD shown in Figure C.1.1 (and also in Figure A.3.3) is a commonly used FAD based on the strip yield model for a crack in an infinitely wide plate. In this diagram, the vertical co-ordinate (K_r) is the ratio of the crack tip stress intensity factor (K_{app}) to the material's fracture toughness (K_{mat}). The horizontal co-ordinate (S_r) is the ratio of the applied net section stress (σ_n) to the material flow strength (σ_f). The crack tip stress intensity factor quantifies the severity of the asymptotic stress-strain field at a crack tip in linear elastic material (i.e., K-field). The derivation of the FAC in this FAD is briefly discussed below.

If the material were to behave in a perfectly linear elastic manner, then the shape of the FAD would be a square bounded by lines at $K_r = 1.0$ and $S_r = 1.0$. The actual driving force for brittle fracture in this case (K_{app}) would be given by:

$$K_{app} = Y\sigma_{app} \cdot T \cdot \sqrt{\pi a}$$

(C.1.2.1)

where K_{app} (also denoted as K_I) is the driving force for crack initiation from a through-thickness crack of half length a that is present in a structural member subject to an applied stress σ_{app}. This is the same equation as B.3.6.3
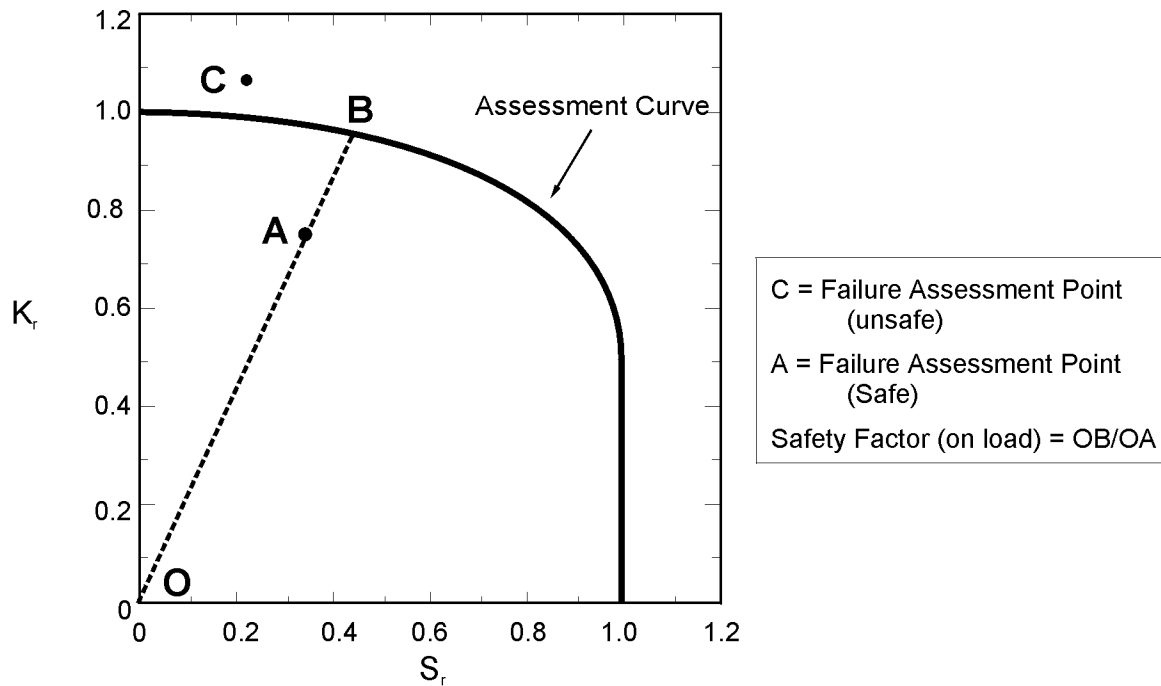

Figure C.1.1: Level 2 Failure Assessment Diagram based on Strip yield Model [Ref. C.3]

In practice, most structural steels display at least some degree of elastic-plastic behaviour so that a certain amount of plasticity develops at the crack tip. In the presence of this plastic zone, the effective driving force for brittle fracture (K_{eff}) is in fact greater than K_{app} calculated on the assumption of linear elastic behaviour. In Irwin's approach [Ref. C.4], this difference is accounted for in the following manner:

$$K_{eff} = Y'\sqrt{\pi(a + r_y)}$$

(C1.2.2)

where, r_y is the radius of the plastic zone size at the crack tip, and the geometry dependent constant Y' now depends on the effective flaw size $(a + r_y)$. The above correction for plastic zone size becomes significant when the applied stress magnitude exceeds about half the material's yield strength (σ_y) and becomes inaccurate when it exceeds about 80% of the yield strength [Ref. C.5].

A more accurate model of the effect of crack tip plasticity on the effective crack driving force is given by the strip yield model [Ref. C.6]. For a through-thickness crack of length **2a** in an infinite plate of an elastic-perfectly plastic material:

$$K_{eff} = s_y \sqrt{pa} \left[\frac{8}{p^2} \ln \sec \left\{ \frac{ps_n}{2s_y} \right\} \right]^{0.5}$$

(C.1.2.3)

By replacing the yield strength (σ_y) in Equation C.1.2.3 by the flow strength (σ_f), one can show from Equations C.1.2.1 and C.1.2.3 that:

$$\frac{K_{app}}{K_{eff}} = \frac{s_n}{s_f} \left[\frac{8}{p^2} \ln \sec \left\{ \frac{ps_n}{2s_f} \right\} \right]^{-0.5}$$

The ratio $\dfrac{K_{app}}{K_{eff}}$ is less than unity in the presence of crack tip plasticity. Also, at the critical point for brittle fracture initiation, $K_{eff} = K_{mat}$, $K_{app}/K_{mat} = K_r$, and $\sigma_n/\sigma_f = S_r$. The above equation may thus be rewritten as:

$$K_r = S_r \left[\frac{8}{p^2} \ln \sec \left\{ \frac{p}{2} S_r \right\} \right]^{-0.5}$$

(C.1.2.4)

This equation defines the FAC in the FAD in Figure C.1.1 (i.e., the ultimate state of a given cracked detail of a given material). This curve or the failure locus for any given value of S_r lies below the line $K_r = 1$ by an amount by which K_{eff} exceeds K_{app}. There are at least two advantages of this approach. First, the non-dimensional crack driving force (K_r) can still be calculated based on linear elastic calculation for K_{app} whereas the material fracture toughness ($K_{mat} = K_{eff}$) can be obtained from full thickness specimens even though these may display crack tip plasticity. Secondly, the approach takes into account failure by brittle fracture as well as plastic collapse. If the structural material has high fracture toughness (high K_{mat}), K_r tends to be small and failure usually occurs by local plastic collapse ($S_r \cong 1$). In the case of a brittle material (low value of K_{mat}), K_r will approach unity very quickly and failure will occur in a brittle mode. In the intermediate region, fracture and collapse interact and fracture occurs in an elastic-plastic manner.

Finally, it should be noted that other FAD's besides those based on the strip yield model have been developed. Some of these FAD's can be used for application to ship structures, depending on the quality of the input parameters and the accuracy desired, and they are discussed in Section C.1.3

C.1.3 Limitations in Application to Ship Structures

The FAD approach for residual strength assessment of a structural member or detail assumes that the far field stresses (away from the flaw but local to the structural member) are well defined and that these do not change as the crack grows. Thus, the FAD, itself, cannot take into account the effect of any redistribution of loads/stresses that might occur as a result of flaw growth or structural redundancy.

In comparison, ship structures are recognised as having a significant degree of structural redundancy, however, quantification of its effect on the stresses in such structures is in its early research stage. Therefore, it is customary to ignore any stress distribution effects, and thus conduct a local residual strength assessment as if the flawed member is isolated from the rest of the structure. If such local residual strength analysis indicates the crack present in a structural member to be larger than the critical size, then, as mentioned in a previous SSC study [Ref. C.7], a normal practice in assessing global structural strength is to completely disregard that member from further consideration.

Another limitation of the FAD approach is that it does not consider buckling which is a common failure mode in ship structures. At this stage, there is little definitive knowledge on the effect of crack like flaws on the buckling residual strength and further research is needed in this area.

Finally, a common limitation in applying the FAD approach to structures is the limited availability of fracture toughness data. This limitation is a particular concern for ship structures because most fracture toughness tests, to the extent that these are indeed performed on materials relevant to ships, are conducted at a quasi-static loading rate whereas the loading rates of extreme wave loads in ship structures are in the intermediate range [C.8]. Clearly, it is necessary to determine fracture toughness values of ship structural steels and weldments at an appropriate loading rate if the application of damage tolerance methodology for residual strength assessment is envisaged. In the meantime, there is no choice but to use the available fracture toughness values with the hope that any degree of unconservatism introduced due to neglect of the loading rate effect will be compensated by conservatism introduced in the selection of the other input parameters.

C.1.4   General Procedure for Determining Residual Strength

There are two principal ways in which FAD's and residual strength assessment procedures can be used. In the first, commonly referred to as **fitness-for-purpose analysis** or **engineering critical assessment**, all the input parameters (applied/service stresses, flaw size, material toughness properties) are known and the main objective is to establish if this particular combination of input parameters is sub-critical (safe) or not. From the known input parameters, K_r and S_r values can be computed and an actual failure assessment point (FAP) can be plotted on the FAD. If this point is within the FAD (e.g., point A in Figure C.1.1), then the structure is safe and its location with respect to the failure assessment curve is indicative of the safety margin. In a deterministic analysis and in the absence of residual stresses, the safety factor on load is OB/OA. An assessment point outside the FAD, point C in Figure C.1.1, would indicate unstable fracture initiation before the peak service stress magnitude is reached.

The second application requires determination of the critical combination of parameters that will lead to failure (i.e., combination of parameters that will lie on the failure assessment curve.). Generally, two of the three inputs would be known and the objective then is to determine the critical value for the third. Thus, for a given known flaw, structural geometry and material properties (strength and fracture toughness), the failure assessment curve can be used to compute the residual strength (maximum allowable applied stress). Conversely, if the maximum magnitude of the in-service applied stresses were known, then the FAC can be used to compute the critical flaw size. Since both the ordinate and the abscissa in the FAD depend on the flaw size and the applied stress, these computations will require an iterative procedure to obtain the final solution. It is, therefore, useful to have a simple computer program to perform these calculations.

C.1.5   Other Commonly used FAD's

The previous section focused on one commonly used FAD based on the strip yield model to explain the FAD concept. However, there are several other FAD's and analysis procedures available for residual strength or critical flaw size analysis. This guide covers FAD's included in Level 1FAD and Level 2 FAD residual strength analysis procedures in Reference C.3, since the 1981 and 1991 editions of this document have been used extensively for flaw assessment and inspection scheduling for offshore structures, bridges, pipelines, storage tanks and pressure vessels. Several revisions and additions were discussed [Ref. C.9] and as this report is completed a new draft BSI document to replace Reference C.3 is being circulated for public comment.[Ref. C.10] To the extent that this information was available, it has been taken into consideration in preparing this Guide.

There are other more sophisticated FAD's and analysis procedures (e.g., Level 3 analysis in Reference C.3 and analysis based on Deformation Plasticity FAD in Reference. C.11), but these are quite complex requiring non-linear, 3-dimensional finite element analysis and specific material properties. These have been developed for tough, ductile materials and enable one to consider ductile tearing, and constraint and weld mismatch effects. These are used mostly in the nuclear industry and are not appropriate for application to ship structures where the accuracy of such procedures is likely to be negated by the uncertainties in the magnitude of the input parameters.

The FAD for **Level 1 FAD analysis** is shown in Figure C.1.2, and the flow diagram for assessing the significance of a known flaw (knowing the service stresses, material fracture toughness, flaw and structural geometry) is shown in Figure C.1.3. The fracture assessment is based on a semi- empirical crack driving force relationship referred to as the CTOD design curve [Ref. C.12] which in turn has been shown to represent an upper bound for the experimental data from a large number of wide plate tests on structural steels and weld metals.

The FAC in this case is defined by two straight lines: K_r or $\sqrt{\delta_r} = 1/\sqrt{2}$ and $S_r = 0.8$ where, K_r is the ratio of the applied crack driving force in terms of the crack tip stress intensity factor (K_I) to the material fracture toughness (K_{mat}), and δ_r is the ratio of the applied crack driving force in terms of CTOD (δ_I) to the corresponding material fracture toughness (δ_{mat}). The value of $1/\sqrt{2}$ for K_r or $\sqrt{\delta_r}$ arises simply from an inclusion of a safety factor of 2 on flaw size in fracture assessment when the applied stress is $\leq 0.5\sigma_y$. At higher applied stresses, the safety factor on flaw size can be slightly different from 2. The CTOD design curve considers fracture only and not failure by plastic collapse and, therefore, to adapt it to the FAD format, an arbitrary cut off for S_r has been established at 0.8. Since there already are safety factors built into this FAD, both on flaw size and on stress ratio, it is advised against the application of additional safety factors in assessing critical stress (residual strength) or critical flaw size.

An assessment based on Level 1 FAD employs upper bound estimates for loading and flaw size, and lower bound estimate for material toughness. In addition, the through-thickness stress distribution at the assessment site is assumed to be uniform for calculating stress intensity factors and net section stresses. These features and the safety factors built into the Level 1 FAD imply that the results of a Level 1 assessment are quite conservative. Since the Level 1 assessment is also relatively easy to perform, it is usually referred to as a **preliminary assessment**. It is appropriate to a Level 2 Load and Stress Analysis as described in Part B. If the analysis finds a flaw to be safe, then no further analysis is deemed necessary. Conversely, if the flaw is found to be unsafe, then one can perform additional assessment based on more complex but more accurate FAD's described in the paragraphs following.
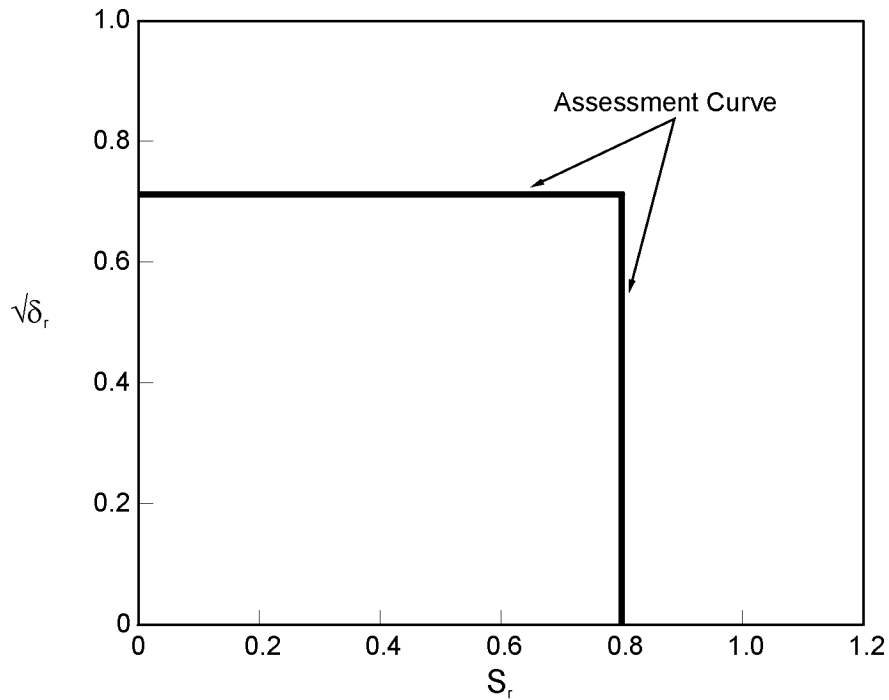
Figure C.1.2: Level 1 Failure Assessment Diagram [Ref. C.3]

Under **Level 2** there are three FAD's that can be used for analysis. These are shown in Figures C.1.1, C.1.4 and C.1.5, respectively and the analysis approach for all three FAD's is summarised in the flow diagram shown in Figure C.1.6. Overall, the three approaches are more accurate than Level 1 assessment, and Reference C.3 refers to Level 2 analyses as normal assessment to assess the susceptibility of a flawed member to unstable fracture. Unlike the Level 1 FAD, there are no built-in safety factors in these FAD's so that any parameters calculated from the FAC (residual strength, flaw size) will be critical values. Therefore, the conservatism of these values in a deterministic assessment will be largely determined by the selected input variables (material fracture toughness, service loads). Guidance on the values for these inputs was provided in Part B.

Level 1
Preliminary Assessment

Define Stresses

Yes — Is Fracture Toughness Data (K, J or δ) Available? — *No*

Determine K_{mat}
δ_{mat}

Estimate Kmat
from Cv

Determine Material Tensile
Properties

Characterize Flaw ← Recharacterize Flaw

Select Analysis Method

Graphical Procedure

Main Procedure

Calculate $\bar{c}$ and $\bar{a}m$

Calculate S_r

Check for Plastic Collapse

Calculate K_r or $\sqrt{\delta_r}$

Plot Assessment Point
$(S_r, K_r$ or $\sqrt{\delta_r})$ on FAD

Assess Significance of
Results

Yes — Defect Tolerable? — *No* — Can Flaw Be Recharacterized? — *Yes*

No

Can Stress Analysis be Refined? — *Yes*

No

Structure Has Been
Demonstrated to be
Safe at Level 1

Structure Cannot be
Demonstrated to be
Safe at Level 1

Figure C.1.3: Flow Chart for Level 1 Assessment [Ref. C.9]

As mentioned earlier, the FAD in Figure C.1.1 is based on the strip yield model and the FAC is given by Equation C.1.2.4. Because of the elastic-perfectly plastic material assumption, it is suitable for low work-hardening materials and therefore recommended for welded steel structures. However, one situation where this Level 2 FAD can become unsafe is when the material displays a yield plateau (Luder band extension) and the applied stresses exceed the yield level so that considerable local strains are involved. To address such situations, one can either impose a cut off for S_r value ≤ 0.83 (1/1.2) or use a material specific FAD (Figure C.1.5).
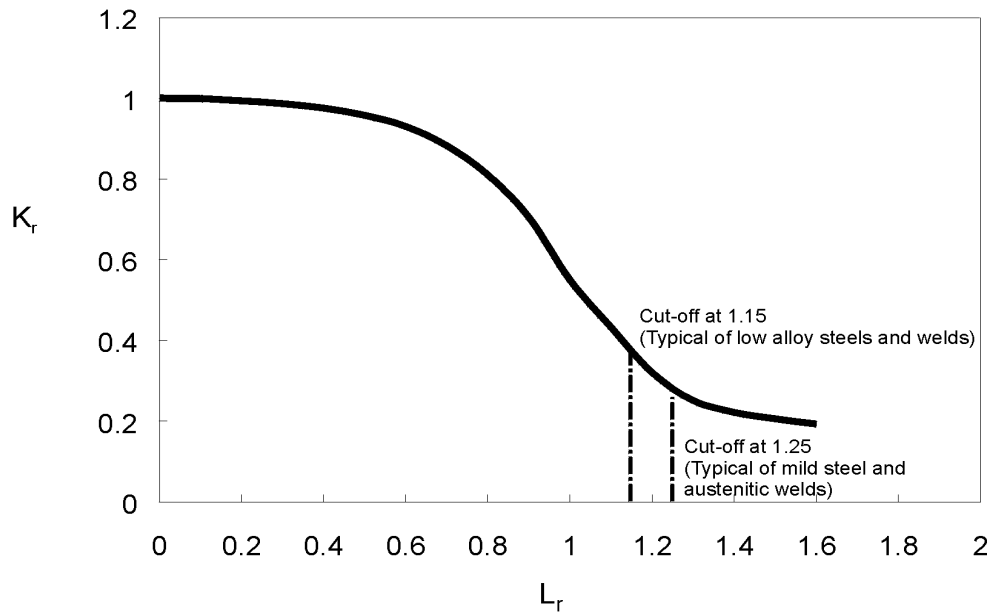
Figure C.1.4: Level 2 Material Non-Specific Failure Assessment Diagram [Ref C.3]

$\sigma_Y = 420$ N/mm^2

$\sigma_U = 560$ N/mm^2
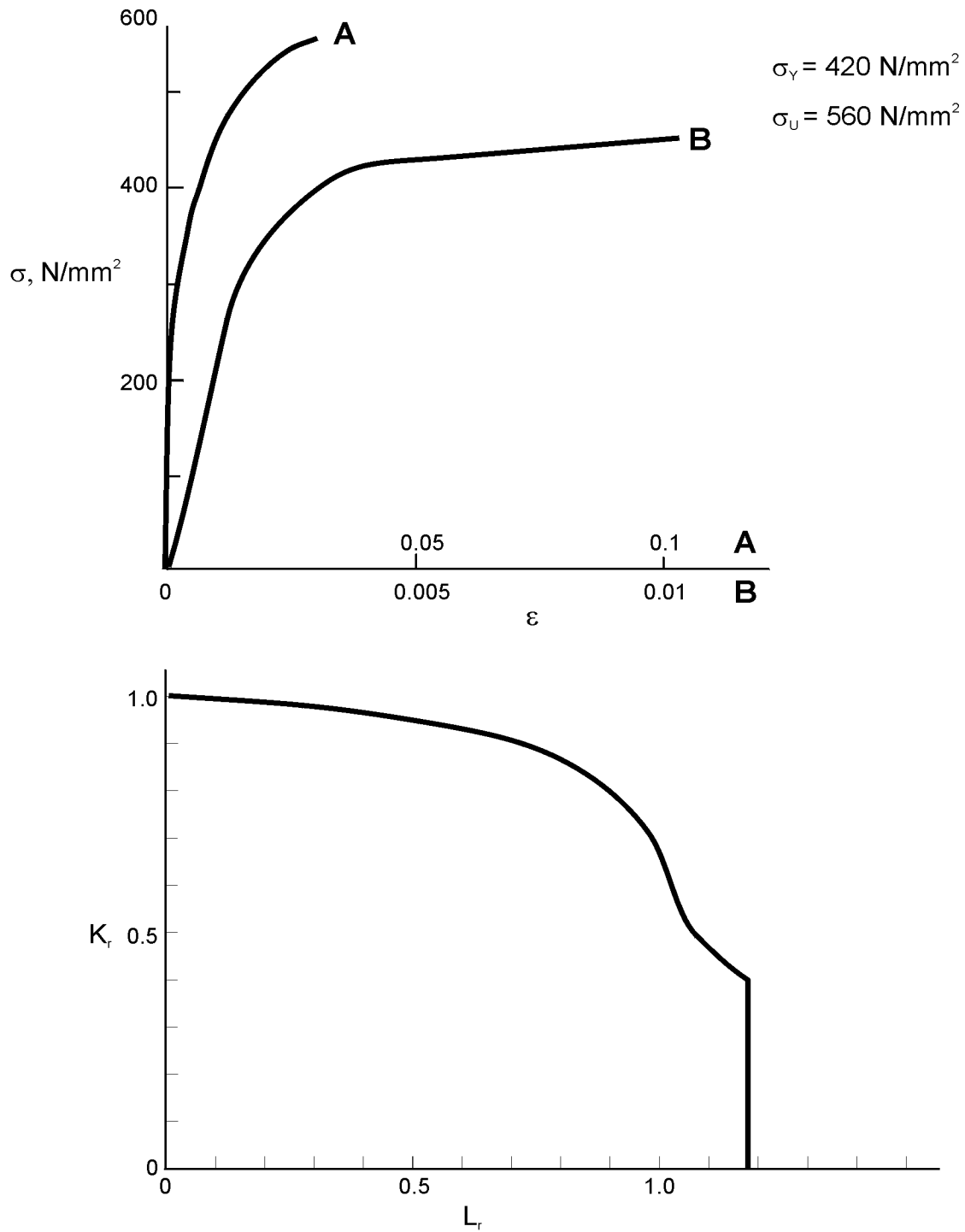
Figure C.1.5(a): Stress-Strain Curve and Material Dependent Failure Assessment Diagram for a Quenched and Tempered Steel [Ref. C.3]

σ_Y = 255 N/mm²

σ_U = 429 N/mm²
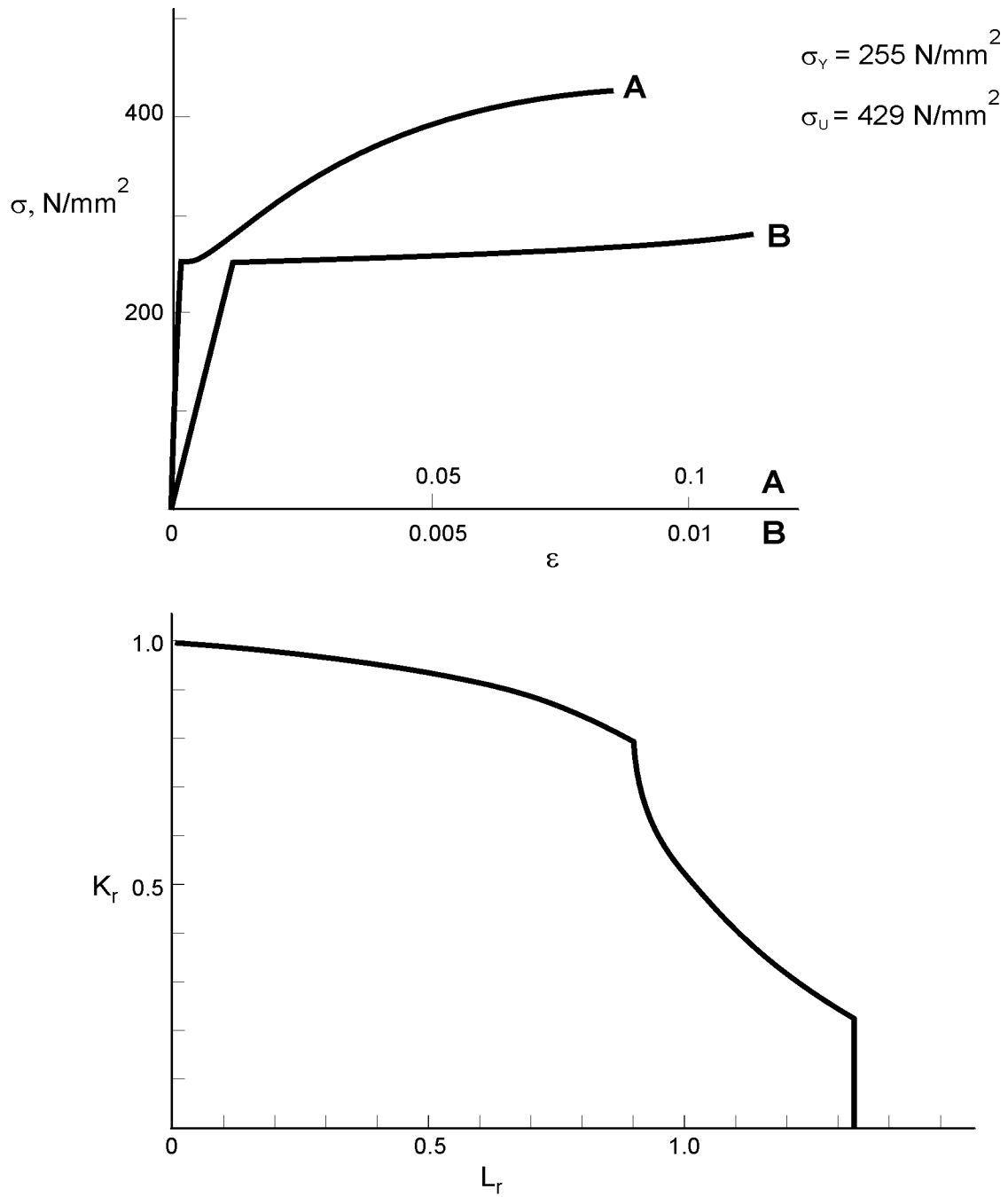
Figure C.1.5(b): Stress- Strain Curve and Material Dependent Failure Assessment Diagram for a Carbon Steel [Ref. C.3]
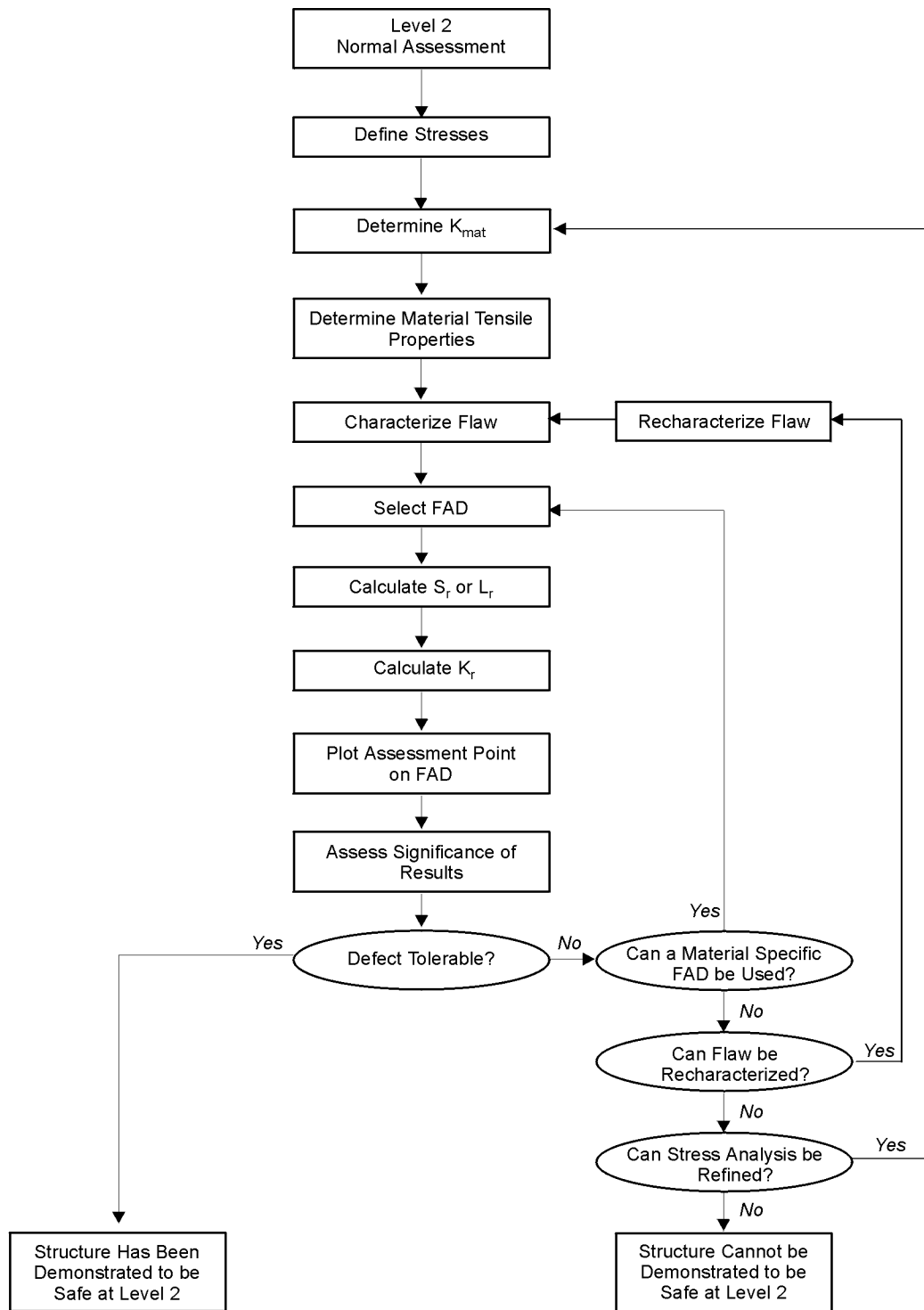
Figure C.1.6: Flow Chart for Level 2 Assessment [Ref. C.9]

The other two Level 2 FAD's (Figures C.1.4 and C.1.5) as presented in Reference C.9 are included in Reference C.3 (1991) as Level 3 FAD's and are more suitable for high work hardening materials (e.g., stainless steels, some low strength ferritic pressure vessel steels). The difference between the FAD's in Figures C.1.4 and C.1.5 is that the former is a lower bound, material non-specific FAD to be used when the stress-strain curve for the material is not available or cannot be easily established (e.g., for heat affected zone), whereas the one in Figure C.1.5 has to be constructed from the actual stress-strain behaviour of the material. The FAC's for these two FAD's are given by the following equations:

Material Non-specific

$$K_r = \left(1 - 0.14 L_r^2\right)\left(0.3 + 0.7 \exp\left(-0.65 L_r^6\right)\right) \quad \text{for } L_r < L_r \text{ max}$$

(C.1.5.1)

$$K_r = 0 \qquad\qquad \text{for } L_r > L_r \text{ max.}$$

Material Specific

$$K_r = \left(\frac{E \ln(1+e)}{s(1+e)} + \frac{s^3(1+e)}{2 s_y^2 E \ln(1+e)} \right)^{-0.5}$$

(C.1.5.2)

$$L_r = \frac{s(1+e)}{s_y}$$

(C.1.5.3)

where; σ is any value of stress along the materials engineering stress strain curve at a strain of ε, and σ_y is the material's lower yield strength or 0.2% offset yield strength. It should be noted that the abscissa in these two FAD's is L_r rather than S_r as in the FAD's in Figures C.1.1 and C.1.2. In the term L_r, now called the load ratio, the net section stress is normalised with respect to the materials yield strength rather than flow stress as for the applied stress ratio, S_r. Thus,

$$L_r = \frac{s_n}{s_y}$$

(C.1.5.4)

where σ_n is the net section stress as defined and calculated for Level 2 strip yield model FAD (Figure C.1.1).

The maximum value of L_r is, however, no longer limited to 1.2 and is given by $(s_y + s_u)/2s_y$. However, if the material displays discontinuous yielding, then L_r is limited to a maximum value of unity. The ordinate of the FAD, K_r, is calculated in exactly the same manner as for the FAD in Figure C.1.1 and the assessment procedure for residual strength or critical flaw size also follow the same approach.

C.1.6   Use of FAD's in Other Industries

In the late 70's and early 80's, the CTOD design curve was the main basis for conducting engineering critical assessments. This approach to evaluate potential for unstable fracture has also been incorporated in non-mandatory appendices in pipeline standards (e.g., CSA Z662, Appendix K, API 1104, Appendix A) to establish flaw acceptance criteria that are usually less restrictive than workmanship criteria. A separate check, however, is needed for considering plastic collapse and the criteria are based on large-scale pipe bend tests. By the mid 80's, a methodology based on the strip yield model FAD had been formalized and used more often for assessments of flaws in offshore structures and pressure vessels.

More recently, Anderson [Ref. C.13] has formalized an engineering critical assessment approach for pressure vessel steels that is based on the material non-specific FAD shown in Figure C.1.4. Since pressure vessel design is based on the ultimate strength of the steel, pressure vessel steels tend to have a relatively higher ultimate strength to yield strength ratio (σ_u/σ_y, greater work hardening) compared to structural steels, especially for higher strength structural steels (yield strength of 350 MPa or more). As mentioned earlier, for such steels it is more appropriate to use one of the FAD's shown in Figures C.1.4 or C.1.5. The lack of conservatism of the failure locus resulting from the use of the strip yield model FAD (Figure C.1.1) for materials with $\sigma_u/\sigma_y > 1$ is shown in Figure C.1.7. Here material specific FACs were calculated by Reemsnyder [Ref. C.14] for steels with different σ_u/σ_y ratios and then after adjusting the load ratio to stress ratio, plotted on to the strip yield model FAD. It is evident that as the σ_u/σ_y ratio increases beyond unity, the strip yield model FAD increasingly becomes more unconservative.

C.1.7   Selection of FAD for Residual Strength Assessment of Ship Structural Members

In light of the comments made in the previous sections, it is recommended that wherever possible, the material specific FAD defined by Equation C.1.6 be used for residual strength assessment. This FAD is henceforth referred to as the **Level 2c FAD**. This FAD, however, requires the stress-strain curve for the material of interest which is often unavailable for steel base materials and never for the heat affected zone. Under such circumstances, either the material non-specific FAD defined by Equation C.1.5 (henceforth referred to as the **Level 2b FAD**) or the strip yield model FAD defined by Equation C.1.4 (henceforth referred to as the **Level 2a FAD**) can be used. These two FAD's are comparable in ease of application, but the **Level 2a FAD** is less suitable for high work hardening materials since: (i) it is less conservative at relatively high S_r values (< 1) , and (ii) and it does not permit net section stresses to exceed $1.2\sigma_y$.

Use of any one of the three Level 2 FAD's presupposes that the material fracture toughness data is available. If that is not the case, then an estimate of the material fracture toughness is obtained indirectly via empirical and conservative correlations between CVN toughness and fracture toughness. In such cases, it is recommended that Level 2 FAD's not be used. Instead, assessments should be based on a Level 1 FAD.

The figure shows a Failure Assessment Diagram plotting K_r versus S_r with multiple PD 6493 curves.

σ_f/σ_y	J_y ksi	σ_u ksi
1.063	80	90
1.125	60	75
1.200	50	70
1.403	36	65
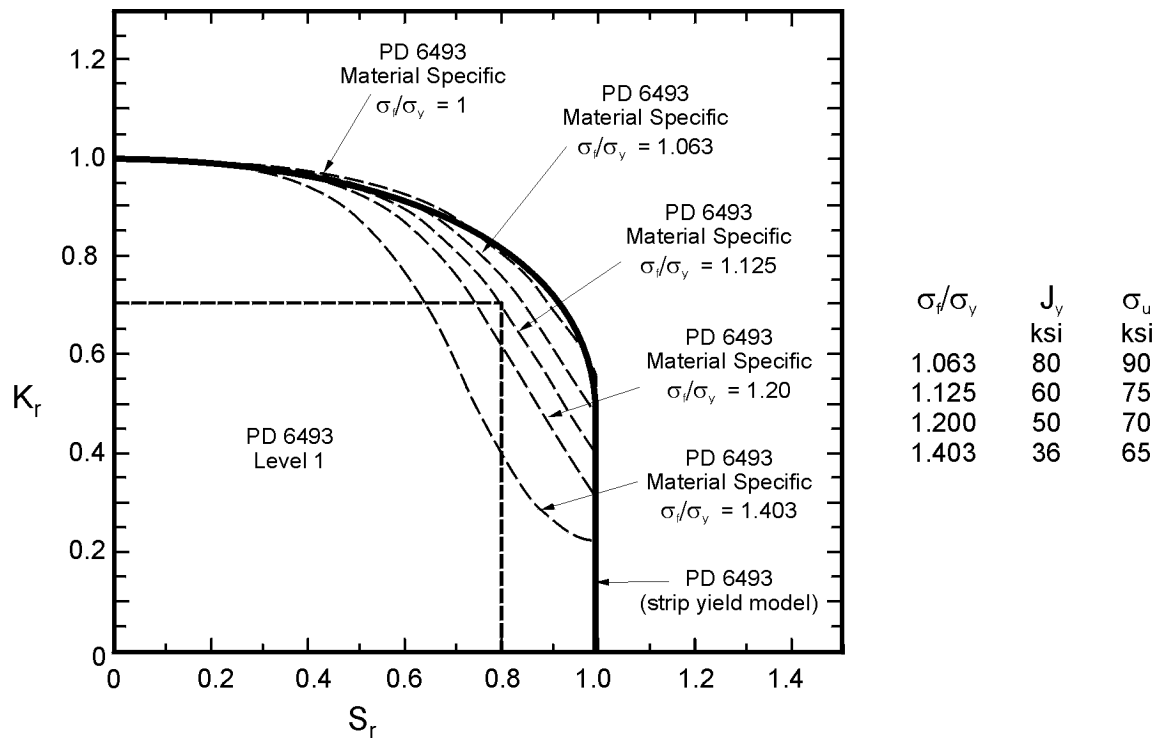
FAILURE ASSESSMENT DIAGRAMS

The Material Specific, FAC Curves represent: (1) elastic-perfectly plastic material, i.e., $\sigma_f/\sigma_y = 1$, (2) A 36, i.e., $\sigma_f/\sigma_y = 1.403$, (3) HSLA 50, i.e., $\sigma_f/\sigma_y = 1.200$ (4) HSLA 60, i.e., $\sigma_f/\sigma_y = 1.125$, and (5) HSLA 80 i.e., $\sigma_f/\sigma_y = 1.063$.

Figure C.1.7: Comparison of Failure Assessment Diagrams for Steels with Different Yield/Ultimate Strength Ratios [Ref. C.14]

In using any of the FAD approaches described above, it should be kept in mind that these cover failure due to Mode I loading (principal stress perpendicular to the crack surface) only.

C.1.8   Crack Driving Force Calculations

The driving force for brittle fracture (K_{app}) and local plastic collapse ($\mathbf{s}_n$) are required inputs for each of the failure assessment diagrams described above. K_{app} depends on the local stress state around a crack tip due to applied loads, welding residual stresses, and fabrication residual stresses, whereas $\mathbf{s}_n$ depends on the local stress state around a crack due to applied loads and only those residual stresses that that do not relax as a result of local net section yielding. Guidance on the calculation of these driving forces and the relevant local stress was given in Part B. Because of the stochastic nature of these calculations, it is necessary to base these calculations on the maximum expected applied loads over the assessment period of interest (usually the inspection period).

C.2   ASSESSMENT OF FATIGUE CRACK GROWTH

C.2.1 Background

This section describes a two level procedure based on linear elastic fracture mechanics for predicting fatigue crack growth in ship structures from an assumed initial crack or from flaws detected in service or during fabrication by non-destructive evaluation. Guidance is given on the preparation of inputs for the procedure, the execution of the procedure and the use of the results to establish safe and efficient schedules for inspection and repairs.

C.2.2   Characterization of Fatigue Crack Growth by Linear Elastic Fracture Mechanics

The resistance of a metal to fatigue crack propagation is normally characterized by a log-log plot of crack growth rate (da/dN) under tensile loading (Mode I) versus the range of the crack tip stress intensity factor (ΔK). Crack growth rates for such plots are extracted from discrete measurements of crack length during fatigue tests of standard specimens with through-thickness edge cracks or center cracks subjected to Mode I constant amplitude loading, and the corresponding stress intensity factor ranges are calculated by linear elastic fracture mechanics. Although fatigue cracks can also propagate by an in-plane shearing mechanism (Mode II) or an out-of-plane tearing mechanism (Mode III), Mode I cracking usually predominates in engineering structures.

The correlation of da/dN against ΔK assumes that identical stress-strain fields exist at the tips of different cracks regardless of crack size, crack shape, applied loads, and structural geometry if the crack tip stress intensity factor, material, R-ratio, and environment remain the same. The crack tip stress intensity factor quantifies the severity of the asymptotic stress-strain field at a crack tip in linear elastic material (i.e., K-field), and ΔK is generally defined in the following manner:

$$\Delta K = \Delta \sigma \cdot Y \sqrt{\pi a} \qquad\qquad (C.2.2.1)$$

where: $\Delta \sigma$ is the tensile portion of the range of the applied stress (e.g., hot spot stress, nominal stress, or local nominal stress) plus total residual stress (due to welding and fabrication) over a load cycle, and Y is, again, a dimensionless factor that depends on the geometry of a crack, the location along a crack front, and the geometry and loading of a structure. The corresponding R-ratio is the ratio of the minimum stress to maximum stress (applied stress plus residual stress) around a crack over a load cycle. Although a plastic zone inevitably develops at a crack tip in ductile materials subjected to cyclic loading, similitude is maintained if the plastic zone is small compared to crack size and surrounded by the elastic K-field. These conditions are usually satisfied in high cycle fatigue problems.

A typical log-log plot of da/dN against ΔK has a sigmoidal shape that can be divided into three regions (Figures C.2.1 and C.2.2):

Region I - Crack growth in Region I ($<10^{-5}$ mm/cycle) can be strongly influenced by microstructure and R-ratio. These rates diminish rapidly with decreasing ΔK, and fatigue cracks are assumed to be non-propagating below a threshold value of the stress intensity factor range (ΔK_{th}) which is usually defined at a growth rate of 10^{-8} mm/cycle to 10^{-7} mm/cycle.

Region II - Crack growth in Region II is characterized by a nearly linear relationship between log da/dN and log ΔK. This relationship is usually approximated by the following power relationship, which is often referred to as the Paris equation [Ref. C.15],

$$\frac{da}{dN} = C\Delta K^m \qquad (C.2.2.2)$$

where C and m are empirical constants. Crack growth rates in Region II (10^{-5} mm/cycle to 10^{-3} mm/cycle) are less sensitive to microstructure and R-ratio than crack growth rates in Region I.

Region III - Crack growth rates in Region III increase asymptotically with increasing ΔK. This acceleration of crack growth is related to the emergence of static failure modes such as fracture, ductile tearing, and plastic collapse, and it is accompanied by an increased sensitivity of crack growth rates to microstructure and R-ratio.

C.2.3   Prediction of Crack Propagation Under Constant Amplitude Loading

The following equation generalizes the relationship between da/dN and ΔK under constant amplitude loading for a given material, R-ratio, and environment:

$$\frac{da}{dN} = f(\Delta K) \qquad (C.2.3.1)$$

If the variation of ΔK with crack size for an idealized two-dimensional edge crack or center crack is known, then the number of load cycles to propagate the crack from an initial length a_i to a final crack length a_f can be determined by integrating equation in the following manner:

$$\Delta N = \int_{a_i}^{a_f} \frac{da}{f(\Delta K)} \qquad (C.2.3.2)$$
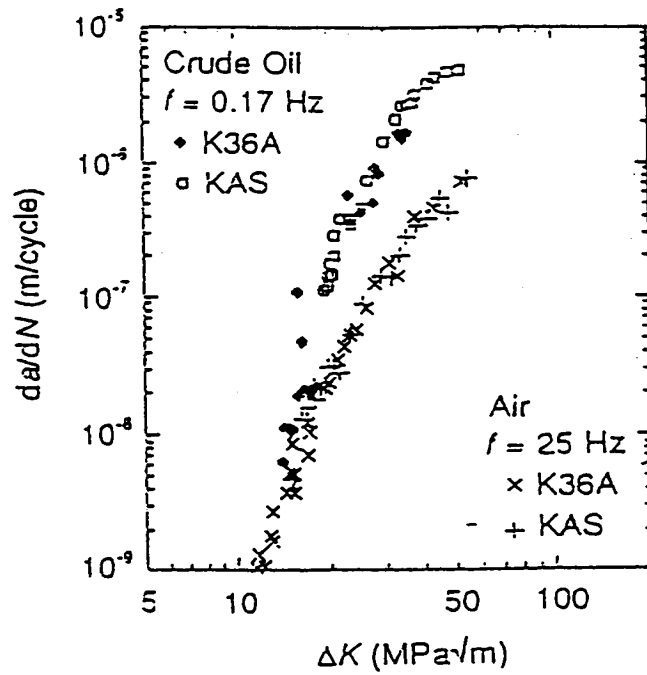
Figure C.2.1: Log-Log Plot of da/dN vs. DK Data
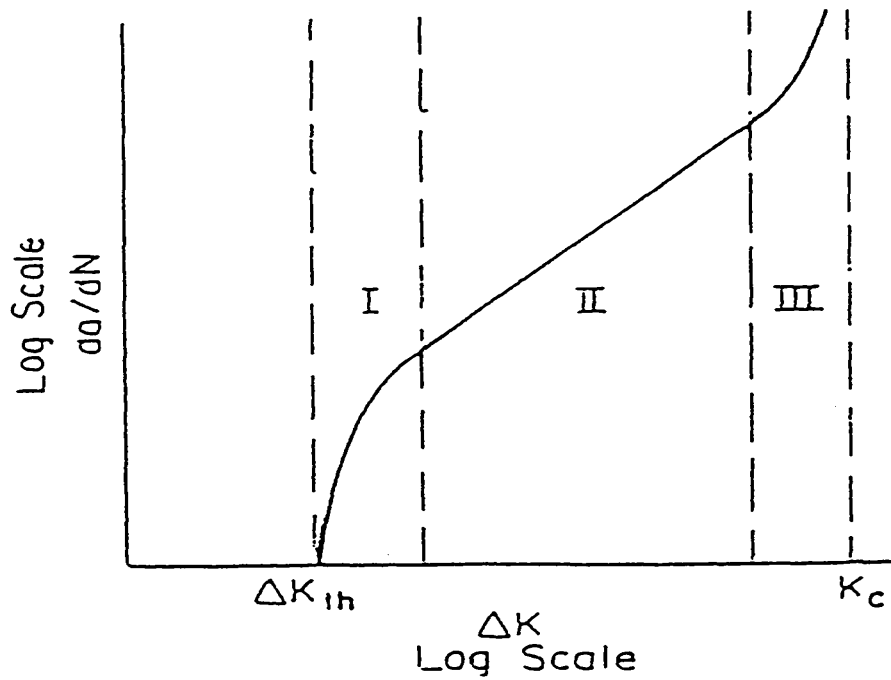
Figure C.2.2: Basic Regions of da/dN vs. DK Curve

Conversely, the incremental crack growth from an initial number of constant amplitude stress cycles N_i to a final number of constant amplitude load cycles N_f can be determined by integrating the equation in the following manner:

$$\Delta a = \int_{N_i}^{N_f} f(\Delta K) dN$$

(C.2.3.3)

A number of empirical equations are available to describe the entire sigmoidal relationship between da/dN and ΔK. This relationship can also be described piecewise by a series of linear segments. However, for many practical applications, it is sufficiently accurate to fit the Paris equation to all values of ΔK from ΔK_{th} up to failure:

$$\frac{da}{dN} = C(\Delta K)^m \qquad \text{for } \Delta K > \Delta K_{th} \qquad (C.2.3.4)$$

$$\frac{da}{dN} = 0 \qquad \text{for } \Delta K \leq \Delta K_{th}$$

In actual engineering structures, edge cracks and through-thickness cracks usually have an irregular or curved crack front. Furthermore, surface cracks and embedded cracks with smooth and irregular curved crack fronts are frequently encountered in such structures. As discussed in the previous Section, ΔK depends on crack size as well as crack shape, and crack shape development can have a significant influence on crack growth rates and accumulated crack growth. In principle, changes in crack shape as well as crack size could be tracked by predicting the incremental crack growth at various locations along the crack front. However, such an approach is time-consuming and impractical. Usually, an embedded flaw is idealized as an elliptic crack, and crack growth is only predicted along the major and minor axes of the idealized flaw. Similarly, a surface flaw is idealized as a semi-elliptic crack, and crack growth is only predicted at the deepest point and surface. It is also customary to idealize a through-thickness edge crack or center crack as a straight-fronted crack and to only predict the average growth along the actual crack front.

C.2.4 Prediction of Crack Propagation Under Variable Amplitude Loading

Most engineering structures, including ships, are subjected to variable amplitude loading rather than constant amplitude loading. Variable amplitude loading can complicate the prediction of fatigue crack growth in several ways:

1. Interaction effects between load cycles of different amplitude can produce temporary departures from da/dN versus ΔK data for constant amplitude loading. In particular, an over-shooting load

spike can retard subsequent crack growth, and to a lesser extent, an under-shooting load spike can temporarily accelerate subsequent crack growth.

These effects tend to cancel out under narrow-banded stationary random loading and under certain types of stationary and non-stationary broad-banded random loading, but they can have a significant influence on accumulated crack growth if there are long sequences of load cycles between one-sided load spikes (Figure C.2.3).

2. The value of ΔK for a given load cycle varies with crack size and shape. In addition, a load cycle that is too small to propagate a small crack (i.e., $\Delta K < \Delta K_{th}$) may be large enough to significantly propagate a larger crack (i.e., $\Delta K > \Delta K_{th}$). As a result, the crack growth produced by each load cycle in a load-time history and the total crack growth over a given number of load cycles can depend on the sequence of the load cycles even if interaction effects are negligible.

3. Individual load cycles in certain load-time histories (e.g., broad-banded random histories) are difficult to define and counting methods such as rainflow and reservoir techniques are needed to decompose such histories into individual load cycles (Figure C.2.4).

4. There is no unique load-time history for forecasting fatigue crack growth under random and pseudo-random loading.

In principle then, a realistic sequence of properly counted load cycles and a crack growth model that accounts for interaction effects between load cycles are needed to predict fatigue crack growth under variable amplitude loading. Furthermore, probabilistic simulation methods and/or calibrated standard load-time histories are required for forecasting fatigue crack growth under random and pseudo-random loading. In practice, however, a rigorous approach is not always needed. A few examples are listed below:

1. If the numbers of load cycles between one-sided spikes in a load history are short, then interaction effects following the spikes have a negligible effect on the accumulated crack growth because the spikes are directly responsible for most of the accumulated crack growth.

2. Retardation and acceleration effects tend to cancel out under narrow-banded stationary random loading and under certain types of stationary and non-stationary broad-banded random loading.

3. The total crack growth over a given number of load cycles is independent of load sequence if interaction effects are negligible and if the ΔK value for each load cycle exceeds $\Delta K_{th.}$ Under these conditions, the total crack growth over a given number of variable amplitude load cycles can be predicted by a cycle by cycle integration of the Paris equation over an arbitrary sequence of the load cycles and their corresponding ΔK values.
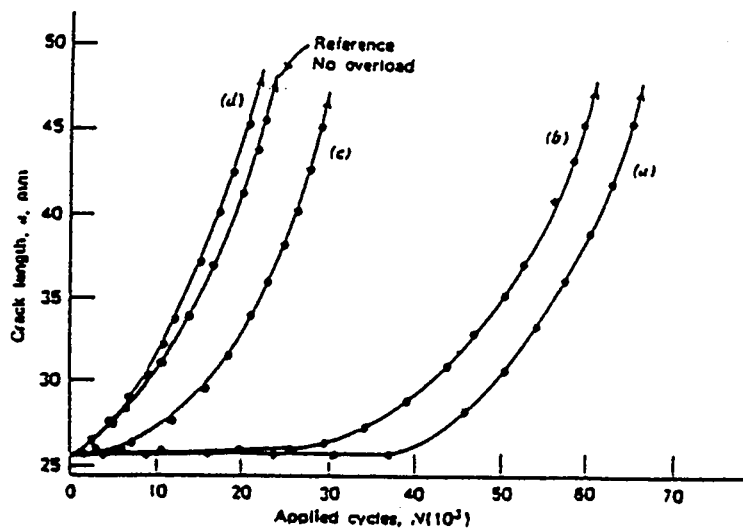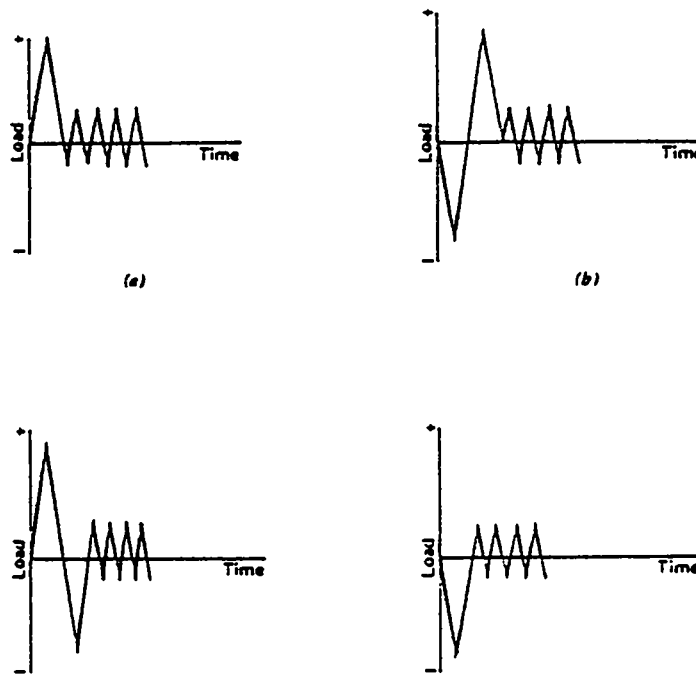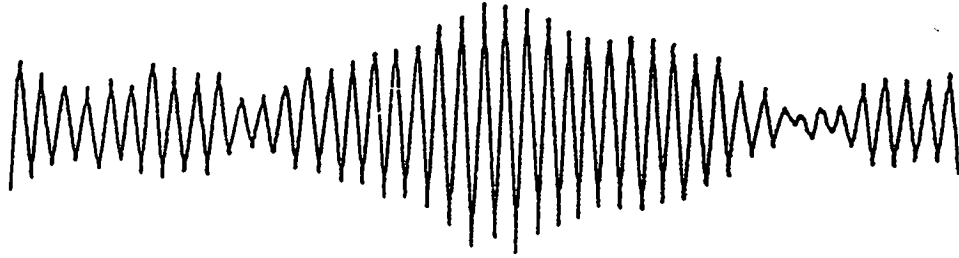
Figure C.2.3: Effects of Different Overload Patterns on Fatigue Crack Growth in 7075-T6 Aluminum [Ref. C.15]

(a)

(b)

Figure C.2.4: Random Load versus Time Histories (a) Narrow Banded (b) Broad Banded

Alternatively, a weighted average of the stress ranges ($\Delta\sigma_{eq}$) associated with the load cycles in the variable amplitude load history can be used to calculate an equivalent stress intensity factor range (ΔK_{eq}) for cycle by cycle integration with the Paris equation [C.2.2.2]:

$$?K_{eq} = Y\,? \boldsymbol{s}_{eq}\sqrt{pa}$$

(C.2.4.1)

$$? s_{eq} = \left[\dfrac{\displaystyle\sum_{j=1}^{j=k} ? s_j^{m} n_j}{N_T}\right]^{1/m}$$

(C.2.4.2)

where; n_i is the number of cycles of magnitude $\Delta\sigma_j$ in the random history, m is the material exponent in the Paris equation, and N_T is the total number of cycles.

C.2.5   Application to Ship Structures

As evident in Figure C.2.5, the variation of stresses at a given point in a ship can be described as a broad-banded non-stationary pseudo-random process. *Broad-banded* means that the frequency content is wide, and *non-stationary* means that the statistics of the process do not remain constant. *Pseudo-random* means that there are deterministic as well as random cyclic stress components. Random components arise from wave-induced bending and torsion of the ship's hull, fluctuations of the external pressure on shell plating, fluctuations of the internal pressure on tank and cargo boundaries as a result of wave-induced motions, and wave-induced dynamic effects such as springing, slamming, and whipping. Deterministic components, on the other hand, arise from thermal effects, changes in still water bending moment as a result of changes in cargo and ballast conditions, seasonal variations in sea states, changes in heading to avoid rough seas, and reductions in speed to minimize slamming.

The prediction of fatigue crack growth in engineering structures is the subject of on-going research, and further work is needed in the following areas before rigorous methods are available for the prediction of fatigue crack growth in ships:

1. Wave-induced loads are responsible for the majority of stress cycles experienced by the hull of a ship over its operational life, and considerable attention has been given to quantifying the statistical distributions of wave-induced cyclic stresses over the short term and long term. In contrast, much less attention has been given to understanding and quantifying the sequence of cyclic stresses in ship structures over time. Realistic sequences of these stresses cannot be re-constructed from the short-term and long-term statistical distributions of wave-induced cyclic stresses by probabilistic simulation methods without an understanding of the deterministic nature of these stresses (e.g., a large peak is generally followed by a large trough, the build up and decay of sea states is gradual rather than random).

    In addition, little is known about the significance and nature of other cyclic stresses in ship structures. For example, changes in still water bending moment can cause relatively large changes in stresses at certain locations in a ship that could retard or accelerate subsequent crack growth. These stress cycles are infrequent and make little direct contribution to the total fatigue damage and accumulated crack growth but the associated retardation effects could have a significant effect on crack growth.

2. Interaction effects under variable amplitude loading are generally attributed to cycle by cycle variations of residual stresses and crack closure at the crack tip. The complexities of these effects have so far precluded a complete theoretical treatment of the problem. Several variants of the Paris equation have been successfully used to model interaction effects, but these empirical models have been calibrated with fatigue crack growth data for specific types of variable amplitude loading and material. In principle, these models could be adapted to ship structures but they would have to be

re-calibrated against data for fatigue crack growth in ships and representative variable amplitude loading for such structures.
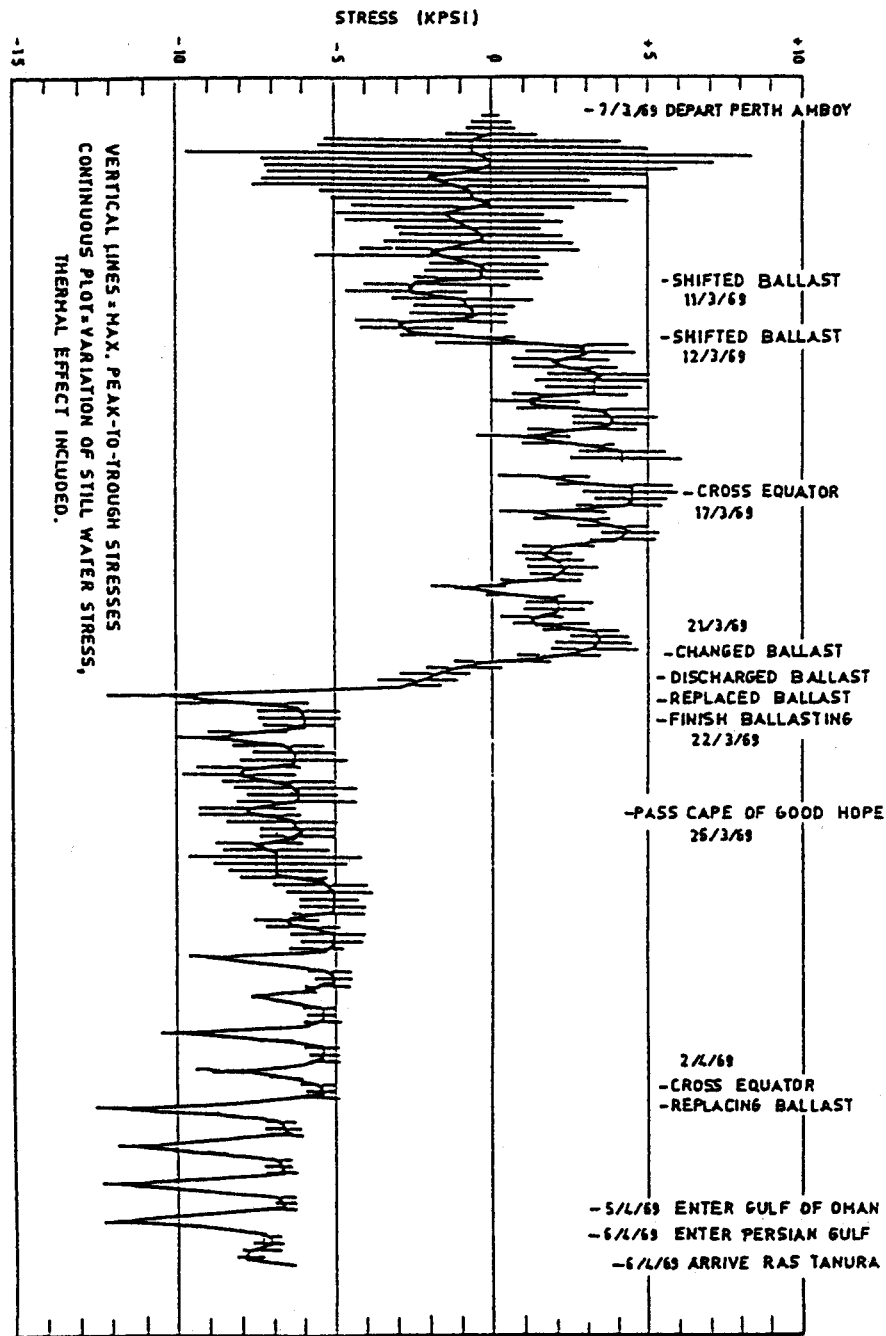
Figure C.2.5: Variation of Midship-Stresses versus Time *SS R.G. Follis* [Ref. C.1]

3. As fatigue cracks propagate away from their initiation sites, load is continuously shed from the damaged areas to surrounding material. The inherent redundancy of ship structures enables them to tolerate a considerable amount of load shedding. Unfortunately, users of this guide cannot fully exploit this redundancy at this time. Stress intensity factor solutions for cracks in basic welded details (handbook solutions or direct calculation by analytical or numerical methods) only account for load shedding around small cracks in ship structures, and little is known about load shedding around large cracks in ship structures. There are many possible paths for the propagation of large fatigue cracks in ships, and a number of large finite element models would be required to quantify load shedding along any given path.

Until further advancements are made in the foregoing areas, procedures for predicting fatigue crack growth in ships structures should be consistent with the sophistication and assumptions of fatigue design procedures recently introduced by classification societies. These procedures only consider wave-induced cyclic stresses and ignore other cyclic stresses in ships. It is assumed that the short-term variation of wave height is a narrow-banded stationary process, and that the structural response is linear. These assumptions enable the short-term distributions of stress range for all possible sea states over a specific voyage route or over the operational life of a ship to be generated by spectral methods. A long-term distribution of stress ranges over a specific voyage route or over the life of a ship is then built-up from the weighted sum of the short-term distributions. Alternatively, the long-term distribution is assumed to be a Weibull distribution characterized by an assumed shape factor and a reference stress range corresponding to a specific probability of exceedance. The long-term distribution of stress ranges is then used in conjunction with fatigue design curves to predict the initiation of relatively large fatigue cracks. These calculations ignore load shedding and interaction effects. It is assumed that the interaction effects are mitigated by the narrow-banded nature of short-term sea states and by the gradual build up and decay of sea states. The calculations also assume that fatigue cracks continue to propagate during the compressive portions of applied stress cycles because of the presence of tensile residual stresses.

The following procedure is, therefore, recommended for predicting fatigue crack growth in ship structures for the purpose of establishing inspection and maintenance schedules or assessing the fitness-for-service of detected flaws.

1. Define the size and shape of an initial crack. See Section C.2.6 for guidance on assuming an idealized initial crack at the design stage, idealizing the size and shape of a crack detected in service by non-destructive evaluation, and selecting the points along the idealized crack front where crack growth will be simulated.

2. Define the statistical distribution of the appropriate stress range (e.g., hot spot stress range, nominal stress range, or local nominal stress range) for stress intensity factor calculations over the interval of interest (e.g., inspection period, voyage route). See Part B for guidance on identifying the appropriate stress range, calculating this stress range from applied loads, and estimating the statistical distribution of this stress range.

3. Approximate the statistical distribution of the applied stress range with a histogram consisting of 10 to 20 levels. Assume that the stress range in each level is constant and equal to the maximum value of the range.

4. Arrange the blocks of stress ranges in the histogram into at least three different sequences including: high-to-low, low-to high, low-high-low. For each stress history, carry out Steps 5 to 9.

5. Calculate the stress intensity factor range ΔK for the first applied stress range in a particular stress history at the simulation points along the idealized crack front. For Level 1FAD analysis, assume that the through-thickness stress distribution is uniform and equal to the magnitude of the maximum peak stress (See Part B, Section B.3.6.2). For Level 2 FAD analysis, use the actual through-thickness stress distribution. The Level 1 crack growth analysis is consistent with the Level 1 residual strength assessment described in Section C.1.7, whereas the Level 2 crack growth analysis is consistent with the Level 2a, 2b and 2c residual strength assessments described in Section C.1.7.

6. Calculate the corresponding increments of crack growth Δa by integrating the Paris equation over the stress range assuming that the crack growth rate is constant over the stress cycle and equal to the crack growth rate at the beginning of the stress cycle.

$$\Delta a = C(\Delta K)^m \qquad \text{for } \Delta K > \Delta K_{th} \qquad (C.2.5.1)$$
$$\Delta a = 0 \qquad \text{for } \Delta K \leq \Delta K_{th}$$

See Part B, Section B.4.3 for guidance on generating C, m, and ΔK_{th} values for a specific steel. Upper bound values for steels are also given there.

7. Update crack size and crack shape.

8. Check to see whether crack has reached a critical size. See Section C.1 for guidance on residual strength assessment.

9. Repeat Steps 6 to 9 for subsequent stress ranges in a given stress history.

The results for each stress history and tracking location along a crack front can be used to construct a curve or table of the accumulated crack growth versus the number of applied stress ranges. In general, the crack growth that accumulates up to any given point of the stress history will depend on the sequence of the applied stress ranges. Therefore, the worst predicted case should be used to establish inspection and maintenance schedules or to assess the fitness-for-service of detected cracks.

Note: If the value of ΔK for every applied stress range in a sequence exceeds ΔK_{th}, the total crack growth would be independent of the sequence of applied stress ranges. Furthermore, the same total crack growth would be predicted by the weighted average stress range approach described in Section C.2.4.

The cycle-by cycle integration procedure can be easily implemented on a personal computer either on a spreadsheet or as a stand-alone program if the variation of the crack tip stress intensity factor with crack size and shape is parametrically defined. If stress intensity factor solutions are only available in tabular or graphical form or if users of this guide do not have access to computing resources, then a manual assessment can be performed with the following block integration procedure:

1. Divide the stress history into blocks of stress ranges of the same magnitude, and carry out Steps 2 and 3 for each block in turn.

2. Calculate ΔK using the crack size, crack shape, and stress range at the beginning of the block.

3. Calculate the crack growth increment (Δa_B) at each simulation point along a crack front over the number of stress ranges in the block (ΔN_B) assuming that the crack growth rate is constant and equal to the crack growth rate at the beginning of the block.

$$\Delta a_B = C\,(\Delta K)^m\,\Delta N_B \qquad \text{for } \Delta K > \Delta K_{th} \qquad (C.2.5.2)$$
$$\Delta a_B = 0 \qquad \text{for } \Delta K \leq \Delta K_{th}$$

Although the approach is inherently non-conservative, results will be close to those obtained by cycle-by-cycle integration if the block size is relatively short (up to 0.1% of the total fatigue life obtained, or the increment of crack growth does not exceed 0.5% of the crack depth at the start of a block).

C.2.6 Flaw Characterisation

C.2.6.1   Idealization of Detected Flaws

Flaws that are detected in service by non-destructive evaluation may be planar or volumetric. The fracture mechanics procedure described is inherently conservative for volumetric flaws and planar flaws that are not cracks because it does not account for the cyclic loading required to initiate fatigue cracks from such flaws.

The fracture mechanics procedure described previously only considers fatigue crack growth under Mode I loading. However, detected flaws are often inclined with respect to the principal stress direction, and fatigue cracks that originate at such flaws may initially propagate under a mixture of Mode I, Mode II, and Mode III loading. Although it is possible to incorporate mixed-mode loading into fatigue rack growth calculations, fatigue cracks tend to curve towards a trajectory that is perpendicular to the principal stress direction. It is simpler albeit conservative to project the detected flaws onto a plane normal to the principal stress direction and to treat the projected flaws as cracks subjected to Mode I loading.

The shapes of detected flaws are often irregular, and a number of closely spaced flaws may be detected. As discussed in Section C.2.2, crack shape development can have a significant influence on crack growth rates and accumulated crack growth. In principle, the growth of multiple cracks could be simulated simultaneously with stress intensity factors that account for interaction effects between closely spaced cracks, and the shape of individual cracks could be tracked by predicting the incremental crack growth at various locations along the crack front. However, such an approach is time-consuming and impractical. In order to minimize the number of simulations and to simplify stress intensity factor calculations, it is necessary to idealize detected flaws in the following manner:

1. Idealize the projected profiles of surface, embedded, and through-thickness flaws as semi-elliptic, elliptic, and straight-fronted cracks, respectively.

2.   Re-characterize closely spaced cracks as a single crack.

3. Assume that the shape of an idealized crack develops in a self-similar manner so that crack growth only needs to be tracked at the major and minor axes of an elliptic crack front, the deepest point and one of the two surface points of a semi-elliptic crack front, or a single point along a straight through-thickness crack front.

4. When an elliptic embedded crack breaks through the top or bottom surface of a plate, re-characterize the elliptic crack as a surface crack for subsequent crack growth calculations. Similarly, when a semi-elliptic surface crack breaks through the top or bottom surface of a plate, re-

characterize the surface crack as a straight-fronted through-thickness crack for subsequent crack growth calculations.

Conservative circumscription methods for idealizing the shape of projected flaws and the re-characterization of idealized cracks during crack growth predictions are given in Appendix D.

C.2.6.2   Assumed Initial Crack

Fatigue cracks in ship structures with properly designed and fabricated welds generally initiate along the toe of a transverse fillet weld or transverse butt weld, usually along the hot spot region of the weld toe where structural stresses (i.e., total stresses minus the stress concentration effect of local weld geometry) are highest. Within this region, multiple surface cracks initiate at microscopic stress raisers such as slag intrusions and macroscopic stress raisers such as weld ripples and undercuts. These cracks coalesce as they propagate through the thickness of a plate, and a dominant crack usually emerges before the fatigue cracking is detected. The spacing and number of crack initiation sites along a weld toe depend on local stresses and welding process. These factors, in turn, influence the size and shape of fatigue cracks during the crack coalescence stage.

Since the fracture mechanics procedure does not explicitly consider fatigue crack initiation, the size, shape, and location of one or more initial cracks must be assumed for fatigue crack growth predictions at the design stage. If statistical information about the size, shape, number, and spacing of initial fatigue cracks along a weld toe are available, then Monte Carlo simulation methods can be used to define an initial array of fatigue cracks along the weld toe. The subsequent growth of these cracks can be simulated simultaneously, and the re-characterization criteria given in Appendix D can be used to conservatively model the coalescence of adjacent cracks. Alternatively, a mean relationship between the aspect ratio and depth of surface cracks along a weld toe can be constructed from experimental observations of crack shape development. This empirical relationship can be used as a forcing function to prescribe the shape of a single surface crack as the growth at the deepest point of the crack is simulated.

In practice, relevant forcing functions and statistical information about crack initiation will rarely be available to users of this guide. In this event, users should assume that a semi-elliptic crack of depth a_i extends across the length of the hot spot region. If the hot spot region extends across the full width of plate, then the surface crack should be re-characterized as an edge crack of constant depth a_i. For comparative assessment of welded joints failing from the weld toe, it is often assumed that a_i lies within the range 0.1 mm to 0.25 mm unless a larger size is known to be relevant. Researchers have found that predicted fatigue lives based on these initial sizes are comparable to the experimental fatigue lives of laboratory specimens.

For establishing inspection intervals at the design stage, however, a_i should be taken as the minimum defect size that can be reliably detected using the relevant NDT technique. The reliability of the inspection technique should be taken into account in the determination of this minimum defect size. This entails the use of probability of detection (POD) curves for a given confidence. A 90% POD with 95% confidence limits has been found to be appropriate in most cases [Ref. C.18].

C.3 REFERENCES

[C.1] Stambaugh, K.A. et al., "Ship Fracture Mechanism Investigation - Part I", SSC Report 337 Part I, Example 3.7, 1990.

[C.2] Graville, B.A. and Morrison, K.G., "Repair Welding of Stiffeners to Hull Plating in Low Temperature Marine Environments without Preheat", Fleet Technology Report submitted to Transport Canada, Report No. TP 1085, 1990.

[C.3] "Guidance on the Methods for Assessing the Acceptability of Flaws in Fusion Welded Structures, PD 6493-1991", published by the British Standards Institution (BSI).

[C.4] Irwin, G.R., "Plastic Zone Near a Crack and Fracture Toughness", Gagamore Research Conference Proceedings, Vol. 4, 1961.

[C.5] Fracture Mechanics: Fundamentals and Applications, by T.L. Anderson, published by CRC Press, 1991.

[C.6] Burdekin, F.M., and Stone, D.E.W., "The Crack Opening Displacement Approach to Fracture Mechanics in Yielding Materials", Journal of Strain Analysis, Vol. 1, 1966, pp. 145-153.

[C.7] Ghose, D.J. et al., "Residual Strength Assessment of Marine Structures", SSC Report 381, 1995.

[C.8] Sumpter, J. D. G. et al. , "Fracture Toughness of Ship Steels", The Royal Institute of Naval Architects, July-August 1989, pp 169-186.

[C.9] Phaal R., et al, "Current Status of Revisions to PD 6493 Assessment Procedures for ` Fusion Welded Structures", IIW Doc. X-1314-95.

[C.10] BSI Document 97/714934 DC "BS 7910 Guide on Methods for Assessing the Acceptability of Flaws in Structures" Draft for Public comment dated 17th Sep. 1999.

[C.11] Bloom, J.M., "Deformation Plasticity Failure Assessment Diagram", Elastic-Plastic Fracture Mechanics Technology, ASTM STP 896, Eds. J.C. Newman, Jr. And F.J. Loss, 1985.

[C.12] Burdekin, F.M., and Dawes, M.G., "Practical Use of Linear Elastic and Yielding Fracture Mechanics with Particular Reference to Pressure Vessels", Proc. IME Conference, London, May 1971, pp28-37.

[C.13] Anderson, T.L., "US Fracture Mechanics Methodologies for Welded Structures", IIW Doc.   X-1315-95.

[C.14] Personal Communication between Dr. H. Reemsnyder (Bethlehem Steel) and Mr. Peter Noble (ABS).

[C.15] Paris, P.C. and Erdogan, F., " A Critical Analysis of Fatigue Propagation Laws", J. Bas. Eng., 1963, 85D, pp528-534.

[C.16] Fuchs, H.O. and Stephens, R.I., Metal Fatigue in Engineering, John Wiley and Sons, 1980.

[C.17] Nibbering, J.J.W., "The Fatigue Problem in Shipbuilding in the Light of New Investigations", Trans. of the RINA, Vol. 118, 1976.

[C.18] Kam, J.C.P., Dover, W.D., and Topp, D.A., "Fracture Mechanics Modelling and Structural Integrity of Welded Tubular Joints in Fatigue", Proc. 6th Int. Symp. on Offshore Mechanics and Arctic Engineering", Vol. 111, pp 279-286, 1987.

PART D EXAMPLES

D.1 OVERVIEW OF EXAMPLES

D.1.1 Scope

This section demonstrates, by way of two hypothetical examples, the damage tolerance assessment procedures presented in this guide. The first example demonstrates the application of these procedures in service, while the second example demonstrates the application of these procedures at the fabrication stage. The fracture assessment and fatigue assessment procedures presented earlier in this guide are fully implemented in both examples. In addition, indirect and direct approaches for stress analysis from Part B of this guide are used in these examples. However, only a Level 2 approach for the determination of loads from Part B.2 and a simplified approach for the determination of stress intensity factors from Part B.3 are used in these examples as they will be the most efficient, if not the only possible, approaches in most practical situations. Demonstration of spectral load analysis is limited to a qualitative "walk-through" of the various steps of such an analysis in Appendix E.

D.1.2 Description of the Problem

A common platform has been selected for the two examples; namely, an 85,000 tons single-skin tanker that was previously analyzed in Reference D.1. The layout and particulars of this tanker are shown in Figure D.1.1, while the mid-ship structural configuration of this tanker is shown in Figure D.1.2.

Example No.1 involves a through-thickness fatigue crack in side shell longitudinal No. 8, which is located in the starboard No. 5 wing ballast tank, about 6 m below the upper deck, near the summer load line (refer to Figures D.1.2 and D.1.3). The crack is located midway between Frames 66 and 67 in the weld metal of a transverse splice weld with ground-off reinforcements, and the plane of this crack is more or less perpendicular to the longitudinal axis of the tanker. The crack had initiated at the outside corner of the longitudinal and had propagated 10 mm into the flange and 10 mm into the web before being detected during a scheduled survey. The ship operator wants to determine if the repairs can be delayed until the next scheduled inspection that is 4 years away.

Example No. 2 considers the fillet weld that joins the flat bracket at Frame 67 to the flange of the aforementioned side shell longitudinal (refer to Figures D.1.2 and D.1.3). A 1.0 mm long undercut has been found along the weld toe at the end of the bracket during a post-fabrication inspection. The undercut is about 0.5 mm deep at the its deepest point. Similar undercuts have been found at other brackets throughout the tanker. Although undercuts of this size are normally found to be acceptable under typical defect acceptance criteria, fatigue cracks initiating at such defects have been found in a number of sister ships after a few years of service.
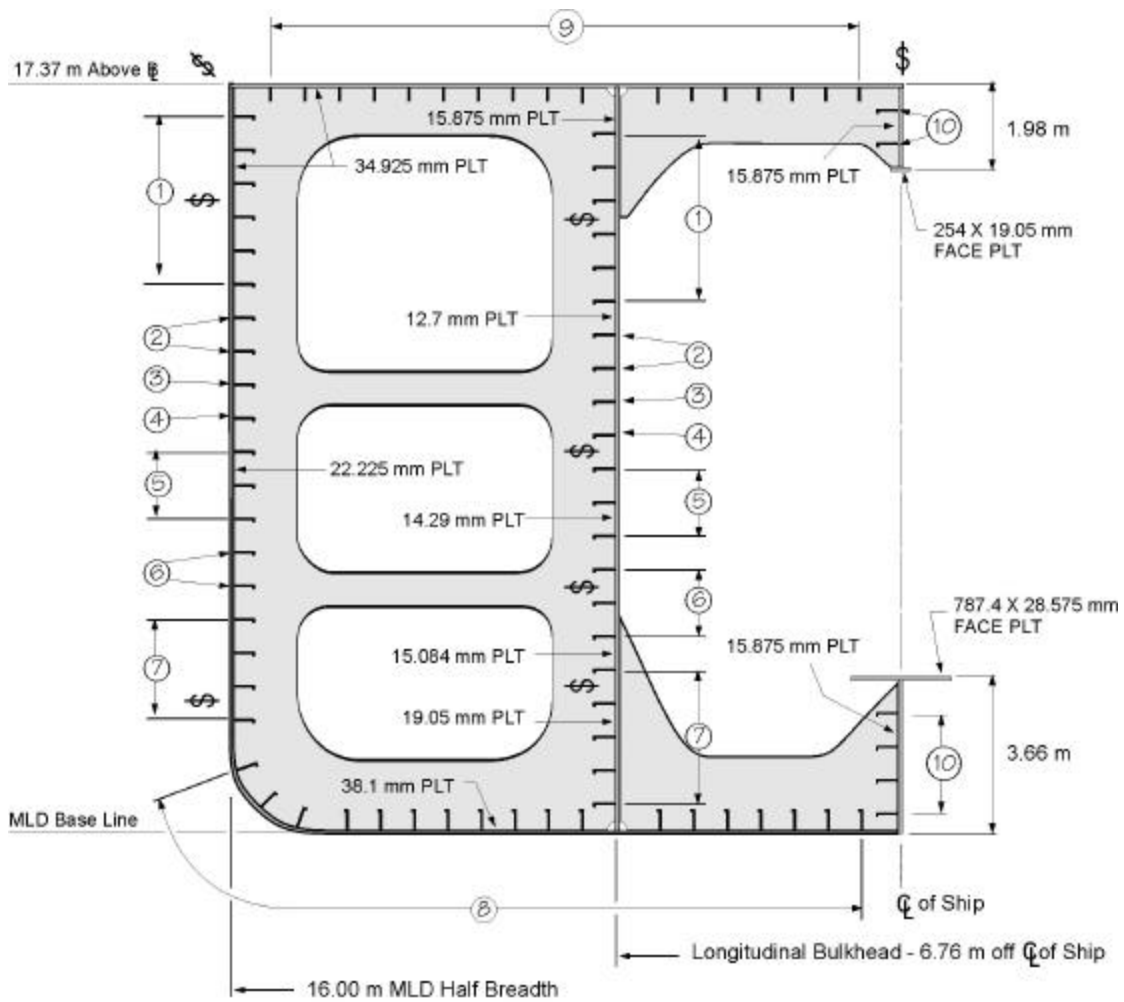
PARTICULARS

Length (O.A.)	246.9 m
Length (B.P.)	239.6 m
Breadth (MLD)	32.0 m
Depth (MLD)	17.37 m
Draft (Summer)	13.26 m
C_b	0.83
Velocity	16 Knots
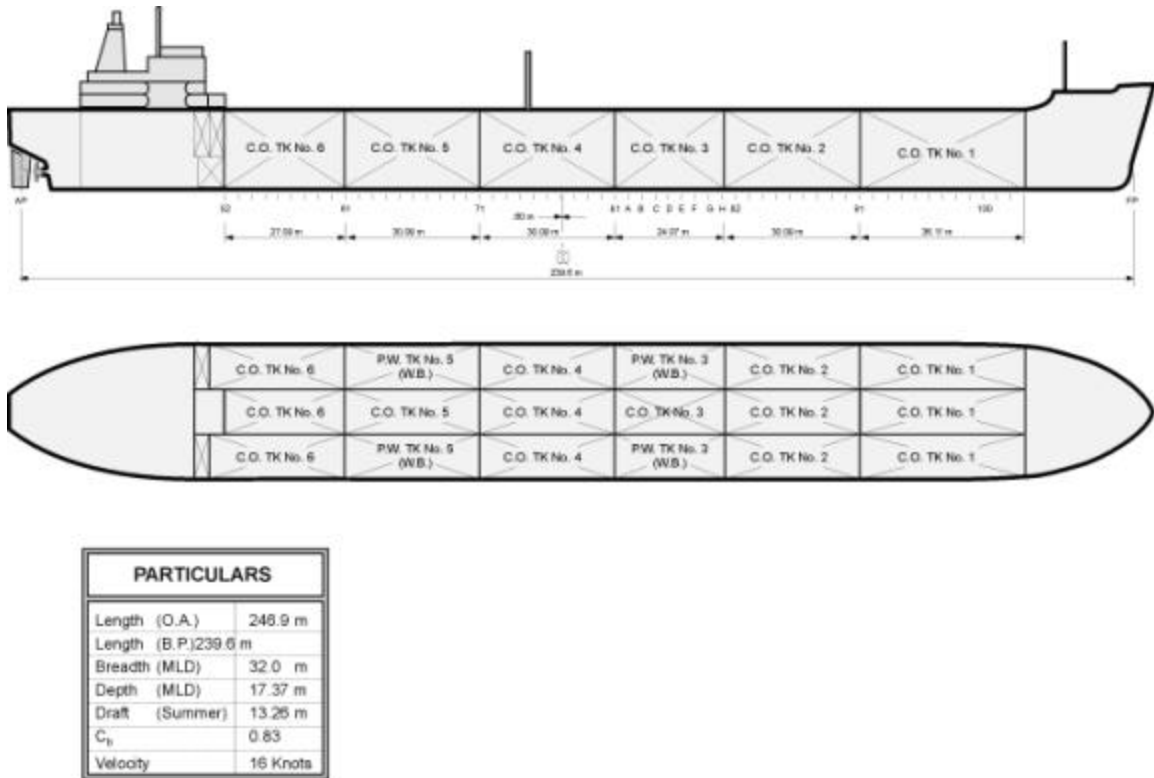
**Figure D.1.1: Platform for Examples-Profile, Plan View
and Particulars of 85,000 Ton Tanker**

Figure D.1.2: Midship Structural Configuration of Tanker

17.37 m Above B

15.875 mm PLT
34.925 mm PLT
1.98 m
15.875 mm PLT
254 X 19.05 mm FACE PLT
12.7 mm PLT
22.225 mm PLT
14.29 mm PLT
787.4 X 28.575 mm FACE PLT
15.084 mm PLT
15.875 mm PLT
19.05 mm PLT
3.66 m
38.1 mm PLT
MLD Base Line
16.00 m MLD Half Breadth
Longitudinal Bulkhead - 6.76 m off C of Ship
C of Ship

STF ID#	d^*	t_w^*	b^*	t_f^*
1	203.2	12.7	101.6	12.7
2	228.6	12.7	101.6	12.7
3	228.6	14.3	101.6	14.3
4	239.4	10.8	101.6	14.6
5	287.0	9.4	88.9	17.8
6	314.7	9.5	101.6	15.5
7	364.5	10.1	85.7	16.5
8	441.3	17.8	101.6	15.9
9	280.0	35.0	00.0	00.0
10	177.8	11.1	101.6	11.1

* All Values in mm
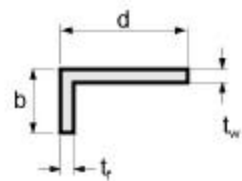
All Material - 'MS' Steel

**Figure D.1.3: Damage Sites along Side Shell Longitudinal No. 8
Between Frames 66 and 67**

The owner and fabricator of the tanker agree that the welds should be repaired before delivery of the vessel because the undercuts are located in regions of high stress concentrations. However, the project is already several months behind schedule and considerably over budget. The fabricator and owner have, therefore, opted for a damage tolerance assessment to determine whether such repairs are necessary.

The side-shell longitudinal, flat bracket, and side-shell plating are fabricated from Grade A mild steel. The nominal yield strength (σ_y) and nominal ultimate tensile strength (UTS)(σ_u) of this material are 235 and 440 MPa respectively. The following CTOD values were obtained from fracture toughness tests on the steel at 0°C (the minimum design temperature): 0.32, 0.37, and 0.25 mm. The failure mode in all three tests was initial ductile tearing followed by unstable cleavage (i.e., Type u).

D.2   LOAD ANALYSIS

Extreme stresses at the damage site for the interval of interest and corresponding to a specific probability of exceedance are required for fracture assessment, while the statistical distribution of stress range at the damage site over the interval of interest are required for fatigue assessment. Method A of the three Level 2 approaches described in Part B, Section B.2.6 of this guide will be used to estimate the statistical stress distribution. This method assumes the basic form of the distribution, and a reference stress range corresponding to a probability of exceedance per wave encounter of 10^{-4} is used as a reference point for the distribution. The extreme stress will correspond to a probability of exceedance of 0.01 over the interval of interest (with the corresponding probability of exceedance per wave encounter equal to 1/n, where n is the number of wave encounters over the interval of interest). This is consistent with the generally accepted value of 0.01 for the ship design life that is typically twenty years. The starting point for the load calculations will, therefore, be the determination of loads for an arbitrary probability of exceedance per wave encounter. The corresponding stresses can then be transformed to the required probability of exceedance for the fatigue and fracture calculations.

The following wave-induced loads can be estimated from parametric equations in Appendix A of Reference D.2.

1. hull girder bending moments (vertical and horizontal);

2. external hydrodynamic pressure range;

3. internal pressure range of tank loads (inertial fluid loads; and added static head due to vessel motion).

The ABS guide does not specify the corresponding probability of exceedance for these loads. However, the equations are intended to give extreme loads so they will be taken to be 10^{-8} per wave encounter. The guide does not take into account wave impact loads, whipping, springing, tank fluid sloshing, or vibrating forces due to machinery or propellers. In this example, however, the latter loads are secondary or insignificant compared to the former three types of loads.

The ABS guide divides the ship cross-section into Zones A and B as shown schematically in Figure D.2.1. The appropriate stress range for each zone is calculated based on the fluctuating load due to two (acting together) of the eight combinations of internal tank loading and draft shown in Figure D.2.2. For Zone A, the greater value of LC1 and LC2 or LC3 and LC4 is used and for Zone B, the greater of LC5 and LC6 or LC7 and LC8. The area of interest in both examples is Zone B so the greater values for LC5 and LC6 or LC7 and LC8 should be used. The values were computed in Reference D.1 and are repeated here in Table D.2.1.

Table D.2.1: Wave-Induced Bending Moments and Pressure Acting on Side Shell Longitudinal No. 8 Between Frames 36 and 37

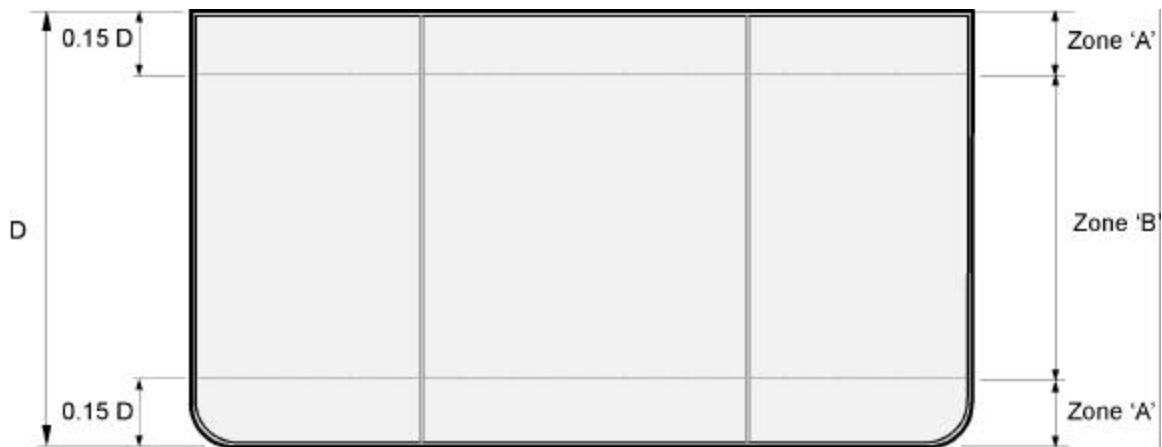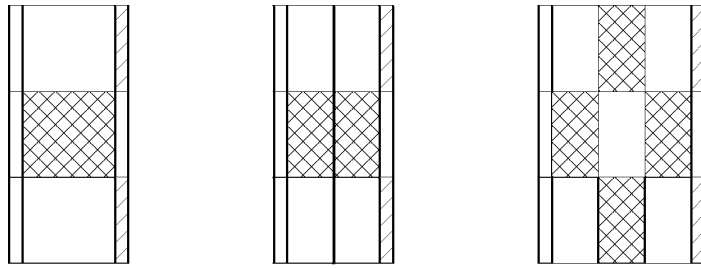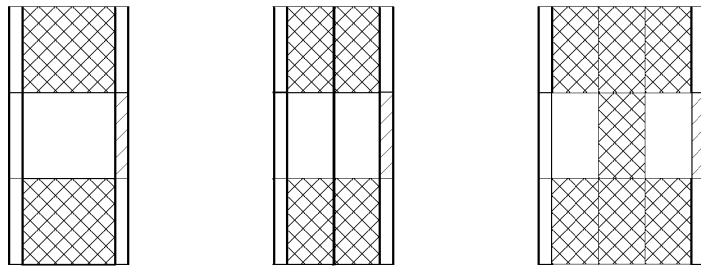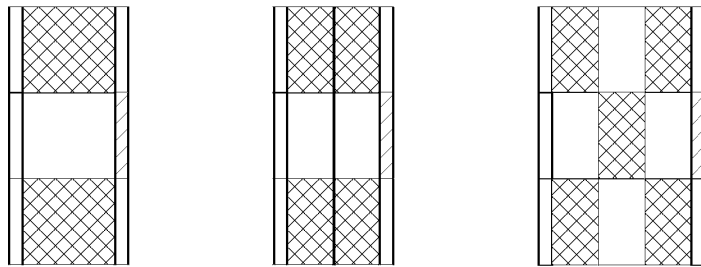| still-water bending moment (M_{sw})	$+2.52 \times 10^9$ N-m
vertical sagging moment (M_{vs})	-1.14×10^9 N-m
vertical hogging moment (M_{vh})	$+1.07 \times 10^9$ N-m
horizontal bending moment (M_h)	$+/- 1.38 \times 10^9$ N-m
side shell pressure range (p)	0.045 MPa

Figure D.2.1: Breakdown of a Ship's Cross-Section for Load Analysis in Accordance with Reference 7.1

a) Load Cases # 1, 3, and 7, 2/3 Design Draft

b) Load Cases # 2, 4, and 8, Design Draft

c) Load Cases # 5, 2/3 Design Draft
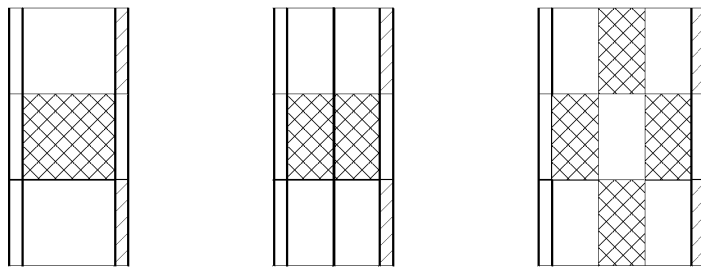
d) Load Cases # 6, 2/3 Design Draft

Figure D.2.2: Loading Cases for Load Analysis in Accordance with Reference 7.1

D.3 STRESS ANALYSIS

D.3.1 Global Nominal Stresses

Estimates of the hull girder bending stresses produced by the bending moments in Table D.2.1 are tabulated in Table D.3.1. These estimates are based on the flexure formula:

$$\sigma_{sw} = M_{sw}y/I_v \qquad \text{(D.3.1.1)}$$

$$\sigma_{vs} = M_{vs}y/I_v \qquad \text{(D.3.1.2)}$$

$$\sigma_{hs} = M_{hs}y/I_v \qquad \text{(D.3.1.3)}$$

$$\sigma_h = M_h z/I_h \qquad \text{(D.3.1.4)}$$

where $I_v = 2.82 \times 10^6 \text{ m}^2\text{-cm}^2 : I_h = 5.51 \times 10^6 \text{ m}^2\text{-cm}^2$

y = vertical distance of side longitudinal No. 8 from horizontal neutral axis = 2.44 m
z = horizontal distance of side longitudinal No. 8 from vertical neutral axis = 16.0 m

Table D.3.1: Stresses Produced By Wave-Induced Bending Moments and Pressure Acting on Side Shell Longitudinal No. 8 Between Frames 36 and 37

still-water bending stress (σ_{sw})	+22.0 MPa
vertical sagging stress (σ_{vs})	-10.0 MPa
vertical hogging stress (σ_{vh})	+9.0 MPa
horizontal bending stress (σ_h)	+/- 40.0 MPa

The estimated global nominal stresses are treated as membrane stresses ($\sigma_{G,m}$) across the cross-section of the longitudinal because the distances between side shell longitudinal No.8 and the horizontal and vertical neutral axes of the ship's cross-section are large with respect to the width and depth of the longitudinal. The worst case from the fatigue and fracture point of view is when the horizontal bending stress is in phase with the vertical bending stress:

$$\sigma_{G,m}^{max} = |\sigma_{sw}| + |\sigma_{hs}| + |\sigma_h| = 22 + 9 + 40 = 71 \text{ Mpa} \qquad \text{(D.3.1.5)}$$

$$\sigma_{G,m}^{min} = |\sigma_{sw}| - |\sigma_{vs}| - |\sigma_h| = 22 - 10 - 40 = -28 \text{ Mpa}$$
(D.3.1.6)

The side shell pressure produces a combination of bending and torsion in side shell longitudinal No. 8. The resulting maximum principal stresses peak at the corner between the flange and web of the longitudinal as evident in the finite element results shown in Figure D.3.1.

The range of this peak stress ($\Delta\sigma_p$) is estimated by the following equations from Section 3.3.3 of Reference D.2 to be 55.4 MPa at the mid-span and 56.6 MPa at the frame ends.
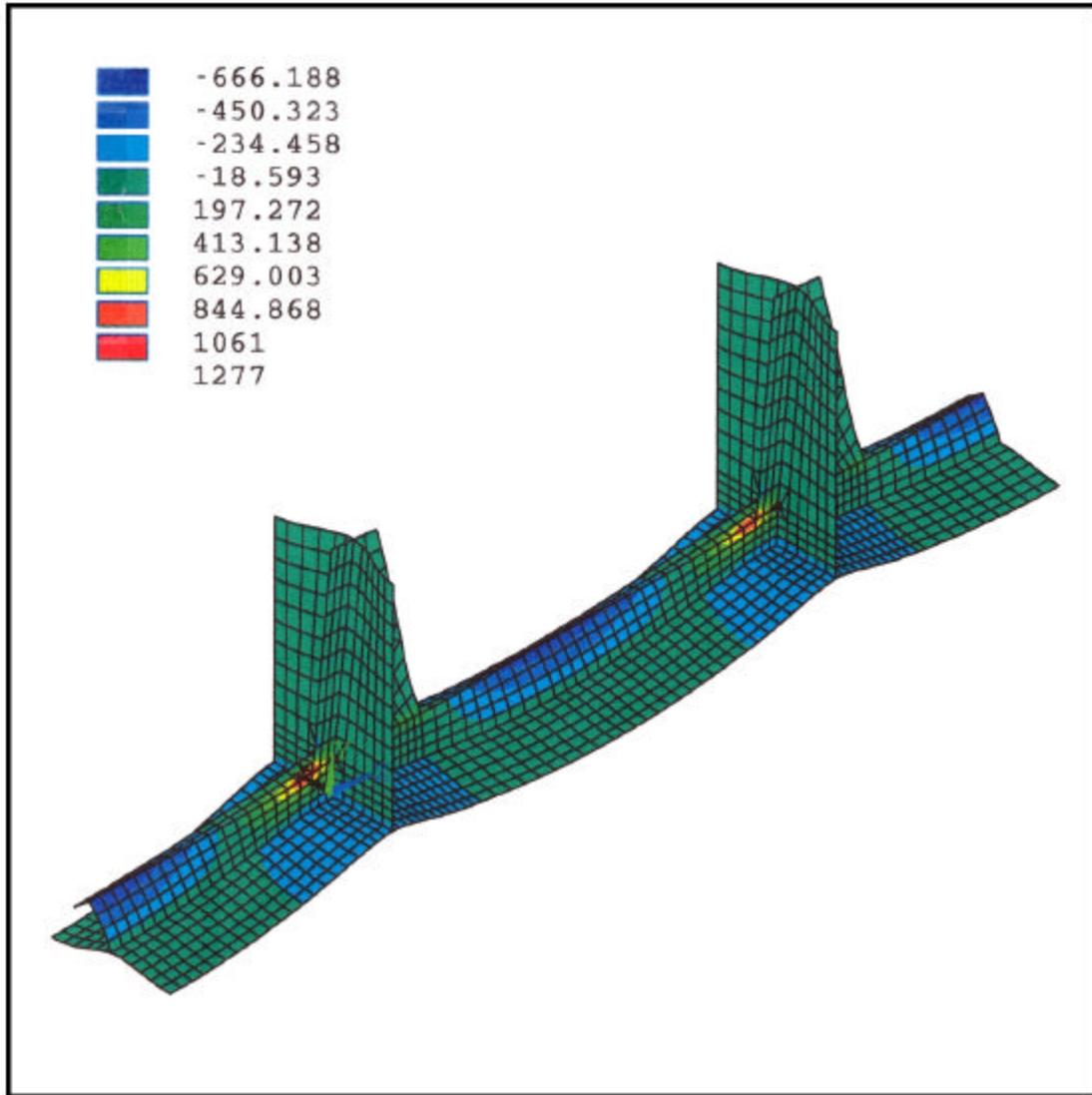
Figure D.3.1: Longitudinal Stresses (MPa) in Side Shell Longitudinal No. 8 Subjected to Unit Inward Pressure (MPa) as Predicted by Finite Element Analysis (ANSYS) with Plate Element Model

$$\Delta\sigma_p = C_t M/Z_4 \qquad\qquad\qquad\qquad (D.3.1.7)$$

$$M = k \cdot p \cdot s \cdot l^2 \qquad\qquad\qquad\qquad (D.3.1.8)$$

where:

C_t	=	correction factor for combined bending and torsional stress = 1.5
Z_l	=	sectional modulus about the vertical axis of the longitudinal and its associated effective side shell plating
	=	473400 mm^3 at mid-span and 463700 mm^3 at frame ends the effective breadth of side shell plating was taken as 351.8 mm at mid-span and 493.7 mm at frame ends
M	=	bending moment at the supported ends of the longitudinal
k	=	factor accounting for the fixity of the stiffener = 1.15/12
s	=	stiffener spacing = 800 mm
l	=	unsupported span of the stiffener = 2250 mm

A horizontal bending stress ($\sigma_{G,b}$) is conservatively assumed to act across the cross-section of the longitudinal. The side shell pressure is also assumed to fully reverse so:

$$\sigma_{G,b}^{max} @ \text{ mid-span} = +27.7 \text{ MPa} \qquad (D.3.1.9)$$

$$\sigma_{G,b}^{min} @ \text{ mid-span} = -27.7 \text{ MPa} \qquad (D.3.1.10)$$

$$\sigma_{G,b}^{max} @ \text{ frame ends} = +28.3 \text{ MPa} \qquad (D.3.1.11)$$

$$\sigma_{G,b}^{min} @ \text{ frame ends} = -28.3 \text{ MPa} \qquad (D.3.1.12)$$

D.3.2 Stress Concentrations

The total stresses (σ_l) and local nominal stresses (σ_L) at the damage sites are related to the global nominal stresses (σ_G) as follows:

$$= K_G \cdot \sigma_G + \sigma_r \qquad (D.3.2.1)$$
$$= K_G \cdot K_w \cdot K_g \cdot K_{te} \cdot K_\alpha \cdot \sigma_G + \sigma_r \qquad (D.3.2.2)$$

(See Nomenclature)

For both sites, welding residual stresses at the damage site are assumed to be uniform through the thickness of the web and flange of the longitudinal and equal in magnitude to the yield strength of the base metal (235 MPa). The determination of K_G requires a global hull finite element analysis, whereas K_{te} and K_α can be estimated from Appendix A of this guide. For the purposes of this demonstration, however, K_{te}, K_α and K_G are assumed to be unity at both damage sites. The product of K_w and K_g at the splice weld in Example 1 is also assumed to be unity. However, the product of K_w and K_g at the toe of the flat bracket in Example 2 is estimated to be 2.2 from Table B2 of Appendix B in this guide.

The values of σ_L and σ_1 corresponding to ${\sigma_{G,m}}^{max}$, ${\sigma_{G,b}}^{max}$, ${\sigma_{G,m}}^{min}$, and ${\sigma_{G,b}}^{min}$ are tabulated in Table D.3.2:

Table D.3.2: Local Nominal Stresses and Total Stresses at Damage Sites

	@ mid-span	@ toe of flat bracket
$\sigma_{L,m}^{max}$	71 + 235 = +306 MPa	71 + 235 = +306 MPa
$\sigma_{L,m}^{min}$	-28 + 235 = +207 MPa	-28 + 235 = +207 MPa
$\Delta\sigma_{L,m} = \sigma_{L,m}^{max} - \sigma_{L,m}^{min}$	99 MPa	99 MPa
$\sigma_{L,b}^{max}$	+27.7 MPa	+28.3 MPa
$\sigma_{L,b}^{min}$	-27.7 MPa	-28.3 MPa
$\Delta\sigma_{L,b} = \sigma_{L,b}^{max} - \sigma_{L,b}^{min}$	55.4 MPa	56.6 MPa
$\sigma_{1,m}^{max}$	71 + 235 = +306 MPa	2(71) + 235 = +376 MPa
$\sigma_{1,m}^{min}$	-28 + 235 = +207 MPa	2(-28) + 235 = +179 MPa
$\Delta\sigma_{1,m} = \sigma_{1,m}^{max} - \sigma_{1,m}^{min}$	99 MPa	198 MPa
$\sigma_{1,b}^{max}$	+27.7 MPa	2(28.3) = +56.6 MPa
$\sigma_{1,b}^{min}$	-27.7 MPa	2(-28.3) = -56.6 MPa
$\Delta\sigma_{1,b} = \sigma_{1,b}^{max} - \sigma_{1,b}^{min}$	55.4 MPa	113.2 MPa

D.3.3 Stress Intensity Factors

In the first example, a fatigue crack has initiated at the corner of side shell longitudinal No. 8 in a splice weld located midway between Frames 36 and 37, and propagated through the thickness of the flange and web before being detected. In the second example, a small undercut has been found along the weld toe at the base of the flat bracket at the Frame 37 end of side shell longitudinal No. 8. It is assumed that a fatigue crack will rapidly initiate from the undercut, so the latter is treated as a pre-existing quarter-elliptic corner crack of the same depth and length as the undercut. It is also assumed that the corner crack will propagate through the thickness of the flange and web in a self-similar manner and that the corner crack will evolve into a through-thickness crack once the flange and web are penetrated.

Matoba and Inoue [Ref. D.3] have developed a relatively simple model for estimating stress intensity factors for the aforementioned types of cracks. Their model considers a semi-elliptic surface crack in an imaginary flat plate subjected to the hot spot stress distribution ($K_g \cdot \sigma_L + \sigma_r$) over the cross-section of an actual longitudinal down to a depth B, where B is the width of the longitudinal's flange (Figure D.3.2). The width and thickness of the imaginary plate are 2B and B, respectively, while the imaginary surface crack has a surface length and depth of 2c and a, respectively, where a and c are the surface lengths of a corner crack or through-thickness crack in the longitudinal.

	$(K_s < 1.17)$	$(K_s > 1.17)$
$\sigma_m{}^*$	σ_m	$0.85\,K_s\,\sigma_m$
$\sigma_b{}^*$	σ_b	$0.85\,K_s\,\sigma_b$
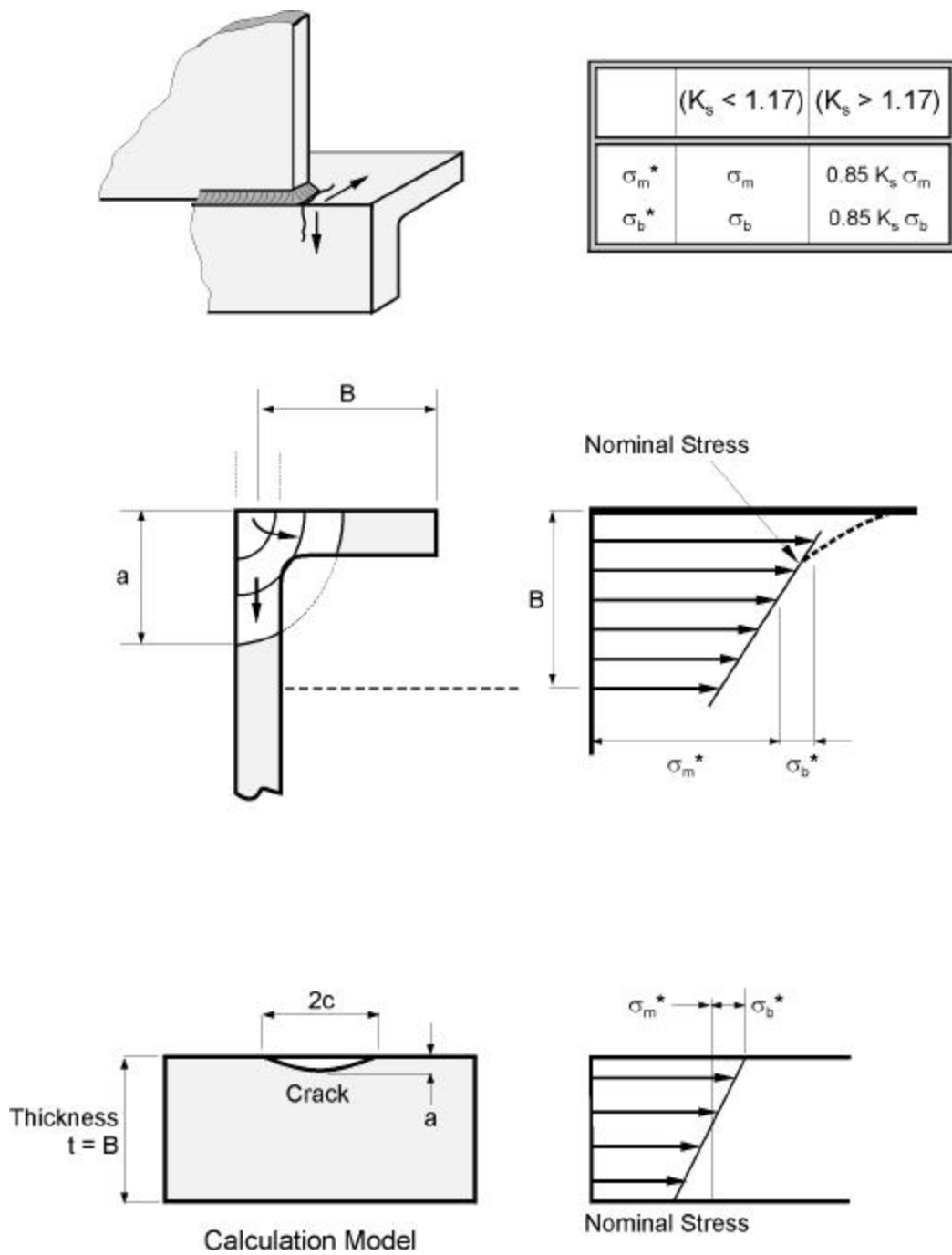
Figure D.3.2: Matoba and Inoue's Model [Ref. D.3] for Calculation of Stress Intensity Factors of Crack in Side Shell Longitudinal No. 8

The stress intensity factor at the deepest point of the semi-elliptic surface crack ($K_{I,a}$) and the stress intensity factor at the ends of the crack ($K_{I,c}$) are defined by the following equations:

for Level 1 FAD (assume through-thickness stress distribution is uniform)

$$K_{I,a} = [Y_{m,a}M_{km,a}\gamma K_g(\sigma_{L,m} + \sigma_{L,b})]\sqrt{\pi a} \qquad (D.3.3.1)$$

$$K_{I,c} = [Y_{m,c}M_{km,c}\gamma K_g(\sigma_{L,m} + \sigma_{L,b})]\sqrt{\pi a} \qquad (D.3.3.2)$$

for Level 2a and Level 2b FAD

$$K_{I,a} = (Y_{m,a}M_{km,a}\gamma K_g\sigma_{L,m} + Y_{b,a}M_{kb,a}\gamma K_g \sigma_{L,b})\sqrt{\pi a} \qquad (D.3.3.3)$$

$$K_{I,c} = (Y_{m,c}M_{km,c}\gamma K_g\sigma_{L,m} + Y_{b,c}M_{kb,c}\gamma K_g\sigma_{L,b})\sqrt{\pi a} \qquad (D.3.3.4)$$

for Level 1 fatigue analysis (assume through-thickness stress distribution is uniform)

$$\Delta K_{I,a} = [Y_{m,a}M_{km,a}\gamma K_g(\Delta\sigma_{L,m} + \Delta\sigma_{L,b})]\sqrt{\pi a} \qquad (D.3.3.5)$$

$$\Delta K_{I,c} = [Y_{m,c}M_{km,c}\gamma K_g(\Delta\sigma_{L,m} + \Delta\sigma_{L,b})]\sqrt{\pi a} \qquad (D.3.3.6)$$

for Level 2 fatigue analysis

$$\Delta K_{I,a} = (Y_{m,a}M_{km,a}\gamma K_g\Delta\sigma_{L,m} + Y_{b,a}M_{kb,a}\gamma K_g\Delta\sigma_{L,b})\sqrt{\pi a} \qquad (D.3.3.7)$$

$$\Delta K_{I,c} = (Y_{m,c}M_{km,c}\gamma K_g\Delta\sigma_{L,m} + Y_{b,c}M_{kb,c}\gamma K_g\Delta\sigma_{L,b})\sqrt{\pi a} \qquad (D.3.3.8)$$

where: $Y_{m,a}$, $Y_{m,c}$, $Y_{b,a}$, and $Y_{b,c}$ are geometry factors for a semi-elliptic crack in a flat plate; $M_{km,a}$, $M_{km,c}$, $M_{kb,a}$, and $M_{kb,c}$ are magnification factors accounting for K_g and K_w in a simple fillet welded joint; and γ is an empirical correction for the local nature of K_g ($\gamma = 1$ for $K_g \leq 1.17$ and .85 for $K_g > 1.17$).

$M_{km,a}$ and $M_{kb,a}$ can be estimated from Equation B.3.6.7 in Part B.3, where α and β are summarized in Table D.3.3, and $M_{km,c}$ and $M_{kb,c}$ are approximated by the values of $M_{km,a}$ and $M_{kb,a}$ for a 0.15 mm deep crack of aspect ratio a/c. $Y_{m,a}$, $Y_{b,a}$, $Y_{m,c}$ and $Y_{b,c}$ can be estimated from parametric equations given in Appendix C.

The value of K_g in Example 1 is set to unity since the crack is located in the weld metal of a ground butt joint. In Example 2, the damage site is located along the weld toe at the base of a flat bracket. The product of K_w and K_g for such a detail is 2.2 according to Table B2 of Appendix B. Although equations for estimating the stress concentration of the weld (K_w) itself are given in Appendix A, K_g is conservatively set to 2 for the purposes for this demonstration.

As evident in the finite element results previously presented in Figure D.3.1, the stress concentration at the base of the flat bracket decays rapidly across the width of the flange of the adjoining longitudinal. This decay is taken into account by the γ correction factor in the equations.

Table D.3.3: **a** and **b** Values for Membrane and Bending Loads where $M_{k, a} = a\,(a/t)^b$

Loading	a/t	α	β
membrane	$\leq .073$	.615	-.31
	$>.073$	.83	-.20
bending	$\leq.03$	.45	-.31
	$>.03$	.68	-.19

D.3.4 Statistical Distribution of Local Nominal Stress Range

The design life for the tanker in Examples 1 and 2 is 20 years. It is assumed that the tanker will encounter 10^8 waves over this period and 500,000 waves per year on average. It is also assumed the ranges of the membrane and bending components of wave-induced local nominal stresses ($\Delta\sigma_{L,m}$ and $\Delta\sigma_{L,b}$) at the damage sites in Examples 1 and 2 follow a Weibull distribution

$$n/n_o = \exp[-(\Delta\sigma/\Delta\sigma_o)^h \ln(n_o)] \qquad (D.3.4.1)$$

or

$$\Delta\sigma/\Delta\sigma_o = [1 - \log(n)/\log(n_o)]^{1/h} \qquad (D.3.4.2)$$

where: $\Delta\sigma$ is either $\Delta\sigma_{L,m}$ or $\Delta\sigma_{L,b}$; $\Delta\sigma_o$ is the stress range exceeded once in n_o cycles (i.e., probability of exceedance = $1/n_o$); n is the number of times $\Delta\sigma$ is exceeded in n_o encounters; and h is the shape factor.

As discussed in Part B.2, the shape factor depends on the location of interest in a ship and the particulars of that ship. The side shell longitudinal in Examples 1 and 2 is located just below the water-line, and the corresponding shape factor is approximately unity according to the following equation from Section B.2.6.1.

$$h = h_o + h_a z_{b\ell}/T_{act} - 0.005(T_{act} - z_{b\ell}) \qquad (D.3.4.3)$$

where:
h_o	=	$2.21 - .54\log_{10}L$
h_a	=	.05
$z_{b\ell}$	=	vertical distance from baseline to load point = 11.01 m
T_{act}	=	draught in m of load condition = 13.26 m
L	=	ship length = 239.6 m

A Weibull distribution with a shape factor of unity reduces to an exponential distribution (Figure D.3.3). Tables D.3.4 and D.3.5 discretize an exponential distribution of stress ranges over 20 years into 21 stress levels. These tables also discretize an exponential distribution of stress ranged over one year into 17 stress levels - the highest four stress levels in the twenty year distribution being clipped off. Histograms of these two distributions are superimposed in Figure D.3.4.

Table D.3.4: Probability of Exceedance

$\dfrac{\Delta\sigma}{\Delta\sigma_{10^{-4}}}$	Probability of Exceedance	No. of Exceedances in 5×10^6 Cycles (1 Year)	No. of Exceedances in 1×10^8 Cycles (20 Years)
0	1.000	5,000,000	100,000,000
0.1	3.981×10^{-1}	1,990,054	39,810,717
0.2	1.585×10^{-1}	792,447	15,848,932
0.3	6.310×10^{-2}	315,479	6,309,573
0.4	2.512×10^{-2}	125,594	2,511,886
0.5	1.000×10^{-2}	50,000	1,000,000
0.6	3.981×10^{-3}	19,905	398,107
0.7	1.585×10^{-3}	7,925	158,489
0.8	6.310×10^{-4}	3,155	63,096
0.9	2.512×10^{-4}	1,256	25,119
1.0	1.000×10^{-4}	500	10,000
1.1	3.981×10^{-5}	199	3,981
1.2	1.585×10^{-5}	79	1,585
1.3	6.310×10^{-6}	32	631
1.4	2.512×10^{-6}	13	251
1.5	1.000×10^{-6}	5	100
1.6	3.981×10^{-7}	2	40
1.7	1.585×10^{-7}	1	16
1.8	6.310×10^{-8}		6
1.9	2.512×10^{-8}		3
2.0	1.000×10^{-8}		1

Table D.3.5: Frequency of Occurrence

$\dfrac{\Delta\sigma}{\Delta\sigma_{10}}{}^{-4}$	No. of Occurrences in 5×10^6 Cycles (1 year)	$\dfrac{\Delta\sigma}{\Delta\sigma_{10}}{}^{-4}$	No. of Occurrences in 1×10^8 Cycles (20 Years)
0.0 - 0.1	3,009,464	0.0 - 0.1	60,189,283
0.1 - 0.2	1,198,089	0.1 - 0.2	23,961,785
0.2 - 0.3	476,968	0.2 - 0.3	9,539,358
0.3 - 0.4	189,884	0.3 - 0.4	3,797,687
0.4 - 0.5	75,594	0.4 - 0.5	1,511,886
0.5 - 0.6	30,095	0.5 - 0.6	601,893
0.6 - 0.7	11,981	0.6 - 0.7	239,618
0.7 - 0.8	4,770	0.7 - 0.8	95,393
0.8 - 0.9	1,899	0.8 - 0.9	37,977
0.9 - 1.0	756	0.9 - 1.0	15,119
1.0 - 1.1	301	1.0 - 1.1	6,019
1.1 - 1.2	120	1.1 - 1.2	2,396
1.2 - 1.3	48	1.2 - 1.3	954
1.3 - 1.4	19	1.3 - 1.4	380
1.4 - 1.5	8	1.4 - 1.5	151
1.5 - 1.6	3	1.5 - 1.6	60
>1.6	1	1.6 - 1.7	24
		1.7 - 1.8	10
		1.8 - 1.9	4
		1.9 - 2.0	2
		> 2.0	1

Figure D.3.3: Probability of Exceedance Diagram for an Exponential Distribution of Stress Ranges with a Reference Stress Range Corresponding to a Probability of Exceedance per Wave Encounter 10^{-4}
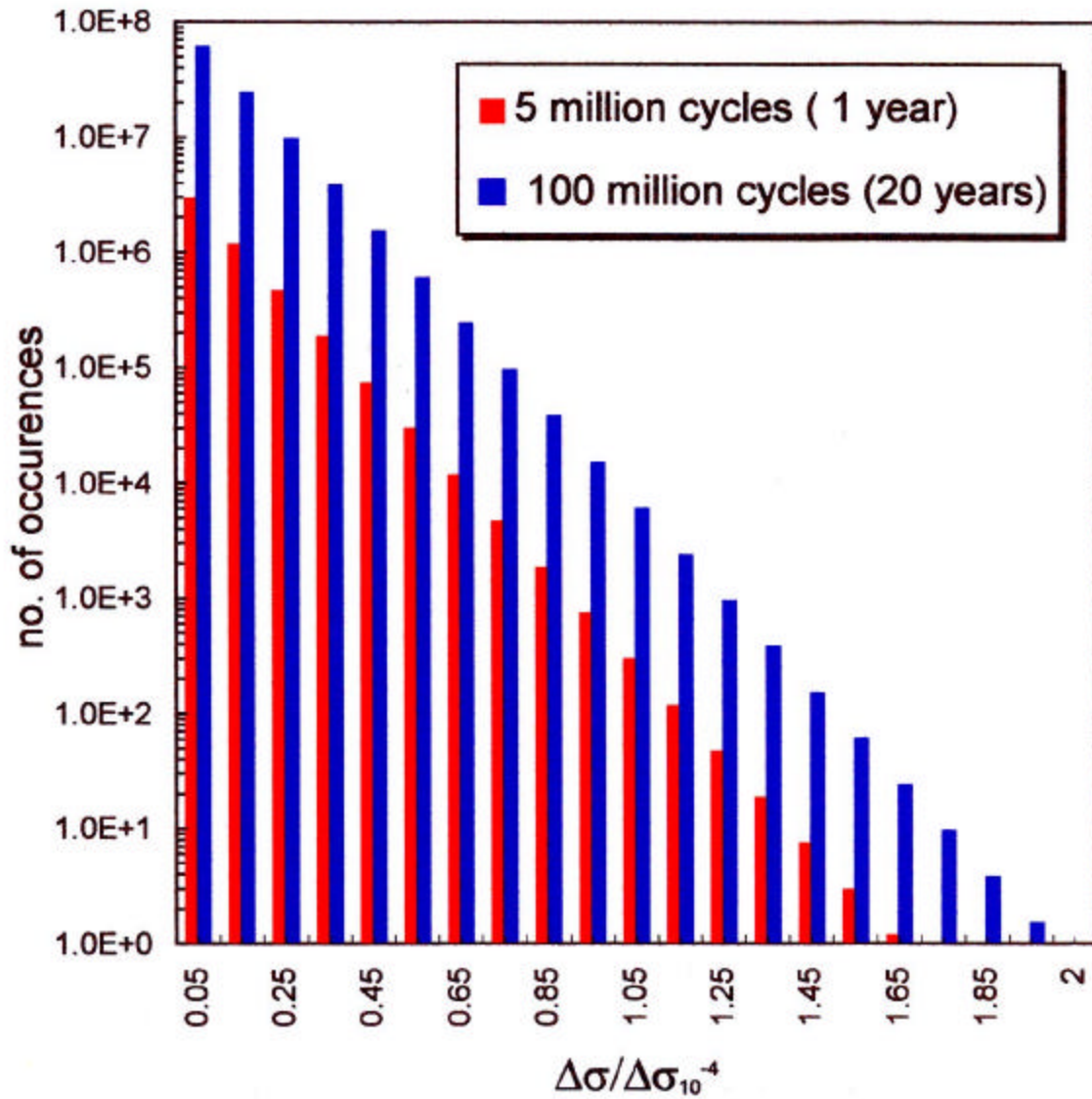
Figure D.3.4: Histogram of Stress Ranges Distributed over One Year and Twenty Years According to an Exponential Distribution with a Reference Stress Range Corresponding to a Probability of Exceedance per Wave Encounter of 10^{-4}

The wave-induced bending moments and pressure acting on the side shell longitudinal and corresponding to a probability of exceedance per wave encounter of 10^{-8} were tabulated in Table D.2.1, and the associated ranges of total stress and local nominal stress were tabulated in Table D.3.1. Because the majority of fatigue damage is usually inflicted by stress ranges corresponding to probability of exceedances between 10^{-3} and 10^{-6}, it is recommended that n_o be set to 10^4 in order to minimize errors associated with differences between the assumed and actual shape factor. The following equation (B.2.6.8) can be used to convert the stress ranges in Table D.3.2 from one probability level (p_2) to another probability level (p_1)

$$\Delta\sigma_2 = \Delta\sigma_1 \, [\log(p_2)/\log(p_1)]^{1/h} \qquad (D.3.4.4)$$

where:

$$\Delta\sigma_2 = 0.5\Delta \qquad (D.3.4.5)$$
for $p_2 = 10^{-8}$ and $p_1 = 10^{-4}$.

D.3.5 Extreme Stress

Extreme values of $\sigma_{L,m}$ and $\sigma_{L,b}$ are required for the calculation of stress intensity factors for residual strength assessment. Design loads for a ship typically correspond to a probability of exceedance of .01 over the design life of the ship, and the associated probability of exceedance per wave encounter is .01/n where n is the number of wave encounters over the design of the ship. As mentioned earlier, the tanker in Examples 1 and 2 has a twenty-year design life and it is assumed that the ship encounters 10^8 waves over this life. Therefore, the values of $s_{L,m}^{max}$ and $s_{L,b}^{max}$ in Table D.3.2, which correspond to a probability of exceedance of 10^{-8} per wave encounter, are suitable for residual strength assessment over the design life of the vessel but too conservative for much shorter assessment intervals. A more sensible approach is to use extreme values that correspond to a constant probability of exceedance of .01 over the assessment interval. To this end, Equation D.3.4.4 can be used to convert the values of $s_{L,m}^{max}$ and $s_{L,b}^{max}$ in Table D.3.2 to values corresponding to a probability of exceedance per wave encounter of $1/n^*$, provided the statistical distribution of stresses remains more or less constant, where n^* is the number of wave encounters over the assessment interval. In Examples 1 and 2, the assessment interval is determined by the number of cycles to propagate a fatigue crack from an initial crack size to a critical crack size, so it is necessary to calculate the extreme stresses and carry out the residual strength assessments simultaneously with the fatigue crack growth calculations.

D.3.6 Net Section Stress

As discussed earlier, the horizontal co-ordinate for a failure assessment diagram (S_r or L_r) is the ratio of the net section stress (σ_n) to either the yield stress (σ_y) or flow stress [$\sigma_f = (\sigma_y + \sigma_y)/2$]. The net section stress for a uniform applied tensile load and symmetric crack configuration is simply the applied load divided by the net cross-sectional area. In contrast, the net section stress for asymmetric crack configurations and/or applied bending loads, is not obvious and usually defined by an imaginary stress that is obtained in the following manner. The distribution of net section stresses prior to plastic collapse is assumed to be identical in form to the distribution of net section stresses at plastic collapse according to a limit load analysis with an elastic-perfectly plastic material model. The net section stress prior to plastic collapse is then obtained by solving the equilibrium equations for moment and forces across the net section simultaneously. Closed form solutions for simple cases are given in Section 3.6. However, an iterative solution is generally required for more complex cases, such as the side shell longitudinal in Examples 1 and 2. See Figure D.3.4 for the development of equilibrium equations for the longitudinal.

Equilibrium of Longitudinal Forces

$$\sigma_m\{t_f \cdot (b - t_w) + d \cdot t_w + b_e \cdot t_s\} = \sigma_n\{t_f \cdot (b - c) + t_w \cdot (d - a) + (t_s - \bar{y}_p) \cdot b_e - \bar{y}_p \cdot b_e\}$$

Equilibrium of Bending Moments

$$\sigma_b (d - \bar{y})/1 + \sigma_m \{ (d - a) \cdot t_w \cdot (d + t_s - a) + b_e \cdot t_s^2/2 \} =$$

$$\sigma_n\{t_f \cdot (b - c) \cdot (d + t_s - t_f/2) + t_w \cdot (d - a) \cdot [(d - a)/2 + t_s] + (b_e \cdot (t_s - \bar{y}_p) \cdot [(t_s \bar{y}_p)/2 + \bar{y}_p] - \bar{y}_p^2 \cdot b_e/2\}$$
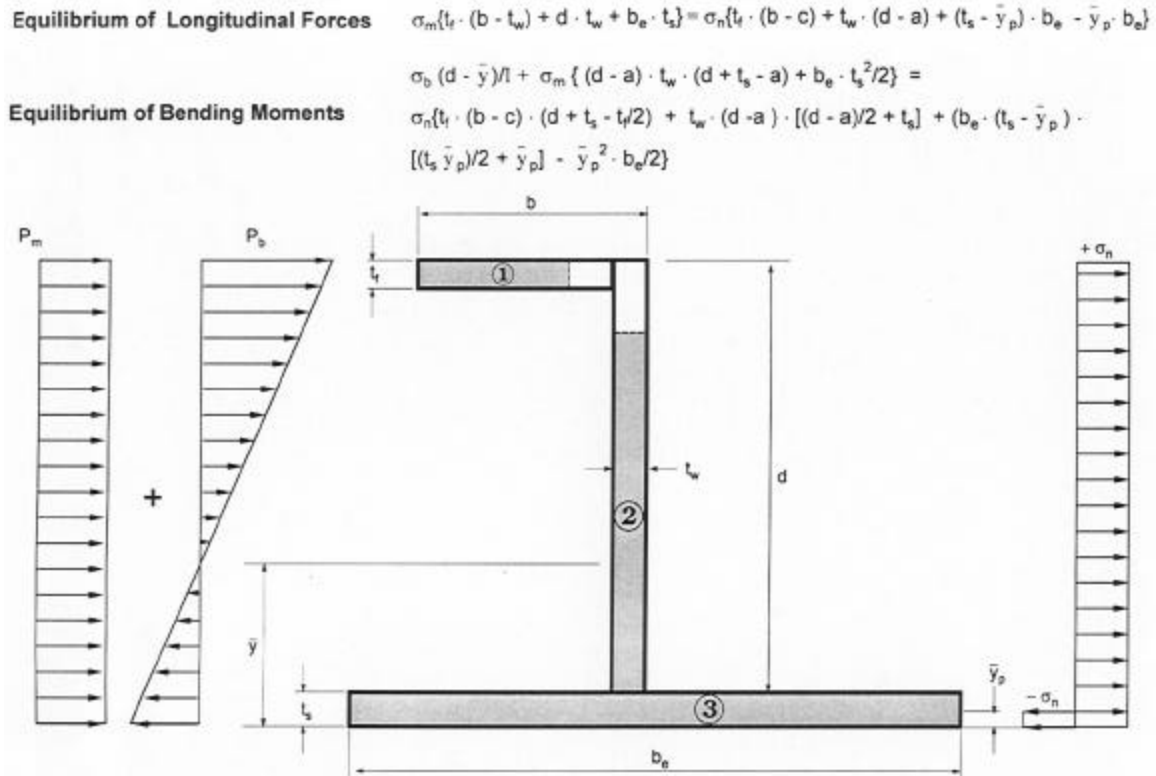
Figure D.3.4: Calculation of Net Section Stress by Simultaneous Solution of Equilibrium Equations for Longitudinal Forces and Bending Moments

D.4 RESIDUAL LIFE ASSESSMENT PROCEDURE

1. Select the level of analysis. Use Level 2 fatigue analysis with Level 1 FAD and Level 3 fatigue analysis with either Level 2a FAD or Level 2b FAD.

2. Arrange the individual blocks of stress ranges in the histograms constructed in Section D.3.4 into three different sequences: high-to-low, low-to high, low-high-low (**Figure D.4.1**).

3. Further divide the blocks of stress ranges in each sequence into sub-blocks of length ΔN_B, where ΔN_B is the lesser of the minimum block length or 10% of the current block length. For each sequence of stress ranges, carry out Steps 4 to 7.

4. Use the approximate model described in Section D.3.3, the relevant values of $\Delta\sigma_{L,m}$ and $\Delta\sigma_{L,b}$ in Table D.3.2 for the damage site of interest, and the appropriate through-thickness stress distribution for the selected level of fatigue crack growth analysis to calculate the stress intensity factor range for the crack tip in the flange of the longitudinal (ΔK_a) and the stress intensity factor range for the crack tip in the web of the longitudinal (ΔK_c).

5. Calculate the incremental crack growth in the web of the longitudinal (Δa) over each sub-block and the incremental crack growth in the flange of the longitudinal (Δc) over each sub-block by integrating the Paris equation assuming that the crack growth rate is constant over the sub-block and equal to the crack growth rate at the beginning of the sub-block.

for $\Delta K > \Delta K_{th}$

$$\Delta a = C(\Delta K_a)^m \Delta N_B \qquad\qquad\qquad (D.3.4.6)$$
$$\Delta c = C(\Delta K_c)^m \Delta N_B \qquad\qquad\qquad (D.3.4.7)$$

for $\Delta K \leq \Delta K_{th}$

$$\Delta a = 0 \qquad\qquad\qquad\qquad\qquad (D.3.4.8)$$
$$\Delta c = 0 \qquad\qquad\qquad\qquad\qquad (D.3.4.9)$$

In the absence of specific values for C and m, use the recommended upper bound values for structural steels in sea water from Section B.4.3.4 (**C** = 2.3×10^{-12} and m =3.0 where: the units for Δa and Δc are mm and the units for ΔK are MPa√mm.). Yield- level tensile residual stresses are assumed to exist at the damage site in both examples so the local R-ratios are greater than 0.5. Use the recommended upper bound value of ΔK_{th} (63 MPa√mm) for such R-ratios from Section B.4. (Equation B.4.3.11).

6. Update crack size and crack shape.

7. Determine whether the crack has reached a critical size. Use either the Level 1 FAD with Level 2 fatigue analysis, or the Level 2a or Level 2b FAD with Level 3 fatigue analysis. Calculate S_r and L_r using the tensile properties defined Table D.2.1 and the net section stresses determined in accordance with Section D.3.3. Calculate K_r using (i) stress intensity factors for extreme stresses calculated in accordance with Section D.3.5 and (ii) a material fracture toughness (K_{mat}) of 5065 MPa$\sqrt{}$mm. The latter value comes from converting a CTOD value of 0.25 mm, which is the minimum value of the three test results obtained for the steel at the minimum service temperature of the tanker (0°C), to an equivalent K_{mat} value using Equation B.4.2.7.

8. Repeat Steps 3 to 7 for subsequent sub-blocks in each stress history.

9. Repeat Steps 2 to 8 with smaller sub-blocks until crack growth converges.
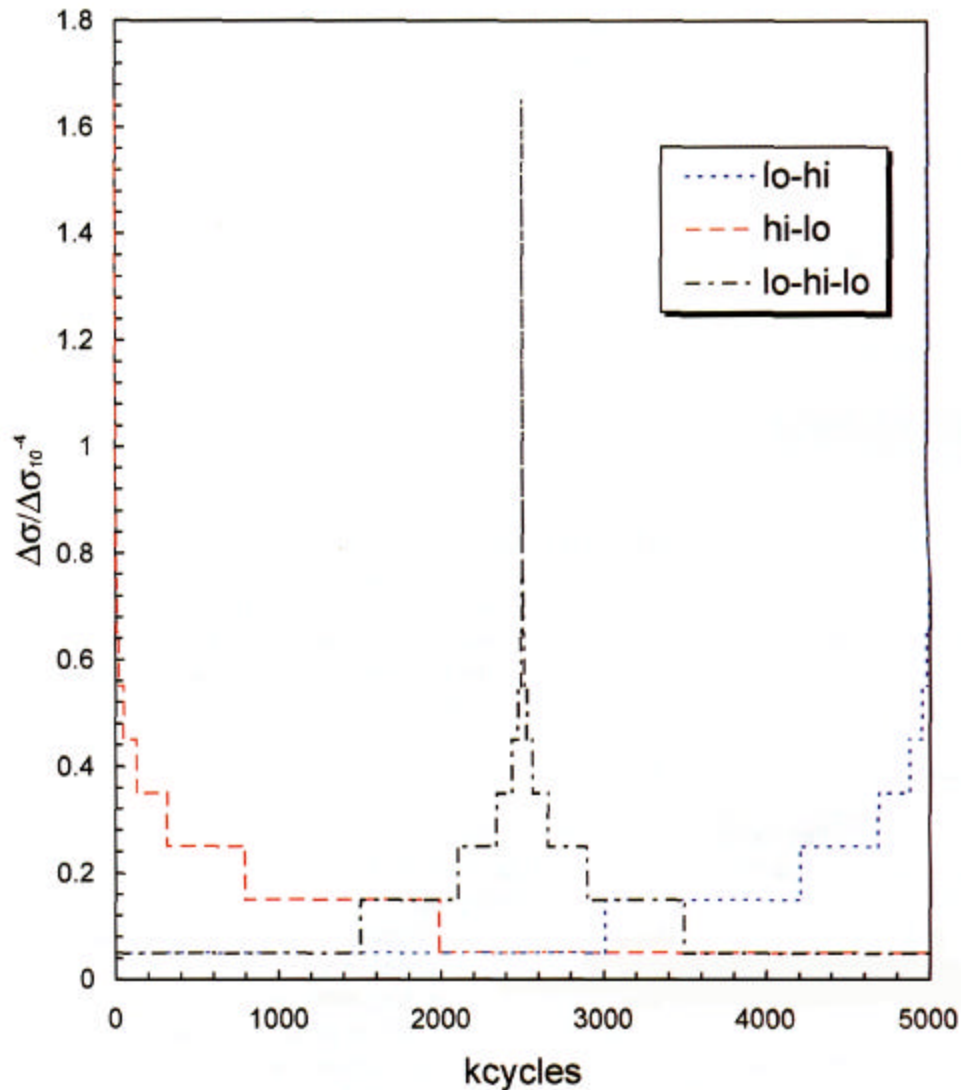
Figure D.4.1: Sequence of Stress Ranges for Fatigue Crack Growth Analysis

D.5   RESULTS

D.5.1 Presentation

At both damage sites and for each stress history, the crack tip in the flange becomes critical before the crack tip in the web. Level 2 predictions of the daily crack advance in the flange are plotted in **Figures D.5.1** and **D.5.2**, while Level 3 predictions of this advance are plotted in **Figures D.5.3** and **D.5.4**. Superimposed on these plots are the predicted critical crack sizes. Failure assessment curves (FAC) and failure assessment points (FAP) for the cases involving lo-hi stress histories are presented in **Figures D.5.5** and **D.5.6**. The predicted critical crack sizes are also tabulated in **Table D.5.1**, while the predicted residual lives are tabulated in **Table D.5.2**.

The following observations can be made about the results:

- For each damage site and level of fatigue analysis, the crack growth curve associated with a hi-lo stress history forms a lower bound on predicted fatigue lives, while the crack growth curve associated with the lo-hi stress history forms an upper bound on predicted fatigue lives. The crack growth curve associated with the lo-hi-lo stress history falls within the aforementioned envelope. The three curves diverge at the beginning of each passing year (i.e., the return period of the stress history) but nearly converge by year's end. Within each year, the maximum difference between the fatigue lives predicted with the lo-hi stress history and the fatigue lives predicted with the hi-lo stress history is about 350 days.

- The predicted residual lives for the damage site at the mid-span of side shell longitudinal No. 8 range from 2238 days to 2784 days, while the predicted residual lives for the damage site at the toe of the flat bracket range from 376 to 949 days. Because of the large geometric stress concentration associated with the flat bracket, the former lives are substantially longer than the latter lives despite the larger initial flaw at the mid-span site. It is also worth noting that the predicted residual lives are greater than the one year return period of the load sequences so the analyses do not have to be repeated with load sequences having shorter return period periods.

- The predicted critical crack sizes (a/c) for the damage site at the mid-span of side shell longitudinal No.8 range from 37.6/43.7 mm to 47.4/58.2 mm, while the predicted critical crack sizes (a/c) for the damage site at the toe of the flat bracket range from 23.1/21.7 mm to 35/38.2 mm. The critical crack sizes at the mid-span are larger than the critical crack sizes at the flat bracket because of the large geometric stress concentration at the toe of the bracket.

- As expected, the shortest residual lives and smallest critical crack sizes are predicted by the Level 1 FAD and Level 1 fatigue analysis, while the longest residual lives and largest critical crack sizes are predicted by the Level 2a FAD and Level 3 fatigue analysis. In most cases, however, the critical crack sizes predicted by the Level 2a FAD and Level 3 fatigue analysis are only 25% longer than the critical crack sizes predicted by the Level 1FAD and Level 2 fatigue analysis, and the percentage difference in terms of residual life is even smaller, viz., 10%.

- The variation of K_r with S_r or L_r is non- linear. This can be attributed to two factors: (i) net section stresses have been calculated for a probability of exceedance per wave encounter that has been constantly updated to maintain a constant probability of exceedance over the assessment interval of 0.01; (ii) the non-linear correction for crack plastic tip plasticity has been applied in both examples because of the assumed presence of yield level welding residual stresses. Therefore, in both examples, the distance of any given failure assessment point (FAP) from the failure assessment curve (FAC) should not be interpreted as a measure of the margin of safety.

Table D.5.1: Critical Crack Lengths

Load History	Damage Site	Level 1		Level 2a		Level 2b	
		a(mm)	c(mm)	a(mm)	c(mm)	a(mm)	c(mm)
lo-hi	mid-span	37.6	43.7	47.4	58	46.1	56.3
	flat bracket	23.1	21.7	33.3	36	25.8	26.5
hi-lo	mid-span	37.8	43.7	47.4	58.2	46.4	56.5
	flat bracket	32.9	33.8	35	38.2	27.2	28.1
lo-hi-lo	mid-span	37.7	43.6	46.2	56.2	43.6	53.9
	flat bracket	32.6	33.3	34.3	37.3	26.2	26.8

Table D.5.2: Residual Fatigue Life in Days (5 ´ 10⁶ Cycles per Year)

Load History	Damage Site	Level 1	Level 2a	Level 2b
lo-hi	mid-span	2525	2784	2545
	flat bracket	723	949	725
hi-lo	mid-span	2191	2238	2331
	flat bracket	376	423	405
lo-hi-lo	mid-span	2356	2379	2370
	flat bracket	546	565	547
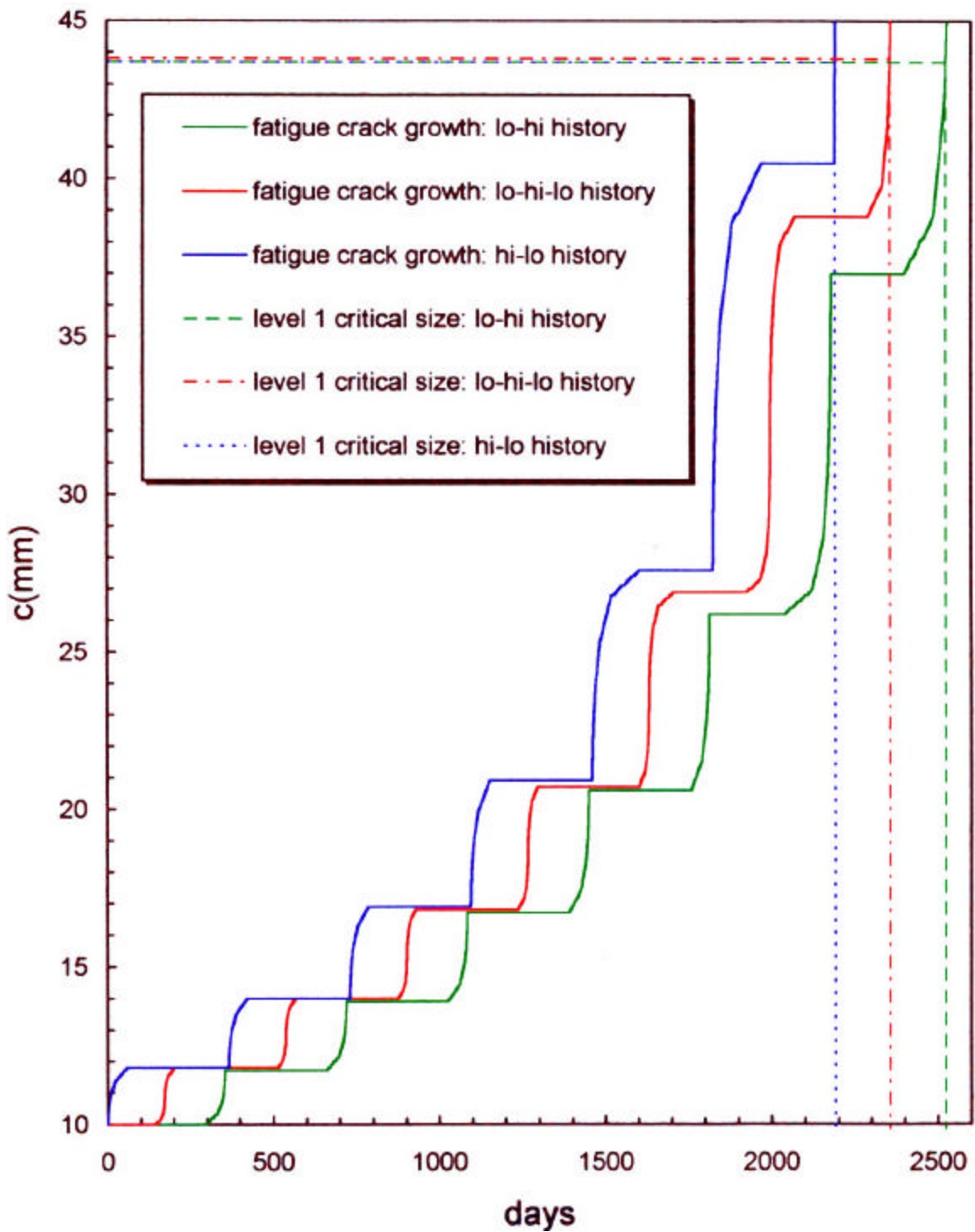
Figure D.5.1: Level 1 Prediction of Flange Crack Length at Mid-Span of Side Shell Longitudinal No. 8 (Example 1) Versus Number of Days of Operation
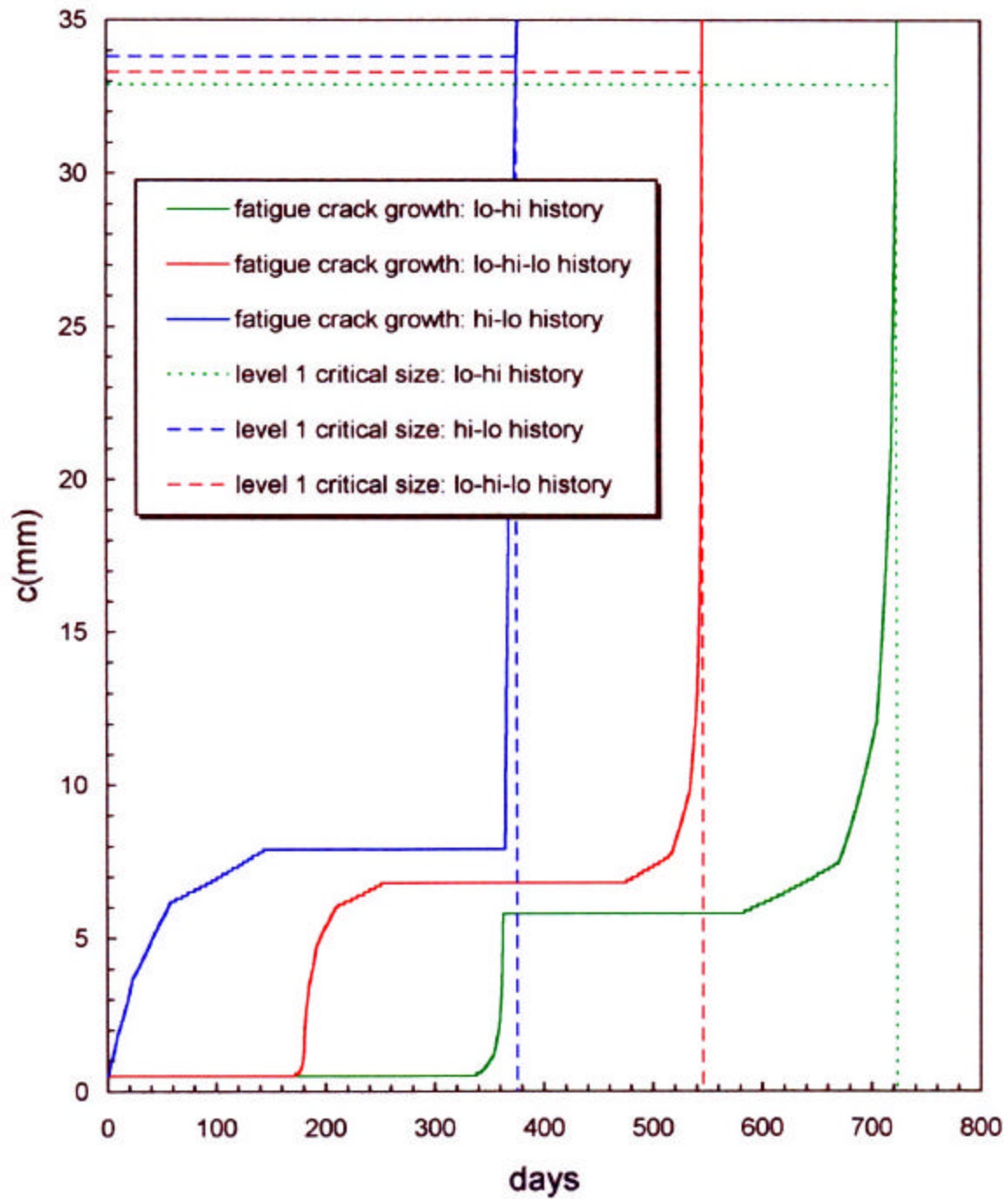
Figure D.5.2: Level 1 Prediction of Flange Crack Length at Flat Bracket at Frame 37 End of Side Shell Longitudinal No. 8 (Example 2) Versus Number of Days of Operation
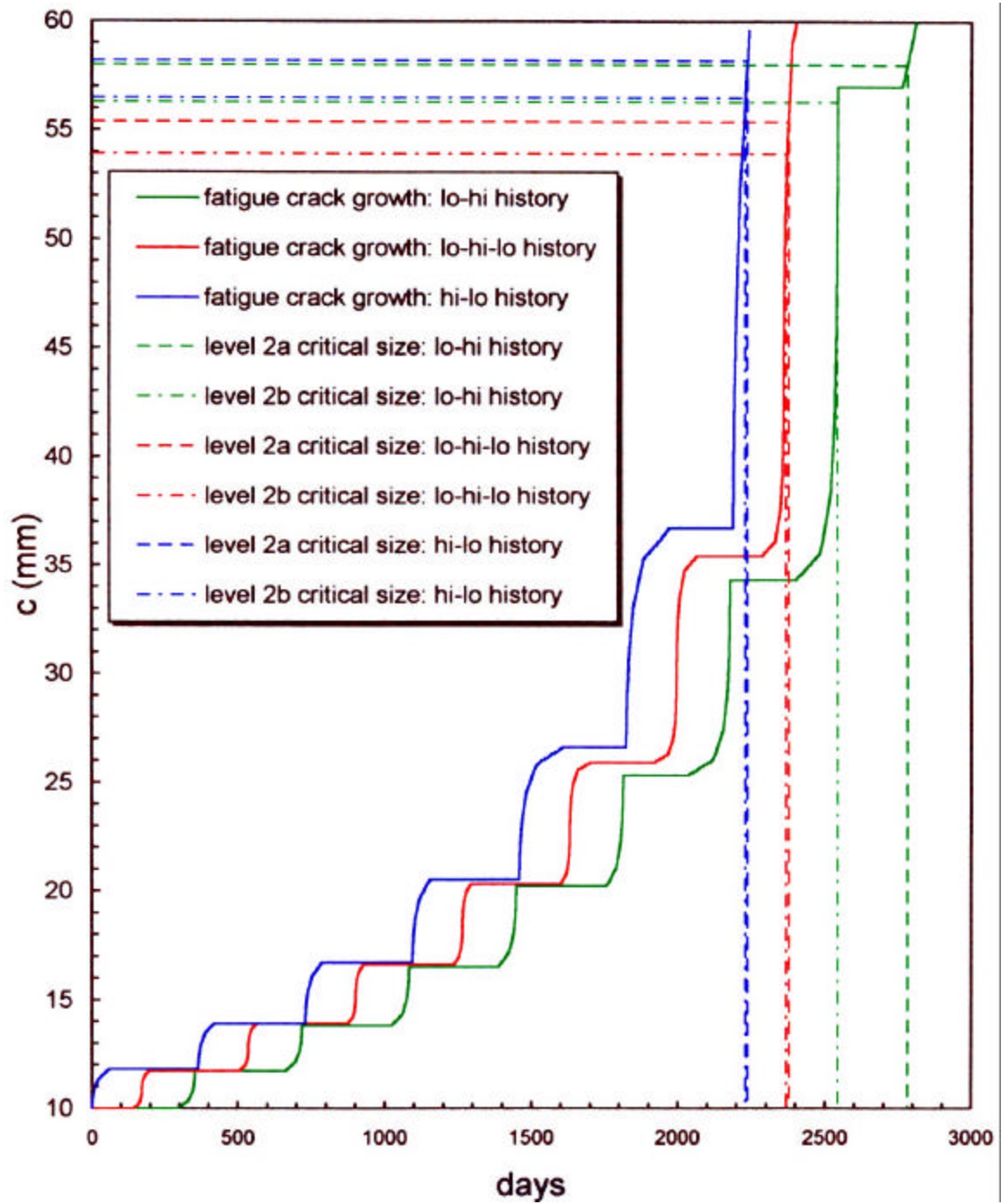
Figure D.5.3: Level 2 Prediction of Flange Crack Length at Mid-Span of Side Shell Longitudinal No. 8 (Example 1) Versus Number of Days of Operation
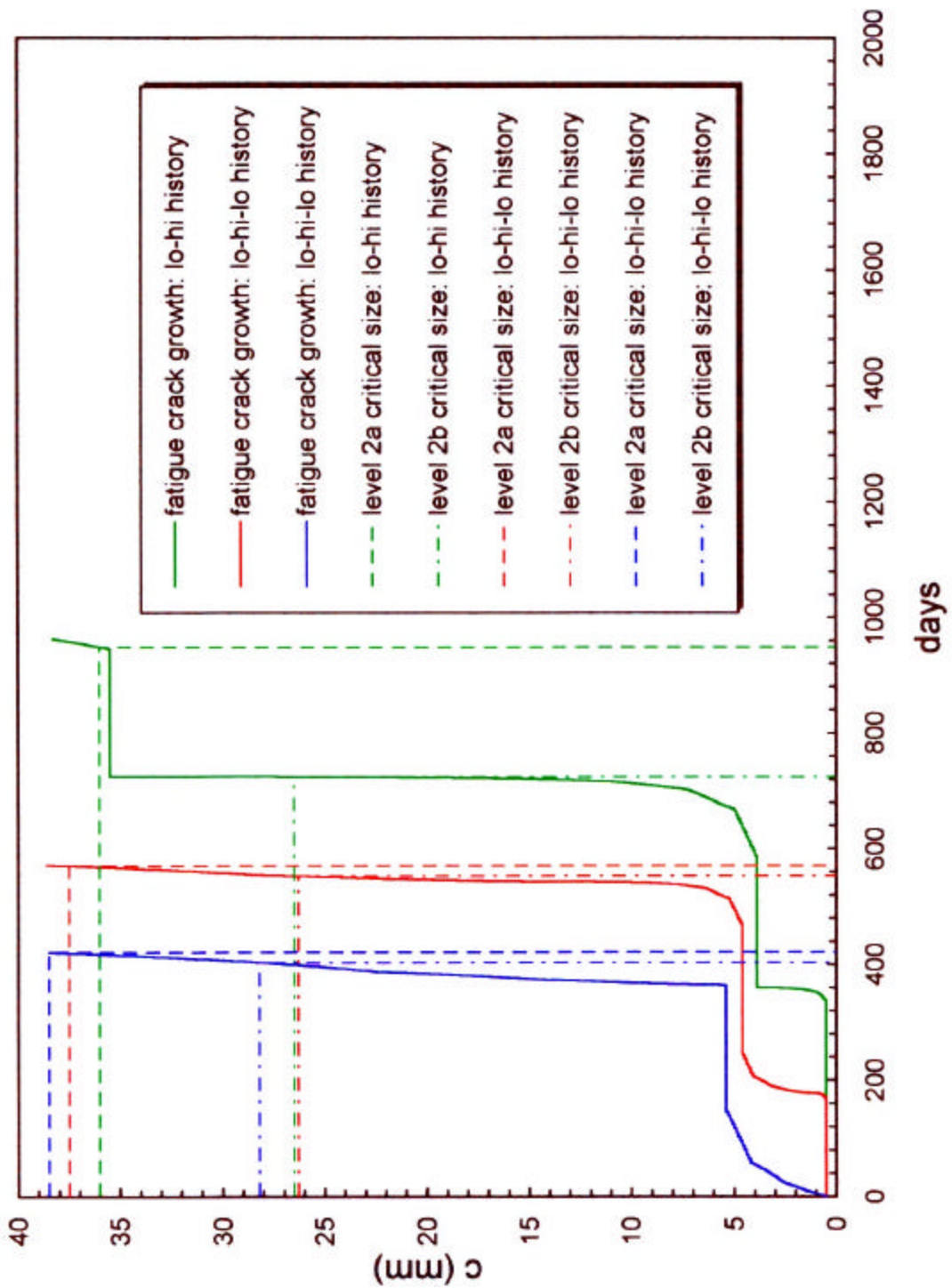
Figure D.5.4: Level 2 Prediction of Flange Crack Length at Mid-Span of Side Shell Longitudinal No. 8 (Example 1) Versus Number of Days of Operation
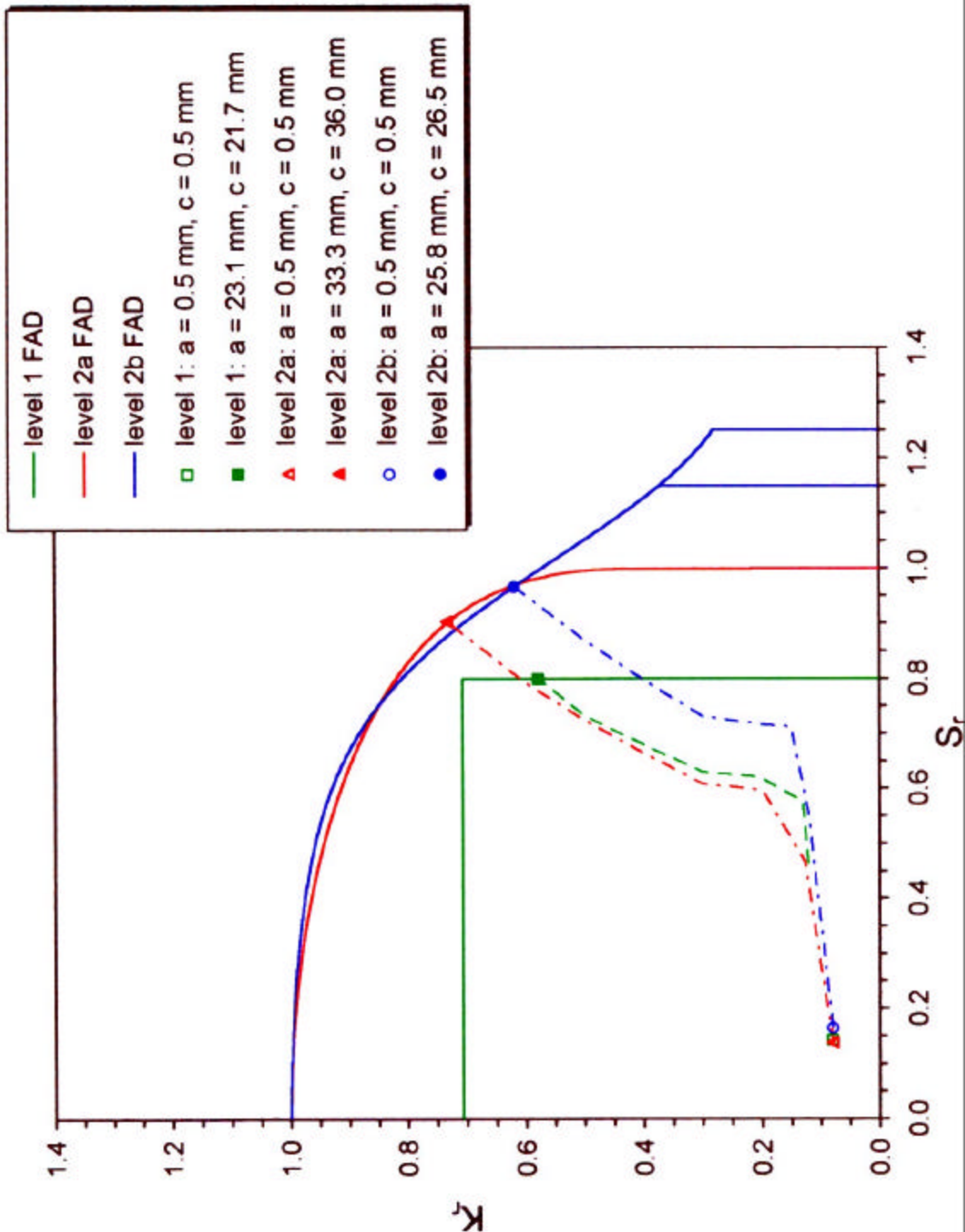
Figure D.5.5: Failure Assessment Diagrams for Damage Site at Mid-Span of Side Shell Longitudinal No. 8 (Example 1) where Fatigue Crack Growth has been Predicted with a Lo-Hi Stress History
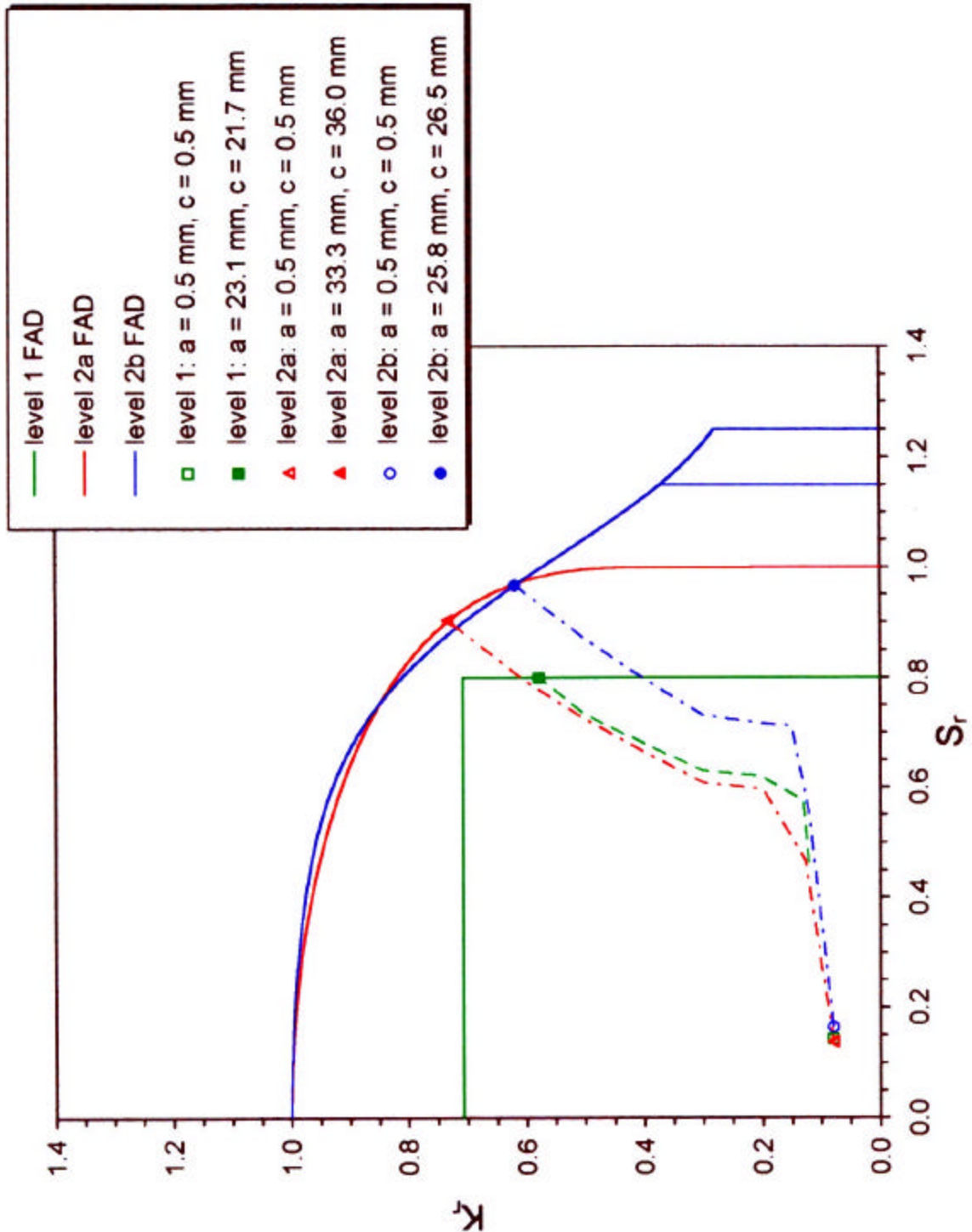
Figure D.5.6: Failure Assessment Diagrams for Damage Site at the Toe of the Flat Bracket at the Frame 37 End of Side Shell Longitudinal No. 8 (Example 2), where Fatigue Crack Growth has been Predicted with a Lo-Hi Stress History

D.5.2 Interpretation of Results

The probability that the stress ranges in Tables D.3.4 and D.3.5 naturally occur in order of increasing magnitude or decreasing magnitude is extremely rare (orders of magnitude less than 10^{-8}). In view of this rarity and the conservatism of the input material properties for fatigue crack growth analysis and residual strength assessment, it is highly unlikely that a critical crack will develop before the residual life predicted by the combination of a Level 1 FAD, Level 1 fatigue analysis, and a hi-lo stress sequence (about 6 years for the mid-span site, just over 1 year for the flat bracket). It is very likely that a critical crack will develop before the residual life predicted by the combination of a Level 2a FAD, Level 2 fatigue analysis, and lo-hi stress sequence (7.5 years for the mid-span site, 1, 2.5 years for the bracket end). The next scheduled survey is in four years. Therefore, the crack detected at the mid-span of side shell longitudinal No. 8 need not be repaired until that time provided the area is subjected to special inspections in the interim. On the other hand, the undercut at the toe of the flat bracket should be repaired before the new ship is delivered by the fabricator.

D.6   REFERENCES

[D.1]   Ghose, D.J., Nappi, N.S., and Wiernicki, C.J., "Residual Strength of Damaged Marine Structures", SSC Report 381, Ship Structure Committee, 1995.

[D.2]   "Guide for the Fatigue Strength Assessment of Tankers", American Bureau of Shipping, 1992.

[D.3]   Matoba, M. and Inoue, K., "Some Stress Intensity Factors for Hull Members in Relation to Fatigue Crack Propagation", IIW-XIII-1081-83.

APPENDIX A

NOTCH STRESS CONCENTRATION FACTORS

This appendix provides guidance on the estimation of notch stress concentration factors (K_W) for welded details. The notch stress concentration factor is that part of the stress concentration due to the geometry of the weld itself. Notch stress concentration factors are required to determine the peak stress at the toe of the weld where cracks tend to initiate. With reference to **Figure A.1**, the notch SCF is defined as:

$$K_W = \sigma_{notch} / \sigma_g$$

The notch SCF may be determined from local fine mesh FEA, or using parametric formulae.
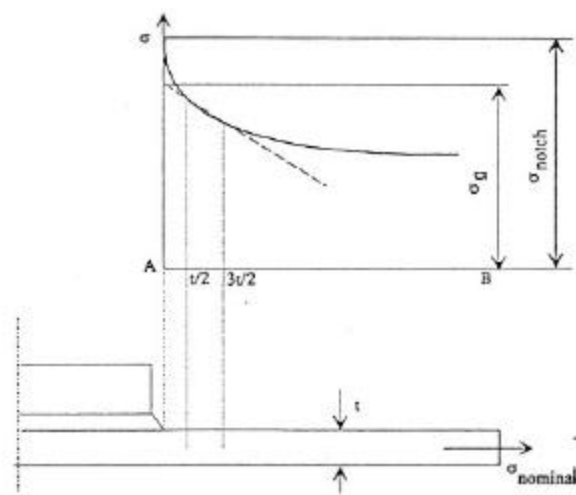
Figure A.1: Definition of Notch Stress Concentration Factor

The main parameters affecting K_W are the weld toe radius (ρ), weld toe angle (θ), plate thickness (**t**):.

$$K_w = 1 + 0.5121 \cdot \theta^{0.572} \, (t/\rho \,)^{0.469}$$

where the angle θ is measured in radians and parameters are as defined in **Figure A.2**.
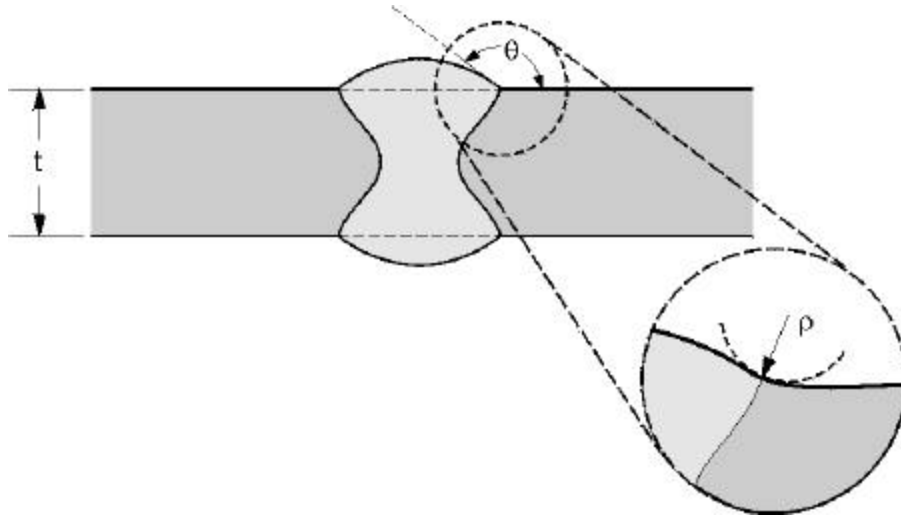
Figure A.2: Weld Toe Geometry

An alternative simpler relationship, independant of the weld toe angle follows:

$$K_w = 1 + \{1 + 0.019 \, (t/\rho \,)\}^{0.5}$$

Reference B.2 recommends a value of $\mathbf{K_w} = 1.5$ for ship structural details, unless stated otherwise in their SCF solutions for welded joints applicable to ship structural details (see Appendix B). However, this value is very low in comparison to the notch SCF values determined from the above equations.

APPENDIX B

STRESS CONCENTRATION FACTORS
FOR SHIP STRUCTURAL DETAILS

This appendix provides guidance on the estimation of stress concentration factors (K_g, K_{te}, K_{ta}) for ship structural details where: K_g is a stress concentration factor due to the gross geometry of the detail, K_{te} is an additional stress concentration factor due to eccentricity tolerance (normally used for plate connections only), and K_{ta} is an additional stress concentration factor due to angular mismatch (normally used for plate connections only).

These stress concentration factors account for the local geometry of the detail, excluding the weld (K_w - see Appendix A). They do not account for the global stress concentration effects of the structure surrounding the detail to be analyzed (K_G). The latter should be determined by global FEA or additional published solutions. The total stress concentration factor for the location, used to determine the peak stress in the load carrying section containing the flaw, is thus defined as follows:

$$K_o = K_G \cdot K_w \cdot K_g \cdot K_{te} \cdot K_{t\alpha}$$

The following SCF solutions have been adapted from Cramer et al. (1995). Alternate solutions may be found in Classification Society documents for fatigue analysis, and previous ship structure committee reports.

Table B.1: SCF For Flange Connections
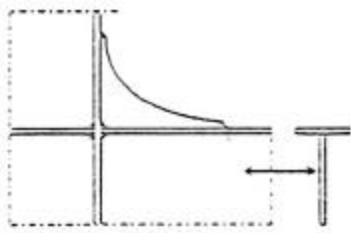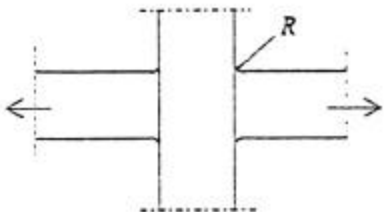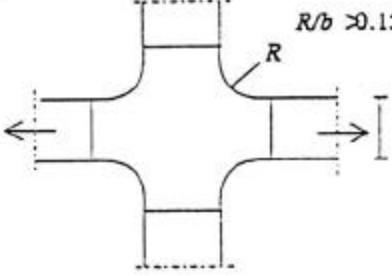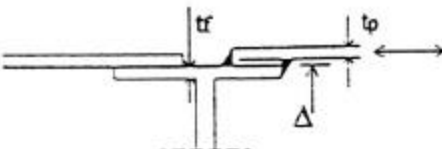
Geometry	K-factor
B.1.a Flange connection with softening toe	$K_t \cdot K_w = 2.2$
B.1.b Crossing of flanges	$K_t \cdot K_w = 2.2$ $R \geq 0.1t$ t = thickness of flange
B.1.c $R/b > 0.15$	$K_t \cdot K_w = 1.9$
B.1.d Overlap connection	$K_t = \left(4\dfrac{t_p}{t_f} + 3\left(\dfrac{t_p}{t_f}\right)^2 + 6\dfrac{\Delta t_p}{t_f^2} \right)$ $\Delta = gap = tolerance$ Default: $\Delta = 1.0\ mm$ $K_w = 1.5$

Table B.2: SCF For Stiffener Supports
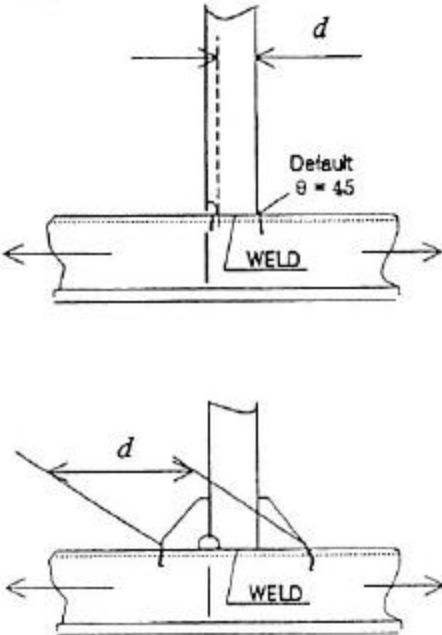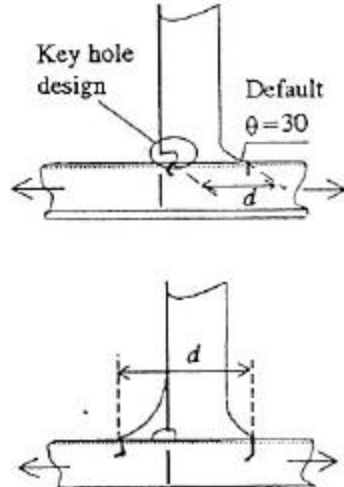
Geometry	K-factor
B.2.a	For supporting members welded to stiffener flange: $\quad K_g \cdot K_w = 1.8 \qquad\qquad d \leq 50$ $\quad K_g \cdot K_w = 1.9 \qquad 50 < d \leq 100$ $\quad K_g \cdot K_w = 2.0 \qquad 100 < d \leq 150$ $\quad K_g \cdot K_w = 2.2 \qquad\qquad d > 150$ For supporting members welded to stiffener web by overlap with weld throat thickness as given in B.5a (Table B.5), the above factors are to be multiplied by a factor 1.15 **Note:** The weld connection area between supporting members and stiffener flange must fulfil the requirements in Rules.
B.2.b	$\quad K_g \cdot K_w = 1.6 \qquad\qquad d \leq 50$ $\quad K_g \cdot K_w = 1.7 \qquad 50 < d \leq 100$ $\quad K_g \cdot K_w = 1.8 \qquad 100 < d \leq 150$ $\quad K_g \cdot K_w = 2.0 \qquad\qquad d > 150$ For supporting member welded to stiffener, flange only. It is assumed that the weld is kept clear of flange edge. **Note:** The weld connection area between supporting members and stiffener flange must fulfil the requirements in Rules

Table B.3: SCF For Termination of Stiffeners on Plates
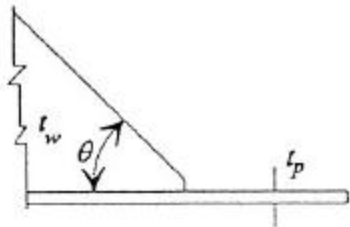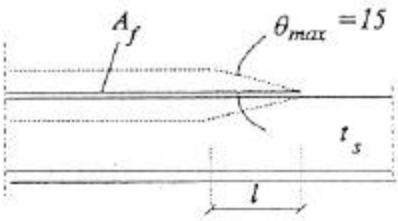
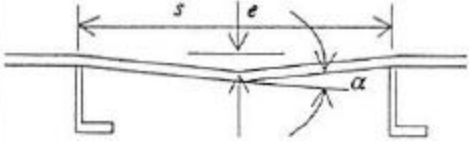| Geometry	K-factor
B.3.a Local elements and stiffeners welded to plates 	$$K_g \cdot K_w = 2\left(1 + \frac{t_w \theta}{t_p 160}\right)$$ θ = angle in degrees of sloping termination
B.3.b Sniping of top flanges: 	$$K_g \cdot K_w = \frac{3A_f}{lt_s}$$ and $K_g \cdot K_w = \min 3.0$

Table B.4: SCF For Butt Welds

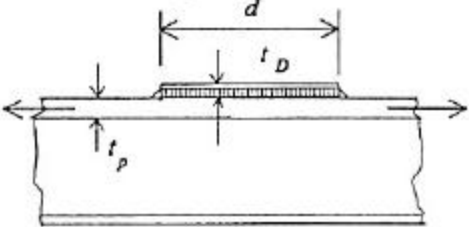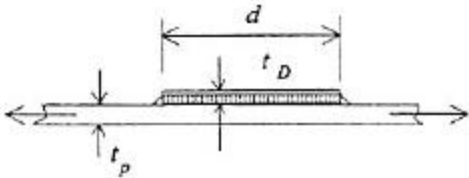| Geometry	K-factor
B.4.a *(diagram of angular mismatch between flat plates with butt weld and stiffener, showing dimensions s, e, and angle α)* Default: $e = 6$ mm	Angular mismatch in joints between flat plates results in additional stresses at the butt weld and the stiffener $$K_{t\alpha} = 1 + \frac{\lambda}{4}\alpha\frac{s}{t}$$ where: $\lambda = 6$ for pinned ends $\lambda = 3$ for fixed ends $\alpha =$ angular mismatch in radians $s =$ plate width $t =$ plate thickness
B.4.b Welding from both sides *(diagram of butt weld with angle θ, eccentricity e, and thickness t)* Default: $e = 0.15\, t$	$$K_g = 1.0$$ $$K_w = 1.0 + 0.5(\tan\theta)^{1/4}$$ Default value $K_w = 1.5$ for $\theta = 45$ deg. $K_{t\alpha}$ from 7.4.a $$K_{te} = 1 + \frac{3e}{t}$$

B.4.c
Plate not restricted in out-of-plane movement

$e = 0.15\ t_1.$

$\Delta t = t_2 - t_1$

$$K_s = 1 + \frac{3\dfrac{\Delta t}{t_1}}{1 + \left(1 + \dfrac{\Delta t}{t_1}\right)^3}$$

$$K_w = 1.4\left(1 + \frac{\Delta t + e}{2a}\right)$$

$$K_{te} = 1 + \frac{6\dfrac{e}{t}}{1 + \left(1 + \dfrac{\Delta t}{t_1}\right)^3}$$

K_{ta} from **B**.4.a

B.4.d
Plate restricted in out-of-plane movement (e.g. flanges)

Default: $e = 0.15\ t_1$

$\Delta t = t_2 - t_1$

$K_s = 1.0$

$$K_w = 1.4\left(1 + \frac{\Delta t + e}{2a}\right)$$

$K_{te} = 1.0$

$K_{ta} = 1.0$

B.4.e
Welding from one side

Default: $e = 0.15\ t.$

Welding from one side is not recommended in areas prone to fatigue due to sensitivity of workmanship and fabrication

$K_s = 1.0$

Default value: $K_w = 2.2$

$$K_{te} = 1 + \frac{3e}{t}$$

K_{ta} from **B**.4.a

Table B.5: SCF For Doubling Plates

Geometry	K-factor
B.5.a Cover plates on beams 	Welded at its end with throat thickness a For $a \geq \dfrac{t_p \cdot t_D}{t_p + t_D}$ $K_s \cdot K_w = 1.8 \qquad d \leq 50$ $K_s \cdot K_w = 1.9 \qquad 50 < d \leq 100$ $K_s \cdot K_w = 2.0 \qquad 100 < d \leq 150$ $K_s \cdot K_w = 2.2 \qquad d > 150$
B.5.b Doubling plates welded to plates 	For $a \geq \dfrac{t_p \cdot t_D}{t_p + t_D}$ $K_s \cdot K_w = 1.8 \qquad d \leq 50$ $K_s \cdot K_w = 1.9 \qquad 50 < d \leq 100$ $K_s \cdot K_w = 2.0 \qquad 100 < d \leq 150$ For $l > 150$: $K_s \cdot K_w = 2.5\left(1 + \dfrac{t_D}{2 t_p}\right)$ if a more detailed analysis is not performed.

Note: If the welds of the doubling plates are placed closer to the member (flange, plate) edges than 10 mm, the K-factors in Table B.5 should be increased by a factor 1.3.

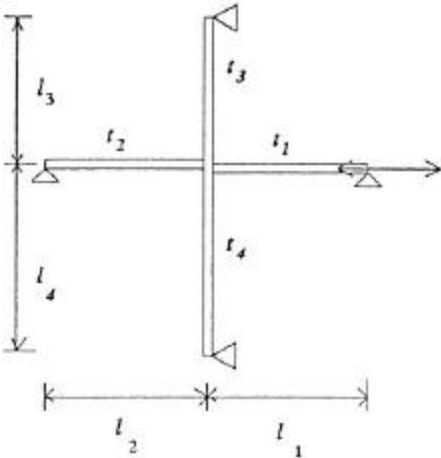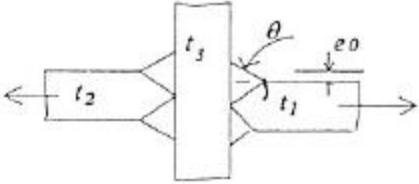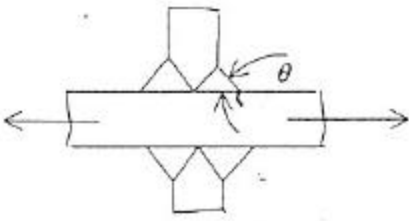# Table B.6: SCF For Cruciform Joints

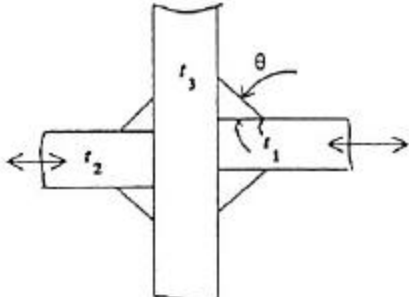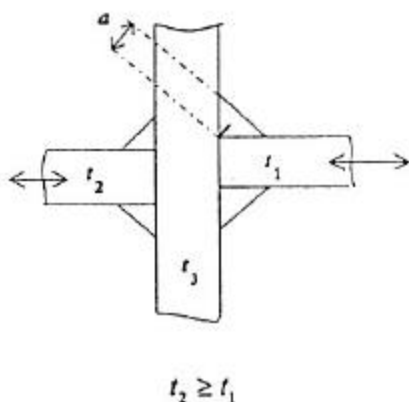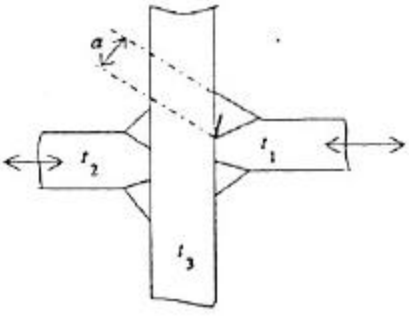| Geometry	K-factor
B.6.a	$$K_{te} = 1 + \frac{6 t^2 \cdot e}{l_1 \left(\dfrac{t_1^3}{l_1} + \dfrac{t_2^3}{l_2} + \dfrac{t_3^3}{l_3} + \dfrac{t_3^3}{l_4} \right)}$$
B.6.b $$e = \frac{t_1}{2} + e_0 - \frac{t_2}{2}$$ $t_1 \le t_2$ $e_0 \le 0.3 t_1$	$K_g = 1.0$ $K_w = 0.90 + 0.90 (\tan \theta)^{1/4}$ Default value: $K_w = 1.8$ K_{te} from **B**.6.a $K_{ta} = 1.0$
B.6.c Applicable also for fillet welds	$K_g = 1.0$ $K_w = 0.90 + 0.90 (\tan \theta)^{1/4}$ Default value: $K_w = 1.8$ $K_{te} = 1.0$ $K_{ta} = 1.0$

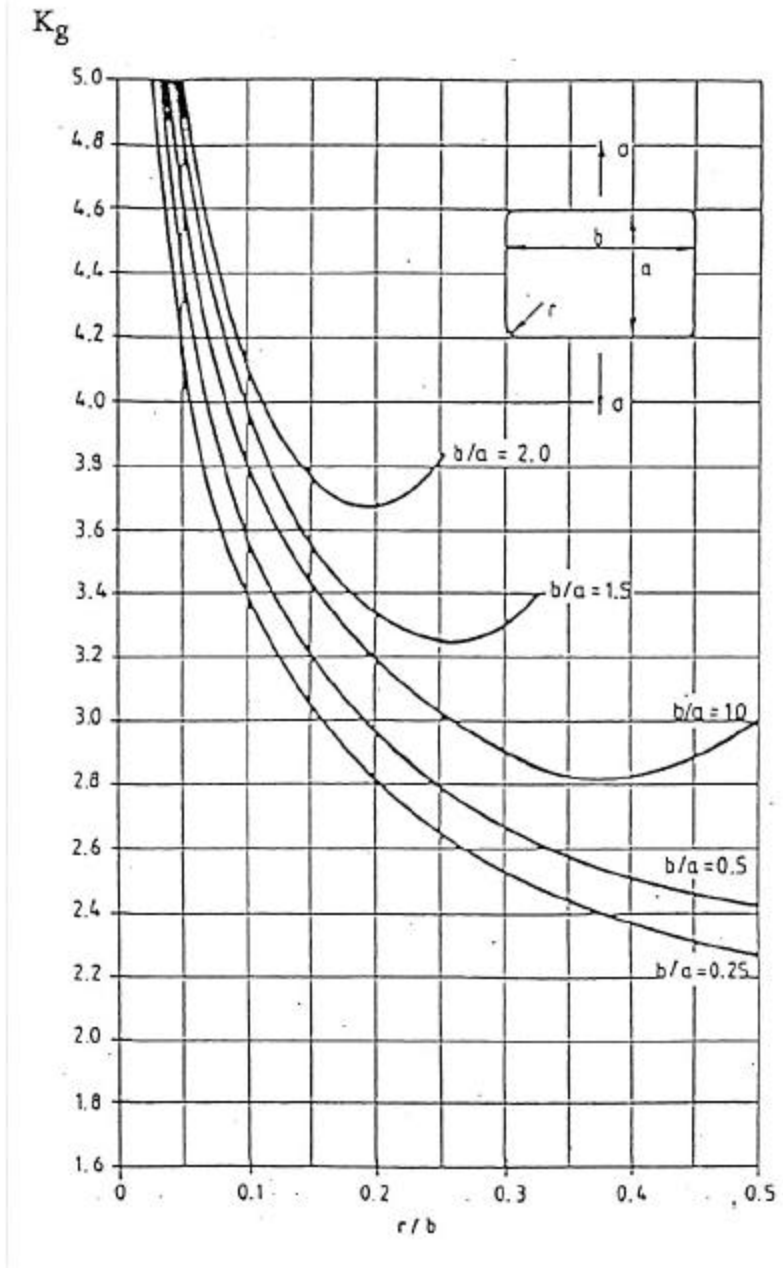# Table B.6: SCF for Cruciform Joints (Continued)

B.6.d	
	$K_{s} \cdot K_{w} = 1.2 + 1.3(\tan \theta)^{1/4}$ Default value : $K_{s} \cdot K_{w} = 2.5$ K_{te} from B.6.a with e as given in B.6. b $K_{ta} = 1.0$
B.6.e	
   $t_2 \geq t_1$	Based on nominal stress in member with thickness t_1 $K_{s} \cdot K_{w} = 1.2 \dfrac{t_1}{a}$ K_{te} from B.6.a with e as given in B.6. b $K_{ta} = 1.0$
B.6.f	
	$K_{s} \cdot K_{w} = 1.2 \dfrac{t_1}{a}$ K_{te} from B.6.a with e as given in B.6.b $K_{ta} = 1.0$

Table B.7: SCF for Cut Outs

APPENDIX C

STRESS INTENSITY FACTORS FOR SHIP STRUCTURAL DETAILS

Stress intensity factor solutions for general crack geometries and stress fields are included in compendia and handbooks by Murikami (1987), Tada et. al (1984), Rooke and Cartwright (1976), Sih (1973), and PD6493:1991. When using such compendia, the SIF solution is obtained either from a simple graphical representation or by evaluating a simple polynomial or analytic expression with given coefficients. The analyst should be careful when using such solutions to ensure that the selected mode adequately represents the geometry and boundary conditions of the actual problem.

The following subsections summarize a few published SIF solutions that are relevant to ship structure fracture mechanics problems.

C.1   Semi-Elliptical Surface Cracks in A Plate

Newman and Raju (1984) developed empirical solutions for Y_m and Y_b derived from a systematic curve-fitting procedure based on their three-dimensional finite element work. The functions Y_m and Y_b correspond to the basic SIF solutions for a semi-elliptical surface crack in a plane plate. Their formulae are generally accepted to be the most comprehensive and are also used in PD6493 (1991). They are as follows:

$$Y_m = 1/\phi \cdot \{M_1 + M_2 \cdot (a/t_s)^2 + M_3 \cdot (a/t_s)^4\} \cdot g \cdot f_\phi \cdot f_W$$
$$Y_b = H \cdot Y_m$$

At the deepest point on the crack front, $\phi = \pi/2$

$$g = f_\phi = 1$$
$$H = H_1$$

At the ends of the crack, $\phi = 0$

$$g = 1.1 + 0.35 \cdot (a/t_s)^2$$
$$f_\phi = (a/c)^{0.5}$$
$$H = H_2$$
$$H_2 = 1 + G_1 \cdot (a/t_s) + G_2 \cdot (a/t_s)^2$$

If $W \geq 20c$, it can be assumed that $c/W = 0$, so that $f_W = 1$. Otherwise use

$$f_W = \{ \sec[(\pi \cdot c/W) \cdot (a/t_s)^{0.5}] \}^{0.5}$$

For Cracks With Aspect Ratios a/2c ≤ 0.5

$\phi = \{1.0 + 1.464(a/c)^{1.65}\}^{0.5}$

$M_1 = 1.13 - 0.09(a/c)$

$M_2 = 0.89 / \{0.2 + (a/c)\} - 0.54$

$M_3 = 0.5 - 1 / \{0.65 + (a/c)\} + 14 \cdot \{1 - (a/c)\}^{24}$

$H_1 = 1 - 0.34(a/t_s) - 0.11 \cdot (a/c) \cdot (a/t_s)$

$G_1 = -1.22 - 0.12(a/c)$

$G_2 = 0.55 - 1.05(a/c)^{0.75} + 0.14 \cdot (a/c)^{1.5}$

For Cracks With Aspect Ratios 0.5 ≤ a/2c ≤ 1.0

$\phi = \{1.0 + 1.464(c/a)^{1.65}\}^{0.5}$

$M_1 = \{1 + 0.04(c/a)\} \cdot (c/a)^{1.65}$

$M_2 = 0.20(c/a)^4$

$M_3 = -0.11(c/a)^4$

$H_1 = 1 - \{0.04 + 0.41(c/a)\} \cdot (a/t_s) + \{0.55 - 1.93(c/a)^{0.75} + 1.38(c/a)^{1.5}\} \cdot (a/t_s)^2$

$G_1 = -2.11 + 0.77(c/a)$
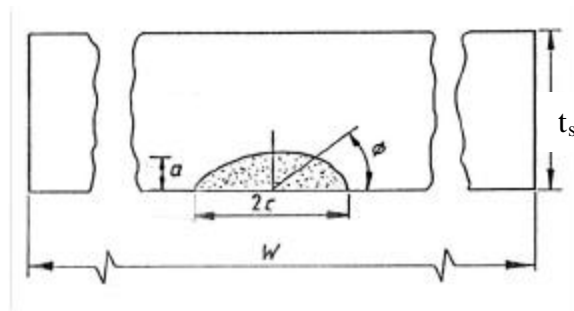
$G_2 = 0.55 - 0.72(c/a)^{0.75} + 0.14(c/a)^{1.5}$

Figure C.1: Semi-Elliptical Surface Crack

C.2   Weld Toe Crack at Transverse Non-Load Carrying Attachment

Parametric formulae for stress intensity factors for 2-D cracks at the toe of a transverse, non-load carrying attachment were developed by Hobbacher (1993) using weight function techniques. The geometry of the problem is shown in **Figure C.2**. Hobbacher states that the effect of the thickness ratio of the two plates is less than 5% for $t_w/t_s < 2$. The same applies for the weld throat **A**. The only significant variable apart from the crack depth is the transition angle, **q**, at the weld toe which is related to the weld dimensions **h** and **w**. The solutions were derived for membrane loading, but it is conservative to apply it for bending.

$$M_k = \alpha(a/t_s)^\beta \qquad\qquad \text{and } M_k \geq 1$$

$$\alpha = 0.8068 - 0.1554(h/t_s) + 0.0429(h/t_s)^2 + 0.0794(w/t_s)$$
$$\beta = -0.1993 - 0.1839(h/t_s) + 0.0495(h/t_s)^2 + 0.0815(w/t_s)$$

The above equations are valid for:

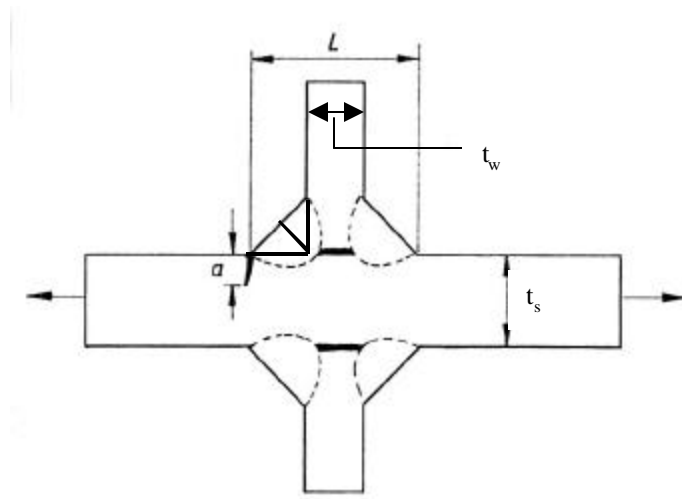|		
$a/t_s \geq 0.0025$	$0.2 \leq h/t_s \leq 1$	$0.2 \leq w/t_s \leq 1$
$15 \leq \theta \leq 60$	$0.175 \leq A/t_s \leq 0.72$	$0.125 \leq b/t_s \leq 2$

Figure C.2: Weld Toe Crack at Transverse Non-Load Carrying Attachment

C.3 Weld Toe Crack at Cruciform Joint with Full Penetration K-Butt Weld

This problem is shown in **Figure C.3** and was also solved by Hobbacher using weight function techniques. The main variables are the crack depth ratio, a/t_s, and the transition angle, **q** , at the weld toe which is related to the weld dimensions **h** and **w**. The solutions were derived for membrane loading, but it is conservative to apply it for bending.

$$M_k = \alpha (a/t_s)^\beta \qquad \text{and } M_k \geq 1$$

$$\alpha = 0.7061 - 0.4091(h/t_s) + 0.1596(h/t_s)^2 + 0.3739(w/t) - 0.1329(w/t_s)^2$$
$$\beta = -0.2434 - 0.3939(h/t_s) + 0.1536(h/t_s)^2 + 0.3004(w/t_s) - 0.0995(w/t_s)^2$$

The above equations are valid for:

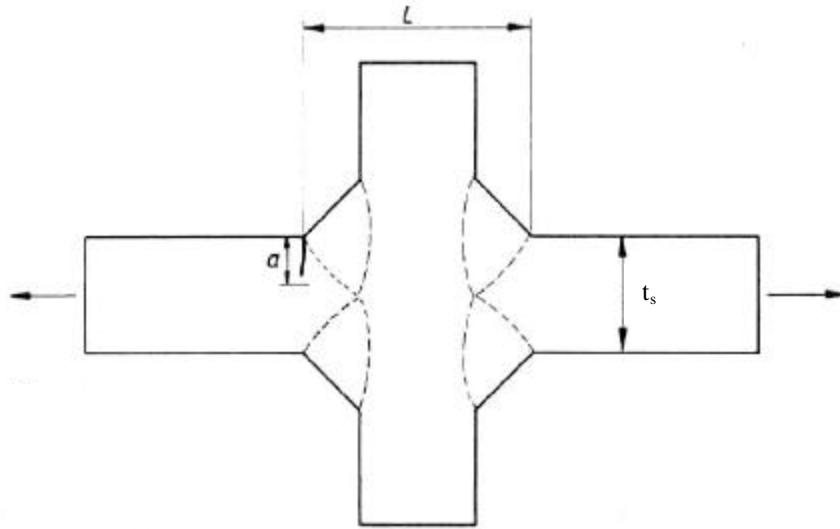|		
$a/t \geq 0.0025$	$0.2 \leq h/t_s \leq 1$	$0.2 \leq w/t_s \leq 1$
$15 \leq \theta \leq 60$	$0.175 \leq A/t_s \leq 1.3$	$0.5 \leq b/t_s \leq 20$

Figure C.3: Weld Toe Crack at Cruciform Joint with Full Penetration K-Butt Weld

C.4 Weld Toe Crack at Cruciform Joint with Partial Penetration Fillet Welds

This problem is shown in **Figure C.4** and was also solved by Hobbacher using weight function techniques. The main variables are the crack depth ratio, a/t_s, the weld throat dimension **A**, and the transition angle, **q**, at the weld toe. Both **A** and **q** can be related to the weld dimensions **h** and **w**. The solutions were derived for membrane loading, but it is conservative to apply it for bending.

$$M_k = \alpha (a/t_s)^\beta \qquad \text{and } M_k \geq 1$$

For $0.2 < h/t_s < 0.5$ and $0.2 < w/t_s < 0.5$ and $0.0025 < a/t_s < 0.07$

$$\alpha = 2.0175 - 0.8056(h/t_s) - 1.2856(w/t_s)$$
$$\beta = -0.3586 - 0.4062(h/t_s) + 0.4654(w/t_s)$$

For $0.2 < h/t_s < 0.5$ and $0.2 < w/t_s < 0.5$ and $a/t_s > 0.07$

$$\alpha = 0.2916 - 0.0620(h/t_s) + 0.6942(w/t_s)$$
$$\beta = -1.1146 - 0.2312(h/t_s) + 1.4319(w/t_s)$$

For $0.5 < h/t_s < 1.5$ or $0.2 < w/t_s < 0.5$

$$\alpha = 0.9055 - 0.4369(h/t_s) + 0.1753(h/t_s)^2 - 0.0665(w/t_s)^2$$
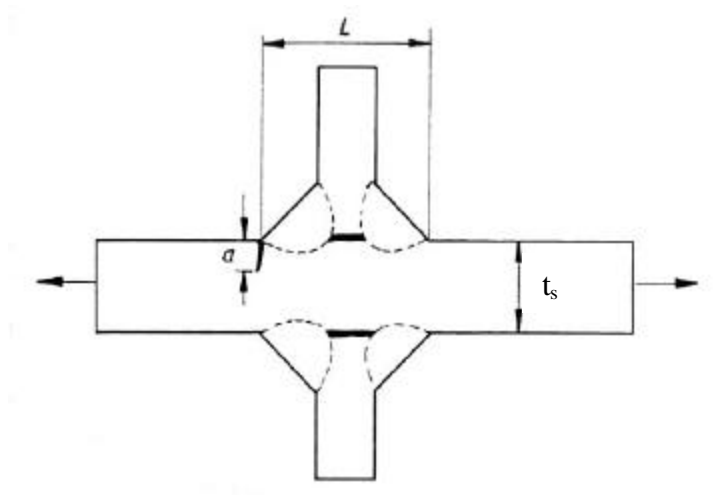$$\beta = -0.2307 - 0.5470(h/t_s) + 0.2167(h/t_s)^2 - 0.2223(w/t_s)$$

Figure C.4: Weld Toe Crack at Cruciform Joint with Partial Penetration Fillet Welds

C.5   Root Crack at Cruciform Joint with Partial Penetration Fillet Welds

The solution for this problem, shown in **Figure C.5**, is given in PD6493 (1991). The solution is derived for membrane loading, but it is conservative to apply it for bending.

$$K_I = \sigma_m \cdot M_k \cdot \{\pi a \cdot \sec(\pi a/W)\}^{0.5}$$

where

$$M_k = \{A_1 + A_2(2a/W)\} / \{1 + (2h/t_s)\} \qquad \text{and} \qquad M_k < 1.0$$

For $0.2 < h/t_s < 1.2$ and $0 < 2a/W < 0.7$

$$A_1 = 0.528 + 3.287(h/t_s) - 4.361(h/t_s)^2 + 3.696(h/t_s)^3 \\ - 1.875(h/t_s)^4 + 0.415(h/t_s)^5$$

$$A_2 = 0.218 + 2.717(h/t_s) - 10.171(h/t_s)^2 + 13.122(h/t_s)^3 \\ - 7.755(h/t_s)^4 + 1.783(h/t_s)^5$$
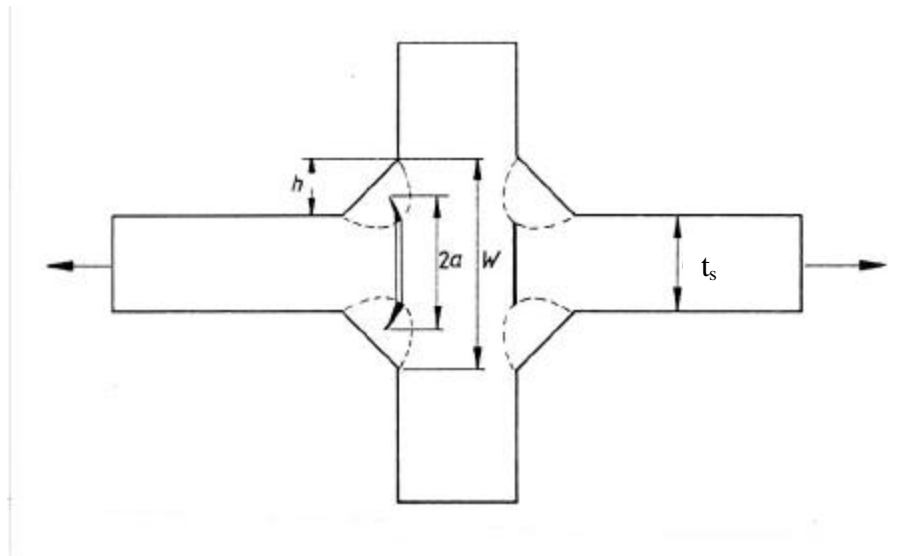
Figure C.5: Root Crack at Cruciform Joint with Partial Penetration Fillet Welds

---

C.6 Lap Joint with Fillet Welds

This problem is shown in **Figure C.6** and was also solved by Hobbacher using weight function techniques. The solutions were derived for membrane loading, but it is conservative to apply it for bending.

$$M_k = \alpha(a/t_s)^\beta \qquad \text{and } M_k \geq 1$$

$\alpha = 1.0210 - 0.3772(h/t_s) + 0.1844(h/t_s)^2 - 0.0187(w/t_s)^2 - 0.1856(u/t_s) + 0.1362(u/t_s)^2$
$\beta = -0.4535 - 0.1121(h/t_s) + 0.3409(h/t_s)^2 - 0.0824(w/t_s)^2 - 0.0877(u/t_s) -0.0417(u/t_s)^2$
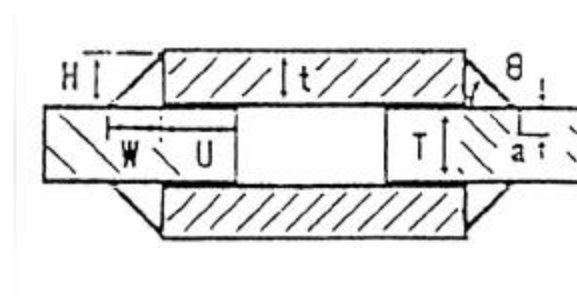
Figure C.6: Lap Joint with Fillet Welds

C.7 Longitudinal Non-Load Carrying Attachments

This problem is shown in **Figure C.7** and was also solved by Hobbacher using weight function techniques. The solutions were derived for membrane loading, but it is conservative to apply it for bending.

$$M_k = \alpha(a/t_s)^\beta \qquad\qquad \text{and } M_k \geq 1$$

$\alpha = 0.9089 - 0.2357(t/t_s) + 0.0249(L/t_s) + 0.0004(L/t_s)^2 + 0.0186(W/t_s) - 1.1414(\theta/t_s)$

$\beta = -0.0229 - 0.0167(t/t_s) + 0.3863(\theta/45°) + 0.1230(\theta/45°)^2$
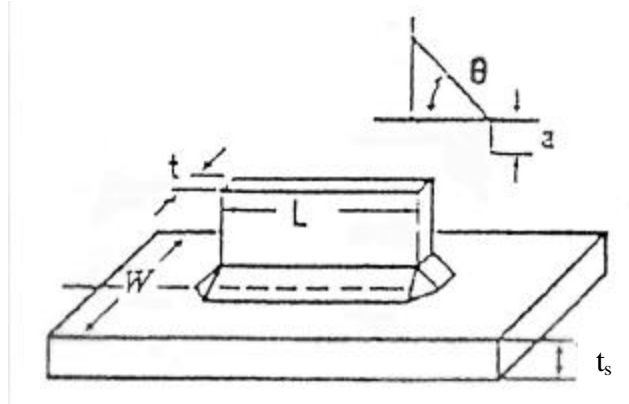
Figure C.7: Longitudinal Non-Load Carrying Attachment

APPENDIX D

FLAW CHARACTERIZATION CRITERIA

(ASME Boiler and Pressure Vessel Code, Section XI)

a

2a

$S \geqslant 0.4a$

$2d_1$

d_2

(whichever is greater)

(whichever is greater)

$S \leqslant 2d_1$ or $2d_2$

$S \leqslant 2d_1$ or $2d_2$

ℓ

Surface flaw #1

Subsurface flaw #2

$2d_2$

ℓ

Liquid metal or cover gas retaining surface

$S \leqslant 2d_2$ or $2d_3$ (whichever is greater)

Unclad surface

$2d_1$

$2d_3$

$S \leqslant 2d_3$ or $2d_2$ (whichever is greater)

d_1

$2d_2$

ℓ

Subsurface flaw #3

$S \geqslant 0.4d_1$

$S \leqslant 2d_1$ or $2d_2$ (whichever is greater)

$2d_3$

$S \geqslant 0.4d_3$

$2a$

$S \geqslant 0.4d_1$

$2d_1$

$2d_2$

$S \geqslant 0.4d_2$

$\ell = 2a$

Subsurface flaw #4

$S \leqslant 2d_1$ or d_2 (whichever is greater)

d, d_1, d_2, d_3
$2d_1, 2d_2, 2d_3$ = depths of individual flaws

$2a$

$S \leqslant 2d_1$ or $2d_2$ (whichever is greater)

$2d_1$

Surface flaw #5

ℓ

$2d_1$

d_2

a

**Figure D.1: Multiple Planar Flaws Oriented in Plane
Normal to Pressure Retaining Surface**

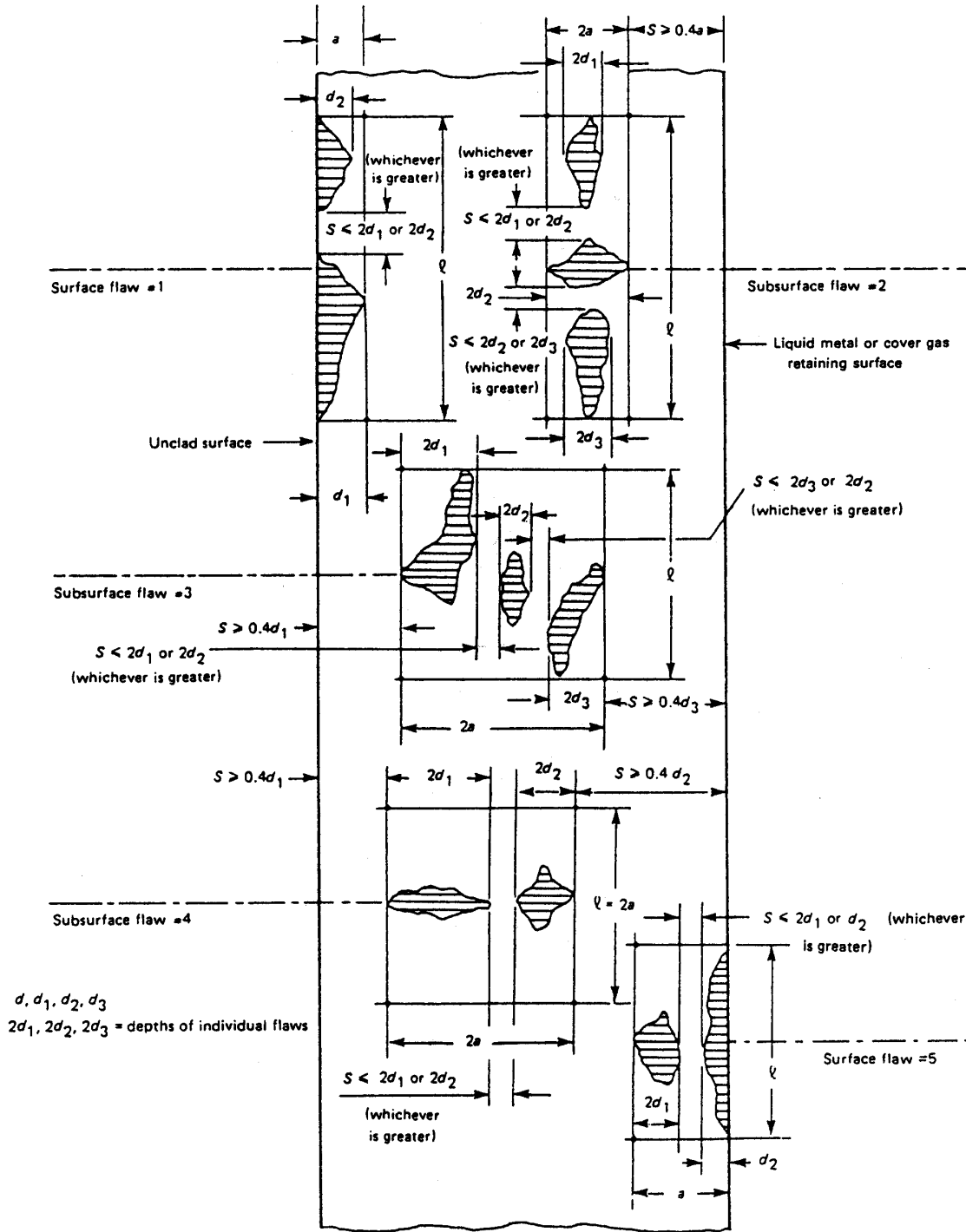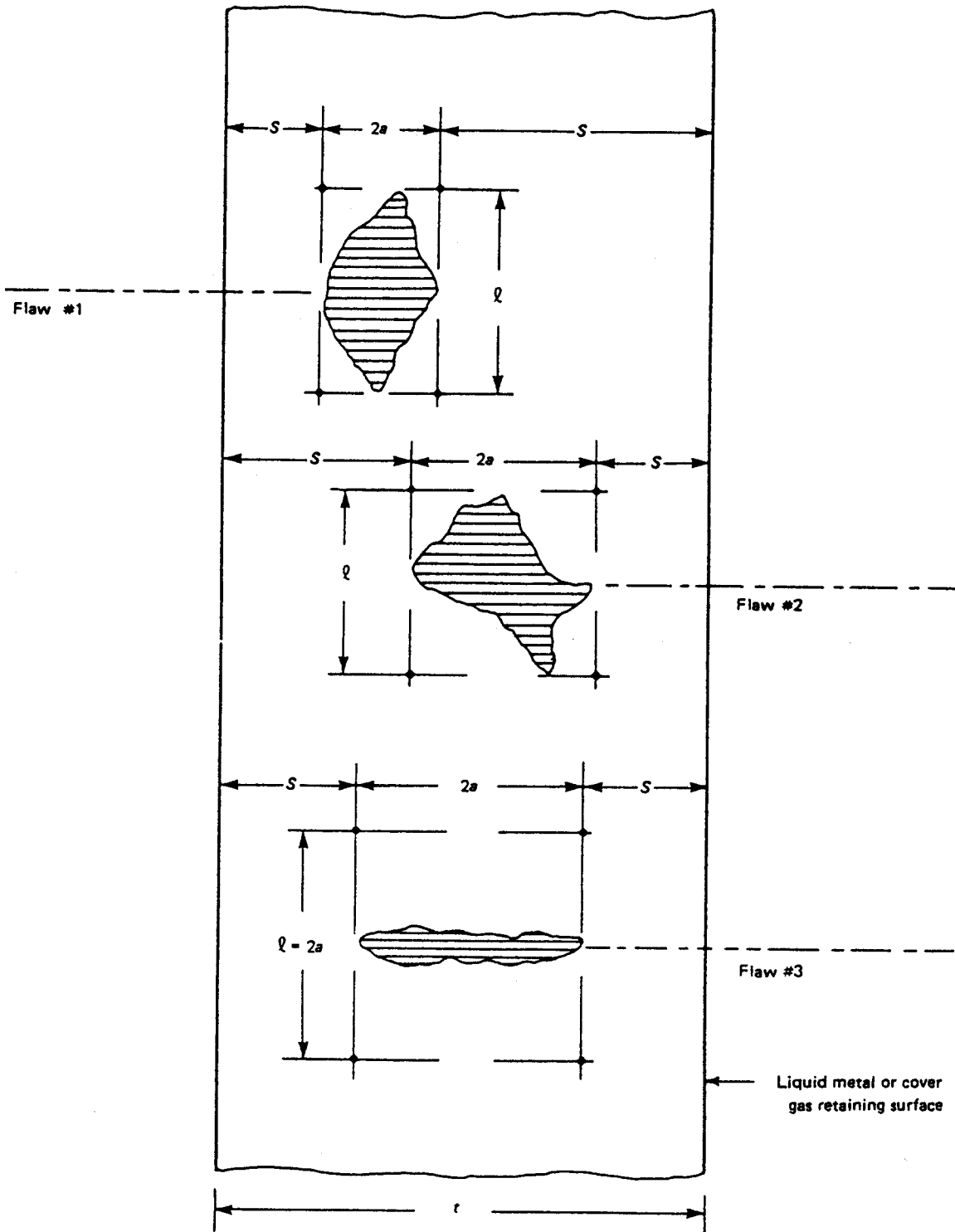**Figure D.2: Subsurface Planar Flaws Oriented in Plane
Normal to Pressure Retaining Surface**
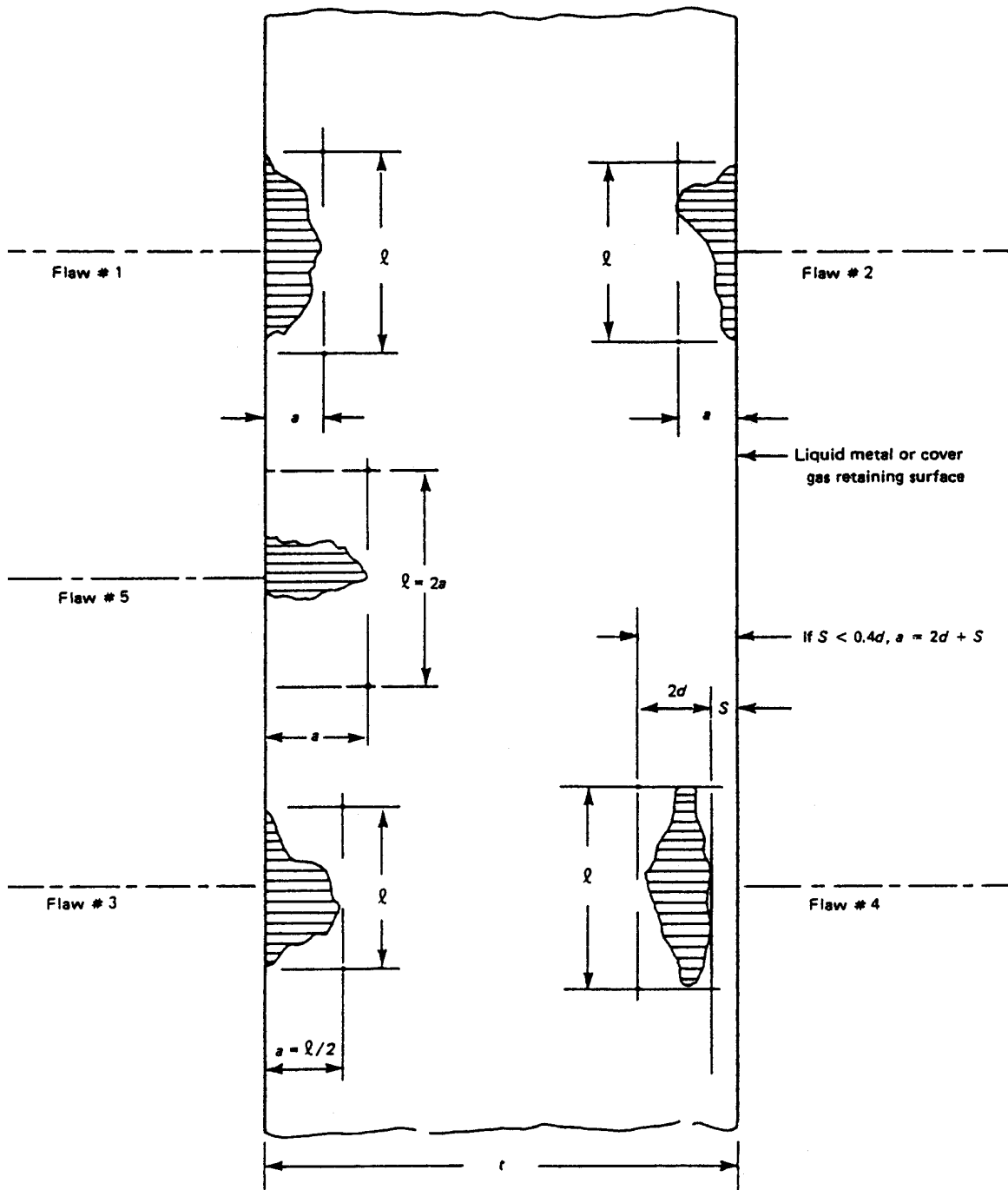
**Figure D.3: Surface Planar Flaws Oriented in Plane
Normal to Pressure Retaining Surface**
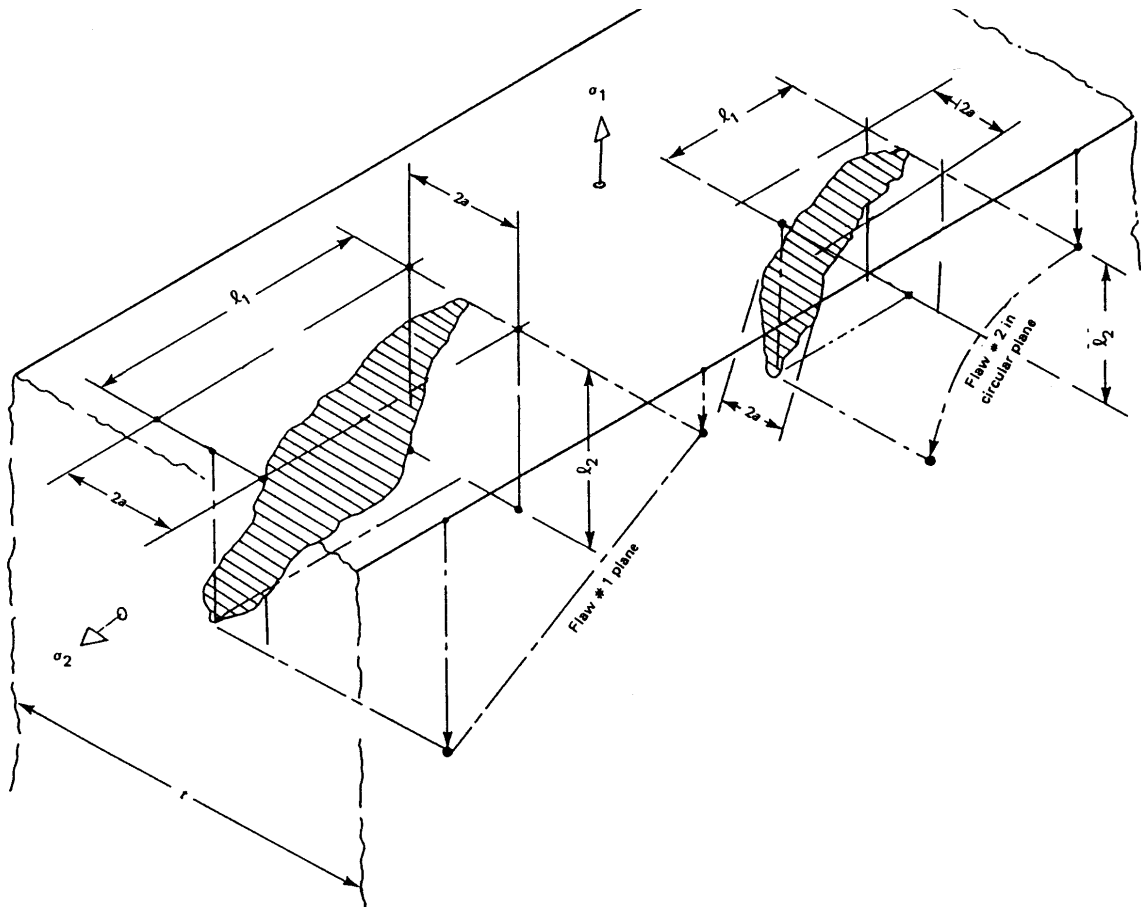
GENERAL NOTE:
Flaw area shall be projected in planes normal
to principal stresses σ_1 and σ_2 to determine critical
orientation for comparison with allowable indication standards.

Figure D.4: Nonplanar Elliptical Subsurface Flaws

Figure D.5: Parallel Planar Flaws

Figure D.6: Laminar Flaws

Figure D.7: Nonaligned Coplanar Flaw in Plane Normal to Pressure Retaining Surface

Figure D.8: Multiple Aligned Planar Indications

APPENDIX E

PROCEDURE FOR LOAD ANALYSIS BY SPECTRAL APPROACH

E.1   Introduction

The elements in the calculation of ship loading due to waves were presented in Section B.2. Three procedures, representing two levels of sophistication, were presented. Level 3 is based on a full spectral method and yields detailed load information for arbitrary ship configurations, w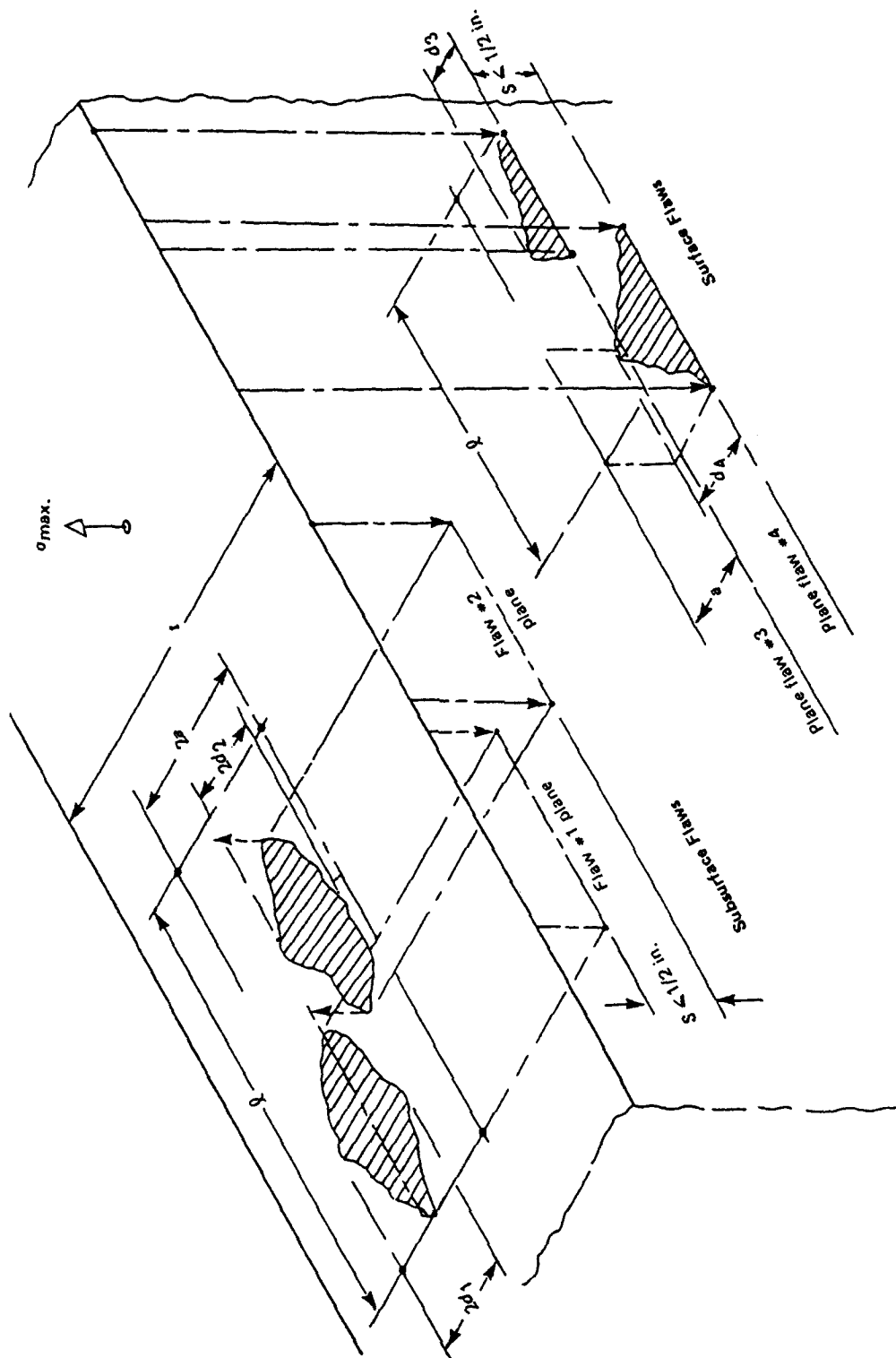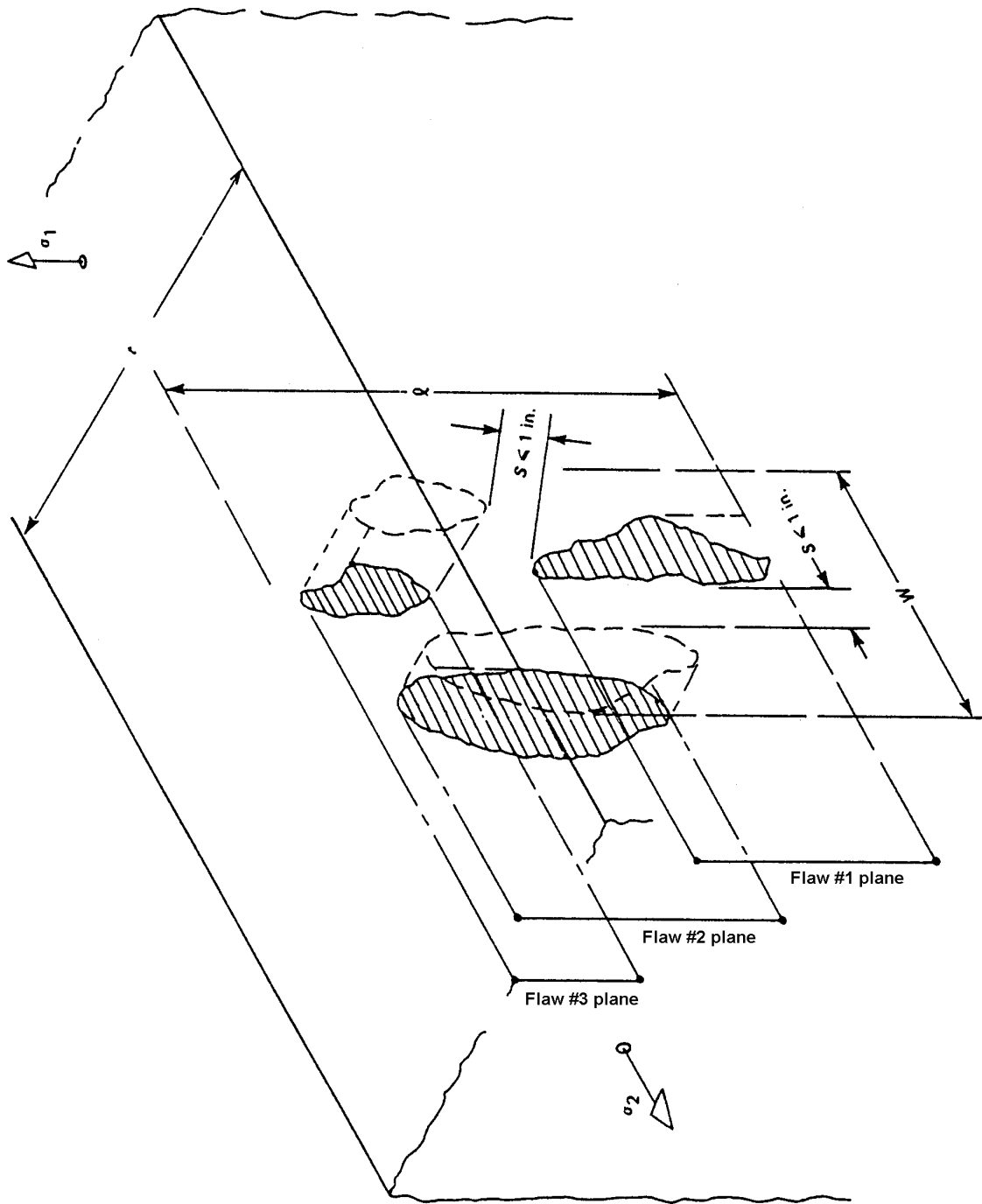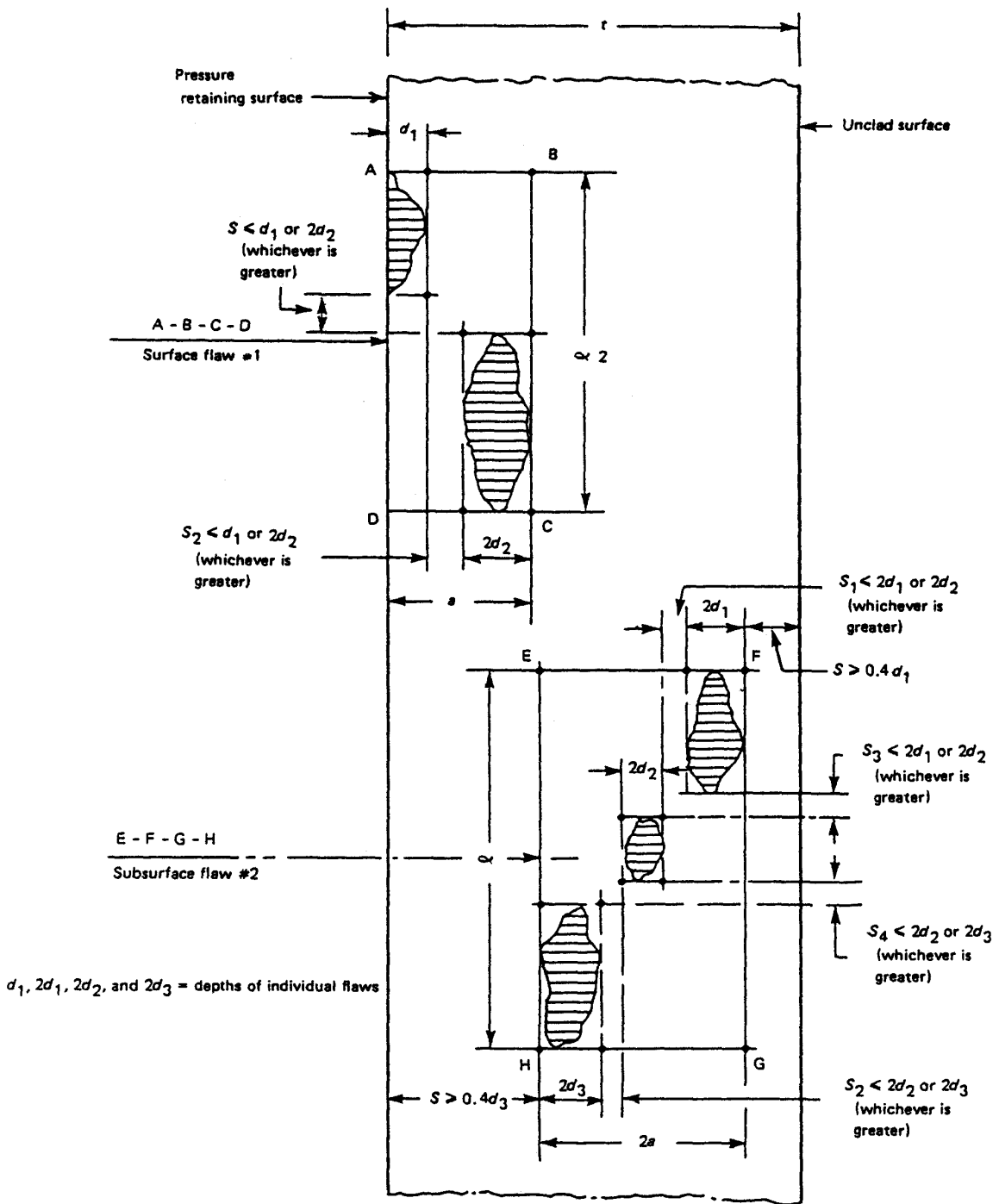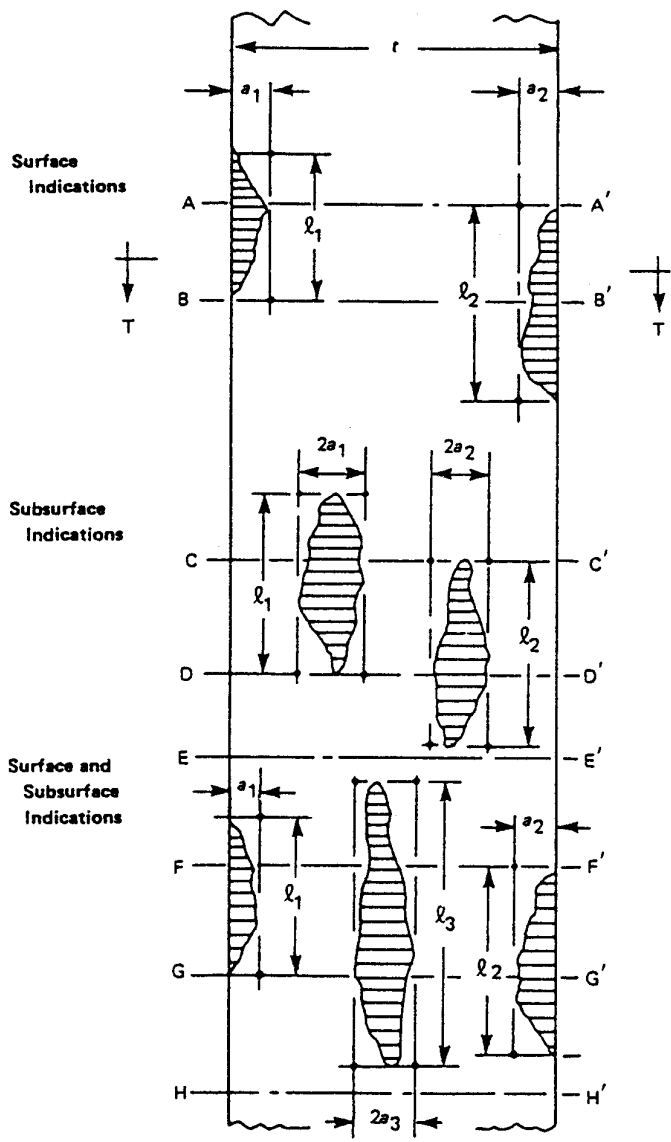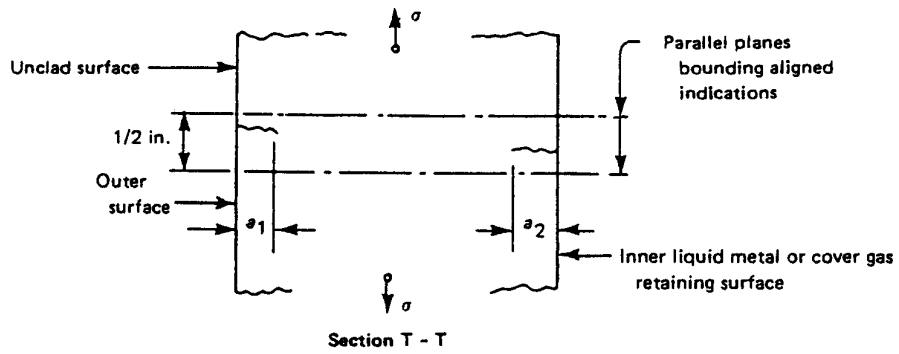ave climates and operational profiles. An alternate method, based on the spectral method but requiring less detailed information on the wave climate, was introduced also (Level 3b). Level 2 methods, of which three are presented, are based on parametric equations. The three methods vary in terms of their comprehensiveness and the effort required to exercise them. The most comprehensive of these methods is based on the DNV approach recommended for fatigue analysis. The DNV methodology is broadly similar to approaches developed by other prominent Classification Societies. The second most refined of the Level 2 methods requires a static wave balance calculation to be performed, the result from which is substituted in parametric equations. The third and final Level 2 method relies entirely on parametric equations where values for a very limited number of basic ship parameters are input. The latter two Level 2 methods are only capable of predicting vertical bending moments.

The Level 1 approach is not covered herein, eing simply "best practice" design and is covered in Reference B.2 (Fatigue Manual).

Clearly, the latter two Level 2 methods are inappropriate for parts of ship structure where the stresses are not dominated by those deriving from overall vertical hull girder bending. In these cases, there is little option but to apply the Level 3 method, as illustrated below.

The steps in the calculation of loading are as follows:

1. Problem definition
2. Operational profile definition
3. Wave climate definition
4. Calculation of RAO's and stress coefficients
5. Computation of response for each combination of H_s and T_z
6. Compilation of stress range spectrum
7. Computation of extreme stress

The purpose of this section is to describe, step-by-step, the calculations to be undertaken in order to compute the stress range spectrum. The steps are presented in the context of the two examples of damage tolerance assessment presented in Part D. In both examples, the platform is an 85,000 ton displacement single skin tanker, and the structural member of interest is a side

shell longitudinal. The computations involved are complicated because a large number of variables need consideration.

The summary provided below identifies the main steps. For detailed discussions of the process the reader is referred to the references given. Particularly relevant are References A.12 and A.18.

The consensus is that linear spectral methods are adequate for fatigue damage calculations, and presumably for crack propagation calculations as well. However, for the calculation of extreme load, non-linear effects may become important. Where they are significant it may be necessary to apply corrections to account for phenomena such as slamming. This consideration also applies to loads induced by rolling which is known to behave non-linearly. The procedure outlined below does not address non-linear effects.

E.2   Problem Definition

The primary tasks under this heading are to define the problem to be analyzed, and gather the required physical ship data.

The following data shall be gathered:

1. Lines plans and/or offset table - to define geometry of hull
2. General arrangement
3. Weights - to define mass distribution of ship
4. Loading arrangements to be considered
5. Scantlings
6. Steel material properties
7. Structural elements selected for study
8. Relevant load types
9. Duration for which assessment is to be performed

Items 1, 2 and 3 are required for the calculation of RAO's. Items 1 through 8 are required for conducting both global and local finite element analyses the purpose of which is to determine stress coefficients. Items 6 through 9 are required for the damage tolerance assessment phase of the work.

The relevant types of loads for the side shell longitudinal analyzed in Part D are:

*   stillwater bending moment
*   vertical hull girder bending moment
*   horizontal hull girder bending moment
*   external hydrodynamic pressure
*   internal tank loads (inertial fluid loads and added static head due to vessel motion)

E.3   Operational Profile Definition

The primary tasks under this heading are to compile operational ship data. This data can be expressed in terms of an operational profile matrix the dimension of which depends on the number of parameters that vary significantly. In general the following data are required:

1. trading patterns
2. loading patterns
3. speed patterns
4. heading angles
5. time at port

The steps in defining the operational profile are as follows:

1. Establish trading patterns by reviewing routes the ship will ply for the duration under consideration. The percentage of time spent in each part of the route (i.e., in each "Marsden" zone as discussed in Part B.2.4) shall be compiled. In the absence of detailed information, the North Atlantic could be assumed.

2. Select loading patterns by considering cargo weight information, including weight, location and centre of gravity, for each weight item and determining likely loading arrangements.

3. Determine speed variations for the vessels. Speed variations are generally not significant for damage tolerance assessment purposes in the case of tankers, bulk carriers, and other large commercial ships.

4. Determine heading angles for the route for each "Marsden" zone that falls on the route.

5. Estimate the proportion of time that the ship will spend alongside. In the absence of detailed information 15% may be assumed for commercial ships such as tankers, bulk carriers and container ships.

6. Compile an operational profile matrix, the dimension of which will depend on the number of parameters that are considered to be variable.

E.4   Wave Climate Definition

The primary tasks under this heading are to compile operational ship data. The following data are required:

1. Select a wave spectrum. In the absence of measured spectra specific to the route of interest, standard spectra as presented in Section F.5 of Appendix F may be used.

2. Select "wave spreading" model to account for short-crestedness.

3. Compile wave scatter diagrams for the route. Using wave scatter diagrams and route and heading data, a composite wave scatter diagram may be compiled.

E.5 Calculation of RAO's and Stress Coefficients

The ultimate objective of this part of the process is to develop stress transfer functions for the structural elements of interest. There are two distinct but related tasks under this heading:

1. Calculation of Response Amplitude Operations (RAO's);
2. Calculation of stress coefficients.

The steps for each calculation are summarized below:

E.5.1 Calculation of RAO's

1. Select a ship motion and ship load program that is capable of computing ship motion and ship load frequency response functions for all relevant components. Programs that employ linear strip theory in the frequency domain are adequate although more advanced programs, which in principle should give better results, are also available.

2. Select the load types relevant to the analysis. These will depend upon the location of structure as discussed under "Problem Definition" above.

3. Select wave headings for which RAO's are to be calculated. This will be based on decisions made in defining the Operational Profile. Generally 45° increments for headings ranging from 0° to 180° is sufficient.

4. Select the range of frequencies for which RAO's are to be calculated. Generally wave frequencies in the range 0.2 to 2 rad/sec in increments of 0.05 rad/sec is sufficient.

5. Select the speed/s for which RAO's are to be calculated. This will be based on decisions made in defining the Operational Profile.

6. Select the ship loading arrangements for which RAO's are to be calculated. This will be based on decisions made in defining the Operational Profile.

7. Use a shipmotion and seaload program to calculate RAO's for the load types identified under "Problem Definition" above. In the cases of local load types (e.g., external hydrodynamic pressure), it is only necessary to calculate the load for the set of wave period and heading angle that produces the maximum value of the corresponding global load type. In general this will vary from load arrangement to load arrangement.

In selecting the "intervals" or "increments" in parameters noted in paras. 3 to 6 (previous) remember that <u>each</u> combination of parameters is a single calculation. Selecting too many increments can lead to many hundreds of calculations which, even with computer programs, can be time-consuming and lead to excessive data generation.

E.5.2   Calculation of Stress Coefficients

In general, stress coefficients should be computed from finite element analyses and this approach is summarized below. Alternative simpler approaches based on hand calculation methods are published by several classification societies.

The steps involved are:

1. Develop global finite element model of the whole ship or part thereof. Exercise the model to determine the stress due to unit sectional load for each load type identified as significant. In general the finite element model shall be designed to allow the following loading effects to be modelled:

    *   vertical hull girder bending including shear lag effects;
    *   vertical shear forces distribution between ship sides and bulkheads;
    *   horizontal bending moment including shear lag effects;
    *   torsion of hull girder (particularly for ships with large openings).

2. As an approximation, it is often possible to restrict calculation, for each load type, to a single wave frequency and a single heading, and apply the same stress to other frequencies and headings.

3. Develop local finite element models for each part of the ship structure of interest. Boundary conditions determined from the global finite element model should be applied.

The reader is referred to Part B.3 for guidance on global and local finite element analysis.

E.6. Computation of Response for Each Combination of Seastate and Heading

The steps to be followed are:

1. For each combination of sea state and heading, compute the following:

$$S_s(?_e) = |H_s(?|?)|^2 S_?(?_e)$$

(equation B.2.4.10)

2. Establish stress range spectrum for each combination of seastate and heading according to: (Equation B.2.4.14)

$$F_{?si}(?s) = 1 - \exp\left(\frac{-?s^2}{8m_{oi}}\right)$$

E.7 Compilation of Stress Range Spectrum

1. The step performed in this section is to combine individual stress range spectra computed in the previous step: (Equation B.2.4.16)

$$F_{?s} = \sum_{i=1}^{\text{all stationary conditions}} r_i F_{?si}(?s) p_i$$

E.8. Computation of Extreme Stress

The following steps are to be followed:

1. Compute probability density function for long-term response: (Equation B.2.4.17)

$$f(s_a) = \frac{\sum_i \sum_j n_* p_i p_j f_*(\sigma)}{\sum_i \sum_j n_* p_i p_j}$$

2. Compute the number of cycles in the period of interest: (Equation B.2.4.19)

$$n = \left(\sum_i \ \sum_j n_* p_i p_j \right) \times T \times (60)^2$$

3. Compute cumulative distribution function incorporating risk parameter: (Equation B.2.4.20)

$$\frac{1}{1 - F\left(\hat{s}\right)} = \frac{n}{a}$$

4. Compute extreme stress due to wave load.

5. Add stress due to stillwater bending moment.

APPENDIX F

INPUT DATA FOR WAVE LOADING

F.1 Introduction

The purpose of this Appendix is to provide information on the input data required for the wave load estimation methodologies presented in Part B.2. This refers primarily to the Level 3 methodologies. The Level 2 methodologies, which are based on parametric equations, are self-sufficient.

F.2 Trading Patterns

In cases where trading patterns are not known, generic trading patterns presented in Table F1 may be used.

Table F1: Fatigue Wave Environment Trading Patterns
[from Reference A.17]

SHIP TYPE/TRADE	TRADING PATTERN		AS % OF SERVICE LIFE
	EXPORTING AREA	IMPORTING AREA	
Large crude oil tanker	Persian Gulf	Europe	33
	(Ballast via Suez, fully loaded via Cape)		
	Persian Gulf	Japan	33
	Persian Gulf	US Gulf	33
Bulk carrier (Coal trade)	Australia	Japan	39
	Australia	Europe	11
	USA	Europe	25
	South Africa	Europe	11
	Canada	Japan	14
Bulk Carrier (Ore trade)	Australia	Far East	44
	Australia	Europe	8
	South America	Europe	23
	South America	Japan	18
	Canada	Europe	7
Large bulk carrier	Ore trade		60
	Coal trade		40
Panamax bulk carrier	Ore trade		23
	Coal trade		46

	Grain trade	31

F.3   Load Conditions

In the absence of specific data, the data in Table F2 may be used:

**Table F2: Fraction of Time at Sea in Loaded and Ballasted Condition
Assuming 85% of Time at Sea** [from Reference B.2]

Vessel Type	Tankers		Container Vessels
Loaded Condition	0.45	0.50	0.65
Ballast Conditions	0.40	0.35	0.20

OBO (oil/bulk/ore) carriers are likely to have a considerably smaller proportion of ballasted voyages.

F.4   Operational Parameters

Operational parameters in this context refer to the ship speed and heading relative to the waves, both of which may be controlled by the operator to reduce loading on the hull, for example, slamming loads.   Data from actual ship operational profiles such as was analysed in Reference B.1 (Glen, et al), can be used to determine the acceptable distribution of ship speed and heading for various sea states.

F.5   Wave Spectra

The Level 3 and 3b approaches require a wave height spectral model. Many wave spectra have been developed since the first ones were proposed in the early fifties, however, it is highly desirable to use wave spectra that require the minimum number of input parameters.   If this restriction is applied, the number of possible wave spectra is reduced to about six. A limited selection is presented below.

(a)   Pierson-Moskowitz

$$S_\eta(f) = \frac{8.10g^2}{10^3(2\pi)^4 f^5} \exp\left[-0.74\left(\frac{g}{\overline{U}_{19.5}\, 2\pi f}\right)^4\right]$$

where
g = acceleration due to gravity (m/s^2)
$U_{19.5}$= mean wind speed at a height of 19.5 m (m/s)

(b)   Bretschneider :

$$S_?(f) = \frac{5H_s^2}{16f_m} \frac{1}{\left(\dfrac{f}{f_m}\right)^5} \exp\left[-\frac{5}{4}\left(\frac{f_m}{f}\right)^4\right]$$

where

H_s = significant wave height
f_m = wave modal frequency, the frequency at which the spectrum is maximum

This form has two variables, **H_s** and **f_m**, and is suitable for partially developed wind-generated seas as well as fully developed seas. In the present context, this formulation is most useful for determining loads using the spectral approach because it can be conveniently used with scatter diagrams which are essentially an expression of the joint probability density function of wave height and wave period. For that purpose, the wave modal frequency can be replaced by the average zero-crossing period using the following relationship:

$$f_m = 0.71 / T$$

Two other parameter spectra, very similar in form to the Bretschneider spectrum, have been proposed by the International Ships and Offshore Structures Congress (1964) and the International Towing Tank Conference (1978).

(c)   The spectra discussed to this point are intended for the open ocean. However, measurements suggest that the general form of spectra based on measurements taken in more confined locations are significantly different. Perhaps the most prominent of this class of spectral model is the so-called JONSWAP spectrum which is based on measurements of waves in the North Sea.

$$S_?(f) = \frac{ag^2}{(2p)^4 f^5} \exp\left[-\frac{5}{4}\left(\frac{f_m}{f}\right)^4\right]?^a$$

where **g** is the ratio of the maximum spectral density to that of the corresponding Pierson-Moskowitz spectrum and is typically about 3.3. Hence, the JONSWAP spectrum is much "peakier" than the Pierson-Moskowitz spectrum which is representative of the open ocean.

The other parameters in the JONSWAP spectrum are defined below:

$$a = \exp\left[\frac{-(f - f_m)^2}{2s^2 f_m^2}\right]$$

$$\sigma = \begin{cases} \sigma_a = 0.07 \\ \sigma_a = 0.09 \end{cases} \quad for \quad \begin{array}{l} f \le f_m \\ f > f_m \end{array}$$

F is the fetch, and the wave modal frequency is given by:

$$f_m = 2.84\left(\frac{gF}{U^2}\right)^{-0.33}$$

The parameter **a** is given by:

$$\alpha = 0.066\left(\frac{gF}{U^2}\right)^{-0.22}$$

F.6   Response Amplitude Operators

The "response amplitude operator" (or RAO) is a term used in the naval architectural word to represent what is more generally known as a "transfer function" or "frequency response function". The essential idea is that an input signal, which may contain energy at a range of frequencies, applied to a transfer function will yield an output signal comprising several frequency components each of which will either be amplified or attenuated. An important feature of transfer functions is that they are complex and contain both a real and an imaginary term; this captures the phase relationship between input and response. The importance of this manifests itself when the response is due to multiple inputs.

In terms of ship motion the input signal is usually represented by a spectrum of wave height. The transfer function (or response amplitude operator) will typically express a range of values of a response parameter (e.g. roll amplitude) as a function of frequency for unit wave amplitude. The output signal will be the spectrum of the response parameter. A typical example for relative motion of the forefoot of a frigate is shown in **Figure F.1**.   The effect on response of applying wave spectra with different dominant frequencies is shown in the figure.

In addition to ship motions programs based on strip theory, several programs have been developed using three-dimensional diffraction theory. Several time domain programs have also been developed that account for non-linearities in wave loading. Specialist programs that model slamming and hydro-elastic response have been developed. However, such programs are still the subject of research and are not widely used in industry.
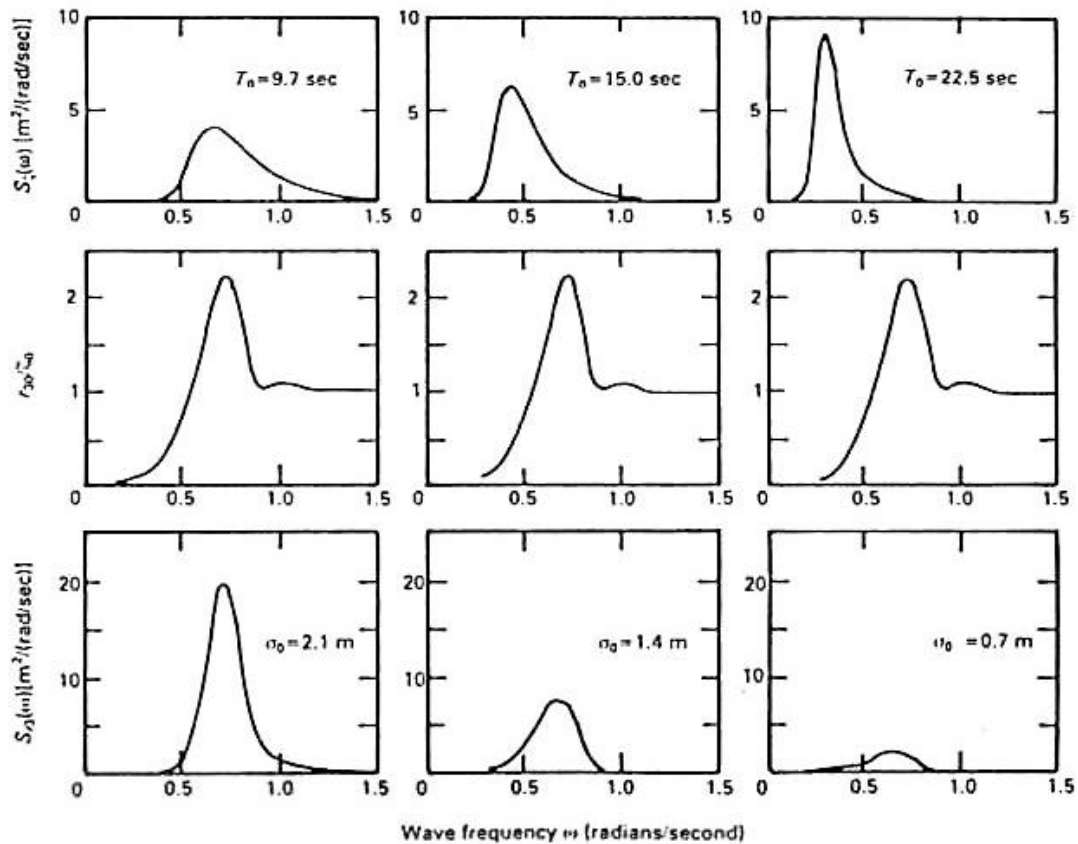

**Figure F.1: Effect on Relative Response of Wave Spectra With
Different Dominant Frequencies (Lloyd, 1989)**

F.7 Stress Coefficients

The stresses caused by the global and local hull girder loads need to be calculated at some point in the damage tolerance assessment process. As with other elements of the calculations there are a number of approaches with varying degrees of complexity and accuracy. The approach employed should, in general, be consistent with complexity and accuracy applied to other elements of the assessment process. The general requirement is to develop stress coefficients that express the field stress at the point of interest for a unit value of the load component (e.g., vertical bending moment). Strictly, the stress coefficients are a function of wave frequency. However, it is acceptable practice to compute stress coefficients for one particular wave frequency, and heading for that matter, and apply it to all wave frequencies and/or headings.

The simple approach is to calculate stresses at the station/s of interest using the computed hull girder bending moments and shear forces and the relevant sectional properties. Estimates of stress can be improved somewhat to account for gross effects such as shear lag, openings in decks and the effect of the superstructure using various rules-of-thumb. This simple approach for computing global stresses is more appropriate for Level 1 FAD methods for damage tolerance assessment.

Stresses at the structural assembly level may be calculated either using hand calculation methods if the structure is fairly regular (e.g., rectangular plates) or can be modelled as a frame. In cases where the structure is irregular and cannot be represented in simple form, the finite element method is the only practical method for determining stresses. Finite element methods offer the most convenient approach for calculating stress coefficients especially for ship structures with significant discontinuities. The application of finite element methods to ship structures is a large subject which cannot be addressed satisfactorily in this appendix.

PROJECT TECHNICAL COMMITTEE MEMBERS

The following persons were members of the Project Technical Committee that represented the Ship Structure Committee to the Contractor as the resident subject matter experts. As such they performed technical review of the initial project proposals to select the contractor, advised the contractor in cognizant matters pertaining to the contract of which the agencies were aware, performed technical review of the work in progress, and edited the final report.

Project Technical Committee Chairperson

Lieutenant Commander Thomas C. Miller   United States Coast Guard

Project Technical Committee Members

Mr. Gabrielle Tam   American Bureau of Shipping

Mr. Harold Reemsnyder   Bethlehem Steel

Executive Director

Lieutenant David J. Martyn   United States Coast Guard

Administrative Assistant

Ms. Jeannette Delaney   Q Systems, INC

SHIP STRUCTURE COMMITTEE PARTNERS AND LIAISON MEMBERS

PARTNERS

The Society of Naval Architects and Marine Engineers

Mr. Jose Femenia
President,
Society of Naval Architects and Marine Engineers

Dr. John Daidola
Chairman,
SNAME Technical & Research Steering Committee

The Gulf Coast Region Maritime Technology Center

Dr. John Crisp
Executive Director,
Gulf Coast Maritime Technology Center

Dr. Bill Vorus
Site Director,
Gulf Coast Maritime Technology Center

LIAISON MEMBERS

American Iron and Steel Institute	Mr. Alexander Wilson
American Society for Testing & Materials	Captain Charles Piersall (Ret.)
American Society of Naval Engineers	Captain Dennis K. Kruse (USN Ret.)
American Welding Society	Mr. Richard Frank
Bethlehem Steel Corporation	Dr. Harold Reemsnyder
Canada Center for Minerals & Energy Technology	Dr. William R. Tyson
Colorado School of Mines	Dr. Stephen Liu
Edison Welding Institute	Mr. Dave Edmonds
International Maritime Organization	Mr. Tom Allen
International Ship and Offshore Structure Congress	Dr. Alaa Mansour
INTERTANKO	Mr. Dragos Rauta
Massachusetts Institute of Technology	Mr. Dave Burke / Captain Chip McCord
Memorial University of Newfoundland	Dr. M. R. Haddara
National Cargo Bureau	Captain Jim McNamara
Office of Naval Research	Dr. Yapa Rajapaksie
Oil Companies International Maritime Forum	Mr. Phillip Murphy
Tanker Structure Cooperative Forum	Mr. Rong Huang
Technical University of Nova Scotia	Dr. C. Hsiung
United States Coast Guard Academy	Commander Kurt Colella
United States Merchant Marine Academy	Dr. C. B. Kim
United States Naval Academy	Dr. Ramswar Bhattacharyya
University of British Columbia	Dr. S. Calisal
University of California Berkeley	Dr. Robert Bea
University of Houston - Composites Eng & Appl.	Dr. Jerry Williams
University of Maryland	Dr. Bilal Ayyub
University of Michigan	Dr. Michael Bernitsas
University of Waterloo	Dr. J. Roorda
Virginia Polytechnic and State Institute	Dr. Alan Brown
Webb Institute	Dr. Kirsi Tikka
Welding Research Council	Dr. Martin Prager
Worchester Polytechnic Institute	Dr. Nick Dembsey
World Maritime Consulting, INC	VADM Gene Henn, USCG Ret.

RECENT SHIP STRUCTURE COMMITTEE PUBLICATIONS

SSC Report Number	Report Bibliography
SSC 408	**Detection Probability Assessment of Visual Inspection of Ships,** L .A. Demsetz, J. Cabrera 1999
SSC 407	**Optimal Strategies for Inspection of Ships for Fatigue and Corrosion Damage,** K. Ma, I. R. Orisamolu, R. G. Bea, 1999
SSC 406	**Sea Operational Profile for Structural Reliability Assessments,** I. F. Glenn, R. B. Paterson, L. Luznik, 1999
SSC 405	**Fatigue Resistant Detail Design Guide for Ship Structures,** I. F. Glenn, A. Dinovitzer, R. B. Paterson, L. Luznik, C. Bayley, 1999
SSC 404	**Ship Structural Integrity Information System (SSIS) Phase III: Ship Quality Information System,** H. P. Reeve, R. G. Bea, 1998
SSC 403	**Design Guide for Marine Applications of Composites,** E. Greene, 1997
SSC 402	**Guide to Damage Tolerance Analysis of Marine Structures,** R. D. Yee, L. Malik, R. Basu, K. Kirkhope, 1997
SSC 401	**State of the Art in Hull Reponse Monitoring Systems,** S. B. Slaughter, Dr. M. C. Cheung, D. Sucharski, B. Cowper, 1997
SSC 400	**Weld Detail Fatigue Life Improvement Techniques,** K. J. Kirkhope, R. Bell, L. Caron, R. I. Basu, 1997
SSC 399	**Strength and Stability of Stiffened Plate Components,** Q. Chen, T. J. E. Zimmerman, D. D. DeGeer, B. W. Kennedy, 1997
SSC 398	**Assessment of Reliability of Ship Structures,** A. Mansour, P. Wirsching, et al. 1997
SSC 397	**Commercial Ship Design and Fabrication for Corrosion Control,** J. Parente, J. Daidola, N. Basar, R. Rodi, 1997
SSC 396	**Optimized Design Parameters for Welded TMCP Steels,** L. Malik, R. Yee, B. Graville, A. Dinovitzer, 1997
SSC 395	**Ship's Maintenance Project, Pt II & III,** B. Bea, T. Xu, K. Ma, R.